

International Atomic Energy Agency

INDC(GCP)-326/L+F

INDC

INTERNATIONAL NUCLEAR DATA COMMITTEE

**NUCLEAR PHYSICS CONSTANTS
FOR THERMONUCLEAR FUSION**

A Reference Handbook

S.N. Abramovich, B.Ya. Guzhovskij, V.A. Zherebtsov,
A.G. Zvenigorodskij

CENTRAL SCIENTIFIC RESEARCH INSTITUTE ON
INFORMATION AND TECHNO-ECONOMIC RESEARCH
ON ATOMIC SCIENCE AND TECHNOLOGY

STATE COMMITTEE ON THE UTILIZATION OF
ATOMIC ENERGY OF THE USSR

Moscow - 1989

Translated by A. Lorenz
for the
International Atomic Energy Agency

March 1991

IAEA NUCLEAR DATA SECTION, WAGRAMERSTRASSE 5, A-1400 VIENNA

**NUCLEAR PHYSICS CONSTANTS
FOR THERMONUCLEAR FUSION**

A Reference Handbook

**S.N. Abramovich, B.Ya. Guzhovskij, V.A. Zherebtsov,
A.G. Zvenigorodskij**

**CENTRAL SCIENTIFIC RESEARCH INSTITUTE ON
INFORMATION AND TECHNO-ECONOMIC RESEARCH
ON ATOMIC SCIENCE AND TECHNOLOGY**

**STATE COMMITTEE ON THE UTILIZATION OF
ATOMIC ENERGY OF THE USSR**

Moscow - 1989

**Translated by A. Lorenz
for the
International Atomic Energy Agency**

March 1991

Reproduced by the IAEA in Austria
March 1991

91-01324

PREFACE

TsNII-ATOMINFORM presents a reference handbook on
"Nuclear-Physics Constants for Thermonuclear Fusion"

UDK 539.17

Light nuclei reactions are required for a number of practical applications: they are used extensively in nuclear physics research as neutron sources, and as standards for the normalization of absolute reaction cross-sections. Nuclear reactions with light nuclei are useful in non-destructive testing and in the determination of isotopic compositions when other analytical methods are not adequate for obtaining the required information.

The information presented in this handbook consists of nuclear reaction cross-sections and scattering cross-sections for the interaction of hydrogen and helium isotopes with nuclei of $Z \leq 5$. The evaluated integral and partial differential cross-sections presented here have been derived from a large body of compiled information, and encompass data for both exo-energetic and endo-energetic reaction channels.

The evaluated data are presented in the form of sets of coefficients for fitted polynomials which ensures reliable interpolation of the data using contemporary computer methods.

The handbook is intended for a wide audience of users in the field of nuclear physics, astrophysics, and biophysics.

The price of this handbook is 40 roubles; it can be obtained by writing to the Collection Laboratory, P.O. Box 971, Moscow, 127434.

Table of Contents

List of Symbols and Abbreviations	9
Foreword	11
Chapter 1. Thermonuclear Reactions for Nuclear Fusion	12
1.1. The $^3\text{H} + \text{d}$ interaction	14
1.2. The $^2\text{H} + \text{d}$ interaction	14
1.3. The $^3\text{H} + \text{t}$ interaction	15
1.4. The $^3\text{He} + \text{d}$ interaction	15
1.5. The $^3\text{He} + \text{t}$ interaction	15
1.6. The $^6\text{Li} + \text{p}$ interaction	16
1.7. The $^6\text{Li} + \text{d}$ interaction	16
1.8. The $^7\text{Li} + \text{d}$ interaction	16
1.9. The $^9\text{Be} + \text{p}$ interaction	17
1.10. The $^{11}\text{B} + \text{p}$ interaction	17
Chapter 2. Evaluation Methodology	18
Chapter 3. Cross-Sections for the Interaction of Hydrogen and Helium Isotopes	22
3.1. Basic Data	22
3.2. The $^2\text{H}(\text{p},\gamma)^3\text{He}$ reaction	22
3.3. The deuteron break-up in the $\text{d} + \text{p}$ interaction	23
The $^2\text{H}(\text{p},\text{p} + \text{n})^1\text{H}$ reaction	23
3.4. The $^2\text{H}(\text{d},\gamma)^4\text{He}$ reaction	23
3.5. The $^2\text{H}(\text{d},\text{n})^3\text{He}$ reaction	24
3.6. The $^2\text{H}(\text{d},\text{p})^3\text{H}$ reaction	24
3.7. The $^2\text{H}(\text{d},\text{p} + \text{n})^2\text{H}$ reaction	25
3.8. The $^3\text{H}(\text{p},\gamma)^4\text{He}$ reaction	25
3.9. Neutron yield in the interactions of protons with tritium nuclei. The $^3\text{H}(\text{p},\text{n})^3\text{He}$ and $^3\text{H}(\text{p},\text{x})\text{n}$ reactions	25
3.10. The $^3\text{H}(\text{d},\gamma)^5\text{He}$	26
3.11. The $^3\text{H}(\text{d},\text{n})^4\text{He}$ reaction	26
3.12. The $^3\text{H}(\text{d},\text{n} + \text{p})^3\text{H}$ and $^3\text{H}(\text{d},2\text{n})^3\text{H}$ reactions	27
3.13. The $^3\text{H}(\text{t},2\text{n})^4\text{He}$ reaction	27
3.14. The $^3\text{H}(\tau,\gamma)^6\text{Li}$ reaction	28
3.15. The $^3\text{He}(\text{d},\gamma)^5\text{Li}$ reaction	28
3.16. The $^3\text{He}(\text{d},\text{p})^4\text{He}$ reaction	29
3.17. The break-up of the deuteron on helium-3 nuclei The $^3\text{He}(\text{d},\text{n} + \text{p})^3\text{He}$ reaction	29
3.18. The interaction of tritium with helium-3 nuclei The $^3\text{He}(\text{t},\text{d})^4\text{He}$, $^3\text{He}(\text{t},\text{n} + \text{p})^4\text{He}$, $^3\text{He}(\text{t},\text{p})^5\text{He}$ and the $^3\text{He}(\text{t},\text{n})^5\text{Li}$ reactions	30
3.19. The $^3\text{He}(\tau,\gamma)^6\text{Be}$ reaction	30
3.20. The $^3\text{He}(\tau,2\text{p})^4\text{He}$ reaction	30
3.21. The $^3\text{He}(\alpha,\gamma)^7\text{Be}$ and $^3\text{H}(\alpha,\gamma)^7\text{Li}$ reactions	31
3.22. The $^4\text{He}(\text{d},\gamma)^6\text{Li}$ reaction	31

Chapter 4.	Cross Sections for the Interaction of Lithium Nuclei with Isotopes of Hydrogen and Helium	41
4.1.	Basic Data	41
4.2.	The ${}^6\text{Li}(p,\gamma){}^7\text{Be}$ reaction	41
4.3.	The ${}^6\text{Li}(p,n){}^6\text{Be}$ reaction	41
4.4.	The ${}^6\text{Li}(p,\alpha){}^3\text{He}$ reaction	42
4.5.	The ${}^6\text{Li}(d,n){}^7\text{Be}$ reaction and the total cross sections for the neutron generation in the Li + d interaction	42
4.6.	The ${}^6\text{Li}(d,p){}^7\text{Li}$ reaction	42
4.7.	The ${}^6\text{Li}(d,t){}^5\text{Li}$ and ${}^6\text{Li}(d,\tau){}^5\text{He}$ reactions	43
4.8.	The ${}^6\text{Li}(d,\alpha){}^4\text{He}$ reaction	43
4.9.	The cross-section for the formation of neutrons and beryllium-7 nuclei in the ${}^6\text{Li}(t,x)n$ and ${}^6\text{Li}(t,2n){}^7\text{Be}$ reactions	44
4.10.	The ${}^6\text{Li}(t,p){}^8\text{Li}$ reaction	45
4.11.	The ${}^6\text{Li}(t,d){}^7\text{Li}$ reaction	45
4.12.	The ${}^6\text{Li}(\tau,n){}^8\text{B}$ reaction	46
4.13.	The ${}^6\text{Li}(\tau,p){}^8\text{Be}$ reaction	46
4.14.	The ${}^6\text{Li}(\tau,d){}^7\text{Be}$ reaction	46
4.15.	The ${}^7\text{Li}(p,\gamma){}^8\text{Be}$ reaction	47
4.16.	The ${}^7\text{Li}(p,n){}^7\text{Be}$ reaction	47
4.17.	The ${}^7\text{Li}(p,\alpha){}^4\text{He}$ reaction	48
4.18.	The cross-section for the formation of tritium in interactions of protons with lithium-7 nuclei	49
4.19.	The cross-section for the formation of beryllium-7 nuclei in the ${}^7\text{Li}(d,x)n$ and ${}^7\text{Li}(d,2n){}^7\text{Be}$ reactions	49
4.20.	The ${}^7\text{Li}(d,p){}^8\text{Li}$ reaction	50
4.21.	The ${}^7\text{Li}(d,t){}^6\text{Li}$ reaction	50
4.22.	Evaluation of the ${}^7\text{Li}(t,p){}^9\text{Li}$ integral reaction cross-section	50
4.23.	Evaluation of the ${}^7\text{Li}(t,d){}^8\text{Li}$ integral reaction cross-section	51
4.24.	Evaluation of the ${}^7\text{Li}(t,\alpha){}^6\text{He}$ partial integral cross-sections	51
4.25.	Evaluation of the integral cross-section for the formation of neutrons in the interaction of tritium with lithium-7 nuclei. The ${}^7\text{Li}(t,x)n$ reaction	52
4.26.	The ${}^7\text{Li}(\tau,n){}^9\text{B}$ reaction	52
4.27.	The ${}^7\text{Li}(\tau,p){}^9\text{Be}$ reaction	52
4.28.	The ${}^7\text{Li}(\tau,d){}^8\text{Be}$ reaction	52
4.29.	The ${}^7\text{Li}(\tau,t){}^7\text{Be}$ reaction	53
4.30.	The ${}^7\text{Li}(\tau,\alpha){}^6\text{Li}$ reaction	53
4.31.	The total integral cross-section for the formation of neutrons in the ${}^7\text{Li}(\alpha,n){}^{10}\text{B}$ reaction	53
Chapter 5.	Cross-Sections for the Interaction of Isotopes of Hydrogen and Helium with Beryllium Nuclei	69
5.1.	Basic data	69
5.2.	The ${}^9\text{Be}(p,\gamma){}^{10}\text{B}$ reaction	69
5.3.	The ${}^9\text{Be}(p,n){}^9\text{B}$ reaction	69
5.4.	The ${}^9\text{Be}(p,d){}^8\text{Be}$ reaction	70
5.5.	The ${}^9\text{Be}(p,\alpha){}^6\text{Li}$ reaction	70
5.6.	The ${}^9\text{Be}(d,\gamma){}^{11}\text{B}$ reaction	71

5.7.	The ${}^9\text{Be}(d,n){}^{10}\text{B}$ reaction	72
5.8.	The ${}^9\text{Be}(d,p){}^{10}\text{Be}$ reaction	73
5.9.	The ${}^9\text{Be}(d,t_0){}^8\text{Be}$ and ${}^9\text{Be}(d,t){}^8\text{B}$ reactions	73
5.10.	The ${}^9\text{Be}(d,\alpha){}^7\text{Li}$ reaction	74
5.11.	The ${}^9\text{Be}(t,n){}^{11}\text{B}$ reaction	74
5.12.	The ${}^9\text{Be}(\tau,n){}^{11}\text{C}$ reaction	75
5.13.	The ${}^9\text{Be}(\tau,p){}^{11}\text{B}$ reaction	76
5.14.	The ${}^9\text{Be}(\alpha,n){}^{12}\text{C}$ reaction	76
Chapter 6. Characteristic Levels of Individual Nuclei		86
BIBLIOGRAPHY		89

LIST OF SYMBOLS AND ABBREVIATIONS

$\sigma(E)$	-	integral cross-section for energy E; if not otherwise indicated in the text, the cross-section is given in millibarn (mb), and the energy in MeV in the laboratory system
$E_{\mu m}$	-	energy in the centre of mass system
$S(E_{\mu m})$	-	S-factor in the Gamow extrapolation equation
E_g	-	energy parameter in Gamow's equation
$\sigma(\theta, E)$	-	differential cross-section for a given angle θ and energy E
E_x	-	excitation energy of the nucleus
$\tau_{1/2}$	-	radionuclide half-life
τ_m	-	mean lifetime of radionuclide
Γ	-	resonance width for a given level in keV
α, β, γ	-	corresponding to alpha, beta and gamma decays
ϵ	-	electron capture
J^π	-	total angular momentum J and parity (/)
T	-	isotopic spin
T_e	-	absolute temperature in degree Kelvin
k	-	Boltzmann constant

Interacting particles

α - alpha particle	p - proton
τ - the ${}^3\text{He}$ nucleus	n - neutron
t - triton	x - any of the outgoing particles in a nuclear reaction
d - deuteron	

Nuclei: Reaction Products

The following convention is adopted in this handbook for the designation of nuclei: ${}^n\text{nA}$, where A is the nucleus symbol, and nn the mass number (e.g. ${}^7\text{Li}$ is the lithium-7 nucleus).

Description of reactions

Nuclear reactions are denoted as: ${}^n\text{A}(\text{particle 1,particle 2}){}^m\text{B}$.
As an example, ${}^7\text{Li}(\text{t,x}){}^8\text{Li}$ describes the interaction of lithium-7 with a triton, leading to the formation of lithium-8 (reaction channels are not defined).

Data types

- EXC - excitation function, the energy dependence of a nuclear reaction
- AND - angular distribution
- DA - differential cross-section
- SIG - integral cross-section
- UND - reaction channels for a given cross-section are not given
- ACT - activation
- TTY - thick target yield

FOREWORD

The production of a specialized handbook of evaluated nuclear data on the interaction of light nuclei ($Z \leq 4$) is justified not only by the fundamental role which these reactions play in nucleosynthesis in the universe, but also by the just as important role which they must play for humanity in the development of the new field of thermonuclear (fusion) power generation. Whereas the usefulness of nuclear data in various aspects of astrophysics have been extensively publicized in review articles and monographs [1], their "terrestrial" applications to problems in the field of nuclear fusion have not been fully exploited.

Nuclear physics data characterizing the interactions of light nuclei are published in numerous scientific journals and publications which are not readily accessible to most potential data users. In addition, experimental cross-section data are often not suitable for direct use in calculations as they are presented in the form of discrete energy points for incoming particles, or as angles of emission escape for outgoing reaction products. In most cases nuclear physics data can be recommended for unambiguous use only after they had gone through the process of evaluation, that is, after all the available experimental cross-section data complemented by data calculated on the basis of proven nuclear reaction models have been rigorously analysed. The evaluation of nuclear physics data requires not only the availability of complete sets of originally measured data, but also a thorough knowledge of the experimental and theoretical methods used in their determination. Because of the extremely large volume of numerical information, the evaluation of nuclear physics data is practically impossible without the utilization of modern computers which facilitate the organization of this information into nuclear data libraries and the development of the necessary computer programs for their processing.

The preparation of the numerical information for this handbook has taken more than ten years. During this time a global bibliographic search was performed and all nuclear physics data for nuclei of $Z \leq 4$ that appeared up to January 1988 in publications accessible to the authors were compiled. A large volume of experimental data has thus been collected and organized: numerical and digitized graphical data, consisting of nuclear interaction cross-sections, were entered into a computerized nuclear physics data library, where they were encoded in a standard (EXFOR) format. A series of computer programs were developed for the input, storage and retrieval of the data, as well as for their statistical analysis and graphical representation [2].

An evaluation methodology was developed for the representation of the evaluated excitation function data in the form of spline-fit curves. In a number of cases, the experimental data were supplemented by theoretically computed data based on phase analysis of few-nucleon systems, on Gamow's analytical formalism in the low energy region, on the optical model for elastic scattering, on the distorted wave approximation and on resonance theory.

The nuclear data which are presented in this handbook are designed primarily to satisfy the requirements for the development of controlled thermonuclear fusion. At the same time this information should also be of interest to specialists in other fields of nuclear science and technology. As an example, some of the light element reactions are used extensively in the generation of monoenergetic neutrons on accelerators where the accuracy achieved in the measurements of neutrons generated by light nuclei reactions depends to a large extent on an exact knowledge of the characteristics of reactions such as ${}^3\text{H}(p,n)$, ${}^2\text{H}(d,n)$, ${}^3\text{H}(d,n)$ and ${}^7\text{Li}(p,n)$. Light nuclei nuclear reactions have also proven to be very useful in non-destructive testing and in the determination of the isotopic composition of fabricated as

well as natural material samples, particularly in those cases where other methods have failed to achieve the desired measurement sensitivity. In practice, however, methods used in the control and analysis of layered and deposited materials rely either on the prompt emission of neutrons, gamma rays and charged particles, or on induced activity. Of particular interest are micro-analytical methods utilizing narrow beams of charged particles which reveal the "topography" of individual isotopic components on the surface of as well as within the analysed sample.

Chapter 1 of the handbook describes basic concepts relating to nuclear reactions in hot plasmas which are of interest for controlled thermonuclear fusion, and presents a brief outline of the possible thermonuclear processes which can occur in plasmas of various compositions.

Chapter 2 outlines the methodology developed for the evaluation of nuclear data which was used in the preparation of this handbook, and describes formulas to be used in the determination of fitted curves giving the energy dependence of the evaluated data.

Chapters 3, 4, and 5 contain the actual evaluated data for reactions of hydrogen isotopes with helium, of lithium with hydrogen and helium, and of beryllium with hydrogen and helium, based on the known experimental data, supplemented by calculated data, for charged particle energies up to 15 MeV.

Chapter 6 contains nuclear structure data for the light elements which take part in these reactions. This information is needed for the analysis of the partial reaction cross-sections and in the calculation of average velocities and energy yields.

1. THERMONUCLEAR REACTIONS FOR NUCLEAR FUSION

Thermonuclear reactions are defined as nuclear reactions between light atomic nuclei at very high temperatures (of the order of 10^6 to 10^{10} K),

reactions in which the relative recoil energy of the nuclei is high enough to overcome the Coulomb (electrostatic repulsion) barrier and the distance between nuclei is of the order of the range of the nuclear-force, giving the possibility for the nuclei to fuse and create a heavier nuclear reaction product with the simultaneous release of energy.

In the universe, thermonuclear reactions play a dual role: they are the basic source of stellar energy and are instrumental in the nucleosynthesis of the light elements. On earth, thermonuclear reactions have so far been realized on a large scale only in the testing of thermonuclear weapons. The utilization of thermonuclear reactions in peaceful applications depends on the attainment of controlled thermonuclear fusion, which would satisfy the growing energy needs of mankind.

In order to describe the dynamic processes occurring in a hot plasma it is important to know the nuclear reaction rate, which either increases the equilibrium temperature, in the case of exothermic reactions with $Q \geq 3/2 kT_e$, or lowers it in the case of endothermic reactions. These reactions can also either add atomic nuclei to a system or remove them from it, nuclei, which in turn act as sources or absorbers of energy. In the case of thermonuclear equilibrium, we have a Maxwellian distribution of ions in the plasma:

$$N(E) = A \cdot \sqrt{E} \cdot \exp(-E/kT_e), \quad (1.1)$$

where E is the ion energy, and kT_e the temperature expressed in energy units. The reaction rate (the number of nuclear reactions per cm^3 per second) is expressed as follows [3]:

$$R/n_1 n_2 = \langle \sigma v \rangle_m = 4 \left(\frac{2\pi}{m_1} \right)^{1/2} \left(\frac{\mu}{m_1 k T_e} \right)^{3/2} \int_0^\infty \sigma \cdot E \cdot \exp(-\mu E / m_1 k T_e) dE, \quad (1.2)$$

where m_1 and E are the mass and energy (in the laboratory system) of the incoming particle, $\mu = \frac{m_1 m_2}{m_1 + m_2}$ is the reduced mass, m_2 the mass of

the target nucleus, and n_1 and n_2 are the nuclear concentrations of the reacting components.

When the equilibrium spectrum differs from the Maxwellian distribution (as in a magnetic mirror machine where ions with a given velocity are escaping into a "loss cone"), the integration of equation (1.2) must be performed with the true distribution.

In the interaction of injected fast ion (or neutral particle) beams with plasma targets, the specific average reaction rate is defined by the following equation [3]:

$$\langle \sigma v \rangle_m = \frac{\rho}{\sqrt{\pi}} \frac{1}{v_0} \int_0^{\infty} \left(\frac{1}{2} n_1 v^2 \right) v^2 \left\{ \sigma \rho [-\beta^2 (v_0 - v)^2] - \exp[-\beta^2 (v_0 + v)^2] \right\} dV, \quad (1.3)$$

where $\beta = m_2 / (2kT_e)$; v_0 and m_1 are the velocity and mass of the injected particles; and m_2 is the mass of a plasma particle.

In order to obtain an effective value for the collision rate $\langle \sigma v \rangle_B$ so as to account for the slowing down of the beam particles in the plasma, we must calculate the integral

$$\int_{v_m}^{v_0} \langle \sigma v \rangle_m f_B(v_0) dv_0, \quad (1.4)$$

where the function $f_B(v_0)$ describes the velocity distribution of beam particles as they are slowed down, and where v_m is the average plasma particle velocity.

The fast product nuclei resulting from thermonuclear reactions (indexed with j), which are slowed down in the plasma (nuclei indexed with i), have a finite probability P_{ij} of undergoing a nuclear reaction $i + j$ "on the fly" (fast fusion):

$$P_{ij} = 1 - \exp(-P'_{ij}), \quad (1.5a)$$

where

$$P'_{ij} = \int_{E_{0j}}^{3/2 kT_e} n_i \langle \sigma v \rangle_{ij} (dt/dE)_j dE. \quad (1.5b)$$

The rate of energy loss of ion j in the plasma $(dE/dT)_j$ is strongly dependent on the electron temperature T_e of the plasma:

$$\left(\frac{dE}{dT} \right)_j \sim - \frac{4\sqrt{2} e^4}{V_j} \left[\frac{n_i}{m_i} + \frac{4}{3\sqrt{2}} \frac{n_e}{m_e} \left(\frac{m_e E_0}{m_j kT_e} \right)^{3/2} \right] \quad (1.6)$$

(on the assumption that Coulomb scattering prevails).

The probability P_{ij} increases as T_e and the energy E_0 of ion j increase, and does not depend on the density of the plasma. To illustrate this, a proton with an energy of 11 MeV (resulting from the $^3\text{He} + ^6\text{Li}$ reaction) has a probability for slowing down in a lithium plasma equal to $P_{ij} = 0.05$ for $kT_e = 100$ keV, and to $P_{ij} = 0.21$ for $kT_e = 300$ keV. Fast secondary charged particles are produced not only as a result of exothermic reactions, but also as a result of elastic scattering of fast primary reaction products, including neutrons, on thermalized plasma nuclei. As an example, neutrons with energy $E_n = 14.07$ MeV resulting from the d-t reaction and undergoing elastic collisions can impart 14.07 MeV to a proton, up to 12.5 MeV to a deuteron, up to 10.55 MeV to a triton and helium-3 particle, up to 9 MeV to an alpha particle, up to 6.89 MeV to lithium-6, and 4.38 MeV to lithium-7.

In order to take the contribution from fast fusion ("on-the-fly reactions") into account, it is necessary to know the total cross-section and the differential scattering cross-sections for particle energies up to 15 MeV.

In a hot plasma, comprising all the stable and long-lived isotopes of hydrogen, helium, lithium and beryllium, we have to take into account the contributions from approximately 40 pairs of interacting nuclei, even if we

include only nuclei with $Z_1 \leq 2$ and $Z_2 \leq 4$. This means considering more than 100 individual exothermic reaction channels leading to the formation of various product nuclei. Reactions between lithium and beryllium need not be considered because of their low interaction probability at temperatures below 100 keV.

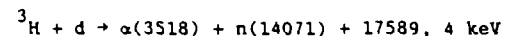
A cursory analysis of the reaction rates listed in Table 1.1 shows that the reactions which are most pertinent to the development of controlled nuclear fusion are the $^2\text{H} + \text{d}$, $^3\text{H} + \text{d}$ and the $^3\text{He} + \text{d}$ reactions. At higher plasma temperatures and densities, it would become possible to utilize reactions of hydrogen isotopes with nuclei of lithium-6 and -7, beryllium and boron-11. Of particular interest is what is referred to as "clean fusion" in which the contributing reactions ($^6\text{Li} + \text{p}$, $^9\text{Be} + \text{p}$ and $^{11}\text{B} + \text{p}$) do not yield any neutrons, as well as catalytic processes which do not involve tritium recovery or tritium breeding. The term catalytic process, as used here, implies a multi-step thermonuclear burn process in which a substantial contribution to total energy production comes from secondary reactions involving nuclei which were not part of the original plasma but were produced in the burn process and act as catalysts.

Neutron-free thermonuclear fusion has the advantage that virtually all the energy produced in the thermonuclear process goes into the heating of the plasma, so that there is no intense neutron radiation that could damage the first wall of the reactor, requiring substantial extra shielding of the installation as a whole.

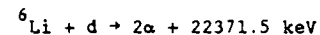
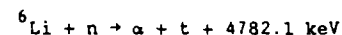
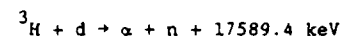
Below we present a number of basic thermonuclear fusion cycles, describing them briefly in terms of reaction rate $\langle\sigma v\rangle$, energy yield and Kerma factor (i.e. the energy fraction transferred to the charged particles). The numbers in parentheses correspond to the particle kinetic energies (in keV) for those cases where the kinetic energy of the two reacting nuclei

is equal to zero. In the case of three-particle interactions the energy distribution is inversely proportional to the masses of the reaction products.

1.1. The $^3\text{H} + \text{d}$ interaction

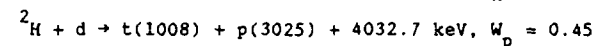
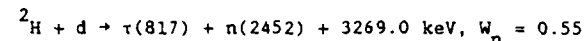


This reaction has the lowest thermonuclear ignition threshold, and is therefore considered as the main reaction for all first-generation controlled thermonuclear fusion schemes. The heating of the plasma during the burning of a one-to-one mixture of deuterium and tritium is brought about by alpha particles only. The energy of the neutrons is deposited in a lithium blanket where large quantities of tritium are produced by the $^7\text{Li}(n, n + t)^4\text{He}$ and $^6\text{Li}(n, \alpha)^3\text{H}$ reactions, thus guaranteeing the existence of a closed fuel cycle:

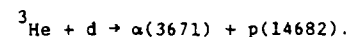
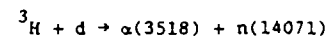


In this case, only 15.73% of the total cycle energy is given off in the burn zone; the rest is deposited in the blanket.

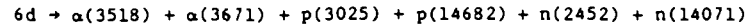
1.2. The $^2\text{H} + \text{d}$ interaction



A thermonuclear burn of pure deuterium requires a considerably higher heating temperature than a deuterium-tritium mixture; however, the heating of a d-d plasma by reaction products proceeds effectively thanks to the additional energy released by the secondary reactions



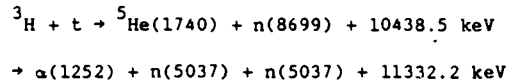
The yield from a complete 6d fuel cycle is then



For every 2d in the cycle, 8907 keV are released in the burn zone, which is 2.53 times the amount of energy released in a d-t reaction. The intermediate reaction products (tritium and helium) play their original role of catalysts in the extended burn cycle; such a cycle is therefore referred to as a catalytic cycle.

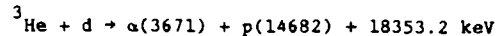
As deuterium is available in unlimited quantities in nature, it is not necessary to have a blanket in a catalytic d-d fuel cycle. For a given thermal power level, a thermonuclear reactor running on pure deuterium would have a fast neutron fluence only a quarter of that found in a reactor running on a d-t mixture.

1.3. The $^3\text{H} + \text{t}$ interaction



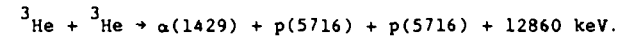
This reaction proceeds as a secondary reaction in a d-t plasma; the reaction rate is two orders of magnitude lower than that of the primary reaction, and the specific energy released in the burn zone is low (1300 keV) owing to the escape of two neutrons. The relationship between the neutron yields from the $^3\text{H} + \text{d}$ ($E_n = 14071 \text{ keV}$), $^2\text{H} + \text{d}$ (2452 keV) and $^3\text{H} + \text{t}$ (8699 keV) reactions is strongly dependent on the ion temperature and can therefore be used for plasma diagnostics.

1.4. The $^3\text{He} + \text{d}$ interaction



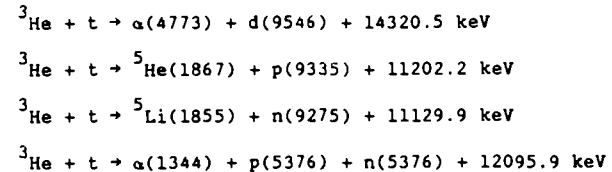
This reaction is ideal for controlled fusion because all the energy released goes into the heating of the plasma in the burn zone and no neutrons are produced. However, at temperatures below 18 keV the reaction rate of the $^2\text{H} + \text{d}$ reaction (at equal concentrations of deuterium and helium-3) is

higher, and it is therefore necessary to take the production of neutrons, tritium and helium-3 into account. At temperatures above 18 keV, the contribution to plasma heating from the secondary $^2\text{H} + \text{d}$ reaction gradually decreases relative to the $^3\text{H} + \text{d}$ reaction until it reaches a level of 13% at $kT_e = 100 \text{ keV}$. A reactor with a d- ^3He mixture is essentially very close to a reactor using the catalytic d-d fuel cycle, and differs only in that it has helium-3 in the initial startup fuel mixture. The other secondary reaction is

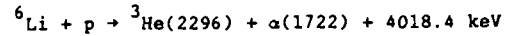


Like the primary one, this reaction yields a large energy contribution and no neutrons, but its contribution to the plasma burn is nevertheless small because of the low reaction rate. The $^3\text{He} + \text{d}$ reaction (along with the $^2\text{H} + \text{d}$ and $^3\text{H} + \text{d}$ reactions) is used for plasma diagnostics by measuring the yield and the energy spectrum of fast neutrons and alpha particles emitted from the burn zone of the plasma.

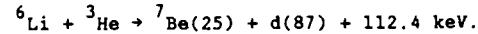
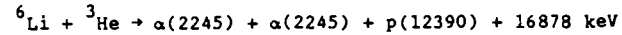
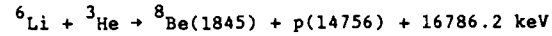
1.5. The $^3\text{He} + \text{t}$ interaction



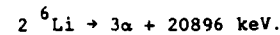
Because of their low concentrations and small reaction rates (in comparison to the $^3\text{H} + \text{d}$ and $^3\text{He} + \text{d}$ competing reactions), these reactions contribute only a relatively small amount of energy to the combustion of the tritium and helium-3 reaction products which are produced in the first stage of the catalytic d-d cycle. Inasmuch as the energy release of the $^3\text{He} + \text{t}$ reaction in the burn zone is dominant, its heating contribution to the catalytic d-d plasma is significant.

1.6. The ${}^6\text{Li} + p$ interaction

At a high enough temperature, it is possible to initiate a catalytic neutron-free burn cycle on the basis of this reaction. The following secondary reactions yield only charged particles



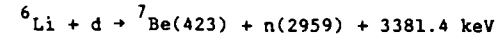
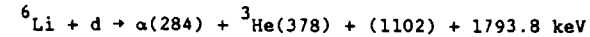
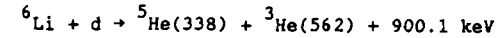
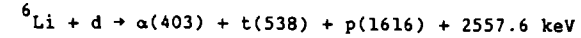
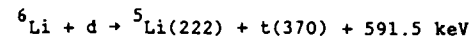
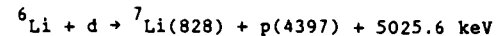
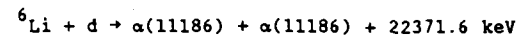
In the next stage, protons react with lithium-6, which is the start of a new cycle. From the balance of the first two stages (without considering the last branch) it follows that only the lithium is consumed and the protons are preserved, i.e. they take part in the burn process as catalysts:



There is a definite probability that the protons will react in flight in the $p + {}^6\text{Li}$ reaction during slowing down, and it is important to take this into consideration in calculating the reaction rate.

The generation of neutrons in a proton- ${}^6\text{Li}$ plasma burn is only possible in the third stage as a result of the ${}^6\text{Li} + d$ reaction and the production of neutrons in the second stage of the ${}^6\text{Li}(\tau, d)$ reaction.

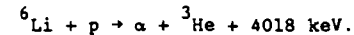
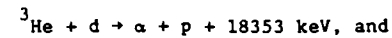
It is expected that the yield of neutrons will be much smaller than that of charged particles; however, in order to obtain a more accurate estimate it is necessary to know the rate of lithium production and the reaction rate of the ${}^6\text{Li} + d$ reaction accompanied by the emission of a neutron.

1.7. The ${}^6\text{Li} + d$ interaction

Concurrent to the $d-{}^6\text{Li}$ plasma burn, the ${}^2\text{H} + d$ reaction produces protons, tritons, helium and neutrons. At temperatures exceeding 100 keV the ${}^6\text{Li} + d$ reaction rate becomes greater than that of the ${}^2\text{H} + d$ reaction.

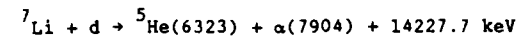
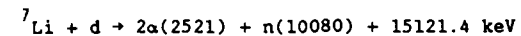
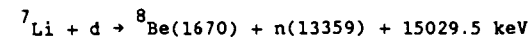
In the second stage, deuterons and lithium-6 interact with reaction products generated during the first stage (see above).

Fast protons, helium-3 nuclei, alpha-particles and neutrons are produced at the end of the second stage. During the third stage two reactions proceed in parallel:

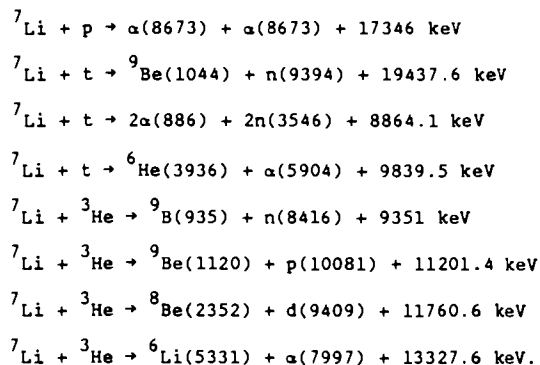


As a result, the burning of deuterium and lithium-6 can proceed not only directly (${}^6\text{Li} + d \rightarrow 2\alpha$), but also with the help of a chain of secondary reactions, involving individual reaction products, notably protons and helium-3 nuclei which play a catalytic role. The effective burning rate in this extended cycle is determined by the slowest ${}^6\text{Li}(p, \alpha){}^3\text{He}$ reaction, whose reaction rate is, however, larger than the direct ${}^6\text{Li}(d, \alpha){}^4\text{He}$ reaction.

In the total burning rate, the contribution of the direct ${}^6\text{Li}(d, \alpha){}^4\text{He}$ reaction decreases with rising temperature: it is 16.3% when $kT_e = 30 \text{ keV}$, and 11.6% when $kT_e = 100 \text{ keV}$; the contribution to the local energy yield from the charged particles is 55.2% when $kT_e = 100 \text{ keV}$.

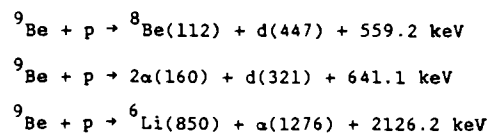
1.8. The ${}^7\text{Li} + d$ interaction

The reaction rates of simultaneously proceeding reactions between deuterons and between deuterons and lithium-7 nuclei become equal when $kT_e = 160$ keV. In addition to catalytic reactions from the d-d cycle (see Section 1.2), it is also possible to have secondary reactions involving products of the d-d cycle, namely protons, tritons and helium-3 with lithium-7 nuclei:



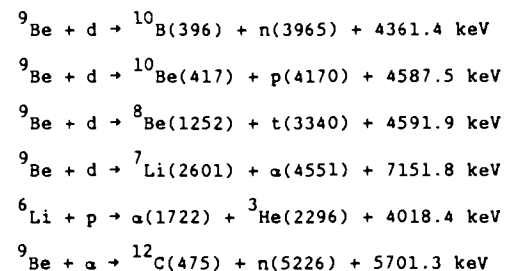
The reaction rates in the interactions of tritium and helium-3 with lithium-7 nuclei at a temperature of $kT_e = 100$ keV are much lower than those of the ${}^3\text{H} + \text{d}$ and ${}^3\text{He} + \text{d}$ reactions (they become equal only when $kT_e = 340$ keV and 490 keV respectively). The presence of lithium-7, rather than lithium-6, in the initial fuel mixture, leads to a much more effective utilization of protons because of the considerably larger reaction energy of the ${}^7\text{Li}(\text{p},\alpha){}^4\text{He}$ reaction, although the reaction rate of the latter is much smaller.

1.9. The ${}^9\text{Be} + \text{p}$ interaction

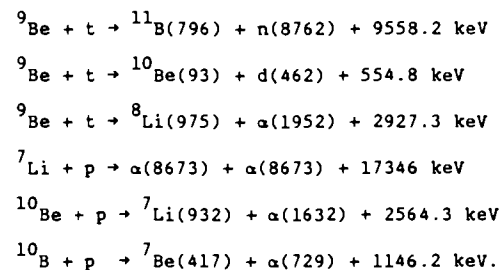


The reaction rates of proton- ${}^9\text{Be}$ reactions and deuteron-deuteron reactions are equal at a temperature of $kT_e = 50$ keV, and this reaction is

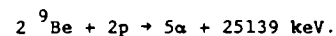
therefore considered to be a good candidate for a neutron-free thermonuclear reactor. The reaction products (deuterons, helium-4 and lithium-6) burn during the second stage of the cycle:



and tritium, lithium-7, beryllium-10 and boron-10 burn in the third stage of the cycle:



The cleanliness of the neutron-free cycle breaks down because of the secondary reactions ${}^9\text{Be}(\text{d},\text{n}){}^{10}\text{B}$ and ${}^9\text{Be}(\alpha,\text{n}){}^{12}\text{C}$, whose contributions are determined by the relative importance of the neutron and non-neutron reaction channels in the second stage of the cycle. The balanced equation of the neutron-free cycle is



The total energy yield of the ${}^9\text{Be} + \text{p}$ cycle is 12.57 MeV, which is 1.41 times larger than the catalytic d-d cycle.

1.10. The ${}^{11}\text{B} + \text{p}$ interaction

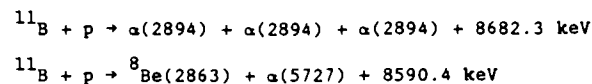
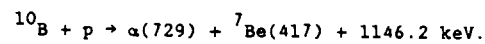


Table 1.1

Reaction rates of thermonuclear reactions $\langle \sigma v \rangle$ in m^3/sec for a few temperatures kT_e in keV

Reaction	Q, keV	kT_e , keV				
		10	30	100	300	1000
${}^3\text{H}+d \rightarrow \alpha+n$	17589	$1,13 \cdot 10^{-22}$	$6,65 \cdot 10^{-22}$	$8,24 \cdot 10^{-22}$	$4,90 \cdot 10^{-22}$	$2,55 \cdot 10^{-22}$
${}^2\text{H}+d \rightarrow \tau+n$	3269	$5,99 \cdot 10^{-25}$	$5,44 \cdot 10^{-24}$	$2,74 \cdot 10^{-23}$	$7,33 \cdot 10^{-23}$	$1,48 \cdot 10^{-22}$
${}^2\text{H}+d \rightarrow t+p$	4033	$5,76 \cdot 10^{-25}$	$4,76 \cdot 10^{-24}$	$2,21 \cdot 10^{-23}$	$6,0 \cdot 10^{-23}$	$1,22 \cdot 10^{-22}$
${}^3\text{H}+t \rightarrow \alpha+2n$	10438	$5,57 \cdot 10^{-25}$	$4,59 \cdot 10^{-24}$	$1,95 \cdot 10^{-23}$	$6,34 \cdot 10^{-23}$	$7,94 \cdot 10^{-23}$
${}^3\text{H}, \tau \rightarrow \alpha+p$	18353	$1,97 \cdot 10^{-25}$	$1,32 \cdot 10^{-23}$	$1,67 \cdot 10^{-22}$	$2,60 \cdot 10^{-22}$	$2,07 \cdot 10^{-22}$
${}^3\text{H}, \tau \rightarrow \alpha+d$	14320	$1,16 \cdot 10^{-26}$	$1,13 \cdot 10^{-24}$	$2,71 \cdot 10^{-23}$	$1,61 \cdot 10^{-22}$	$5,16 \cdot 10^{-22}$
${}^3\text{He}, \tau \rightarrow \alpha+2p$	12860	$4,86 \cdot 10^{-30}$	$4,92 \cdot 10^{-27}$	$6,31 \cdot 10^{-25}$	$9,82 \cdot 10^{-24}$	$1,25 \cdot 10^{-22}$
${}^6\text{Li}+p \rightarrow \tau+\alpha$	4018	$7,17 \cdot 10^{-27}$	$6,95 \cdot 10^{-25}$	$1,33 \cdot 10^{-23}$	$6,36 \cdot 10^{-23}$	$1,82 \cdot 10^{-22}$
${}^7\text{Li}+p \rightarrow 2\alpha$	17346	$1,78 \cdot 10^{-28}$	$1,86 \cdot 10^{-26}$	$5,55 \cdot 10^{-25}$	$3,89 \cdot 10^{-24}$	$4,01 \cdot 10^{-23}$
${}^6\text{Li}+d \rightarrow 2\alpha$	22371	$1,02 \cdot 10^{-27}$	$2,05 \cdot 10^{-25}$	$4,84 \cdot 10^{-24}$	$1,56 \cdot 10^{-23}$	$2,81 \cdot 10^{-23}$
${}^6\text{Li}+d \rightarrow {}^7\text{Be}+n$	3381	$1,44 \cdot 10^{-27}$	$3,06 \cdot 10^{-25}$	$8,89 \cdot 10^{-24}$	$4,49 \cdot 10^{-23}$	$1,04 \cdot 10^{-22}$
${}^6\text{Li}+d \rightarrow {}^7\text{Li}+p$	5026	$1,38 \cdot 10^{-27}$	$3,07 \cdot 10^{-25}$	$9,40 \cdot 10^{-24}$	$4,48 \cdot 10^{-23}$	$1,64 \cdot 10^{-22}$
${}^6\text{Li}+d \rightarrow \alpha+p+t$	2558	$1,02 \cdot 10^{-27}$	$2,76 \cdot 10^{-25}$	$1,30 \cdot 10^{-23}$	$6,82 \cdot 10^{-23}$	$2,71 \cdot 10^{-22}$
${}^6\text{Li}+d \rightarrow \alpha+n+\tau$	1793	$7,24 \cdot 10^{-28}$	$1,63 \cdot 10^{-25}$	$5,59 \cdot 10^{-24}$	$3,74 \cdot 10^{-23}$	$1,06 \cdot 10^{-22}$
${}^7\text{Li}+d \rightarrow 2\alpha+n$	15121	$1,53 \cdot 10^{-27}$	$4,61 \cdot 10^{-25}$	$2,54 \cdot 10^{-23}$	$2,44 \cdot 10^{-22}$	$1,03 \cdot 10^{-21}$
${}^9\text{Be}+p \rightarrow d+2\alpha$	641	$1,34 \cdot 10^{-27}$	$9,75 \cdot 10^{-25}$	$7,00 \cdot 10^{-23}$	$2,21 \cdot 10^{-22}$	$2,02 \cdot 10^{-21}$
${}^9\text{Be}+p \rightarrow \alpha+{}^6\text{Li}$	8126	$1,34 \cdot 10^{-27}$	$8,77 \cdot 10^{-25}$	$5,99 \cdot 10^{-23}$	$1,90 \cdot 10^{-22}$	$1,62 \cdot 10^{-21}$
${}^{11}\text{B}+p \rightarrow 3\alpha$	8682	$1,38 \cdot 10^{-28}$	$4,06 \cdot 10^{-23}$	$4,06 \cdot 10^{-23}$	$2,39 \cdot 10^{-22}$	$3,50 \cdot 10^{-22}$

Since all other channels are closed, the cycle is neutron-free. However, the presence of boron-10 in the initial fuel mixture (natural boron) leads to another reaction, namely



The reaction rate of the interaction of protons with boron-11 nuclei is 3.2 times lower at $kT_e = 100 \text{ keV}$ than the interaction of protons with beryllium-9 nuclei, and the energy yield is also lower by a factor of 1.45.

2. EVALUATION METHODOLOGY

The method used to obtain curves of evaluated data has been described in Ref. [4]; it consists of fitting the experimental data with approximating functions using the spline polynomial [5] of a given degree p in a fixed lattice:

$$E_N = X_0 < X_1 < \dots < X_{n-1} < X_n = E_k$$

A significant improvement of the evaluation quality was achieved by supplementing the initial data. The authors decided not to fix the knots of the spline function, but used them instead as parameters in the minimization process. It was therefore essential to use not only first order defect splines (when all the derivatives of degree up to $p-1$ are continuous at the knots) but also those of higher order. The statistical model used in this evaluation method was formulated for N sets of experimental data as follows:

$$\{x_j^r, y_j^r, \Delta y_j^r; j = 1, \dots, n_r\}, r = 1, \dots, N$$

It is assumed that the independent variable (for nuclear data it is usually the energy) x_j^r is known exactly, and that y_j^r is a function of x_j^r . This quantity, known to a given degree of accuracy, has a normal distribution $N(0, \sigma_j^r)$ with a root-mean-square deviation $\sigma_j^r \equiv \Delta y_j^r$. In addition, each set of data has a systematic error which has a distribution $N(0, \zeta(r))$. The experimental data can thus be represented by

$$Y_j^r = \bar{Y}_j^r + \epsilon_j^r + b^r \quad (2.1)$$

where \bar{Y}_j^r is the actual value of the function which is to be determined; ϵ_j^r is a random quantity which has the distribution $N(0, \sigma_j^r)$, and b^r is a random quantity which has the distribution $N(0, \zeta^r)$.

It is assumed that each pair of ξ_j^r is independent for given values of j , and that the quantity b^r is also independent for different values of r . Note that the y_j^r will not be independent random quantities because they all contain the same random quantity b^r . It follows from these considerations that the data in different sets are independent of each other, and that the probability function for each set can therefore be calculated independently. The logarithm of the general probability function can thus be obtained by adding the logarithms of the probability functions for all data sets [6]. The probability function for a given set can be determined as follows.

Let us introduce the random quantities $\xi_j^r = Y_j^r - \bar{y}_j^r$ and consider case A with its associated condition $\delta_j^r \leq \xi_j^r \leq \delta_j^r + d\delta_j^r$ and case B with its condition $\beta^r \leq b^r \leq \beta^r + d\beta^r$. The probability $P(A \cap B)$ can then be calculated according to the equation $P(A \cap B) = P(A/B) \cdot P(B)$. As can be seen from (2.1), if one considers the conditions of B, the quantity ξ_j^r will have a distribution given by $N(\beta^r, \sigma_j^r)$.

It follows then that

$$P(A \cap B) = \kappa \cdot \exp \left[- \sum_{j=1}^n \frac{(\xi_j^r - \beta^r)^2}{2(\sigma_j^r)^2} \right] \prod_{j=1}^n d\delta_j^r \exp \left[- \frac{(\beta^r)^2}{2(\xi_j^r)^2} \right] \quad (2.2)$$

where κ is an arbitrary coefficient independent of both δ_j^r and β^r .

Next, let us find the evaluated values of y_j^r , which depend on the random quantities of ξ_j^r , but not on b^r . For this purpose we must find from equation (2.2) the marginal distribution for the ξ_j^r array, integrating (2.2) over β^r from $-\infty$ to $+\infty$. After performing the integration, taking the logarithm, discarding the constant term and summing over all sets,

we obtain the final expression for the logarithm of the probability function:

$$\ln P = - \sum_{r=1}^N \left[\frac{(\xi_j^r)^2}{1 + \sum_j \left(\frac{\xi_j^r}{\sigma_j^r} \right)^2} \right] \cdot \phi \quad (2.3)$$

where

$$\phi = \left[\sum_{j=1}^{n_r} \frac{y_j^r - \bar{y}_j^r}{(\sigma_j^r)^2} \right]^2 - \sum_{j=1}^{n_r} \left[\frac{y_j^r - \bar{y}_j^r}{(\sigma_j^r)^2} \right]^2$$

We shall now look for \bar{y}_j^r as the value at point x_j^r of a spline function dependent on parameters $\alpha_1, \dots, \alpha_k$. These parameters we shall take to be a function of the location of the spline knots and of the values at these knots. The values we can determine by maximizing the logarithm of the probability function. The spline degree, the number of knots and defects are considered to be fixed. It is known that the spline function is linearly dependent on its value at the knot, and has a non-linear dependence on the location of the knot. Let us define the spline knots as $\{x_i\}$, $i = 0, \dots, n+1$.

Since they determine the interval which is being evaluated, the values of x_0 and x_{n+1} are fixed. In order to find the values of x_i , it is convenient to represent the spline function in the form

$$S(x) = \sum_{j=1}^l C_j B_j(x, x_1, x_2, \dots, x_n) \quad (2.4)$$

where $l + n = k$, and k is the total number of parameters.

We shall use a spline of order p . Although the spline order is normally taken as 3, it is more convenient not to be limited to a cubic spline, especially if such a generalization does not introduce any difficulties. As a base element which has a defect k at the knot x_j

($1 \leq k \leq (p + 1)$) and is non-zero only in the interval $(x_i, x_{i+p+2-k})$, we shall take the function

$$Q_{ik} = \begin{cases} \psi(x) & \text{for } x \geq x_i \\ 0 & \text{for } x < x_i \end{cases} \quad (2.5)$$

where

$$\psi(x) = \sum_{j=1}^{p+1-k} \frac{(x_{j+i} - x)_+^p}{(x_{j+i} - x_i)^{k-1} \prod_{m=0}^{i+j} (x_{j+i} - x_{m+i})}$$

and where

$$\begin{aligned} (x_{j+i} - x)_+^p &= (x_{j+i} - x)^p \quad \text{when } x_{j+i} - x \geq 0, \\ \text{and } (x_{j+i} - x)_+^p &= 0 \quad \text{when } x_{j+i} - x < 0. \end{aligned}$$

In order that these functions be defined at the end points of the evaluation range, it is necessary to extend the lattice $\{x_i\}$ by p points to the left, beyond x_0 , and to the right, beyond x_{n+1} . As the results of this evaluation will not depend on the method by which this extension is implemented, for the sake of clarity we can choose

$$x_{j+1} - x_j = \begin{cases} x_1 - x_0 & \text{for } i < 0 \\ x_{n+1} - x_n & \text{for } i > n+1 \end{cases} \quad (2.6)$$

In order to be sure that Q_{ik} is indeed a spline having the required properties, it is only necessary to check that

$$\begin{aligned} Q_{i,k}^{(l)}(x_i) &= 0 \quad \text{when } 1 \leq (p-k), \\ \text{and } Q_{i,k}^{p+1-k}(x_i) &\neq 0 \end{aligned} \quad (2.7)$$

This can be shown by induction on p . Substituting in equation (2.3) an expression for y_j^r in the spline form from (2.4), we arrive at the minimization of the function $\phi(c_1, \dots, c_k; x_1, \dots, x_n)$ whose parameters c_j are entered bi-linearly; the x_i parameters are, however, more complex. As it is impossible to minimize on x_i exactly, we need to use an approximation method. The authors chose to use Newton's method where the minimization is performed on the function

$$\phi_1(x_1, \dots, x_n) = \min_{c_j} \phi(c_1, \dots, c_k; x_1, \dots, x_n)$$

rather than on the function ϕ , because it is easier to find $\min \phi$ for given values of x_i (which requires the solution of a system of linear equations). At the same time there is a significant reduction in the number of parameters which must be found by Newton's method. The following obvious limiting conditions are applied in the solution of this problem:

$$x_0 < x_1 < x_2 \dots < x_n < x_{n+1}$$

In the process of solving this problem, it is possible that two spline knots would tend to merge. In such a case, the two knots are combined into one and the defect order is increased by one. The reason for proceeding in this manner can be seen from equation (2.5) if one changes its limits to $x_{i+1} \rightarrow x_i$. It can be seen that within these limits one would indeed have a base spline with a defect order of $k + 1$ in x_i . In order to evaluate the error of this approximation, consider the fact that with fixed knots, the problem is one of maximizing the probability with linear parameters; the inverse matrix for the solution of this problem, as we know, is the covariance matrix with coefficients c_j . The standard deviation of the spline in (2.4) can then be found from the equation

$$D(S(x)) = \sum_{i,j} \text{COV}(C_i, C_j) B_i(x) \cdot B_j(x) \quad (2.8)$$

As can be seen, the contribution to $D(s(x))$ of terms containing $\text{cov}(c_i, x_j)$ and $\text{cov}(x_i, x_j)$ has been omitted; their inclusion would have led to a very

complex expression. The question is whether it is necessary to include this contribution. The problem is that expressions such as (2.8) yield an evaluation only in those cases where real values of σ_j^r and ξ_j^r are included in the input data. In most cases they are not, so the values of σ_j^r and ξ_j^r must almost always be taken from the evaluation and re-entered into the evaluation to yield an improved value. In addition there is the philosophical question: "Would equation (2.8) be valid if the knots were not adjusted, and the existing optimum knots were regarded as fixed and used as such?" This shows that the errors in the approximation are determined in a rather random fashion, and that the error values quoted in the results must be considered only as tentative.

The spline approximation curves obtained in the course of this investigation are presented in this handbook in the form of tabulated cubic spline coefficients, determined on an appropriate lattice.

The value of the spline function can be calculated from the equation

$$y(x) = \sum_{k=0}^3 A_k (x-x_j)^k \quad (2.9)$$

where A_0 , A_1 , A_2 and A_3 are the spline curve coefficients corresponding to the j -th knot and x is the value of the argument in the j -th range defined by the condition $x_j \leq x \leq x_{j+1}$.

Depending on which of the four representational forms is used for the spline approximation (linear-linear, linear-log, log-linear or log-log), the evaluated value of $\sigma(E)$ for a given energy E can be calculated for the four respective representational forms by using the following equations:

$$\sigma(E) = \sum_{k=0}^3 A_k (E-E_j)^k \quad (2.10)$$

$$\sigma(E) = \sum_{k=0}^3 A_k \left(\ln \left(\frac{E}{E_j} \right) \right)^k \quad (2.11)$$

$$\ln \sigma(E) = \sum_{k=0}^3 A_k (E-E_j)^k \quad (2.12)$$

$$\ln \sigma(E) = \sum_{k=0}^3 A_k \left(\ln \left(\frac{E}{E_j} \right) \right)^k \quad (2.13)$$

The dependence of the extrapolated cross-section in the low-energy region can be conveniently calculated by the approximation method of non-resonance charged particle interaction described originally by Gamow [7] and by Gurney and Condon [8].

In accordance with these authors, it is convenient to separate the energy dependence of the Coulomb barrier penetration in the form of a factor and to represent the cross-section $\sigma(E)$ as

$$\sigma(E_{c.m.}) = \left(\frac{S(E_{c.m.})}{E_{c.m.}} \right) \exp \left[- \sqrt{\frac{E_g}{E_{c.m.}}} \right] \quad (2.14)$$

where the expression for the kinetic energy is $E_{c.m.} = (m_1/(m_1 + m_2))E$.

Here m_1 and m_2 are the masses of the interacting particles, and E is the energy in the laboratory system of the second particle, where the first particle is at rest.

The Gamow energy E_g is defined by the following equation:

$$E_g = (0.98948 Z_1 Z_2 \sqrt{A})^2 \text{ MeV} \quad (2.15)$$

where Z_1 and Z_2 are the charges of the charged particles in proton charge units, and $A = A_1 \cdot A_2 / (A_1 + A_2)$ is the reduced mass in atomic mass units.

Far from nuclear resonances, the astrophysical factor $S(E_{c.m.})$ is slowly varying as a function of the energy $E_{c.m.}$, and it is convenient to represent it in the form of the power series

$$S(E_{c.m.}) = S(0) + S'(0) \cdot E_{c.m.} + \frac{S''(0) \cdot E_{c.m.}^2}{2} \quad (2.16)$$

where the prime represents differentiation with respect to the energy in the centre of mass system. Both quantities, $S(E_{c.m.})$ and E_g are given in the handbook in the centre of mass system.

It has to be taken into consideration, however, that the evaluated cross-sections obtained from the tabulated spline approximations are generally in the laboratory system.

In a number of cases, such as for the reactions ${}^3\text{H}(d,n){}^4\text{He}$, ${}^2\text{H}(d,n){}^3\text{He}$, ${}^2\text{H}(d,p){}^3\text{He}$, ${}^3\text{H}(t,2n){}^4\text{He}$, ${}^3\text{He}(d,p){}^4\text{He}$ and ${}^3\text{He}(\tau,2p){}^4\text{He}$, the evaluations are presented in the form of S-factors instead of cross-sections, and are expressed as a function of the cross-section by the following relationship:

$$S(E_{\text{CM}}) = \sigma \cdot E_{\text{CM}} \cdot \exp \sqrt{\frac{E_g}{E_{\text{CM}}}} \quad (2.17)$$

The evaluated values of the S-factors can be calculated from the approximate spline function coefficients using the following expression:

$$\ln S(E) = \sum_{k=0}^3 A_k \left(\ln \left(\frac{E}{E_j} \right) \right)^k \quad (2.18)$$

The angular distributions of the differential cross-sections for some of the reactions are given in the form of the following Legendre polynomials:

$$\sigma(\theta, E) = \frac{\sigma(E)}{4\pi} \left(1 + \sum_{k=1}^N B_k \cdot P_k(\cos\theta) \right) \quad (2.19)$$

$$\sigma(\theta, E) = \sigma(0^\circ, E) \cdot \sum_{k=0}^N B_k \cdot P_k(\cos\theta) \quad (2.20)$$

$$\sigma(\theta, E) = \sigma(90^\circ, E) \cdot \sum_{k=0}^N B_k \cdot P_k(\cos\theta) \quad (2.21)$$

3. CROSS-SECTIONS FOR THE INTERACTIONS OF HYDROGEN AND HELIUM ISOTOPES

3.1. Basic data

Hydrogen: atomic number - 1

Stable isotopes:

- protium, atomic mass 1.007825, abundance 99.985%
- deuterium, atomic mass 2.014102, abundance 0.015%

Radioactive isotope:

- tritium, atomic mass 3.016049, $T_{1/2} = 12.26$ years

Protium is the basic element of the Universe; the protium nucleus, the proton, is an elementary particle which, together with the neutron, is a constituent of all nuclei. The coupling of protium and deuterium with oxygen forms water (H_2O) and heavy water (D_2O) respectively. Heavy water is used in nuclear reactors as a moderator of neutrons. Deuterium and tritium are used as fuel in thermonuclear explosive devices. Tritium is used as a radioactive tracer.

Helium: atomic mass - 2

Stable isotopes:

- helium-3, atomic mass 3.016029, abundance 0.000138%
- helium-4, atomic mass 4.002603, abundance 99.999862%

Helium-4 is used in cryogenic technology, as a cooling agent in reactors, in dirigibles, and in breathing mixtures to avoid ill-effects from deep sea diving. Helium-3 is used extensively in nuclear technology.

3.2. The ${}^2\text{H}(p,\gamma){}^3\text{He}$ reaction

This reaction has been studied in the energy range (see Table 3.2) from a few x 10 keV to several tens of MeV. It has been of interest to astrophysicists, to physicists in the study of three-body problems, and this in turn has also led to a better understanding of the mirror reaction ${}^2\text{H}(n,\gamma){}^3\text{H}$.

The ${}^2\text{H}(p,\gamma){}^3\text{He}$ reaction was first investigated by Curran and Strothers [9]. The gamma-ray emission from this reaction is in the form of a single line with an energy of $E_\gamma = (5.49 + 2/3 E_p)$ MeV. Its cross-section grows uniformly with energy. Both the angular distribution (which has a dominant $\sin^2\theta$ term) and the polarization [10] indicate that this reaction is due to a capture process from a 2p state in a continuous spectrum transition to the final 2s state of the helium-3 nucleus with the emission of a gamma ray.

At low energies, with $E_p < 0.03$ MeV, the integral reaction cross-section can be described by equation (2.14) using the following parameters: $E_g = 0.657$ MeV and $S(E_{c.m.}) = (0.146 + 9.12 E_{c.m.}) \cdot 10^{-3}$ MeV·b. In the energy range $E_p = 0.02$ to 20 MeV the integral cross-section can be calculated with the corresponding spline parameters using equation (2.13). The spline coefficients are listed in Table 3.3. A comparison with the experimental data is shown in Fig. 3.1.

3.3. The deuteron break-up in the d + p interaction

The ${}^2\text{H}(p,p+n){}^1\text{H}$ reaction

The ${}^2\text{H}(p,p+n){}^1\text{H}$ reaction was first investigated by Barkas and White [19] at the energy of 5.1 MeV. Interest in this reaction stemmed from the general interest in three-body problems, as well as from the need to assess the contribution of the continuous neutron spectrum for neutron sources based on the d-d and d-t interactions. The data used to evaluate the integral cross-section of this reaction were taken from a number of papers listed in Table 3.4.

There have been no direct measurements of this reaction at proton energies above 10 MeV. The evaluation curve at those energies was constructed on the basis of data from Ref. [25], which contains evaluations obtained from the symmetrical reaction ${}^2\text{H}(n,n+p)n$. Table 3.5 lists the spline coefficients

obtained from the above-mentioned integral cross-section data from the ${}^2\text{H}(p,p+n){}^1\text{H}$ reaction. A comparison of the evaluated data with the experimental data is shown in Fig. 3.2.

3.4. The ${}^2\text{H}(d,\gamma){}^4\text{He}$ reaction

Interest in the ${}^2\text{H}(d,\gamma){}^4\text{He}$ reaction is based on its usefulness in high-temperature plasma diagnostics [26] for fusion research. This reaction, and the reverse reaction ${}^4\text{He}(\gamma,d){}^2\text{H}$, have been studied at high energies by various groups of investigators in order to obtain information on the structure of the ${}^4\text{He}$ nucleus. A brief tabulation of the data used in the construction of the evaluated excitation function of the integral cross-section is given in Table 3.6.

Integral cross-section data for the ${}^2\text{H}(d,\gamma){}^4\text{He}$ reaction compiled in Ref. [28] were used to derive the spline coefficient data given in Table 3.7. (These data were adjusted and corrected on the basis of the original measurements.) This approach was taken primarily because the authors of Ref. [28] had themselves converted most of the data to an integral representation, using for the purpose information obtained directly from the authors of the original work. A comparison of the experimental data with the recommended excitation function of the integral cross-section for the ${}^2\text{H}(d,\gamma){}^4\text{He}$ reaction is given in Fig. 3.3.

Analysis of the angular distribution of the emitted gamma rays indicates that, within the experimental accuracy limits, the data have the following dependence:

$$\sigma(\theta) = A \sin^2\theta \cdot \cos^2\theta$$

which would seem to point to a dominant role of electric quadrupole excitation.

For extrapolation to the low energy range we use Eq. (2.14) with the following parameters: $E_g = 0.98565$ MeV and $S_0(E_{c.m.}) = 3.865 \times 10^{-3}$ MeV·b.

3.5. The ${}^2\text{H}(d,n){}^3\text{He}$ reaction

Table 3.8 lists all of the references used for the evaluation of this reaction.

The form of the excitation function of the total cross-section for all of the ${}^2\text{H} + d$ reaction channels in the vicinity of the threshold of the break-up of the helium-4 compound nucleus into two deuterons is determined by the absence of compound nucleus levels in the vicinity (both above as well as below) of the threshold [54]. In addition, the closest levels have negative parity: this means that their effect on the ${}^2\text{H} + d$ reaction is weakened by the presence of the centrifugal barrier as they cannot be excited by an S-wave in the input channel. Levels located above the threshold are assumed to have an isospin of $T = 1$; and therefore, because of the isospin conservation law, their excitation to the ${}^2\text{H} + d$ channel is forbidden.

Indeed, there are no signs of any resonance characteristics in the excitation functions of the ${}^2\text{H}(d,\gamma){}^4\text{He}$, ${}^2\text{H}(d,p){}^3\text{H}$ and ${}^2\text{H}(d,n){}^3\text{He}$ reactions in the energy range $E_d < 10$ MeV; and phase analysis of d-d elastic scattering also shows the same results [54]. Accordingly, experimental results on the ${}^2\text{H}(d,n){}^3\text{He}$ and ${}^2\text{H}(d,p){}^3\text{H}$ reactions at low energies can be satisfactorily approximated by Gamow's equations, (2.14) and (2.16). However, the use of these equations is unreliable when it comes to extrapolating the cross-sections to lower energies, where experimental data are absent because measured angular distributions for these reactions have revealed significant anisotropy [32, 34] due to an appreciable contribution from partial waves with $l > 0$ in the input channel. The separation of the individual partial cross-sections is not a simple task. At any rate, it is not enough to measure angular distributions to resolve a "clean" P-wave. For this reason, extrapolation of the ${}^2\text{H}(d,n){}^3\text{He}$ and ${}^2\text{H}(d,p){}^3\text{H}$ reaction cross-sections to the low-energy region for which there are no experimental data was

performed by the R-matrix method, whose parameters are based on experimental data which had been subjected to a least-squares analysis. The ${}^2\text{H}(d,n){}^3\text{He}$ reaction cross-sections calculated by this method were then used as a basis for our evaluation in the 0-120 keV energy range. Evaluated data published in Ref. [55] were used in the 0.120-6 MeV, and data from Ref. [33] in the 6 to 20 MeV energy ranges. The evaluation procedure used in this case was the same as in the evaluation of the ${}^3\text{H}(d,n){}^4\text{He}$ reaction. The data from all references were first converted to s-factors. Then, a first-order spline fit approximation was obtained from the data in Refs [33, 55] and the R-matrix calculation results. Then a least-squares analysis was performed to find the spline curve giving the best fit to the experimental data used in the evaluation (allowing for the individual weights assigned to them).

The spline coefficients are listed in Table 3.9.

The excitation function of the total ${}^2\text{H}(d,n){}^3\text{He}$ reaction cross-section, calculated on the basis of these coefficients, is shown in Fig. 3.4. The experimental data used in the evaluation are plotted in the same figure.

3.6. The ${}^2\text{H}(d,p){}^3\text{H}$ reaction

This is a mirror reaction of the ${}^2\text{H}(d,n){}^3\text{He}$ reaction and all properties of their excitation functions are therefore analogous. As in the case of the ${}^2\text{H}(d,n){}^3\text{He}$ reaction, its total cross-section at low energies, i.e. $E_d < 120$ keV, was approximated with the R-matrix formula whose parameters were obtained on the basis of least-squares fitted experimental data [32, 34]. The reaction cross-section calculated in this way was used as a basis for the evaluation in the energy range of 0-120 keV. Evaluated data from Ref. [56] were used in the energy range $E_d > 0.12$ MeV. The results from all references were converted to s-factors. The evaluated data from Ref. [56] and the R-matrix calculation results were used to obtain a first order spline fit curve approximation. A least-squares analysis was then

performed to find the spline curve giving the best fit to the experimental data used in the evaluation (allowing for the individual weights assigned to them).

The data used in the evaluation of this reaction are tabulated in Table 3.10. The total evaluated ${}^2\text{H}(\text{d},\text{p}){}^3\text{H}$ cross-section, and the experimental data used in the evaluation, are plotted in Fig. 3.5. The spline fit coefficients are listed in Table 3.11.

3.7. The ${}^2\text{H}(\text{d},\text{p} + \text{n}){}^2\text{H}$ reaction

Deuteron interaction reactions are important as a source of monoenergetic neutrons, and so it is important to take account of this reaction, which produces a continuous neutron spectrum, above the three-body break-up threshold. The most exhaustive study of the deuteron-deuteron break-up has been published in Ref. [33]. Included in that survey is an evaluation of the differential cross-section of this reaction at an angle of zero degrees; the results of this evaluation are given in Table 3.12.

3.8. The ${}^3\text{H}(\text{p},\gamma){}^4\text{He}$ reaction

The ${}^3\text{H}(\text{p},\gamma){}^4\text{He}$ reaction is often used as a source of monoenergetic gamma rays to investigate photonuclear processes. This reaction is characterized by a high Q-value (19.81 MeV), and a relatively large differential cross-section at an angle $\theta = 90^\circ$. At this angle, the gamma-ray energy can be expressed in the form $E_\gamma = Q + 0.75 E_p$, and the differential cross-section, according to Ref. [63], behaves according to the expression $d\sigma/\Omega(\text{mb}/\text{sr}) = 3.50 E_p$ for $(0.1 < E_p < 2 \text{ MeV})$. Because of the relatively large cross-section of this reaction, it can be used for the diagnostics of low-temperature plasmas containing tritium and hydrogen. Excitation function measurements [63] of the differential cross-section $\sigma(E,90^\circ)$ were taken as a basis for determining the evaluated integral reaction curve. Gamma-ray angular distributions from all references listed in

Table 3.13 were used to obtain values for the integral cross-section. This analysis showed that integral cross-sections could be calculated with an acceptable uncertainty from differential cross-sections at 90° using the expression $\sigma(E) = 4\pi\sigma(E,90^\circ)/1.3$. As the deviation from this relationship for various energy values did not exceed 10%, it was used to calculate values of the integral cross-section from the differential cross-section.

At higher energies, the evaluation of the energy dependence of the ${}^3\text{H}(\text{p},\gamma){}^4\text{He}$ integral cross-section was based on data from Ref. [65] normalized at a proton energy of 4.0 MeV on the basis of data from Ref. [63]. The reliability of the absolute differential cross-section values [65] obtained in this fashion was checked by comparing them with results of absolute measurements [68] which do not deviate from the data of Ref. [63] by more than 5%.

Spline fit coefficients for the excitation function of the ${}^3\text{H}(\text{p},\gamma){}^4\text{He}$ integral reaction cross-section are given in Table 3.14. A comparison of the fitted curve with the experimental data is shown in Fig. 3.6.

3.9. Neutron yield from interactions of protons with tritium nuclei

The ${}^3\text{H}(\text{p},\text{n}){}^3\text{He}$ and ${}^3\text{H}(\text{p},\text{x})\text{n}$ reactions

The ${}^3\text{H}(\text{p},\text{n}){}^3\text{He}$ reaction is widely used as a source of monoenergetic neutrons with energies ranging from 0.6 to 4 MeV.

The cross-sections for this reaction have been compiled in a number of publications [69, 70] and their evaluations performed by a number of authors [33, 55]. Inasmuch as there have been no new evaluations of this reaction since the last evaluation [33], our determination of the evaluated curve for the energy range of interest to us (10–20 MeV) is based on the evaluated data of Ref. [55] ($E_p = 1.2$ to 10 MeV) and Ref. [33] ($E_p = 6$ –17 MeV). In matching these evaluations we have relied on the uncertainties quoted by the

respective authors: 5% for the data from Ref. [55] and 2% for the data from Ref. [33]. The spline fit coefficients for the description of the excitation function for the integral ${}^3\text{H}(p,n){}^3\text{He}$ reaction cross-section are given in Table 3.15, and Fig. 3.7 compares the most representative experimental data from Refs [3, 71-76], with the evaluated curve.

The neutron angular distribution for this reaction in the centre of mass system can be obtained from the expression

$$\sigma(\theta, E) = \sigma(0^\circ, E) \cdot \sum_{k=0}^4 B_k \cdot P_k(\cos\theta)$$

using the evaluated differential cross-sections at 0° (Table 3.16) and the corresponding Legendre coefficients given in Table 3.17. In the expansion given in equation 2.18, only the first five Legendre coefficients are taken into account; inclusion of higher order coefficients leads to changes in the differential cross-section in the $2 < E_p < 10$ MeV energy range which fall within the uncertainty limits of 1% to 3%. At higher energies, as implied by the data from Ref. [33], the omission of higher order coefficients may increase the uncertainty of the differential cross-sections to about 5%-7%.

For proton energies larger than 8.35 MeV there may be production of neutrons due to the three-body break-up of the ${}^3\text{H}(p, n + p){}^2\text{H}$ reaction ($Q = -6.258$ MeV); then, beyond $E_p = 11.32$ MeV, there is an additional source of continuous spectrum neutrons from the ${}^3\text{H}(p, 2n){}^1\text{H}$ reaction, which has a Q-value of -8.482 MeV. For neutron sources, the number of such background neutrons at 0° is of particular interest. This problem is thoroughly investigated in Refs [33] and [77]. Mean values of the differential spectral neutron production cross-sections from Refs [33] and [77] are given in Table 3.18.

3.10. The ${}^3\text{H}(d, \gamma){}^5\text{He}$ reaction

This reaction has been studied extensively during the last thirty years. The most important references for it are listed in Table 3.19. In early research emphasis was put mainly on obtaining information on the properties of systems which involved $A = 5$ nuclides. More recently [27, 79] there has been increased interest in this reaction because of its possible utilization as a tool in the diagnostics of high-temperature d-t plasmas.

References [27, 79, 81] were taken into consideration in this evaluation because they report on relative gamma-ray and neutron yields. Cross-section values for the ${}^3\text{H}(d, \gamma){}^5\text{He}$ reaction and evaluated cross-section values for the ${}^3\text{H}(d, n){}^4\text{He}$ reaction (see Section 3.11) were obtained from Ref. [80] in order to arrive at the $\sigma(d, \gamma)/\sigma(d, n)$ cross-section ratio.

The reaction cross-section ratio ${}^3\text{H}(d, \gamma){}^5\text{He}/{}^3\text{H}(d, n){}^4\text{He}$ is compared with the experimental data in Fig. 3.8; the parameters of the evaluated curve are given in Table 3.20.

3.11. The ${}^3\text{H}(d, n){}^4\text{He}$ reaction

This reaction, together with the ${}^2\text{H}(d, n){}^3\text{He}$ and the ${}^2\text{H}(d, p){}^3\text{H}$ reactions, has determined the energy and neutron yield characteristics of practically all existing thermonuclear devices. It was investigated extensively in the 50s and 60s in laboratories abroad as well as in the Soviet Union (see Table 3.21).

The accuracy of these cross-section measurements was approximately 5%. However, the importance of these reactions in thermonuclear processes prompted investigators to make even more exact measurements using the most sophisticated contemporary technology. The most significant efforts in the measurement of nuclear data for thermonuclear reactions have been made by research teams in the United States (at the Los Alamos National Laboratory),

in the Federal Republic of Germany and in China. The results of these efforts produced data with accuracies ranging from 1% to 1.5%, which stimulated a review of the existing evaluated data for these reactions.

The behaviour of the excitation function for the total ${}^3\text{H}(d,n){}^4\text{He}$ reaction cross-section at energies below 1 MeV is determined essentially by a strong resonance in the compound helium-5 system with an excitation energy $E_x = 16.76$ MeV, $J^\pi = 3/2^+$ and $T = 1/2$.

The threshold of the ${}^3\text{H}(d,pn){}^3\text{H}$ reaction is at a deuteron energy of $E_d^- = 3.709$ MeV, which corresponds to an excitation energy of the compound system of $E_x = 18.92$ MeV. The next resonance, at $E_d = 5.17$ MeV, has an excitation energy of $E_x = 19.8$ MeV, with $J^\pi = 3/2^+$ or $5/2^+$, and $T = 1/2$. Because of the level structure of the helium-5 nucleus it is possible to obtain a satisfactory description of the ${}^3\text{H}(d,n){}^4\text{He}$ total reaction cross-section for deuteron energies below a few hundred keV using the single level approximation of the R-matrix formalism; this is possible because of the dominant position of the resonance at $E_x = 16.76$ MeV, with $J^\pi = 3/2^+$, in this range of excitation energies. In Ref. [83] this approach was used to evaluate the total cross-section of this reaction in the deuteron energy range between 0 and 250 keV. Satisfied that the data from more recent measurements [35, 82] were in good agreement with that evaluation, we have based the construction of the evaluated spline curve in the 0-200 keV energy range on the R-matrix equation using parameters from Ref. [83]. Evaluated data from Ref. [55] were used in the energy range between 0.2 and 3 MeV, and data from Refs [33, 60] were used in the energy range from 3 to 20 MeV. The data were evaluated in the following manner. First, data from all references were converted to s-factors; then, the first approximation of the spline fit was constructed on the basis of data published in Refs [33, 55, 60, 83]. An improved approximation of the spline fit was then constructed

with the aid of the least-squares method using all experimental data weighted by the accuracy of their measurements. A brief description of all references used in this evaluation is given in Table 3.21. The spline coefficients are tabulated in Table 3.22.

Figure 3.9 shows the calculated excitation function of the ${}^3\text{H}(d,n){}^4\text{He}$ total cross-section and the experimental data points used in this evaluation.

3.12. The ${}^3\text{H}(d,n+p){}^3\text{H}$ and ${}^3\text{H}(d,2n){}^3\text{He}$ reactions

The break-up of the deuteron upon collision with tritium nuclei has been studied in Ref. [20] for energy region $3.75 < E_d < 6.2$ MeV and in Refs [91, 92] for $4.8 < E_d < 11.9$ MeV. Reference [92] gives neutron angular distributions as well as energy distributions at 0° . Whereas according to Ref. [33] the ${}^3\text{H}(d,n){}^4\text{He}$ monochromatic neutron yield at 0° in the energy range $4 < E < 17$ MeV does not deviate significantly from a value of 25 mb/sr, the continuous neutron spectrum varies over the same energy range virtually from 0 to 200 mb/sr [91]. The magnitudes of the continuous neutron spectrum at 4.8 MeV, given in Refs [20] and [91] respectively, differ by a factor of four. Recommended values of the differential cross-sections for the production of neutrons at 0° in the ${}^3\text{H} + d$ interaction, normalized to the data from Ref. [91], are listed in Table 3.23.

3.13. The ${}^3\text{H}(t,2n){}^4\text{He}$ reaction

This reaction occurs in all thermonuclear experiments based on the ${}^3\text{H}(d,n){}^4\text{He}$ reaction. However, it does not contribute appreciably to the energetic or kinetic burning process, because its reaction rate under normal operating conditions is 2 to 3 times lower than the reaction rate of the ${}^3\text{H}(d,n){}^4\text{He}$ reaction.

The primary interest in this reaction lies in the fact that it can be used for plasma diagnostics in various fusion devices - diagnostics relying on

the substantially different temperature dependence of the reaction rates for the ${}^2\text{H}(d,n)$, ${}^3\text{H}(t,2n)$ and ${}^3\text{H}(d,n)$ reactions, which means that spectral differentiation can be used to determine their individual contributions.

The evaluation was based on the R-matrix analysis results published in Ref. [78], after we had ascertained that they were in agreement with subsequent results published in Ref. [93]. The results from Ref. [78] were then converted to s-factors and used in determining the first approximation of the spline function. The spline coefficients, listed in Table 3.25, were then calculated by the least-squares method to fit all of the data listed in Table 3.24. Note that this evaluation was performed in the energy range of $E_t < 2.8$ MeV, where there are experimental data. At energies above 2.8 MeV it was assumed that the s-factors are constant and equal to the value at $E_t = 2.8$ MeV.

The evaluated curve and the experimental points used in this evaluation are plotted in Fig. 3.10.

3.14. The ${}^3\text{H}(\tau,\gamma){}^6\text{Li}$ reaction

This reaction, which describes the fusion of tritium and helium-3 nuclei, was studied primarily in order to obtain information on the cluster-like structure of the low-lying levels of lithium-6. The analysis of the gamma-ray spectra [99, 100] shows that the principal contribution to the gamma-ray production cross-section of this reaction comes from channels corresponding to the ground and first excited states of lithium-6.

The evaluation of the integral cross-sections of the ${}^3\text{H}(\tau,\gamma_0){}^6\text{Li}$ and ${}^3\text{H}(\tau,\gamma_1){}^6\text{Li}$ reactions was obtained with the use of data published in Ref. [101], supplemented by results given in Ref. [99] and [102] after the latter had been normalized to the data from Ref. [101]. Inasmuch as the data used in the evaluation described above were presented for the most part in the form of

excitation functions of the partial differential cross-sections at an angle of 90° , these were converted to integral cross-sections taking into account information on the angular distribution of the gamma rays tabulated in Table 3.26. A comparison of the evaluated excitation functions for the integral ${}^3\text{H}(\tau,\gamma){}^6\text{Li}$ reaction cross-sections with the experimental data is given in Fig. 3.11. The spline curve coefficients are listed in Table 3.27.

3.15. The ${}^3\text{He}(d,\gamma){}^5\text{Li}$ reaction

This reaction has been investigated thoroughly with the objective of obtaining information on the states of the residual lithium-5 nucleus (see Table 3.28). In addition, measurements of this reaction can be utilized for the diagnostics of high-temperature plasmas which contain a mixture of deuterium and helium-3. For this purpose, the cross-section of the ${}^3\text{He}(d,\gamma){}^5\text{Li}$ reaction was measured in the $E = 0.048-0.095$ MeV energy range and the results published in Ref. [27].

The cross-section reaction ratio ${}^3\text{He}(d,\gamma){}^5\text{Li}/{}^3\text{He}(d,p){}^4\text{He}$ measured in Ref. [27] was used to evaluate the ${}^3\text{He}(d,\gamma){}^5\text{Li}$ reaction cross-section with the help of the evaluated ${}^3\text{He}(d,p){}^4\text{He}$ cross-section values quoted in Section 3.16. With the assumption that there are two gamma-ray lines corresponding to the ground and first excited states of the lithium-5 nucleus, respectively, the authors of Ref. [27] concluded from their gamma-ray spectrum analysis that, for the given energy range, the ratios of the two radiative branches of the ${}^3\text{H} + d$ interaction to the proton branch are constant and equal to

$$\frac{\Gamma_{\gamma_0}}{\Gamma_p} = (4.5 \pm 1.2) \cdot 10^{-5} \quad \text{and} \quad \frac{\Gamma_{\gamma_1}}{\Gamma_p} = (8 \pm 3) \cdot 10^{-5}$$

respectively.

Since the data presented in the references are in the form of excitation functions of differential cross-sections at an angle of 90° , the

values for the integral cross-sections were obtained from the following recommended equation [107]:

$$\sigma(E) = \frac{4\pi\sigma(90^\circ, E)}{\left[1 - \frac{B_2}{2B_0}\right]}$$

where B_0 and B_2 are the corresponding coefficients for the Legendre expansion of the angular distribution. The values for the B_2/B_0 ratio are given in Table 3.29.

The evaluated curve was calculated from relative measurements [104] which were normalized to the total gamma-ray yield cross-section at an incoming deuteron energy of $E = 0.575$ MeV given in Ref. [105] ($\sigma(0.575) = 39\mu\text{b}$). Spline coefficients for determining the total integral cross-section of the ${}^3\text{He}(d,\gamma){}^5\text{Li}$ reaction are given in Table 3.30. A comparison of the evaluated curve with the experimental data is shown on Fig. 3.12. A rough estimate of the partial integral cross-sections corresponding to the ground and first excited states of lithium-5 can be made by using the following relationships taken from Refs [27] and [107]:

$$\text{for } E = 0.06 \text{ MeV } \sigma_{\gamma_1}/\sigma_{\gamma_0} = 2$$

$$\text{for } E = 10.0 \text{ MeV } \sigma_{\gamma_1}/\sigma_{\gamma_0} = 0$$

$$\text{for } E = 23.0 \text{ MeV } \sigma_{\gamma_1}/\sigma_{\gamma_0} = 0.8$$

In lower energy regions, it is possible to use the extrapolation equation (2.14) with the following values (in the centre of mass):

$$E_g = 4.726 \text{ MeV}, S(0) = 1.51 \text{ mb}\cdot\text{MeV}, \text{ and } S'(0) = 0.01 \text{ mb}.$$

3.16. The ${}^3\text{He}(d,p){}^4\text{He}$ reaction

Because this is a mirror reaction to the ${}^3\text{H}(d,n){}^4\text{He}$ reaction, most early publications tried to shed some light on these reactions by studying the charge symmetry of nuclear forces on the basis of comparisons of their respective excitation functions. Recent publications show significant disagreement with some of the early work as regards the absolute values of the

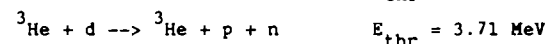
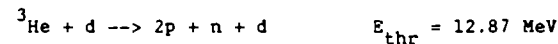
cross-sections and the shape of the excitation functions. The behaviour of the excitation function in the low energy region $E_d < 1$ MeV is determined by the level structure of the compound nucleus of lithium-5, which is analogous to the structure of the mirror nucleus of helium-5 that determines the properties of the ${}^3\text{He}(d,n){}^4\text{He}$ reaction. These circumstances explain the analogous behaviour of the excitation functions brought about by the dominating level $J^\pi = 3/2^+$, $T = 1/2$, $E_x = 16.66$ MeV [108].

The evaluation of this reaction was performed in the same manner as for the ${}^3\text{H}(d,n){}^4\text{He}$ reaction, namely with the aid of s-factors.

The first approximation of the spline curve was calculated by using the R-matrix formalism with input parameters based on the fitted experimental data from Refs [34, 109] and [110, 111]. An improved approximation of the spline fit was then constructed with the aid of the least-squares method using all experimental data weighted by the accuracy of their measurements. A brief description of all references used in this evaluation is given in Table 3.31. The spline coefficients are tabulated in Table 3.32, and Figure 3.13 shows the calculated excitation function of the ${}^3\text{He}(d,p){}^4\text{He}$ total cross-section as well as the experimental data points used in this evaluation.

3.17. The break-up of the deuteron upon interaction with helium-3 nuclei The ${}^3\text{He}(d,n+p){}^3\text{He}$ reaction

The interactions of fast deuterons with light nuclei (in particular helium-3 nuclei) give rise to a continuous neutron spectrum as a result of the three-body reaction channels which have substantial cross-sections. The following three neutron producing reaction channels are possible when helium-3 is bombarded with deuterons:

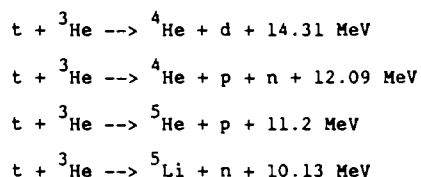


The differential cross-sections for the ${}^3\text{He}(d,n+p){}^3\text{He}$ reaction for an angle of 0° , listed in Table 3.33, are based on the measurements published in Refs [20, 22 and 125]. More complete information on neutron spectra and angular distributions will be found in Ref. [125].

3.18. The interaction of tritium with helium-3 nuclei

The ${}^3\text{He}(t,d){}^4\text{He}$, ${}^3\text{He}(t,n+p){}^4\text{He}$, ${}^3\text{He}(t,p){}^5\text{He}$ and ${}^3\text{He}(t,n){}^5\text{Li}$ reactions

Investigations of the interaction of tritium with helium-3 nuclei for tritium energies ranging from 0.5 to 1.6 MeV have been reported by only a few authors (see Table 3.34). The interaction of tritium and helium-3 can lead to the following four reactions:



The reaction probabilities for all four channels are practically constant over the energy range under consideration [126]; they are 45% for channel 1, 48% for channel 2, and 7% for channels 3 and 4.

The evaluation of the cross-sections for the interaction of tritium with helium-3 nuclei is based on the information from Ref. [126]. The total integral cross-section values for the ${}^3\text{He} + t$ interactions published in that reference are in good agreement with the data from Ref. [127], but disagree considerably with the values given in Ref. [129]. In the evaluation of the cross-section curve, the weights of the cross-sections from Ref. [129] were therefore reduced by a factor of three. The information on the total cross-section of the ${}^3\text{He} + t$ reaction is available only in the narrow energy range of $E_t = 0.1$ to 1.0 MeV. At higher energies, measurements have been made only for individual reaction channels [128]. In particular, results for the ${}^3\text{He}(t,d){}^4\text{He}$ reaction cross-section published in Ref. [128], together

with the reaction channel probability given above, were used in the evaluation of the total cross-section. The experimental data used in the evaluation are compared with the evaluated curve in Fig. 3.14; the spline coefficients are listed in Table 3.35.

3.19. The ${}^3\text{He}(\tau,\gamma){}^6\text{Be}$ reaction

The ${}^3\text{He} + \tau$ radiative capture reaction has been considered as one of the end reactions of the proton-proton cycle. We know of two papers - Refs [132] and [133] - that are devoted to the investigation of this reaction. The first reports measurements of the excitation function of the differential cross-section at an angle of 90° in the energy range $E_{\text{lab}} = 0.86$ - 11.8 MeV; the second extends the measurement of the excitation function to the energy range 12 - 27 MeV, and reports measurements of gamma-ray angular distributions at a number of points of the energy range. Experimental values of the differential cross-section at 90° from the papers mentioned above are tabulated in Table 3.36.

The gamma-ray angular distributions reported in Ref. [133] are symmetrical with reference to 90° in the centre of mass system, and can be represented by a second order Legendre polynomial of the type $W(\theta) = 1 - a_2 \cdot P_2(\cos\theta)$. The Legendre polynomial coefficient a_2 varies between 0.25 and 0.37 in the energy range of $12 < E < 24$ MeV.

3.20. The ${}^3\text{He}(\tau,2p){}^4\text{He}$ reaction

This reaction is primarily of interest to astrophysicists, particularly in their efforts to explain the observed deficit in the flux of solar neutrinos relative to the calculated flux by the presumed existence of a resonance in the cross-section of this reaction at low collision energies of helium-3 nuclei [134, 135]. However, the rather thorough measurements performed by the authors of Ref. [134] have failed to find any indication of a

resonance, and this result seems to be confirmed by measurements of the ${}^3\text{H}(t,2n){}^4\text{He}$ mirror reaction.

The evaluation of this reaction was performed in the following manner. All of the data were first converted to s-factors, then the best approximation of the spline curve was calculated by the least-squares method. A brief description of the references used in the evaluation is given in Table 3.37, the spline coefficients are given in Table 3.38, and the experimental data and the evaluated curve are compared in Fig. 3.15.

3.21. The ${}^3\text{He}(\alpha,\gamma){}^7\text{Be}$ and ${}^3\text{H}(\alpha,\gamma){}^7\text{Li}$ reactions

These two mirror reactions are of interest for both fusion and astrophysics. According to the evaluation by Fowler [139], the first reaction could be an essential mechanism of the energy balance of many stars in particular stages of their evolution. The astrophysical interest in these reactions has stimulated a significant number of measurements of their cross-sections at low energies (see Table 3.39).

Although most measurements have been done in a geometry where the detector is placed at an angle of 90° to the beam, and the particles measured are prompt radiative capture gamma rays, the isotropy of the gamma rays allows for easy conversion of the differential quantities to integral cross-sections. It has been shown [144] that in the ${}^3\text{He}(\alpha,\gamma){}^7\text{Be}$ reaction the branching ratio of the gamma transitions, proceeding through the first excited state of beryllium-7 and directly to the ground state, is equal to $\sigma_1/\sigma_0 = 0.41 \pm 0.02$, and is essentially constant over the energy range $E_{c.m.} = 0.16$ to 1.2 MeV.

A reliable description of the energy dependence of the ${}^3\text{He}(\alpha,\gamma){}^7\text{Be}$ integral reaction cross-section at "stellar" energies (i.e. $E_{c.m.} = 10$ to 20 keV) can be obtained by an extrapolation such as that in Eq. (2.14). The data published in Ref. [143] - normalized to the value $S(0) = 0.575$ keV·b

obtained from an analysis of the data published in Refs [144-146] - were used to determine the energy dependence of the s-factors. In this case the analytical description of the integral cross-section for the reaction ${}^3\text{He}(\alpha,\gamma){}^7\text{Be}$ was obtained from equation (2.14) using the following input parameters: $E_g = 26.82$ MeV, and $S(E_{c.m.}) = (0.575 - 0.44 E_{c.m.} + 0.19 \cdot E_{c.m.}^2)$ MeV·mb for $0 < E_{c.m.} < 1.5$ MeV.

The s-factors for the ${}^3\text{H}(\alpha,\gamma){}^7\text{Li}$ reaction were taken directly from Refs [140] and [147]. Since both reactions had been measured in Ref. [140], it was possible to use the normalization obtained earlier for the ${}^3\text{He}(\alpha,\gamma){}^7\text{Li}$ reaction. At the same time, it was found that the cross-section value for the ${}^3\text{He}(\alpha,\gamma){}^7\text{Be}$ reaction in Ref. [140] was a factor of 1.54 too high. After the renormalization, the ${}^3\text{H}(\alpha,\gamma){}^7\text{Li}$ reaction cross-section values in Refs [140] and [147] differed by a factor of 2 to 4. As a result, only the renormalized values given in Ref. [140] were used in determining of the s-factors for the ${}^3\text{H}(\alpha,\gamma){}^7\text{Li}$ reaction. The parameters that can be used to calculate the s-factors for the integral cross-section of the ${}^3\text{H}(\alpha,\gamma){}^7\text{Li}$ reaction are: $S(0) = 0.100 - 0.31 \cdot E + 0.44 \cdot E^2$ mb·MeV; and $E_x = 6.735$ MeV.

3.22. The ${}^4\text{He}(d,\gamma){}^6\text{Li}$ reaction

This reaction has been studied most extensively in Ref. [148] in connection with astrophysical applications. The data given there for deuteron energies below 3 MeV agree quite well with the direct-capture theoretical calculations, taking into account the resonance at $E_d = 1.07$ MeV for $E_x({}^6\text{Li}) = 2.185$ MeV.

The approximate curve shown in Fig. 3.16 is based on the experimental data given in Ref. [148] as well as on theoretical calculations. For practical applications, the following analytical expression is recommended to obtain an approximation of the excitation function for the ${}^4\text{He}(d,\gamma){}^6\text{Li}$ reaction

$$\sigma(E_{CM}) = \left[10.05 - 20.18 E_{CM} + 52.54 E_{CM}^2 + \frac{0.1811}{(0.711 - E_{CM})^2 + 173 \cdot 10^{-6}} \right] \cdot \phi$$

where

$$\phi = \frac{\exp\left[-\sqrt{\frac{5.22}{E_{CM}}}\right]}{E_{CM}}$$

where $E_{c.m.}$ is the reaction energy in MeV and $\sigma(E_{c.m.})$ is the integral cross-section in units of 10^{-6} mb. The uncertainty in the cross-section varies from 30% at $E_{c.m.} = 0.1$ MeV to 15% at $E_{c.m.} = 0.992$ MeV.

For centre-of-mass energies larger than 0.992 MeV, the following expression can be used to describe the integral ${}^4\text{He}(d,\gamma){}^6\text{Li}$ reaction cross-section in the range $0.922 < E_{c.m.} < 9$ MeV:

$$\sigma(E_{CM}) = \exp[1.498 + 1.674 A + 0.408 A^2 - 0.3 A^3]$$

where

$$A = \ln\left[\frac{E_{CM}}{0.922}\right]$$

Table 3.1

Energy characteristics of interaction channels for hydrogen and helium isotopes

Input channel	Output channel	Energy, MeV	Reaction product decay	Decay energy, MeV
${}^2\text{H}+p$	${}^3\text{He}+\gamma$	5,494	-	-
${}^2\text{H}+p$	$2p+n$	-2,225	-	-
${}^2\text{H}+d$	${}^4\text{He}+\gamma$	23,847	-	-
${}^2\text{H}+d$	${}^3\text{He}+n$	3,269	-	-
${}^2\text{H}+d$	$t+p$	4,033	$t(\beta){}^3\text{He}$	0,0186
${}^2\text{H}+d$	$d+p+n$	-2,225	-	-
${}^2\text{H}+d$	$2p+2n$	-4,449	-	-
${}^3\text{H}+p$	${}^4\text{He}+\gamma$	19,814	-	-
${}^3\text{H}+p$	${}^3\text{He}+n$	-0,764	-	-
${}^3\text{H}+d$	${}^5\text{He}+\gamma$	16,700	${}^5\text{He}-{}^4\text{He}+n$	0,89
${}^3\text{H}+d$	${}^4\text{He}+n$	17,589	-	-
${}^3\text{H}+d$	$t+p+n$	-2,225	$t(\beta){}^3\text{He}$	0,0186
${}^3\text{H}+d$	${}^3\text{He}+2n$	-2,988	-	-
${}^3\text{H}+t$	${}^6\text{He}+\gamma$	12,308	${}^6\text{He}(\beta){}^6\text{Li}$	3,507
${}^3\text{H}+t$	${}^5\text{He}+n$	10,44	${}^5\text{He}-{}^4\text{He}+n$	0,89
${}^3\text{H}+t$	${}^4\text{He}+2n$	11,332	-	-
${}^3\text{He}+d$	${}^5\text{Li}+\gamma$	16,39	${}^5\text{Li}-p+{}^4\text{He}$	1,96
${}^3\text{He}+d$	${}^4\text{He}+p$	18,353	-	-
${}^3\text{He}+d$	${}^3\text{He}+p+n$	-2,225	-	-
${}^3\text{He}+d$	$t+2p$	-1,461	$t(\beta){}^3\text{He}$	0,0186
${}^3\text{He}+t$	${}^6\text{Li}+\gamma$	15,796	-	-
${}^3\text{He}+t$	${}^4\text{He}+d$	14,321	-	-
${}^3\text{He}+t$	${}^4\text{He}+p+n$	12,096	-	-
${}^3\text{He}+t$	${}^5\text{Li}+n$	10,13	${}^5\text{Li}-p+{}^4\text{He}$	1,96
${}^3\text{He}+t$	${}^5\text{He}+p$	11,21	${}^5\text{He}-n+{}^4\text{He}$	0,89
${}^4\text{He}+t$	${}^7\text{Li}+\gamma$	2,468	-	-
${}^4\text{He}+t$	${}^6\text{Li}+n$	-4,782	-	-
${}^3\text{He}+\tau$	${}^6\text{Be}+\gamma$	11,489	${}^6\text{Be}-{}^4\text{He}+2p$	1,371
${}^3\text{He}+\tau$	${}^4\text{He}+2p$	12,860	-	-
${}^3\text{He}+\tau$	${}^5\text{Li}+p$	10,90	${}^5\text{Li}-p+{}^4\text{He}$	-
${}^4\text{He}+\tau$	${}^7\text{Be}+\gamma$	1,5876	${}^7\text{Be}(\beta){}^7\text{Li}$	0,862
${}^4\text{He}+d$	${}^6\text{Li}+\gamma$	1,4753	-	-

Table 3.2

Brief data content of references used in the evaluation of the ${}^2\text{H}(p,\gamma){}^3\text{He}$ reaction cross-section

Energy range, MeV	Range of angles, deg.	Type of data	Uncertainty, %		Ref.
			random	system.	
0,024-0,048	0; 90	EXC,DA	10	15	[1]
0,275-1,750	0;45;90;135	EXC,DA	10	12	[12]
2,5-3,7	90	EXC,DA	3	-	[13]
5,0-8,0	90	EXC,DA	3	10	[14]
9,9-22,6	10-170	AND,DA	10	14	[15]
- 16	32-152	AND,DA	1	3	[16]
6,5-16,0	32-152	AND,DA	1	-	[17]
9,9; 14,8	5-175	AND,DA	2	7	[18]

Table 3.3

Spline fit coefficients for the description of the ${}^2\text{H}(p,\gamma){}^3\text{He}$ integral reaction cross-section (The cross-section can be calculated using equation (2.13))

Knot No.	Knot energy, MeV	Spline fit coefficients				Cross-section uncert., %
		λ_0	λ_1	λ_2	λ_3	
1	0,024	-10,390	2,693	-1,382	0,5683	23,34
2	0,0502	- 8,927	1,582	-0,123	-0,0028	17,77
3	22,6	- 4,494	0	0	0	6,941

Table 3.4

Brief data content of references used in the evaluation of the ${}^2\text{H}(p,p+n){}^1\text{H}$ reaction cross-section

Energy range, MeV	Range of angles, deg.	Type of data	Uncertainty, %		Ref.
			random	system.	
3,47-5,51	0	EXC,DA	2	30	[20]
3,40-5,55	4 π	EXC,SIG	4	12	[21]
8,6	0	DA	10	10	[22]
6,5	4 π	SIG	15	15	[23]
9,0	20-152	AND,DA	6	6	[24]

Table 3.5

Spline fit coefficients for the description of the ${}^2\text{H}(p,p+n){}^1\text{H}$ integral reaction cross-section (The cross-section can be calculated using equation (2.13))

Knot No.	Knot energy, MeV	Spline fit coefficients				Cross-section uncert., %
		λ_0	λ_1	λ_2	λ_3	
1	3,4	-4,657	93,36	-554,5	1291,4	10
2	3,897	1,038	14,17	-26,02	19,72	4
3	5,896	3,847	2,773	-1,514	0,171	4
4	39,85	4,815	0	0	0	5

Table 3.6

Brief data content of references used in the evaluation of the ${}^2\text{H}(d,\gamma){}^4\text{He}$ reaction cross-section

Energy range, MeV	Range of angles, deg.	Type of data	Uncertainty, %		Ref.
			random	system.	
0,05 -20	-	EXC,TTY	15	30	[27]
0,7-4,5	130	EXC,DA	5	15	[28]
1,4;2;10; 15	45 - 135	AND,DA	5	15	[28]
6-19	135	EXC,DA	10	25	[29]
0,8;1,4; 2,2	0; 45;90	DA	30	80	[30]
4-12,5	132	EXC,DA	25	36	[31]
6;9;12	0 - 132	AND,DA	25	36	[31]

Table 3.7

Spline fit coefficients for the description of the ${}^2\text{H}(d,\gamma){}^4\text{He}$ integral reaction cross-section (The cross-section can be calculated using equation (2.13))

Knot No.	Knot energy, MeV	Spline fit coefficients				Cross-section uncert., %
		λ_0	λ_1	λ_2	λ_3	
1	0,026	-16,83	1,550	-0,157	-0,0252	23
2	7,547	- 9,261	0,520	-0,272	-0,682	23
3	18,92	-9,403	-0,520	0	0	10

Table 3.8

Brief data content of references used in the evaluation of the ${}^2\text{H}(d,n){}^3\text{He}$ reaction cross-section

Energy range, MeV	Range of angles, deg.	Type of data	Uncertainty, %		Ref.
			random	system.	
0,02-0,12	45-150	EXC,DA	1	2	[32]
6-17	0-88	EXC,DA	2	1	[33]
0,006-0,325	15-85	EXC,DA	1	6	[34]
0,012-0,16	90	EXC,DA	3	-	[35]
0,25-0,825	0-82	EXC,DA	3	-	[36]
3-6	0	EXC,SIG	2	-	[37]
0,119-0,294	0	EXC,SIG	-	-	[38]
0,1-1	15-60	EXC,DA	3,5	6	[39]
0,02-0,22	0	EXC,SIG	-	20	[40]
0,5-3,5	0-90	EXC,DA	-	-	[41]
2-6,2	25-155	EXC,DA	-	-	[42]
13,2	6-90	AND,DA	-	2	[43]
0,156-0,466	0	EXC,SIG	1	3	[44]
0,0522; 0,0869	20-90	AND,DA	1,4	3	[45]
12,305	10-40	AND,DA	2	0,4	[46]
1-3,5	16-91	AND,DA	-	-	[47]
0,298-0,703	20-160	EXC,DA	6	-	[48]
12-18	20-160	AND,DA	-	-	[49]
5,8-13,8	20-170	EXC,DA	-	-	[50]
5-10	20-90	EXC,DA	3	-	[51]
0,013-0,12	90	EXC,SIG	2	4	[52]
5-12,2	0-90	EXC,DA	3	5	[53]

Table 3.9

Spline fit coefficients for the description of the S-factors for the ${}^2\text{H}(d,n){}^3\text{He}$ reaction (The evaluated total cross-section of the ${}^2\text{H}(d,n){}^3\text{He}$ reaction can be calculated using equations (2.14) and (2.18))

Knot No.	Knot energy, MeV	Spline fit coefficients				S-factor coefficient uncertainty, %
		λ_0	λ_1	λ_2	λ_3	
1	0,005	3,9345	0,022224	0,016557	-0,022414	4,6
2	0,008851	3,9484	0,019206	-0,021842	0,018866	4,7
3	0,42334	4,7875	0,69691	-0,12960	0,026336	3,3
4	4,0875	6,0084	0,51538	0,049548	-0,059482	3,4
5	20,0	6,7136	0	0	0	4,6

Table 3.10

Brief data content of references used in the evaluation of the ${}^2\text{H}(d,p){}^3\text{H}$ reaction cross-section

Energy range, MeV	Range of angles, deg	Type of data	Uncertainty, %		Ref.
			random	system.	
0,298-0,703	20-160	EXC,DA	6	-	[48]
5,8-13,8	20-170	EXC,DA	-	-	[50]
0,013-0,12	4%	EXC,SIG	2	4	[52]
0,02-0,12	45-150	EXC,DA	I	2	[32]
0,006-0,325	15-85	EXC,DA	I	6	[34]
0,012-0,16	90	EXC,DA	3	-	[35]
3-II,5	30-170	EXC,DA	1,5	3	[57]
0,08-I,07	0-140	EXC,DA	2,5	3	[39]
0,2-I,77	10-90	EXC,DA	2	5	[58]
0,2-0,5	80-170	EXC,DA	-	-	[59]
I-3	30-170	EXC,DA	I	2	[60]
I2,305	2I-146	AMD,DA	I	0,43	[61]
I-3,5	II-85	AMD,DA	-	-	[47]
0,052-0,087	20-90	AMD,DA	I,4	3	[45]
0,156-0,466	90	EXC,SIG	I	3	[44]
13,2	6-90	AMD,DA	-	2	[43]
10,3	I4-I76	AMD,DA	-	5	[62]

Table 3.11

Spline fit coefficients for the description of the S-factors for the ${}^2\text{H}(d,p){}^3\text{H}$ reaction (The evaluated total cross-section of the ${}^2\text{H}(d,p){}^3\text{H}$ reaction can be calculated using equations (2.14) and (2.18))

Knot No.	Knot energy, MeV	Spline fit coefficients				S-factor coefficient uncertainty, %
		A_0	A_1	A_2	A_3	
1	0,005	3,9658	0,059150	-0,063862	0,01892	4,3
2	0,16002	4,1914	0,29829	0,13286	-0,031631	4,5
3	0,64162	4,7771	0,48429	0,22627	-0,10071	3,7
4	1,3855	5,2381	0,65362	-0,006308	-0,011246	3,2
5	14,0	6,5770	0	0	0	5,5

Table 3.12

Differential cross-section at 0° for the ${}^2\text{H}(d,p+n){}^2\text{H}$ reaction in the laboratory system

Energy, MeV	Cross section, mb/sr	Energy, MeV	Cross section, mb/sr
5,0	0,8	8,0	50
5,25	1,6	9,0	80
5,50	3,4	10,0	120
6,0	8,5	11,0	160
6,5	16,0	14,0	230
7,0	27,0	17,0	290
7,5	40,0	20,0	300

Table 3.13

Brief data content of references used in the evaluation of the ${}^3\text{H}(p,\gamma){}^4\text{He}$ integral reaction cross-section

Energy range, MeV	Range of angles, deg	Type of data	Uncertainty, %		Ref.
			random	system.	
0,46-0,93	0-135	AMD,DA	5	-	[64]
0,I-6,2	90	EXC,DA	5	10	[63]
2; 3,4;4;5,6	15-160	AMD,DA	5	10	[63]
3-18	90	EXC,DA	10	-	[65]
4-II	45; 90; 135	EXC,DA	3	10	[66]
4-II	0-135	AMD,DA	3	10	[66]
5,8-9,2	90	EXC,DA	5	15	[67]
8;3;13,6	90	DA	3	7	[68]

Table 3.14

Spline fit coefficients for approximating the excitation function of the ${}^3\text{H}(p,\gamma){}^4\text{He}$ integral reaction cross-section (The cross-section can be calculated using equation (2.13))

Knot No.	Knot energy, MeV	Spline fit coefficients				Cross section uncertainty, %
		A_0	A_1	A_2	A_3	
1	0,100	-5,686	0,9610	0,0316	-0,0054	6
2	2,030	-2,655	1,003	-0,9736	0,2801	4
3	6,599	-2,367	-0,1244	0,0123	-1017,0	3
4	6,602	-2,367	-0,1249	-1,149	0,6480	3
5	17,80	-2,988	0	0	0	4

Table 3.15

Spline fit coefficients for the description of the ${}^3\text{H}(p,n){}^3\text{He}$ integral reaction cross-section (The cross-section can be calculated using equation (2.11))

Knot No.	Knot energy, MeV	Spline fit coefficients				Cross section uncertainty, mb
		A_0	A_1	A_2	A_3	
1	1,2000	218,09	332,92	243,69	-143,73	I4
2	2,2000	477,40	469,92	-598,58	-286,86	I5
3	2,9665	556,73	35,174	-855,82	-208,97	20
4	4,0000	485,19	-532,48	232,46	-2,6394	I5
5	5,9817	308,40	-346,70	229,27	-30,195	I0
6	8,9442	204,06	-176,87	192,82	-250,30	8
7	13,375	147,80	-143,26	-109,31	316,91	7
8	19,999	93,109	0	0	0	I0

Table 3.16

Spline fit coefficients for the description of the excitation function of the ${}^3\text{H}(p,n){}^3\text{He}$ differential cross-section at 0° in the center-of-mass system. The energy is given in the laboratory system. (The cross-section can be calculated using equation (2.11))

Knot No.	Knot energy, MeV	Spline fit coefficients				Cross section uncertainty, mb
		A_0	A_2	A_3	A_4	
1	1,2000	16,2	16,832	4,5464	51,644	3,2
2	1,3802	18,786	21,137	26,222	-45,529	2,7
3	1,5874	22,131	25,801	7,1131	130,53	2,5
4	1,8258	26,237	35,456	61,899	154,69	2,4
5	2,1000	32,833	61,859	316,34	-835,01	2,0
6	2,6086	52,610	81,246	-226,94	38,497	1,7
7	3,2404	59,948	-11,759	-201,90	239,84	2,6
8	4,0253	50,348	-65,489	-45,853	174,25	2,6
9	5,0000	35,766	-60,791	4,6181	72,214	1,5
10	6,5976	20,805	-41,577	64,604	3,1471	1,1
11	8,7059	14,317	-4,9826	67,301	-52,261	0,9
12	11,487	16,996	20,285	23,832	-55,698	1,3
13	15,158	23,265	20,655	-22,497	15,536	1,2
14	19,999	27,593	0	0	0	2,1

Table 3.17

Spline fit coefficients for the description of the energy dependence of the Legendre polynomial coefficients for determining the ${}^3\text{H}(p,n){}^3\text{He}$ differential cross-section in the center-of-mass system.
(The Legendre coefficients can be calculated using equation (2.11))
Energy is given in the laboratory system.

Legendre coeff. No.	Knot No.	Knot energy, MeV	Spline fit coefficients				Legendre coeff. uncert., mb
			A_0	A_1	A_2	A_3	
B_0	I	1,2000	1,0560	1,1943	-8,6483	30,858	0,10
	2	1,3240	1,1257	0,3935	0,8096	-10,414	0,10
	3	1,4720	1,1582	0,2328	-2,3822	12,130	0,10
	4	1,6304	1,1701	0,1259	1,3357	-15,958	0,09
	5	1,8217	1,1798	-0,1008	-3,5554	10,854	0,08
	6	2,0000	1,1440	-0,4875	-7,4251	17,014	0,07
	7	2,5317	0,8394	-1,1518	4,6068	-6,3717	0,05
	8	3,2046	0,7404	-0,0421	0,1008	1,3432	0,08
	9	4,0564	0,7536	0,2294	1,0507	-0,7536	0,05
	10	5,1351	0,8562	0,5991	0,5178	1,2708	0,04
	11	6,4999	1,0429	1,0551	-1,2023	-3,7240	0,03
	12	8,6089	1,1618	-0,5026	-4,3414	5,8283	0,05
	13	11,402	0,8071	-1,5619	0,5715	1,3967	0,04
	14	15,100	0,4443	-0,9099	1,7488	-2,5736	0,04
	15	19,999	0,2696	0	0	0	0,08
B_1	I	1,2000	-0,0761	-1,8985	1,2298	0,1937	0,06
	2	1,6613	-0,5569	-1,0369	1,4188	4,6813	0,03
	3	2,3000	-0,5829	1,3722	-5,0372	6,9575	0,03
	4	2,6864	-0,4652	0,3111	-1,7956	2,1396	0,04
	5	3,1377	-0,4522	-0,0918	-0,7987	0,0030	0,06
	6	3,6649	-0,4857	-0,3397	-0,7973	1,6468	0,06
	7	4,2806	-0,5515	-0,4682	-0,0301	-4,2353	0,06
	8	4,9998	-0,6408	-0,7840	1,9028	-7,8473	0,04
	9	5,8538	-0,7479	-0,7693	-1,8096	9,3658	0,03
	10	6,8538	-0,8775	-0,6414	2,6211	5,5210	0,03
	11	8,0245	-0,8918	0,5972	5,2330	-6,1889	0,03
	12	9,3952	-0,6918	1,7858	2,3051	-11,406	0,03
	13	11,000	-0,3976	1,6619	-1,1188	-0,4532	0,04
	14	14,832	-0,0129	0,8726	-1,5252	1,4893	0,03
	15	19,999	0,1511	0	0	0	0,05
B_2	I	1,2000	0,0132	1,3331	-0,6814	0,1008	0,07
	2	2,1909	0,5908	0,6223	-0,4993	0,5778	0,03
	3	4,0000	0,9105	0,6493	-0,1973	2,8578	0,07
	4	4,5594	0,9986	0,7446	0,9249	-3,4865	0,07
	5	5,1971	1,1040	0,8075	-0,4442	4,4154	0,05
	6	5,9239	1,2120	0,9182	1,2897	-12,595	0,05

Table 3.17 (continued)

Legendre coeff. No.	Knot No.	Knot energy, MeV	Spline fit coefficients				Legendre coeff. uncert., mb
			A_0	A_1	A_2	A_3	
B_2	7	6,7524	1,3261	0,6084	-3,6564	-8,9995	0,05
	8	7,6968	1,3229	-0,8115	-7,1905	11,752	0,04
	9	8,7732	1,1198	-2,0899	-2,5757	8,4497	0,04
	10	10,000	0,8211	-2,3298	3,2729	-1,6673	0,04
	11	14,143	0,3373	-0,6620	1,5394	-1,5011	0,04
	12	19,999	0,2303	0	0	0	0,08
B_3	I	2,1000	-0,0036	-0,0687	-0,0124	-0,4133	0,03
	2	3,2404	-0,0695	-0,3127	-0,5502	-0,6592	0,03
	3	4,9998	-0,3624	-1,1621	-1,0658	-1,8624	0,02
	4	6,0527	-0,6364	-1,7734	-2,1335	13,262	0,02
	5	7,3272	-0,9607	-1,1359	5,4696	-0,7794	0,02
	6	8,8702	-0,9835	0,8692	5,0227	-8,6870	0,02
	7	10,738	-0,6946	1,8372	0,0424	-1,7808	0,03
	8	12,999	-0,3543	1,6583	-3,1961	3,5751	0,03
	9	16,124	-0,1097	0,7790	-0,8860	0,7018	0,05
	10	19,999	0,0240	0	0	0	0,06
B_4	I	4,0000	0,0439	0,2760	-0,4665	2,1075	0,04
	2	5,3666	0,1382	0,5479	1,3916	-1,3451	0,02
	3	7,2001	0,3852	1,0173	0,6562	-5,5636	0,02
	4	8,8322	0,5730	0,5886	-2,7543	1,3654	0,02
	5	10,834	0,5900	-0,3659	-1,9173	3,4695	0,03
	6	13,291	0,4647	-0,7149	0,2095	0,5983	0,03
	7	16,304	0,3325	-0,5543	0,5763	-1,0375	0,04
	8	19,999	0,2345	0	0	0	0,05

Note: The differential cross-section of the ${}^3\text{H}(p,n){}^3\text{He}$ reaction in the centre-of-mass system can be calculated using equation (2.20).

Table 3.18

Differential cross-sections at 0° for the production of a continuous neutron spectrum in the laboratory system in p-t reactions

E_p , MeV	Continuous spectrum	Two-particle channel
	$\sigma(E,0^\circ)$, mb/sr	
9,77	11,4 \pm 0,8	41,5
10,77	0,91 \pm 0,2	27,0
11,77	2,2 \pm 0,1	29,2
12,77	4,1 \pm 0,4	32,1
13,77	5,4 \pm 0,4	35,3
14,77	8,2 \pm 0,4	38,4

Table 3.19

Brief data content of references used in the evaluation of the ${}^3\text{H}(d,\gamma){}^3\text{He}/{}^3\text{H}(d,n){}^3\text{He}$ integral reaction cross-sections ratio

Energy range, MeV	Type of data	Uncertainty, %		Ref.
		random	system.	
0,04-0,15	$\text{TTY}(d,\gamma)/\text{TTY}(d,n)$	3	7	[27]
0,14-0,62	$\text{TTY}(d,\gamma)/\text{TTY}(d,n)$	4	12	[79]
0,16-1,4	$\text{TTY}(d,\gamma)$	5	30	[80]
2,0-5,0	$\text{TTY}(d,\gamma)/\text{TTY}(d,n)$	-	-	[27]
0,025-0,1	σ_p/σ_n	-	30	[81]

Table 3.20

Spline fit coefficients for approximating the ${}^3\text{H}(d,\gamma){}^3\text{He}/{}^3\text{H}(d,n){}^3\text{He}$ cross-section ratios
(The ratios can be calculated using equation (2.11))

Knot No.	Knot energy, MeV	Spline fit coefficients ($\times 10^{-5}$)				Ratio uncert.
		A_0	A_1	A_2	A_3	
1	0,042	5,452	0,4267	-1,296	0,6385	0,85
2	5,0	47,6	0	0	0	1,2

Table 3.21

Brief data content of references used in the evaluation of the ${}^3\text{H}(d,n){}^4\text{He}$ reaction cross-section

Energy range, MeV	Range of angles, deg	Type of data	Uncertainty, %		Ref.
			random	system.	
0,08-0,116	45-150	EXC, DA	I	I,3	[82]
0,08-0,078	45-150	EXC, DA	I	I,4	[83]
7-16,5	0-132	EXC, DA	I,5	2	[33]
0,014-0,114	90	EXC, DA	5	-	[35]
5-15,7	0-140	EXC, DA	3	4	[84]
0,019-0,12	90	EXC, DA	2	4	[52]
0,025-0,225	-	EXC, SIG	-	-	[40]
I,5-6	0-150	EXC, DA	3	10	[85]
8-16	0-145	EXC, SIG	6,5	-	[86]
0,048-0,73	-	EXC, SIG	5	5	[87]
I	10-140	AND, DA	-	3	[88]
0,5-7	0-165	EXC, DA	3,5	5	[89]
0,053-0,8	-	EXC, SIG	-	8	[90]

Table 3.22

Spline fit coefficients for the description of the S-factors for the ${}^3\text{H}(d,n){}^4\text{He}$ reaction (The evaluated total cross-section of this reaction can be calculated using equations (2.14) and (2.18))

Knot No.	Knot energy, MeV	Spline fit coefficients				S-factor coeffic. uncert., %
		Λ_0	Λ_1	Λ_2	Λ_3	
I	0,005	2,5038	0,021225	0,036332	0,025539	1,98
2	0,069024	3,2719	0,73991	-2,6114	0,65548	1,37
3	0,18022	2,1561	-2,4613	0,597705	-0,046018	1,41
4	1,9177	-0,93401	-0,40958	0,27059	0,45441	3,23
5	4,0943	-0,89073	0,78512	-1,1275	0,50776	4,36
6	10,104	-0,72726	0,008837	0,24856	-0,11710	3,34
7	19,000	-0,66320	0	0	0	4,92

Table 3.23

Differential cross-section at 0° for the production of a continuous neutron spectrum in the laboratory system in a ${}^3\text{H}+d$ reaction

Energy, MeV	Cross section, mb/sr	Energy, MeV	Cross section, mb/sr
3,75	0,7	6,84	165
4,03	7,2	7,38	175
4,30	24	7,83	200
4,58	45	8,33	160
4,82	72	8,83	150
5,08	90	9,81	165
5,37	108	10,89	180
5,64	120	11,89	200
6,32	130	-	-

Table 3.24

Brief data content of references used in the evaluation of the ${}^3\text{H}(t,2n){}^4\text{He}$ reaction cross-section

Energy range, MeV	Range of angles, deg	Type of data	Uncertainty, %		Ref.
			random	system.	
0,076-0,116	20-160	EXC, DA	6	5	[32]
0,04-0,2	0	EXC, SIG	-	15	[94]
0,031-0,155	0-150	EXC, DA	8	10	[95]
0,95-2,1	30-120	EXC, DA	7	7	[93]
0,06-1,14	45	EXC, SIG	10	5	[96]
0,2-1	90	EXC, SIG	-	20	[97]
0,04-2,2	0	EXC, SIG	15	10	[98]

Table 3.25

Spline fit coefficients for the description of the S-factors for the ${}^3\text{H}(t,2n){}^4\text{He}$ reaction (The evaluated total cross-section of this reaction can be calculated using equations (2.14) and (2.18))

Knot No.	Knot energy, MeV	Spline fit coefficients				S-factor coeffic. uncert., %
		Λ_0	Λ_1	Λ_2	Λ_3	
I	0,01	182,15	-5,6435	6,3212	-2,6523	6,5
2	0,068957	175,72	-10,899	-9,0427	6,2428	5,86
3	0,37559	161,67	12,255	22,703	47,985	5,75
4	1,6255	379,25	387,76	425,84	-175,19	5,6
5	2,680	460,61	-10,706	50,478	-69,506	5,3
6	4,0	459,95	0	0	0	9,3

Table 3.26

Gamma ray angular distribution $W(\theta)$ for the ${}^3\text{H}(t,\gamma){}^6\text{Li}$ reaction

Channel	E_γ , MeV	$W(\theta) = 1 + \sum_{\mu=1}^2 a_\mu P_\mu(\cos\theta)$	Ref.
γ_0	2,7	$1 - (I \pm 0, I) P_2$	[99]
	13,1	$1 + (0,16 \pm 0,03) P_1 - (0,9 \pm 0,1) P_2$	[100]
	21,7	$1 - (1,07 \pm 0,07) P_2$	[100]
γ_1	13,1	$1 - (0,14 \pm 0,05) P_1 + (0,41 \pm 0,07) P_2$	[100]
	21,7	$1 - (0,11 \pm 0,02) P_1 - (0,28 \pm 0,04) P_2$	[100]

Table 3.27

Spline fit coefficients for the description of the ${}^3\text{H}(t,\gamma){}^6\text{Li}$ and ${}^3\text{H}(t,\gamma_1){}^6\text{Li}$ integral partial cross-section (The cross-sections can be calculated using equation (2.13))

Knot Channel	Knot No.	Energy, MeV	Spline fit coefficients				Spline curve uncert., %
			Λ_0	Λ_1	Λ_2	Λ_3	
γ_0	I	0,4444	-7,704	1,196	0,6031	-0,2108	12
	2	11,051	-4,628	-1,458	-1,429	3,035	5
	3	20,000	-5,362	0	0	0	12
γ_1	I	0,510	-6,853	0,715	1,446	-0,494	20
	2	4,798	-3,554	-0,2555	-1,879	157,48	7
	3	5,139	-3,529	1,721	3,450	-4,335	8
	4	12,83	-2,386	0	0	0	7

Table 3.28

Brief data content of references used in the evaluation of the ${}^3\text{He}(d,\gamma){}^5\text{Li}$ integral reaction cross-section

Energy range, MeV	Range of angles, deg	Type of data	Uncertainty, %		Ref.
			random	system.	
0,05-0,100	135	$\sigma_{\text{tot}}/\sigma_{\text{p}}; \gamma_0, \gamma_1$	15	30	[27]
0,12-4,6	90	EXC, DA; γ_0, γ_1	12	30	[103]
0,17-2,4	90	EXC, DA; γ_0, γ_1	10	-	[104]
0,2-1,2	90	EXC, DA; γ_0	7	20	[105]
2,5-8,0	30; 130	EXC, DA; γ_0, γ_1	10	40	[106]
-	0-143	AND, DA; γ_0, γ_1	10	40	[106]
I,13-16,8	90	EXC, DA; γ_0, γ_1	8	15	[107]
-	0-140	AND; γ_0, γ_1	8	15	[107]

Table 3.29

Values of the B_2/B_0 ratio for the description of the angular distribution of gamma rays emitted from the ${}^3\text{He}(d,\gamma){}^5\text{Li}$ reaction

$E({}^5\text{Li})$ MeV	18.1	19.5	20.7	23.2	25.7
B_2/B_0	0.03/0.1	0.14/0.08	-0.11/0.07	-0.37/10.06	-0.53/0.16

Table 3.30

Spline fit coefficients for the description of the ${}^3\text{He}(d,\gamma){}^5\text{Li}$ total integral reaction cross-section

(The cross-section can be calculated using equation (2.13))

Knot No.	Energy, MeV	Spline fit coefficients				Cross-section uncer., %
		A_0	A_1	A_2	A_3	
1	0,048	-8,855	3,198	I,214	-I,011	I4
2	0,1700	-4,533	I,72I	0,1193	-0,6098	6
3	0,4646	-3,30I	0,1114	-I,720	I,311	4
4	I,270	-3,596	0,6287	-0,7712	0,3639	3
5	4,724	-3,276	0,4864	0,6629	-0,7017	3
6	7,722	-2,960	0,6297	-3,714	3,467	3
7	II,39	-3,073	-0,6864	0,3282	I,619	3
8	16,80	-3,195	0	0	0	7

Table 3.31

Brief data content of references used in the evaluation of the ${}^3\text{He}(d,p){}^4\text{He}$ reaction cross-section

Energy range, MeV	Range of angles, deg	Type of data	Uncertainty, %		Ref.
			random	system.	
0,012-0,3	30-160	EXC, DA	I	6	[34]
14,6-39,9	10-165	EXC, DA	I	10	[112]
0,38-0,58	16,3	EXC, SIG	-	10	[113]
0,1-1,5	90	EXC, SIG	-	5	[114]
0,26-3,56	18-150	EXC, DA	-	7	[115]
10,215-160	15-160	AND, DA	5	-	[116]
2,23-13	20-170	EXC, DA	2	-	[110]
0,2-1,5	0-90	EXC, DA	2	3,5	[117]
0,029-0,044	48-128	EXC, DA	-	10	[118]
0,036-0,093	90	EXC, DA	2	4	[52]
10-18	15-45	EXC, DA	-	5	[119]
3-10	30-150	EXC, DA	-	-	[111]

Table 3.31 (cont.)

Energy range, MeV	Range of angles, deg	Type of data	Uncertainty, %		Ref.
			random	system.	
5,9-13,7	12-170	AND, DA	-	5	[120]
10	130-170	AND, DA	2,5	0,33	[61]
2,8-II,5	30-160	EXC, DA	I	3	[121]
0,2-2,15	-	EXC, SIG	-	5	[109]
0,1-0,8	0-140	EXC, DA	2	6	[122]
0,387-1,46	90	EXC, SIG	3	5	[123]
17-44	5-175	EXC, DA	-	3	[124]

Table 3.32

Spline fit coefficients for the description of the S-factors for the ${}^3\text{He}(d,p){}^4\text{He}$ reaction (The evaluated total cross-section of this reaction can be calculated using equations (2.14) and 2.18))

Knot No.	Knot energy, MeV	Spline fit coefficients				S-factor coeffic. uncer., %
		A_0	A_1	A_2	A_3	
1	0,01	8,7403	0,0035619	0,014882	0,0047493	4,5
2	0,039385	8,7854	0,071135	0,034413	0,082523	2,3
3	0,19970	9,3447	0,83533	1,3109	-2,4558	1,7
4	0,38695	9,7600	-0,65421	-3,5627	2,1482	1,5
5	0,99510	7,7739	-1,6347	0,45197	0,066942	1,9
6	3,1628	6,5914	-0,32091	0,68420	-0,38870	2,0
7	9,2313	6,5550	-0,19308	-0,56486	0,76488	1,4
8	20,0	6,4216	0	0	0	3,2

Table 3.33

Differential cross-section at 0° for the ${}^3\text{He}(d,n+p){}^3\text{He}$ reaction in the laboratory system

Energy, MeV	Cross-section, mb/sr	Energy, MeV	Cross-section, mb/sr	Energy, MeV	Cross-section, mb/sr
3,89	0,11	5,08	4,23	8,85	57,0
4,14	0,27	5,22	4,67	9,88	69,2
4,40	1,07	5,35	5,56	10,85	89,2
4,66	2,11	5,51	6,01	11,9	109,1
4,81	2,71	6,91	33,1	18,6	190,0
4,95	3,49	7,82	41,0		

Table 3.34

Brief data content of references used in the evaluation of the ${}^3\text{He}, {}^3\text{He}$ integral reaction cross-sections

Energy range, MeV	Range of angles, deg	Type of data	Uncertainty, %		Ref.
			random	system.	
0,15-0,97	90	EXC, DA; d, n	6	20	[127]
1,0-1,5	0-160	AND, DA; d	1,5	7	[128]
0,5-1,1	0-170	AND, DA; d, n	2	5	[126]
0,1-0,8	90	EXC, DA; d, n	5	20	[129]
0,3-0,8	10;90	EXC, DA; d	1,5	-	[130]
0,7-3,8	0;40	EXC, DA; ${}^5\text{Li}$	2	10	[131]
2,7;3,6	0-140	AND, DA; ${}^5\text{Li}$	2	10	[131]

Table 3.35

Spline fit coefficients for the description of the ${}^3\text{He}+$ integral reaction cross-section (The cross-section can be calculated using equation (2.13))

Knot No.	Knot energy, MeV	Spline fit coefficients				Cross section uncer., %
		A_0	A_1	A_2	A_3	
1	0,1000	-1,760	5,759	-1,921	0,2173	9,6
2	1,521	4,062	0	0	0	4,2

Table 3.36

Differential cross-section at $\theta=90^\circ$ for the ${}^3\text{He}(r,\gamma){}^6\text{Be}$ reaction

Energy, MeV	$d\sigma/d\Omega$, $\mu\text{b/sr}$	Energy, MeV	$d\sigma/d\Omega$, $\mu\text{b/sr}$
0,86	0,032	11,74	0,770
1,40	0,061	13,74	0,800
1,72	0,077	14,69	0,84
2,20	0,143	15,73	0,91
3,01	0,200	16,83	0,90
3,83	0,278	17,88	0,92
4,62	0,326	18,94	0,97
5,66	0,374	19,99	1,03
7,72	0,526	20,82	1,09
9,77	0,624	21,88	1,14
10,78	0,700	22,77	1,07
		23,83	1,01

Table 3.37

Brief data content of references used in the evaluation of the ${}^3\text{He}(\tau, p){}^4\text{He}$ reaction cross-section

Energy range, MeV	Range of angles, deg	Type of data	Uncertainty, %		Ref.
			random	system.	
0,3-6	-	EXC, DA	5	10	[136]
17,9-24	-	EXC, DA	4	4	[137]
0,06-0,3	90	EXC, SIG	-	20	[138]
0,2-2,2	30-140	EXC, DA	6	6	[134]
0,45-1,5	0-135	AMD, DA	2	7	[123]
0,036-0,7	30-140	EXC, SIG	5	3,5	[135]

Table 3.38

Spline fit coefficients for the description of the S-factors for the ${}^3\text{He}(\tau, p){}^4\text{He}$ reaction (The evaluated total cross-section of this reaction can be calculated using equations (2.14) and (2.18))

Knot No.	Knot energy, MeV	Spline fit coefficients				S-factor coeff. uncert., %
		A_0	A_1	A_2	A_3	
1	0,040	5264,56	-48,2137	-6,74799	-16,8251	3,44
2	0,303255	4999,35	-282,675	-108,995	-208,334	3,29
3	0,428087	4880,41	-432,111	-308,414	143,609	3,34
4	1,6228	4082,15	-472,513	278,771	619,432	5,23
5	5,20028	4808,65	2550,44	-6786,64	124829	5,38
6	6,00	5400,0	0	0	0	5,45
7	24,0	5400,0	0	0	0	4,41

Table 3.39

Brief data content of references used in the evaluation of the ${}^3\text{He}(\alpha, \gamma){}^7\text{Be}$ and ${}^3\text{H}(\alpha, \gamma){}^7\text{Li}$ reaction cross-sections

Energy range, MeV	Range of angles, deg	Type of data, Reaction number	Uncertainty, %		Ref.
			random	system.	
0,5-1,3	90	EXC, DA; 1, 2	6	30	[140]
0,42-5,8	4	EXC, SIG; 1	3	10	[141]
0,37-0,56	90	EXC, DA; 1	5	10	[142]
0,25-2,95	90	EXC, DA; 1	15	20	[143]
0,25-2,95	39; 90; 116	AMD, DA; 1	15	20	[143]
0,37-2,73	90	EXC, DA; 1	3	7	[144]
2,09	4	I	-	4	[145]
1,22	0	I	-	8	[146]
0,5-1,9	90	EXC, DA; 2	5	15	[147]
1,6	0; 45; 90; 135	AMD, DA; 2	5	15	[147]

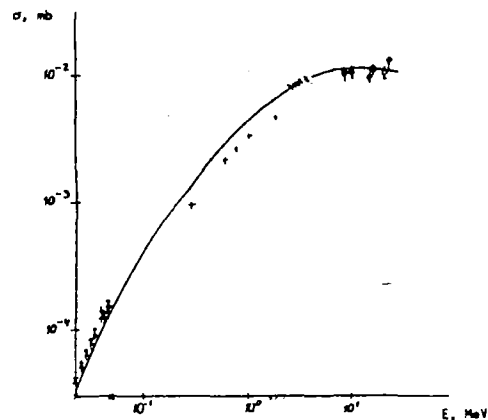


Fig. 3.1.

Energy dependence of the integral proton radiative capture cross-section of deuterium. Spline fit given by continuous curve. Experimental data: Σ - [11], + - [12], x - [13], \diamond - [15], \square - [16], \bullet - [18].

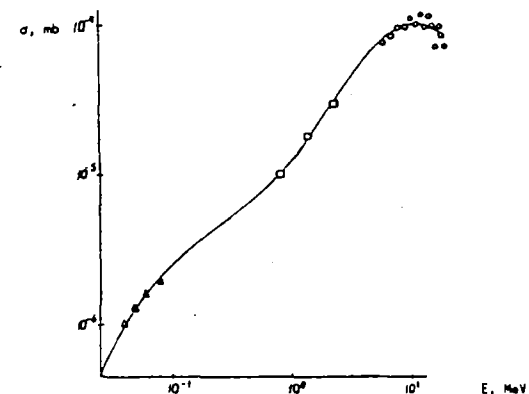


Fig. 3.3.

Energy dependence of the integral ${}^2\text{H}(d, \gamma){}^4\text{He}$ reaction cross-section. Spline fit given by continuous curve. Experimental data: Δ - [27], o - [29], \square - [30], \diamond - [15], \square - [16], \bullet - [18].

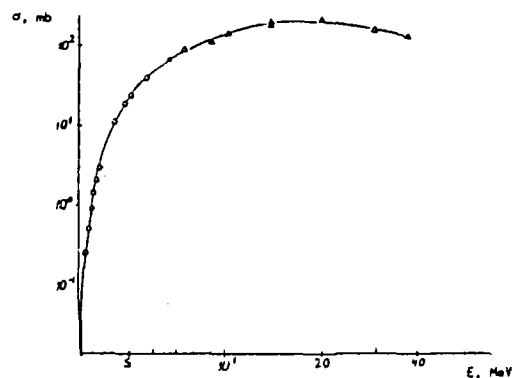


Fig. 3.2.

Energy dependence of the integral deuteron break-up cross-section in a d-p interaction. Spline fit given by continuous curve. Experimental data: o - [21], x - [23], Δ - [25].

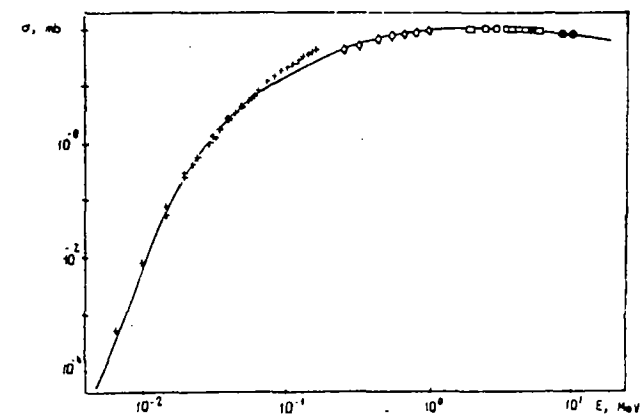


Fig. 3.4.

Energy dependence of the integral ${}^2\text{H}(d, n){}^3\text{He}$ reaction cross-section. Spline fit given by continuous curve. Experimental data: \bullet - [32], + - [34], \diamond - [39], \square - [42], \bullet - [51].

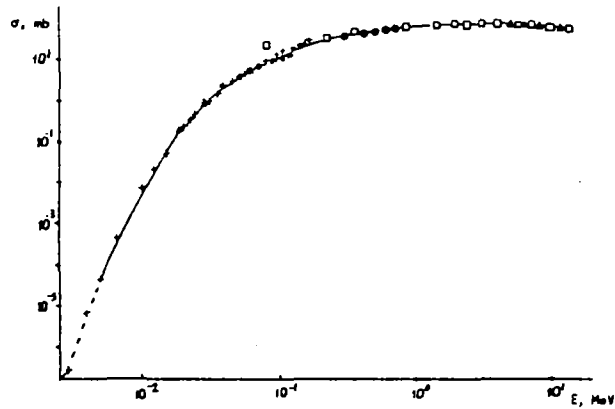


Fig. 3.5. Energy dependence of the integral ${}^2\text{H}(d,p){}^3\text{H}$ reaction cross-section. Spline fit given by continuous curve. Experimental data: \circ - [32], $+$ - [34], \bullet - [48], \blacktriangle - [57], \square - [60].

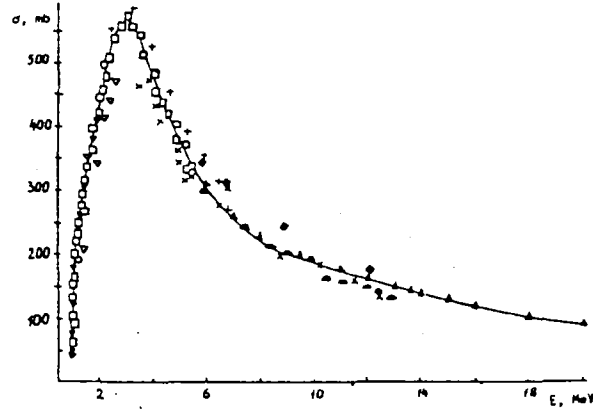


Fig. 3.7. Energy dependence of the integral ${}^3\text{H}(p,n){}^3\text{He}$ reaction cross-section. Spline fit given by continuous curve. Experimental data: ∇ - [21], \blacktriangle - [33], \circ - [71], \ominus - [72], \times - [73], \blacklozenge - [74], \square - [75], $+$ - [76].

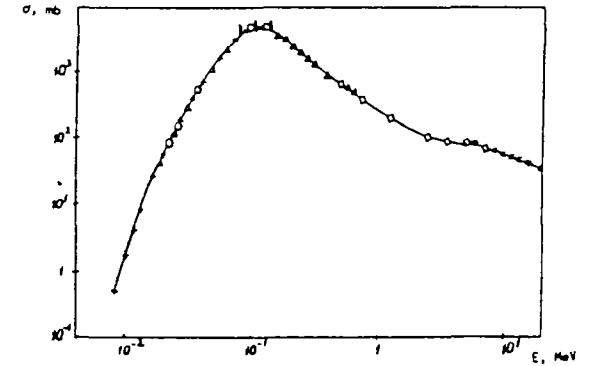


Fig. 3.9. Energy dependence of the integral ${}^3\text{H}(d,n){}^4\text{He}$ reaction cross-section. Spline fit given by continuous curve. Experimental data: \circ - [33], Δ - [35], \blacksquare - [40], \circ - [52], \times - [82], $+$ - [83], \blacktriangle - [87], \diamond - [89].

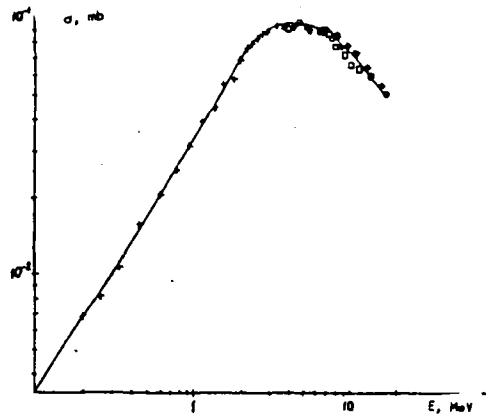


Fig. 3.6. Energy dependence of the integral ${}^3\text{H}(p,\gamma){}^4\text{He}$ reaction cross-section. Spline fit given by continuous curve. Experimental data: $+$ - [63], \blacklozenge - [65], \square - [66], \bullet - [68].

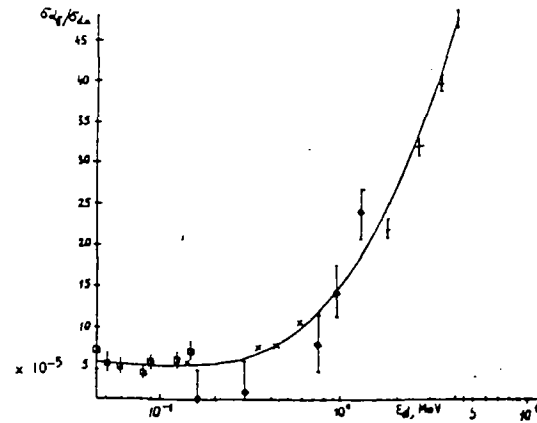


Fig. 3.8. Energy dependence of the ${}^3\text{H}(d,\gamma){}^3\text{He}/{}^3\text{H}(d,n){}^4\text{He}$ reaction cross-section ratio. Spline fit given by continuous curve. Experimental data: \square - [27], \times - [79], \blacklozenge - [80], $+$ - [27].

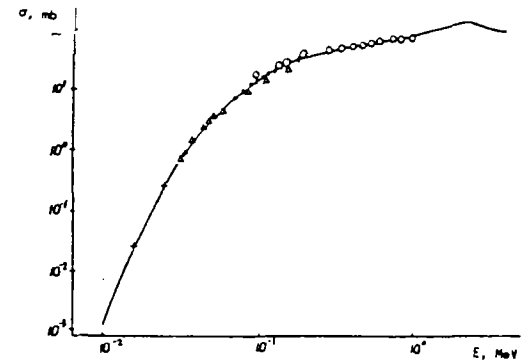


Fig. 3.10. Energy dependence of the integral ${}^3\text{H}(t,2n){}^4\text{He}$ reaction cross-section. Spline fit given by continuous curve. Experimental data: $+$ - [32], Δ - [95], \circ - [96].

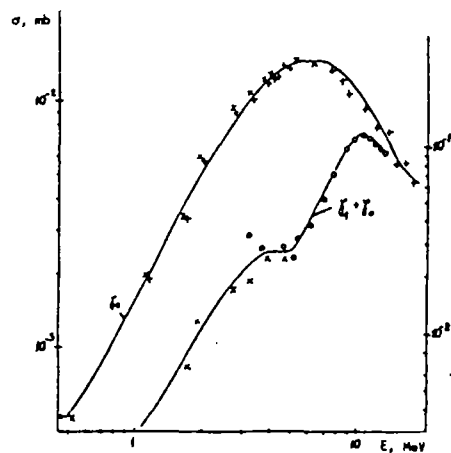


Fig. 3.11. Energy dependence of the excitation functions of the partial ${}^3\text{H}(t, \gamma){}^6\text{Li}$ reaction cross-section (left-hand scale), and of the ${}^3\text{H}(t, \gamma){}^6\text{Li}$ reaction cross-section (right-hand scale). Spline fit given by the continuous curve. Experimental data: x - [99], o - [100], + - [102].

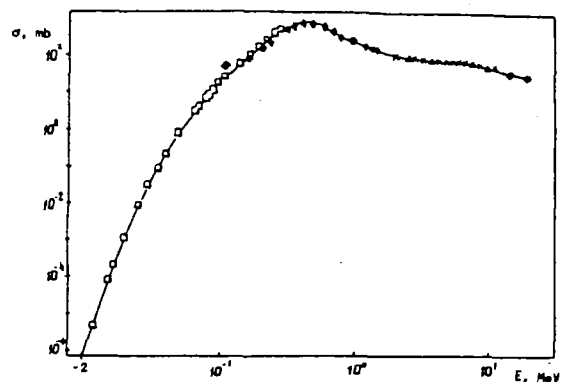


Fig. 3.13. Energy dependence of the integral ${}^3\text{He}(d, p){}^4\text{He}$ reaction cross-section. Spline fit given by continuous curve. Experimental data: \square - [34], x - [110], Δ - [111], \circ - [112], \blacklozenge - [114].

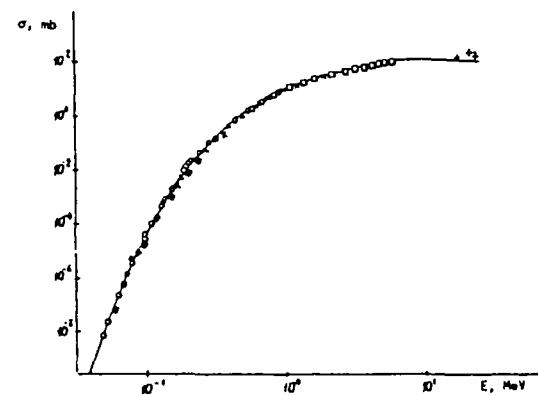


Fig. 3.15. Energy dependence of the integral ${}^3\text{He}(t, 2p){}^4\text{He}$ reaction cross-section. Spline fit given by continuous curve. Experimental data: \circ - [123], x - [134], o - [135], \square - [136], + - [137], \oplus - [138].

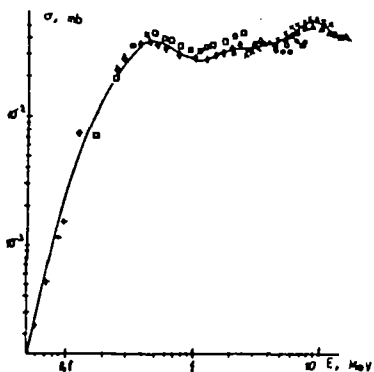


Fig. 3.12. Energy dependence of the integral ${}^3\text{He}(d, \gamma){}^5\text{Li}$ reaction cross-section. Spline fit given by continuous curve. Experimental data: + - [27], \blacklozenge - [103], \square - [104], o - [105], x - [106], Δ - [107].

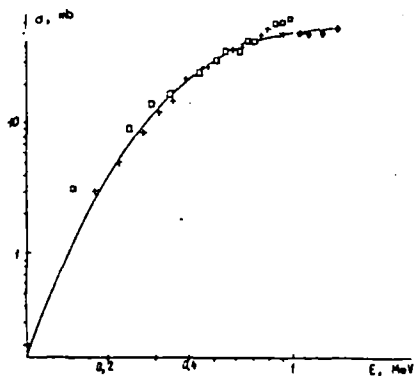


Fig. 3.14. Energy dependence of the total integral ${}^3\text{He}(t, x)$ cross-section for the interaction of helium-3 and tritium. Spline fit given by continuous curve. Experimental data: x - [126], \square - [127], \blacklozenge - [128], + - [129].

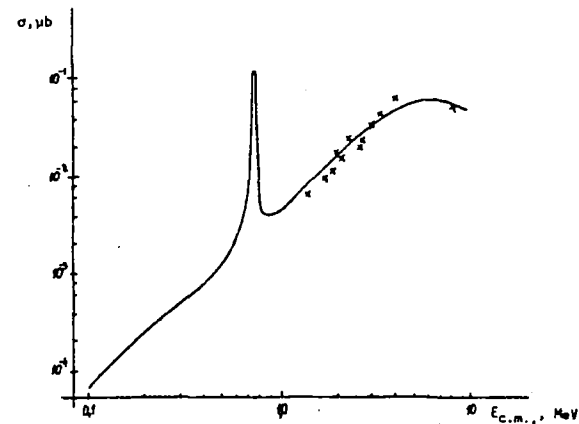


Fig. 3.16. Energy dependence of the integral ${}^4\text{He}(d, \gamma){}^6\text{Li}$ reaction cross-section. Spline fit given by continuous curve. Experimental data: x - [148].

4. CROSS-SECTIONS FOR THE INTERACTION OF LITHIUM NUCLEI WITH ISOTOPES OF HYDROGEN AND HELIUM

4.1. Basic data

Lithium: atomic number - 3
atomic mass - 6.939
Isotopic composition: lithium-6 7.52%
lithium-7 92.48%
Density: 0.534 g/cm³ at 20°C
Melting temperature: 180.5°C

Fields of application: nuclear technology, production of tritium through the ${}^6\text{Li} + n \rightarrow {}^3\text{H} + {}^4\text{He}$ reaction in the shielding of nuclear reactors (the thermal neutron absorption cross-section in lithium-6 is 945 barns). Liquid lithium-7 is used as a coolant in uranium fuelled reactors. Lithium is also used in the silicon industry and in metallurgy.

The energy characteristics of nuclear reactions of lithium-6 and lithium-7 nuclei with nuclei of hydrogen and helium isotopes considered in this evaluation are listed in Table 4.1.

4.2. The ${}^6\text{Li}(p,\gamma){}^7\text{Be}$ reaction

The integral cross-section for radiative capture of protons by the lithium-6 nucleus was derived from data given in Ref. [149]. The spline coefficients to describe the integral cross-section curve are listed in Table 4.2. The plotted evaluated curve is compared with the experimental data in Fig. 4.1.

The partial differential cross-section data corresponding to the ground state and first excited state of beryllium-7 were taken from Ref. [150] and were used to obtain the partial cross-section ratios tabulated in Table 4.3.

4.3. The ${}^6\text{Li}(p,n){}^6\text{Be}$ reaction

The total integral neutron production cross-section for this reaction, from threshold to a proton energy of 14 MeV, is presented in Ref. [151]. The authors report an estimated relative uncertainty of 15%, and an evaluated value of $32 \pm 50\%$ mb at $E_p = 8$ MeV.

An evaluated contribution of 30 mb by the ground state channel (${}^6\text{Li}(p,n_0){}^6\text{Be}$) at a proton energy of 11.6 MeV is reported in Ref. [152]. An evaluation of the relative contribution of the dual channel of the ${}^6\text{Li} + p$ reaction to the neutron yield at a proton energy of 10.5 MeV can be made on the basis of neutron spectrum data reported in Ref. [153]. This contribution does not amount to more than 30%, however, which gives a lower limit of 100 mb for the total neutron production cross-section at $E_p = 11.6$ MeV. If one took the relative neutron yield data for the ${}^6\text{Li}(p,n)$ reaction reported in Ref. [151] and normalized them to the recommended value of the total cross-section at $E_p = 8$ MeV, a value of 70 mb at a proton energy of 11 MeV could be inferred. Taking into account the systematic variation of the detector efficiency for the measurements reported in Ref. [151], which decreases from its initial value at $E_p = 2$ MeV to 75% of that value at $E_p = 9$ MeV, an evaluated value of 100 mb at $E_p = 11.6$ MeV for the total integral neutron yield for that reaction will be obtained. The normalization of the relative excitation function given in Ref. [151] was performed in a similar manner using the above-mentioned reference values for the total integral neutron yield. Values for the neutron yield cross-section as a function of energy, which are tabulated in Table 4.4, were taken from the evaluated curve drawn through the experimental values.

4.4. The ${}^6\text{Li}(p,\alpha){}^3\text{He}$ reaction

The total cross-section of this reaction, measured in the E_p energy range 0.023 to 16 MeV, has been described in a large number of references published between 1936 and 1980 (see Table 4.5).

The values for this reaction cross-section, taken principally from Ref. [158], are in good agreement in the low-energy range with the values published in Refs [154] and [156]. Extrapolation to low energies can be done by using Eq. (2.14) with the following parameters in the centre-of-mass system: $S(E_{c.m.}) = S(0) \cdot (1 + aE_{c.m.} + bE_{c.m.}^2)$ where $S(0) = 3.145 \text{ MeV}\cdot\text{b}$; $a = -0.70 \text{ MeV}^{-1}$; $b = 0.06 \text{ MeV}^{-2}$; and $E_g = 6.521 \text{ MeV}$.

In the energy range $0.02 < E < 14 \text{ MeV}$, values for the integral ${}^6\text{Li}(p,\alpha){}^3\text{He}$ reaction cross-section can be derived from Eq. (2.13) using the spline coefficients listed in Table 4.6. The latter were derived from integral data reported in the references listed in Table 4.5. The evaluated spline curve for the ${}^6\text{Li}(p,\alpha){}^3\text{He}$ reaction and the experimental points used in the evaluation are plotted in Fig. 4.2.

4.5. The ${}^6\text{Li}(d,n){}^7\text{Be}$ reaction and the total neutron production cross-section in the ${}^6\text{Li} + d$ interaction

In view of the fact that the ${}^6\text{Li}(d,n){}^7\text{Be}$ and the ${}^6\text{Li}(d,p){}^7\text{Li}$ reactions are charge-symmetric, the ratios of their partial channel cross-sections corresponding to the ground and first excited states of the residual lithium-7 and beryllium-7 nuclei can be expected to be equal. Since the partial integral cross-sections of the d-p reaction channels are known (see Section 4.6), only the integral cross-sections of the d-n reaction channel are considered here. Their values were derived from the references listed in Table 4.7.

Extrapolation to lower energies was performed with the aid of Eq. (4.1), given in Section 4.6, which was proposed in Ref. [175]. Values for the corresponding parameters to calculate the integral cross-sections for the

${}^6\text{Li}(d,n){}^7\text{Be}$ reaction in the energy range $E_d < 0.016 \text{ MeV}$ are listed in Table 4.13. With due allowance for the above extrapolation, a spline curve was constructed for the 0.016 to 17 MeV energy range using the coefficients listed in Table 4.8. A comparison of the evaluated curve with the experimental data is shown in Fig. 4.3. The extrapolation of the data above 12 MeV was performed with data given in Ref. [170] after they had been normalized at 12 MeV to values given in Ref. [169].

The angular distributions of the neutrons from this reaction are essentially isotropic at deuteron energies lower than 0.2 MeV. At higher energies the distribution is sharply peaked forward, which is characteristic of significant contributions from direct processes. Detailed measurements of angular distributions are reported only in Ref. [167].

Neutron production cross-sections for interactions of deuterons with lithium-6 have been studied in Refs [172, 173] and [174] (see Table 4.7). The data from Ref. [172] can be taken as fairly reliable. References [173] and [174] include only differential cross-sections at 90° and 0° respectively, and it is impossible to derive integral cross-section information from them. For that reason, the evaluated integral neutron production cross-sections for ${}^6\text{Li} + d$ interactions given in Table 4.9 are based exclusively on the data given in Ref. [172].

4.6. The ${}^6\text{Li}(d,p){}^7\text{Li}$ reaction

This reaction is of great interest both to nuclear astrophysics and to the development of controlled thermonuclear fusion. The study of the interaction of deuterons with lithium-6 nuclei resulting in the emission of protons helps improve the cross-section values in the charge symmetric interaction channels of the ${}^7\text{Be} + n$ reaction.

The evaluation of the partial integral cross-sections corresponding to the ground and first excited states of lithium-7 in the 0.3 to 12 MeV deuteron

energy range is expressed in the form of spline curves, based on the least-square fit of the input data, including their relative and absolute errors, as listed in Table 4.10. The coefficients of these curves are given in Table 4.11.

The cross-section ratios $\sigma(E)dp_0/\sigma(E)dp_1$ and $\sigma(E)dn_0/\sigma(E)dn_1$ for the partial ${}^6\text{Li}(d,p){}^7\text{Li}$ and ${}^6\text{Li}(d,n){}^7\text{Be}$ reaction channels are equal, and so, knowing the total neutron yield, we can make use of this fact to determine the partial integral neutron cross-sections for the reaction channels. The ratios for the proton emission channels thus have an independent interest of their own and are listed separately in Table 4.12.

Extrapolation to low energies can be done by using Eq. (2.14) with the following parameters in the centre of mass: $E_g = 13.23$ MeV; dp_0 : $S(E_{c.m.}) = 28.3(1 - 6.8E_{c.m.} + 20E_{c.m.}^2)$ MeV·b; and dp_1 : $S(0) = 3.2$ MeV·b.

A more exact extrapolation can be obtained by using an equation proposed by the authors of Ref. [175], who used the R-matrix approach:

$$\sigma(E) = \frac{P_c(E)}{E} \left[\frac{t}{(1 - \gamma_c S_c^0(E))^2 + (\gamma_c P_c(E))^2} \right] \quad (4.1)$$

where $S_c^0(E) = S_c(E) - B_c$; $P_c(E) = \rho_c / (F_c^2 + G_c^2)$, which is the penetrability of a hard Coulomb sphere of radius r ; $S_c(E) = P_c(E) \cdot [F_c \cdot F_c' + G_c \cdot G_c']$ is the displacement function; and F_c , G_c , F_c' and G_c' are the regular and irregular Coulomb functions and their derivatives. The t and γ parameters are tabulated in Table 4.13 [175].

Comparisons of the experimental data with the evaluated excitation function curve for the integral ${}^6\text{Li}(d,p_0){}^7\text{Li}$ and ${}^6\text{Li}(d,p_1){}^7\text{Li}$ reaction cross-sections are given in Fig. 4.4 and Fig. 4.5 respectively.

4.7. The ${}^6\text{Li}(d,t){}^5\text{Li}$ and ${}^6\text{Li}(d,\tau){}^5\text{He}$ reactions

These two mirror reactions are very similar and should therefore be considered together. Since the reaction products, lithium-5 and helium-5, are

unstable and decay into an alpha particle and into a neutron or a proton, these reactions must be considered as three body reactions, and the tritons and the τ -particles are observed in the form of continuous spectra.

The integral tritium production cross-section of the ${}^6\text{Li}(d,t){}^5\text{Li}$ reaction was studied by the authors of Ref. [179] in the 0.4 to 4.0 MeV energy range, and by the authors of Ref. [180] in the 0.1 to 0.8 MeV energy range. Although the measurements reported in these two references were made at different times and by different experimental methods, they are in excellent agreement. The recommended approximating spline curve, whose coefficients are tabulated in Table 4.14, is based on the data from both references. For extrapolation to lower energies Eq. (2.14) can be used with the following parameters (in the centre-of-mass system): $E_g = 13.2$ MeV and $S(0) = 23.0$ MeV·b. A comparison of the experimental data with the evaluated curve will be found in Fig. 4.6.

Reference [180] also reports measurements of differential cross-sections for the mirror reaction ${}^6\text{Li}(d,\tau+n){}^4\text{He}$. Since there are no other data for this reaction, the neutron angular distributions (in the laboratory system) reported in Ref. [180] are presented directly in Table 4.15 in the form of Legendre coefficients.

These reactions were also studied at high deuteron energies ($E_d = 15$ MeV) in Ref. [181]. The measurements were of triton and helium-3 spectra at 13.8° to 88° in the centre-of-mass system. The authors also proposed a model to describe the observed spectra on the basis of Butler's theory of direct reactions.

4.8. The ${}^6\text{Li}(d,\alpha){}^4\text{He}$ reaction

Of all possible alpha producing reactions, this reaction has the highest energy yield and is therefore of great interest for thermonuclear

fusion. It is not surprising therefore that it has been studied by numerous authors and over a broad energy range (see Table 4.16).

The basic data for the determination of the evaluated curve were taken from Refs [167, 168, 188], and these were assigned minimal systematic errors. The data from Refs [185, 187, 189 and 190] were normalized at a deuteron energy of 2.5 MeV to an average value based on data from Refs [168] and [188]. Evaluated data from Refs [175] and [191], which are in close agreement, were used in the low-energy region of the evaluation.

An evaluated spline curve, whose coefficients are listed in Table 4.17, was constructed over the energy range for which experimental data are available, namely $E_d = 0.03$ to 14.8 MeV. A comparison of the evaluated curve with the experimental values is shown in Fig. 4.7.

The approaches used in Refs [191] and [175] can be used for the extrapolation to low-energy regions. The authors of Ref. [191] propose an equation similar to Eq. (2.14) with the following parameters (in the centre-of-mass system): $E_g = 13.32$ MeV and $S(0) = 7.222$ MeV·b.

Then, if we adopt the extrapolation dependence given by Eq. (2.14), we obtain at a deuteron energy of 0.016 MeV a cross-section value equal to 2.02 nb - practically an order of magnitude lower than the recommended value given in Ref. [182], which was obtained by using the extrapolation formula (4.1) from Ref. [175]. If we accept the evaluation given by equation (2.14), then the cross-section at low energies, $E_d < 100$ keV, can be described very well by the parameters $E_g = 13.32$ MeV and $S(0) = 25.1$ MeV·b, which are accordingly recommended.

4.9. The cross-section for the formation of neutrons and beryllium-7 nuclei in the ${}^6\text{Li}(t,x)n$ and ${}^6\text{Li}(t,2n){}^7\text{Be}$ reactions

The total cross-section for the production of neutrons in these reactions is composed of contributions from the following two reaction

channels: ${}^6\text{Li}(t,n){}^8\text{Be} + 10.44$ MeV and ${}^6\text{Li}(t,2n){}^7\text{Be} + 8.77$ MeV. The first of these has a large energy yield and is the dominant channel in determining the total production of neutrons. A list of references devoted to the study of the neutron production cross-section in the ${}^6\text{Li} + t$ interaction is given in Table 4.18.

As shown in Table 4.18, data have been measured down to an incoming triton energy of 0.1 MeV. Extrapolation of the data to lower energies was performed with Eq. (2.14). The data used to construct the evaluated curve were taken from Refs [172, 192, 194]. The parameters used in the calculation of the S-factors with the help of Eq. (2.14) were derived from Ref. [192] and are (in the centre-of-mass system): $E_g = 17.56$ MeV and $S(0) = (1.78 \pm 0.27) \cdot 10^{-4}$ mb·MeV.

The spline curve constructed from the experimental data, with a value at $E = 0.198$ MeV corresponding to the analytical representation obtained from Eq. (2.14), will be found in Fig. 4.8. The spline coefficients are tabulated in Table 4.19.

Because it is important for a number of practical applications to know the total beryllium-7 production cross-section, it was decided to separate this reaction channel from all other neutron production channels in the ${}^6\text{Li} + t$ interaction. Because of the endothermic character of the ${}^6\text{Li}(t,2n){}^7\text{Be}$ reaction, it is not essential to describe the behaviour of the excitation function at low energies. Therefore, the total cross-section of the ${}^6\text{Li}(t,2n){}^7\text{Be}$ reaction was represented only by the spline approximation. The spline coefficients are listed in Table 4.20. Data from Ref. [169] were used in the construction of the spline curve. Experimental cross-section data for the production of the ground and first excited states of beryllium-7 and the associated spline curves are shown in Fig. 4.8.

4.10. The ${}^6\text{Li}(t,p){}^8\text{Li}$ reaction

Measurements of the total lithium-8 production cross-section of the ${}^6\text{Li}(t,p){}^8\text{Li}$ reaction in the energy range 0.3 to 10 MeV are described in Refs [195, 196]. Information on measurements of the partial cross-section for the production of the first excited state of lithium-8 is also available in Ref. [171]. A brief description of the references is given in Table 4.21.

Analysis of the excitation function of the total lithium-8 production cross-section of the ${}^6\text{Li}(t,p){}^8\text{Li}$ reaction (Fig. 4.9) reveals a distinct resonance at $E_t = 4.4$ MeV which corresponds to the compound nucleus excitation energy of $E({}^9\text{Be}) = 20.6$ MeV. Another excited state, with an excitation energy of $E({}^9\text{Be}) = 19.4$ MeV, corresponding to an incident triton energy of 1.7 MeV, was taken into account in determining the cross-section energy dependence for triton energies ranging from 1 to 2.5 MeV.

Relative measurements reported in Ref. [196], normalized at a triton energy of 1.0 MeV to a cross-section value of 20 mb, were used in the construction of the low-energy part of the excitation function for the total lithium-8 production cross-section. To extend the evaluated curve to the low-energy region, $E_t < 0.3$ MeV, where no experimental data exist, we used the following expression:

$$\sigma(E) = (3750/E) \cdot \exp(-26.4/E)^{1/2}$$

In extrapolating the total evaluated lithium-8 production cross-section curve to higher energies, $10 < E < 20$ MeV, it was assumed that the energy dependence behaves as $1/E$. An excitation function for the ${}^6\text{Li}(t,p){}^8\text{Li}$ reaction reflecting the above considerations is shown in Fig. 4.9 and its coefficients are listed in Table 4.22.

In order to evaluate the contribution to the total lithium-8 production cross-section of the partial reaction channels leading to the ground and first excited states of the stable lithium-8 nucleus, one can use the measured

${}^6\text{Li}(t,p_1){}^8\text{Li}$ reaction cross-section data given in Ref. [171]. These data were derived from measurements of the gamma rays emitted at an angle of 55° ; they are tabulated in Table 4.23.

If one assumes that the 0.981 MeV transition in the lithium-8 nucleus is a pure M1-multipole transition, which would imply that the angular distribution for such a transition would have the form

$$W(\theta) = B_0 P_0 + B_2 P_2(\cos(\theta))$$

where P_0 and P_2 are Legendre polynomials, then the total gamma-ray production cross-section can be expressed by

$$\sigma(E) = 4\pi\sigma(55^\circ, E)$$

If we now compare the partial cross-section obtained in this way with the total lithium production cross-section, we will see that the former makes up approximately 3/8 of the latter. This agrees very well with the relative contributions of the ground and first excited states derived exclusively on the basis of spin statistical weights.

4.11. The ${}^6\text{Li}(t,d){}^7\text{Li}$ reaction

The only data reported in the literature for this reaction are measurements of the partial cross-section leading to the first excited state of lithium-7 [171]. An analytical expression in the form of a spline fit was constructed by drawing a curve through the only available experimental data; the corresponding spline coefficients are listed in Table 4.24. Since the energy range over which the experimental data had been measured extended only from 2.7 to 10 MeV, the excitation function of the ${}^6\text{Li}(t,d_1){}^7\text{Li}$ total cross-section was extended to the region below 2.7 MeV by means of the following expression:

$$\sigma(E) = 9000/E \cdot \exp(-26.4/E)^{1/2}$$

This curve is shown in Fig. 4.10. The evaluated curve for the cross-section of the ${}^6\text{Li}(t,d_0){}^7\text{Li}$ reaction, leading to the ground state

of lithium-7, was arrived at by using data for the inverse reaction ${}^7\text{Li}(d,t){}^6\text{Li}$ published in Ref. [179]. The conversion of the data was done with the following relationship based on the principle of detailed balance:

$$\sigma(E)_{dt} \sigma(E)_{td} = 0.5(k_t/k_d)$$

where k_t is the wave number of the relative motion in the ${}^6\text{Li} + t$ system and k_d the corresponding wave number for the ${}^7\text{Li} + d$ system.

Since the cross-sections of the ${}^7\text{Li}(d,t){}^6\text{Li}$ reaction were derived from cross-sections of the ${}^6\text{Li}(t,d){}^7\text{Li}$ reaction, the most convenient approach is to express the energies in the energy scale of the incident deuterons. In this case, $0.5(k_t/k_d)^2 = 0.64286 - 0.8207/E_d$ and $E_t = 1.6667E_d - 1.4985$, where E_d is the deuteron energy in the laboratory system.

Using this conversion, it has been possible to evaluate the cross-section for the ${}^6\text{Li}(t,d_0){}^7\text{Li}$ reaction leading to the ground state of lithium-7 in the energy range of 0.3 to 4.12 MeV. For extrapolation to higher energies, it was assumed that the behaviour of the excitation function for the t,d_0 reaction channel would be similar to the behaviour of the excitation function for the t,d_1 reaction channel.

4.12. The ${}^6\text{Li}(\tau,n){}^8\text{B}$ reaction

The total cross-section for this reaction, which has been measured [168, 197] from threshold to an energy of $E(\tau) = 3.5$ MeV, exhibits a monotonic increase up to a value of 4.3 mb, which it reaches at 3.5 MeV. The total boron-8 yield has been measured at energies of $E(\tau) = 8.9$ to 26.5 MeV [198, 199]. The spline curve obtained on the basis of these data is shown in Fig. 4.11, and the parameters for the curve are given in Table 4.25.

4.13. The ${}^6\text{Li}(\tau,p){}^8\text{Be}$ reaction

This reaction is interesting from the point of view of its use in the realization of neutron-free fusion. The interaction of helium-3 with

lithium-6 accompanied by the production of protons has three possible reaction channels:

- the production of beryllium-8 in the ${}^6\text{Li}(\tau,p){}^8\text{Be}$ reaction;
- the production of lithium-5 in the ${}^6\text{Li}(\tau,\alpha){}^5\text{Li}$ reaction;
- the three-particle break-up in the ${}^6\text{Li}(\tau,p){}^4\text{He} + {}^4\text{He}$ reaction.

In these reactions, the nuclei of beryllium-8 and lithium-5 are not stable and decay into two alpha particles or into an alpha particle and a proton, respectively.

The basic data which were used to obtain evaluated values of the ${}^6\text{Li}(\tau,p){}^8\text{Be}$ reaction cross-section were taken from Ref. [200] (see Table 4.26). The results given in Refs [201] and [202] were normalized to these data. The effect of such an interdependence revealed a significant discrepancy (up to a factor of 1.5) between the data of Refs [201] and [203]. It was therefore felt to be justified to renormalize the data from [203]. The resulting spline curves for the two reaction channels of the reaction are plotted in Figs 4.12 and 4.13; the spline coefficients are listed in Table 4.27.

At low energies, the integral cross-sections for the ${}^6\text{Li}(\tau,p){}^8\text{Be}$ reaction leading to the ground state, and for the ${}^6\text{Li}(\tau,p_1){}^8\text{Be}$ reaction leading to the first excited state can be described by Eq. (2.14) using the following parameters (centre of mass): $E_g = 71.25$ MeV; $P_0:S(0) = 14.0$ MeV·b; and $P_1:S(0) = 35$ MeV·b.

The cross-sections for the ${}^6\text{Li}(\tau,p){}^8\text{Be}$ reaction channels corresponding to excitation levels of 16.63 MeV and 16.92 MeV and to the contribution from continuous spectrum protons follow Ref. [200] (see Table 4.28).

4.14. The ${}^6\text{Li}(\tau,d){}^7\text{Be}$ reaction

This reaction is of interest because of its importance in the ${}^6\text{Li} + p$ fuel cycle of fusion reactors [204]. An additional attraction is that it

provides a possibility of studying the nuclear structure of the beryllium-7 nucleus. Table 4.29 lists the references used in the evaluation of this reaction.

Partial integral reaction cross-sections are reported in Ref. [200]. The summed integral cross-section is in good agreement with the data of Barr and Gilmore measured by activation analysis and reported in Ref. [200]. At an energy of $E(\tau) = 1.55$ MeV, the excitation function has a resonance corresponding to the 17.64 MeV level of beryllium-9 [178]. At $E(\tau) = 2.0$ MeV the data of Barr and Gilmore are in very good agreement with the data given in Ref. [205]. The latter allow an evaluation of the total integral cross-section of the ${}^6\text{Li}(\tau, d){}^7\text{Be}$ reaction up to an energy of $E(\tau) = 6.0$ MeV.

For energies higher than 8 MeV we have information on the angular distributions of deuterons corresponding to the ground and first excited states of the beryllium-7 nucleus [208]. The summed integral cross-section for these two channels adds up to approximately half of the total integral cross-section of the reaction, which is an indication of a substantial contribution corresponding to higher energy states of the beryllium-7 nucleus [200]. Table 4.30 gives spline coefficients for a curve approximating the summed integral cross-section of the ${}^6\text{Li}(\tau, d){}^7\text{Be}$ reaction. The evaluated curve is compared with the experimental data in Fig. 4.14.

Extrapolation to lower energies can be done with the aid of Eq. (2.14) using the following parameters (in the centre-of-mass system): $E_g = 71.25$ MeV and $S(0) = 2144$ MeV·b.

4.15. The ${}^7\text{Li}(p, \gamma){}^8\text{Be}$ reaction

This reaction has been extensively studied (see Table 4.31). The highly excited states of the beryllium-8 nucleus formed in the course of proton capture decay to the ground (0^+) and the first excited (2^+ , $E_x =$

3.04 MeV) states accompanied by the emission of gamma rays with energies of $17.2 + (7/8)E_p$ and $14.3 + (7/8)E_p$ MeV respectively, where E_p is the energy of the incident proton.

The probability for decays to higher excited states of the beryllium-8 nucleus is low (of the order of 0.1% of the first two states). The energy dependence of the reaction cross-section reveals the well known resonance at an incident proton energy of 0.440 MeV, as well as two smaller resonances at 1.03 and 2.1 MeV respectively, superimposed on a substantial background which some authors have attempted to explain by the existence of a giant resonance at a higher energy. The 0.440 MeV resonance can be described reasonably well by the simple Breit-Wigner formula with the following parameters:

$$E_{\text{res}} = 441.4 \text{ keV}, l_p = 1, \Gamma_{\text{lab}} = 12.2 \text{ keV}, J^\pi = 1^+ \text{ and } \omega \cdot \Gamma_\gamma = 9.4 \text{ eV}.$$

For convenience, the cross-section of the ${}^7\text{Li}(p, \gamma){}^8\text{Be}$ reaction is represented by a single spline curve over the full energy range, including the resonance at 0.441 MeV. The experimental data on the gamma-ray production cross-section are compared to the evaluated curve in Fig. 4.15. The spline parameters are listed in Table 4.32.

4.16. The ${}^7\text{Li}(p, n){}^7\text{Be}$ reaction

Because of its high neutron yield, the ease of its application and its relatively low threshold, this reaction is used extensively as a neutron source. The only disadvantages are the existence of a significant gamma-ray background at reaction energies above 2.38 MeV, and the comparatively narrow energy range over which monoenergetic neutrons are produced. At energies above 3.68 MeV we see a continuous neutron spectrum due to the contribution of the multi-particle break-up reaction ${}^7\text{Li}(p, n + \alpha){}^3\text{He}$. The contribution of these spectral neutrons increases gradually and reaches 40% to 50% of the total neutron yield at proton energies above 7 MeV.

The evaluation of this reaction is based on results given in Ref. [216], as well as on data published subsequently. The neutron yield from this reaction has been measured up to a proton energy of 26 MeV. Furthermore, there have been a few measurements which have produced high precision results in the monoenergetic neutron yield region. There is also additional information on the multi-particle channels of this reaction and on measurements of the total neutron yield.

A brief description of references supplementing the information given in Ref. [216] is given in Table 4.33.

The data given in Ref. [217] have made it possible to improve the accuracy of the energy dependence of the integral cross-section for the ground state channel of this reaction in the threshold region as well as in the $E_p < 4$ MeV energy region. These data, supplemented by information from Refs [217] and [218], are tabulated in Table 4.34 and plotted in Fig. 4.16.

The data on the partial integral cross-section of the ${}^7\text{Li}(p,n_1){}^7\text{Be}$ reaction (leading to the first excited state of beryllium-7) published in Ref. [216] have been re-evaluated on the basis of data from Refs [219] and [171]. In the former, the integral p-n reaction cross-section was normalized using the ratio pn_1/pp_1 , and in the latter, the normalization was performed on the basis of results given in Ref. [219]. The evaluation above 10 MeV was based on data given in Ref. [218]. The evaluated integral cross-section curve for the ${}^7\text{Li}(p,n_1){}^7\text{Be}$ reaction (leading to the first excited state) is plotted in Fig. 4.17; the numerical values for this cross-section are listed in Table 4.35.

Three-particle reaction channels in the interaction of neutrons and protons contribute substantially to the total neutron yield at energies above 6 MeV. Measurements of the total neutron yield (for neutron energies ranging from 4 to 14 MeV) resulting from the bombardment of lithium-7 with protons

have been reported in Ref. [151]. As the energy dependence of this neutron yield from the ${}^7\text{Li}(p,n)$ reaction is reported by the authors of Ref. [151] in relative units, the data were normalized at a proton energy of 4.0 MeV under the assumption that the neutron yield results from the first two channels of the ${}^7\text{Li}(p,n){}^7\text{Be}$ reaction. The resulting neutron yield data are listed in Table 4.36, and the excitation function for the summed integral yield of neutrons from the ${}^7\text{Li}(p,n){}^7\text{Be}$ reaction is plotted in Fig. 4.18.

4.17. The ${}^7\text{Li}(p,\alpha){}^4\text{He}$ reaction

Because of its intrinsic scientific interest (e.g. in the investigation of clustering effects and for astrophysical studies) and its pertinence to the development of controlled fusion, the ${}^7\text{Li}(p,\alpha){}^4\text{He}$ reaction, as well as its inverse, the ${}^4\text{He}(\alpha,p){}^7\text{Li}$ reaction, have been studied extensively in many laboratories of the world.

The integral cross-section for this reaction has been measured in the proton energy range of 0.023 to 12 MeV. At low energies the dependence of the excitation function can be described by Eq. (2.14). At energies above 1 MeV, the cross-section is strongly influenced by resonances corresponding to the levels of the compound nucleus of beryllium-8.

Practically all of the measurements (see Table 4.37) which have been performed to study the ${}^7\text{Li}(p,\alpha){}^4\text{He}$ reaction can be divided into two groups. The first group consists of relative measurements which were normalized to data given in Ref. [220], or which are in agreement with the absolute values presented in [220]. The second group consists of absolute measurements which are in agreement with the data given in Ref. [221]. The differential cross-sections from these two groups of data differ by a factor of two. The reasons for such a significant discrepancy are investigated in Refs [215, 222 and 223] as well as in those references which are devoted to the study of the inverse reaction [224, 225]. The results of these investigations oblige us to

review all of these data [159, 226-228]. As a consequence the evaluated curve has been reduced by a factor of two.

A comparison of the experimental data with the evaluated curve is shown in Fig. 4.19. The recommended values of the integral cross-section data for proton energies (in the laboratory system) above 0.02 MeV can be calculated with the aid of Eq. (2.13) using the coefficients listed in Table 4.38.

Extrapolation of the experimental data to stellar energies can be done by

using Eq. (2.14) with the following parameters: $E_g = 7.765$ MeV,

$$S(E_{c.m.}) = 65.0(1 + 1.82 E_{c.m.} - 2.51 E_{c.m.}^2) \text{ MeV}\cdot\text{mb.}$$

4.18. The cross-section for the formation of tritium in interactions of protons with lithium-7 nuclei

When lithium-7 nuclei are bombarded by protons, tritium can be produced by the following three reactions:

1. ${}^7\text{Li}(p,t){}^5\text{Li}$ $Q = -4.434$ MeV
2. ${}^7\text{Li}(p,t){}^4\text{He} + p$ $Q = -2.468$ MeV
3. ${}^7\text{Li}(p,p){}^7\text{Li} \rightarrow {}^4\text{He} + t$ $Q = -4.6$ MeV

Inasmuch as the only information available for the evaluation of the ${}^7\text{Li}(p,t)$ interaction was Ref. [229], all deductions and conclusions were necessarily based on that reference. In the measured spectra reported in Ref. [229], groups of tritons which correspond to the formation of the ground state of the lithium-5 nucleus can be clearly distinguished. The contribution of the tritons from the ${}^7\text{Li}(p,t){}^5\text{Li}$ reaction decreases gradually as the angle increases, until at angles larger than 90° their peak merges completely with the continuous spectrum.

It is impossible to infer from the shape of the spectrum which of two reactions (2 or 3) is the main contributor to the formation of the continuous spectrum. However, theoretical considerations would suggest that the

${}^7\text{Li}(p,t + p){}^4\text{He}$ reaction does not contribute significantly to the spectrum because of the low probability for simultaneous three-particle formation.

The curve in Fig. 4.20 approximating the energy dependence of the tritium production cross-section in the ${}^7\text{Li}(p,x){}^3\text{H}$ reaction can be described analytically by the expression

$$\sigma(E) = \frac{255}{\pi} \times \left[\frac{\pi}{2} + \arctan \frac{(E-6.6)}{0.1859} \right]$$

4.19. Cross-sections for the formation of neutrons and beryllium-7 nuclei in the ${}^7\text{Li}(d,x)n$ and ${}^7\text{Li}(d,2n){}^7\text{Be}$ reactions

The production of neutrons in the ${}^7\text{Li} + d$ interaction occurs through a number of channels, and this leads to a complex neutron spectrum [230]. The difficulties which arise in studying the multi-particle neutron-producing ${}^7\text{Li} + d$ interactions limit our opportunities to perform thorough analyses of each separate reaction channel, yet, at the same time, in practical applications it is often desirable to know, first and foremost, the total yield of neutrons. With regard to specific measurements of total neutron yields from the ${}^7\text{Li}(d,x)n$ reaction, from among the relatively dependable sources of information we can cite here only Ref. [173], which reports measurements of the differential cross-section of this reaction for deuteron energies from 0.2 to 2 MeV at an angle of 90° , and Ref. [172], which reports differential data for $E_d = 2.8$ to 11 MeV (see Table 4.39).

The absolute value of the cross-section data from Ref. [172] was found by using the ratio method with the ${}^7\text{Li}(p,n){}^7\text{Be}$ reaction; this procedure introduces an uncertainty of $\leq 15\%$.

An analysis of neutron angular distributions [231, 232] from the various ${}^7\text{Li} + d$ reaction channels for incident deuteron energies smaller than 2 MeV indicates that values for the total ${}^7\text{Li}(d,x)n$ cross-section can be obtained within 10%-15% by multiplying the differential cross-section at 90° by 4π .

On the basis of these considerations, an evaluated curve in the deuteron energy range from 0.2 to 11 MeV was produced from the Ref. [172] data, using also the data from Ref. [173] multiplied by the 4π factor. The excitation function of the ${}^7\text{Li}(d,x)n$ total neutron production cross-section is plotted in Fig. 4.21. The spline coefficients as well as the uncertainty of the cross-section at the spline knots are listed in Table 4.40.

With regard to the total neutron production cross-section, the neutron reaction channel leading to the formation of the beryllium-7 nucleus is of special interest for astrophysical applications and a number of other practical applications. The total integral beryllium-7 production cross-sections and the partial integral cross-sections for the production of the first excited state of beryllium-7, based on the data published in Refs [169] and [171], are tabulated in Table 4.41.

4.20. The ${}^7\text{Li}(d,p){}^8\text{Li}$ reaction

Absolute values of the integral cross-section for this reaction at low energies are of interest in connection with a controlled fusion fuel cycle based on a reaction chain involving charged particles and nuclei of lithium-6, lithium-7 and beryllium-9. A brief description of the most important references used in deriving evaluated cross-section data for this reaction is given in Table 4.42.

The data from Refs [168] and [235] differ by 24%, a discrepancy larger than the sum of the root-mean-square errors of the data reported by these authors. The large discrepancy prompted measurements of the total cross-section of this reaction by two separate methods [237, 238]: by measuring the total proton yield, and by measuring the activity of lithium-8. The results yielded by the two methods are in good agreement and are close to the values reported in Ref. [168], which in turn agree with the data published in Ref. [236]. The data for the total ${}^7\text{Li}(d,p){}^8\text{Be}$ reaction cross-section

published in the literature cover the energy range from threshold to a deuteron energy of 10 MeV.

Values of the total cross-section for this reaction can be calculated using Eq. (2.11) with the spline coefficients listed in Table 4.43. As can be seen from Fig. 4.22, the evaluated curve relies largely on the measured data in Refs [168, 236-238] and reflects well the resonance character of the excitation function of the ${}^8\text{Li}(d,p){}^8\text{Be}$ reaction cross-section.

4.21. The ${}^7\text{Li}(d,t){}^6\text{Li}$ reaction

Data on this reaction would be of particular interest for the solution of certain practical problems, but are unfortunately extremely scarce. Measurements of the total integral tritium production cross-section in the ${}^7\text{Li} + d$ interaction, measured from threshold to $E_d = 4.71$ MeV, were reported in Ref. [179] and the results are listed in Table 4.44. The only data at high energies are partial differential cross-sections of the ${}^7\text{Li}(d,t_0){}^6\text{Li}$ (ground state) reaction in the energy range 10-12 MeV at an angle (in the lab system) of 155° , and information on the angular distribution of tritons for a deuteron energy of 12 MeV, both reported in Ref. [239]. The partial cross-section reported in Ref. [239] at $E_d = 12$ MeV is 66.5 mb. If we assume that the contribution of the partial cross-section corresponding to the ground state of the lithium-6 nucleus is approximately 30% of the total tritium production cross-section (which is deduced from a rough analysis of the spectra reported in Refs [239] and [240]), then the total tritium production cross-section at $E_d = 12$ MeV is 200 mb.

4.22. Evaluation of the integral ${}^7\text{Li}(t,p){}^9\text{Li}$ reaction cross-section

Lithium-9 has only two stable states whose levels contribute to the total lithium-9 production cross-section. The total lithium-9 production cross-section for this reaction, measured by the activation method, has been reported in Refs [195, 241].

The references used in evaluating the integral ${}^7\text{Li}(t,p){}^9\text{Li}$ reaction cross-sections are listed in Table 4.45. The shape of the excitation function in the tritium energy range from 10 to 15 MeV was constructed on the assumption that the cross-section is strongly affected by a "giant" threshold anomaly [195]. The spline curve, obtained with the use of data published in Refs [195] and [243], is shown in Fig. 4.23, and the spline coefficients are tabulated in Table 4.46.

4.23. Evaluation of the integral ${}^7\text{Li}(t,d){}^8\text{Li}$ reaction cross-section

The spline curve which describes the excitation function of the total lithium-8 production cross-section for the ${}^7\text{Li}(t,d){}^8\text{Li}$ reaction was based on the data published in Refs [171] and [195]. The spline curve is plotted in Fig. 4.24 and the spline coefficients are listed in Table 4.47.

The lithium-8 nucleus has only two stable levels which can contribute to the total cross-section, and the experimental data therefore correspond to the summed cross-sections for the two channels: ${}^7\text{Li}(t,d_0)$ and ${}^7\text{Li}(t,d_1)$.

4.24. Evaluation of the partial integral ${}^7\text{Li}(t,\alpha){}^6\text{He}$ reaction cross-sections

The helium-6 nucleus which results from the ${}^7\text{Li}(t,\alpha){}^6\text{He}$ reaction has only one stable state, namely the ground state. All other helium-6 states lead to decay resulting in two neutrons and an alpha particle. If we know the cross-section for this reaction channel, which is taken into account in the total neutron production cross-section discussed in Section 4.25, we have the possibility of separating out other neutron producing channels. The formation of the helium-6 nucleus is interesting in itself, and is taken into account in astrophysical calculations. A brief description of the references which report on the ${}^7\text{Li}(t,\alpha){}^6\text{He}$ reaction is given in Table 4.48.

The angular distribution of the alpha particles is isotropic for the ${}^7\text{Li}(t,\alpha_1){}^6\text{He}$ reaction channel at low reaction energies, and is subject to the

$W(\theta) = A + B\cos^2(\theta)$ dependence for the ${}^7\text{Li}(t,\alpha_0){}^6\text{He}$ reaction channel.

Furthermore, for tritium energies smaller than 0.3 MeV, the partial cross-section leading to the first excited state is an order of magnitude larger than the partial cross-section leading to the ground state [244, 249]. This ratio decreases gradually as the tritium energy increases and assumes a practically constant value (approximately equal to 2) over a broad energy range, $E_t = 2$ to 20 MeV [246-248]. As a result, the following procedure was used to evaluate the excitation functions of the partial cross-sections for the reaction channels under consideration.

On the assumption that the alpha particle angular distribution is isotropic, data from Refs [244, 249] were used to determine the integral partial cross-section for the ${}^7\text{Li}(t,\alpha_1){}^6\text{He}$ reaction channel in the 0.04-0.5 MeV energy range. The excitation function for this reaction channel was extended to the energy range 1.15 to 1.95 MeV by using integral values obtained by the integration of differential data given in Ref. [246]. In the 3.0 to 10.0 MeV energy range, the excitation function of the ${}^7\text{Li}(t,\alpha_1){}^6\text{He}$ reaction channel cross-section (leading to the first excited state) was derived from the energy dependence of the integral partial ${}^7\text{Li}(t,\alpha){}^6\text{He}$ reaction cross-section (leading to the ground state) [195] on the assumption that it is two times smaller than the integral partial reaction cross-section leading to the first excited state. The spline curves for the cross-sections of these reaction channels are shown in Figs 4.25 and 4.26, and their coefficients are listed in Table 4.49.

The excitation function for the partial ${}^7\text{Li}(t,\alpha_0){}^6\text{He}$ reaction channel in the energy range $E_t = 0.039$ to 0.5 MeV was derived from the excitation function corresponding to the first excited state on the assumption that its value is 1/10 of the latter. The justification for such an assumption is based on the values at reference points at $E_t = 0.055$ MeV [244], and

$E_t = 0.151$ MeV and 0.272 MeV [249]. Data from Refs [195, 246 and 247] were used for higher energies.

The summed cross-section (for both reaction channels) of the ${}^7\text{Li}(t,\alpha){}^6\text{He}$ reaction can be extrapolated to lower energies - $E_t \leq 0.055$ MeV - by means of the following expression:

$$\sigma(E) = (19827/E) \exp[-(26.5/E)^{1/2}] \text{ mb}$$

4.25. Evaluation of the integral cross-section for the production of neutrons in the interaction of tritium with lithium-7 nuclei

The ${}^7\text{Li}(t,x)n$ reaction

In the interaction of tritium with lithium-7 nuclei, neutrons are produced by way of the following two channels:

1. Two-particle channel: ${}^9\text{Be} + n + 10.455$ MeV
2. Multi-particle channel: $2{}^4\text{He} + 2n + 8.865$ MeV

Most publications present results in the form of differential neutron production cross-sections (see Table 4.50). In order to be able to use these data, we analysed the angular distributions in Ref. [194] and obtained normalizing coefficients with the help of which integral cross-section data were obtained from differential data at 0° .

The total neutron production cross-section for low triton incident energies can be approximated by the following expression [251]:

$$\sigma(E) = \left[\frac{3.52 \cdot 10^4}{(E - 0.1172)^2 + 0.1267} \right] \cdot \exp\left(-\sqrt{\frac{28.09}{E}}\right) \cdot \frac{1}{E}$$

A spline fit in the energy range $E \leq 0.13$ MeV, constructed on the basis of existing experimental data, is plotted together with the experimental data in Fig. 4.27; the spline coefficients are listed in Table 4.51.

4.26. The ${}^7\text{Li}(t,n){}^9\text{B}$ reaction

Data on this reaction is scarce and incomplete. The reaction channel leading to the ground state of the boron-9 nucleus has been studied relatively

well (see Table 4.52). The total cross-section has been investigated only in Ref. [192]. The rest of the references report on measurements of partial differential cross-sections corresponding to the ground state of the boron-9 nucleus; analysis of the neutron time-of-flight spectrum described in Ref. [235], shows that the ground state reaction channel, for an energy $E_t = 2.1$ MeV, contributes 11% of the total neutron yield. The values of the total neutron yield differential cross-sections at 0° given in Ref. [192] are listed in Table 4.53. Neutron angular distributions corresponding to the ground state of boron-9 in the energy range $E_t = 1.5$ to 5.5 MeV are reported in Ref. [252]; Legendre coefficients for these distributions, and the integral cross-sections for the ${}^7\text{Li}(t,n_0){}^9\text{B}$ reaction, are tabulated in Table 4.54.

4.27. The ${}^7\text{Li}(t,p){}^9\text{Be}$ reaction

This reaction has not been investigated extensively. The references used in the evaluation are described in Table 4.55. The measured excitation functions of the partial differential cross-sections and the associated angular distributions show that, in the energy range $E_t = 0.6$ to 1.4 MeV, this reaction proceeds primarily by way of the compound nucleus of boron-10 with an excitation energy of 18.5 MeV. In the range from $E_t = 2.2$ to 11 MeV, the excitation functions are relatively flat, without any resonance structure. The angular distributions have a very strong isotropic component [254]. In view of the paucity of experimental data, it has been impossible to make an evaluation of this reaction. The only available partial differential cross-section data, from Ref. [252], are tabulated in Table 4.56.

4.28. The ${}^7\text{Li}(t,d){}^8\text{Be}$ reaction

Data for this reaction are very scarce and incomplete. Measured excitation functions and differential cross-sections of angular distributions of the residual deuterons, corresponding to the ground state of beryllium-8 in

the energy range $E_{\tau} = 1.0$ to 2.6 MeV, were reported in Ref. [257]. In that energy range, the partial differential cross-section at 70° and 130° increases monotonically from 0.1 to 0.7 mb/sr. The total deuteron production cross-section in this reaction is composed of two channels, corresponding to the ground and first excited states of the beryllium-8 nucleus. Measured yields of d_0 and d_1 deuterons for energies of $E_{\tau} = 3.0$ MeV [258] and 10.0 MeV [254] indicate that the ratio of the deuteron yield corresponding to the first excited state to the d_0 deuteron yield obeys the $(2J + 1)$ rule. This substantiates the assumption that compound nucleus processes contribute considerably to the ${}^7\text{Li}(\tau, d){}^8\text{Be}$ reaction. Reference [254] shows that for a τ energy of 10 MeV:

$$\sigma({}^3\text{He}, d_0) = 5.0 \pm 0.6 \text{ mb, and } \sigma({}^3\text{He}, d_1) = 25 \pm 3 \text{ mb.}$$

4.29. The ${}^7\text{Li}(\tau, t){}^7\text{Be}$ reaction

Data for this reaction can be obtained from references devoted to the study of the total beryllium-7 production cross-section in the helium-3 interaction with lithium-7 (see Table 4.57). The data used in the evaluation of this reaction and in the construction of the spline fitted curve were taken from Ref. [209]. The differential data given in Ref. [260] were integrated, and the resulting total beryllium-7 production cross-sections normalized using data published in Ref. [209]. The results of this evaluation are shown in Table 4.58 and Fig. 4.28.

4.30 The ${}^7\text{Li}(\tau/\alpha){}^6\text{Li}$ reaction

In spite of its large energy yield ($Q = 13.328$ MeV) this reaction has not attracted the attention of fusion researchers. Data that could be used for the evaluation of this reaction (see Table 4.59) have been dedicated primarily to the study of the mechanism of direct reactions in the energy region $E_{\tau} = 1$ to 10 MeV.

These measurements include partial reaction channels corresponding to the ground, first excited and second excited states of lithium-6. The angular distributions of the α_0 and α_2 groups exhibit substantial forward peaking at angles larger than 160° which indicates the presence of a cluster structure (${}^3\text{He} + t$) in the resultant lithium-6 nucleus.

Partial integral cross-sections given in Refs [261-264] were used in the derivation of the summed integral cross-section of the ${}^7\text{Li}(\tau, \alpha){}^6\text{Li}$ reaction. The data from this reaction used in constructing the evaluated partial cross-section curves were not normalized. The approximating curve representing the summed cross-section, whose coefficients are listed in Table 4.60, was obtained by adding the spline curves for the individual partial cross-sections. The evaluated curve is compared with the experimental data in Fig. 4.29. The partial integral cross-sections can be calculated by means of the summed cross-sections and corresponding ratios for the individual levels given at discrete energy points which are tabulated in Table 4.61.

4.31. The total integral cross-section for the production of neutrons in the ${}^7\text{Li}(\alpha, n){}^{10}\text{B}$ reaction

This reaction, which leads to the ground state of the boron-10 nucleus, is the inverse of the ${}^{10}\text{B}(n, \alpha){}^7\text{Li}$ reaction. Inasmuch as this (inverse) reaction is used extensively in neutron detection and neutron flux measurements, study of the boron-10 nucleus and its associated structure for excitation energies above 11.456 MeV should be of considerable interest.

The integral cross-section of the ${}^7\text{Li}(\alpha, n){}^{10}\text{B}$ reaction in the energy range from threshold to 5.5 MeV is determined by the partial integral cross-section corresponding to the ground state of the boron-10 nucleus. This energy range has been investigated in a number of experiments [265-267], but with disagreeing results. The evaluated curve was obtained on the basis of

results published in Ref. [265] which had been lowered by the authors by 10%; this corresponds to the discrepancy in the cross-section values of the ${}^7\text{Li}(p,n){}^7\text{Be}$ reference reaction which had been used by the authors of Ref. [265], and which are now considered as accepted.

Information on the integral neutron production cross-section at energies higher than 5.5 MeV, and on the total neutron yield up to 8 MeV, has been published in Ref. [21]. For high energies we have only data on the total differential cross-section at 0° , from which it appears that, in addition to the prominent peak of the excitation function of the total neutron yield cross-section at 7 MeV, three additional peaks can be seen at 10.2 MeV, 12.5 MeV and 13.7 MeV.

Values of the evaluated total integral cross-section of the ${}^7\text{Li}(\alpha,n){}^{10}\text{B}$ reaction are listed in Table 4.62; the excitation function of the differential cross-section for the total neutron yield at 0° , which was taken from Ref. [268] and normalized to results published in Ref. [265], is plotted in Fig. 4.30.

Table 4.1

Energy characteristics of individual channels for the interaction of hydrogen and helium isotopes with lithium nuclei

Input Channel	Output Channel	Energy in MeV	Reaction product decay	Decay Energy in MeV
${}^6\text{Li}+p$	${}^7\text{Be}+\gamma$	5,6064	${}^7\text{Be}(\epsilon){}^7\text{Li}$	0,8618
${}^6\text{Li}+p$	${}^6\text{Be}+n$	-5,070	${}^6\text{Be} \rightarrow {}^4\text{He}+2p$	1,372
${}^6\text{Li}+p$	${}^4\text{He}+{}^3\text{He}$	4,020	-	-
${}^6\text{Li}+d$	${}^8\text{Be}+\gamma$	22,282	${}^8\text{Be} \rightarrow 2{}^4\text{He}$	0,092
${}^6\text{Li}+d$	${}^7\text{Be}+n$	3,3818	${}^7\text{Be}(\epsilon){}^7\text{Li}$	0,862
${}^6\text{Li}+d$	${}^7\text{Li}+p$	5,026	-	-
${}^6\text{Li}+d$	${}^4\text{He}+t+p$	2,559	-	-
${}^6\text{Li}+d$	$t+{}^5\text{Li}$	0,59	${}^5\text{Li} \rightarrow {}^4\text{He}+p$	1,97
${}^6\text{Li}+d$	${}^3\text{He}+{}^5\text{He}$	0,90	${}^5\text{He} \rightarrow {}^4\text{He}+n$	0,89
${}^6\text{Li}+d$	${}^4\text{He}+{}^4\text{He}$	22,374	-	-

Table 4.1 (continued)

Input Channel	Output Channel	Energy in MeV	Reaction product decay	Decay Energy in MeV
${}^6\text{Li}+d$	${}^4\text{He}+n+{}^3\text{He}$	1,795	-	-
${}^6\text{Li}+t$	$n+{}^8\text{Be}$	16,024	${}^8\text{Be} \rightarrow 2\alpha$	0,092
${}^6\text{Li}+t$	$\alpha+{}^5\text{He}$	15,22	${}^5\text{He} \rightarrow {}^4\text{He}+n$	0,89
${}^6\text{Li}+t$	$p+{}^8\text{Li}$	0,801	${}^8\text{Li}(\beta^-){}^8\text{Be}$	16,006
${}^6\text{Li}+t$	$2n+{}^7\text{Be}$	-2,876	${}^7\text{Be}(\epsilon){}^7\text{Li}$	0,862
${}^6\text{Li}+t$	${}^3\text{He}+{}^6\text{He}$	-3,488	${}^6\text{He}(\beta^-){}^6\text{Li}$	3,507
${}^6\text{Li}+t$	$d+{}^7\text{Li}$	0,993	-	-
${}^6\text{Li}+t$	${}^9\text{B}+\gamma$	16,601	${}^9\text{B} \rightarrow {}^8\text{Be}+p$	0,185
${}^6\text{Li}+t$	${}^8\text{B}+n$	-1,975	${}^8\text{B}(\beta^+){}^8\text{Be}$	17,979
${}^6\text{Li}+t$	${}^8\text{Be}+p$	16,786	${}^8\text{Be} \rightarrow 2\alpha$	0,092
${}^6\text{Li}+t$	${}^5\text{Li}+\alpha$	14,91	${}^5\text{Li} \rightarrow p+\alpha$	1,97
${}^6\text{Li}+t$	${}^7\text{Be}+d$	0,112	${}^7\text{Be}(\epsilon){}^7\text{Li}$	0,862
${}^6\text{Li}+t$	${}^6\text{Be}+t$	-4,307	${}^6\text{Be} \rightarrow {}^4\text{He}+2p$	1,371
${}^6\text{Li}+d$	${}^{10}\text{B}+\gamma$	4,460	-	-
${}^6\text{Li}+d$	$n+{}^9\text{B}$	-3,977	${}^9\text{B} \rightarrow {}^8\text{Be}+p$	0,185
${}^7\text{Li}+p$	${}^8\text{Be}+\gamma$	17,254	${}^8\text{Be} \rightarrow 2\alpha$	0,092
${}^7\text{Li}+p$	${}^7\text{Be}+n$	-1,644	${}^7\text{Be}(\epsilon){}^7\text{Li}$	0,862
${}^7\text{Li}+p$	${}^5\text{Li}+t$	-4,43	${}^5\text{Li} \rightarrow p+\alpha$	0,89
${}^7\text{Li}+p$	${}^4\text{He}+\alpha$	17,346	-	-
${}^7\text{Li}+d$	${}^9\text{Be}+\gamma$	16,695	-	-
${}^7\text{Li}+d$	${}^8\text{Be}+n$	15,030	${}^8\text{Be} \rightarrow 2\alpha$	0,092
${}^7\text{Li}+d$	${}^4\text{He}+{}^5\text{He}$	14,23	${}^5\text{He} \rightarrow {}^4\text{He}+n$	0,89
${}^7\text{Li}+d$	${}^7\text{Be}+2n$	-3,869	${}^7\text{Be}(\epsilon){}^7\text{Li}$	0,862
${}^7\text{Li}+d$	${}^8\text{Li}+p$	-0,192	${}^8\text{Li}(\beta^-){}^8\text{Be}$	16,006
${}^7\text{Li}+d$	${}^6\text{Li}+t$	-0,993	-	-
${}^7\text{Li}+t$	${}^{10}\text{B}+\gamma$	17,250	${}^{10}\text{B}(\beta^-){}^{10}\text{B}$	0,557
${}^7\text{Li}+t$	${}^9\text{Be}+n$	10,438	-	-
${}^7\text{Li}+t$	${}^6\text{Be}+\alpha$	9,839	${}^6\text{Be}(\beta^-){}^6\text{Li}$	3,507
${}^7\text{Li}+t$	$2n+{}^8\text{Be}$	8,772	${}^8\text{Be} \rightarrow 2\alpha$	0,092
${}^7\text{Li}+t$	${}^9\text{Li}+p$	-2,386	${}^9\text{Li}(\beta^-){}^9\text{Be}$	13,606
${}^7\text{Li}+t$	${}^8\text{Li}+d$	-4,225	${}^8\text{Li}(\beta^-){}^8\text{Be}$	16,006
${}^7\text{Li}+t$	${}^{10}\text{B}+\gamma$	17,788	-	-
${}^7\text{Li}+t$	${}^9\text{B}+n$	9,351	${}^9\text{B} \rightarrow {}^8\text{Be}+p$	0,185
${}^7\text{Li}+t$	${}^9\text{Be}+p$	11,201	-	-
${}^7\text{Li}+t$	${}^8\text{Be}+d$	11,761	${}^8\text{Be} \rightarrow 2\alpha$	0,092
${}^7\text{Li}+t$	${}^7\text{Be}+t$	-0,881	${}^7\text{Be}(\epsilon){}^7\text{Li}$	0,862
${}^7\text{Li}+t$	${}^6\text{Li}+\alpha$	13,321	-	-
${}^7\text{Li}+\alpha$	${}^{10}\text{B}+n$	-2,790	-	-

Table 4.2

Spline fit coefficients for the description of the ${}^6\text{Li}(p,\gamma){}^7\text{Be}$ integral reaction cross-section (The cross-section can be calculated using Eq. (2.13))

Knot no.	Knot energy in MeV	Spline fit coefficients				Cross section uncert., %
		A_0	A_1	A_2	A_3	
I	0,157	-8,471	5,622	-5,182	1,931	15
2	0,345	-6,314	1,055	-0,623	0,160	7
3	1,174	-5,663	0	0	0	14

Table 4.3

Ratios of partial cross-section values for the ${}^6\text{Li}(p,\gamma_0){}^7\text{Be}$ and ${}^6\text{Li}(p,\gamma_1){}^7\text{Be}$ reactions

Energy in MeV	$\sigma_{\gamma_0}/\sigma_{\gamma_1}$	Energy in MeV	$\sigma_{\gamma_0}/\sigma_{\gamma_1}$
0,4	2	0,8	1,7
0,5	1,6	0,9	1,6
0,6	1,6	1,0	1,7
0,7	1,8	1,1	1,7

Table 4.4

Integral neutron production cross-sections of the ${}^6\text{Li}(p,x)n$ reaction

Energy in MeV	Cross Sect.	Uncertainty	Energy in MeV	Cross Sect.	Uncertainty
5,700	0,00	0,00	6,700	22,30	2,50
5,800	2,10	0,00	6,800	24,40	2,70
5,900	5,30	0,50	6,900	26,40	3,00
6,000	8,40	0,80	7,000	29,50	3,40
6,100	9,40	0,90	7,100	30,50	3,70
6,200	11,80	1,20	7,200	32,60	4,00
6,300	14,00	1,40	7,300	34,70	4,30
6,400	16,10	1,60	7,400	36,80	4,60
6,500	18,20	2,00	7,500	39,00	4,90

Table 4.4 (continued)

Energy in MeV	Cross Sect.	Uncertainty	Energy in MeV	Cross Sect.	Uncertainty
6,600	20,20	2,20	7,600	41,00	5,20
7,700	42,90	5,50	10,600	94,70	13,70
7,800	44,80	5,80	10,700	95,90	14,00
7,900	46,70	6,00	10,800	97,00	14,20
8,000	48,60	6,30	10,900	98,00	14,40
8,100	50,50	6,60	11,000	98,90	14,60
8,200	52,40	6,90	11,100	99,80	14,80
8,300	54,30	7,20	11,200	100,60	15,00
8,400	56,20	7,50	11,300	101,50	15,20
8,500	58,10	7,80	11,400	102,20	15,40
8,600	60,00	8,00	11,500	104,00	15,60
8,700	62,00	8,30	11,600	104,70	15,80
8,800	64,00	8,60	11,700	105,40	16,00
8,900	66,00	8,90	11,800	106,10	16,20
9,000	68,00	9,20	11,900	106,80	16,40
9,100	69,90	9,50	12,000	107,50	16,60
9,200	71,80	9,80	12,100	108,20	16,80
9,300	73,70	10,10	12,200	108,90	17,00
9,400	75,60	10,40	12,300	109,80	17,10
9,500	77,50	10,70	12,400	110,40	17,20
9,600	79,20	11,00	12,500	111,00	17,30
9,700	80,90	11,30	12,600	111,60	17,40
9,800	82,60	11,60	12,700	112,20	17,50
9,900	84,30	11,90	12,800	112,80	17,60
10,000	86,00	12,20	12,900	113,40	17,70
10,100	87,50	12,40	13,000	114,00	17,80
10,200	89,00	12,70	13,100	114,60	17,90
10,300	90,30	12,90	13,200	115,20	18,00
10,400	91,80	13,20	13,300	115,80	18,00
10,500	93,20	13,50	13,400	116,40	18,00
13,500	117,00	18,00	13,800	118,20	18,00
13,600	117,60	18,00	13,900	119,40	18,00
13,700	118,20	18,00	14,000	120,00	18,00

Table 4.5

Brief data content of references used in the evaluation of the ${}^6\text{Li}(p,\alpha){}^3\text{He}$ reaction cross-section

Energy range in MeV	Range of angles in deg	Type of data	Uncertainty in %		Ref.
			random	system.	
0,025-0,05	4 π	EXC, SIG	15	20	[154]
0,04 -0,24	90	EXC, DA	30	50	[155]
0,05 -0,19	60-120	AND, DA	10	10	[156]
0,1 -0,7	37-160	AND, DA	10	14	[157]
0,14 -3,0	35-155	AND, DA	7	10	[158]
0,15; 0,317	35-150	AND, DA	8	12	[159]
0,3 -1,0	10-160	AND, DA	10	20	[160]
1,9 -5,0	20-160	AND, DA	15	20	[161]
0,1 -0,18	4 π	EXC, SIG	10	15	[162]
3,0 -12,0	25-155	AND, DA	10	15	[163]
9,0 -12,0	10-170	AND, DA	10	20	[164]
12 -18,5	10-170	AND, DA	4	10	[165]

Table 4.6

Spline fit coefficients to describe the ${}^6\text{Li}(p,\alpha){}^3\text{He}$ integral reaction cross-section
(The cross-section can be calculated using Eq. (2.13)) -

Knot no.	Knot energy in MeV	Spline fit coefficients				Cross section uncert., %
		λ_0	λ_1	λ_2	λ_3	
1	0,010	-16,89	13,84	-3,318	0,2728	20
2	0,050	-2,069	5,285	-1,148	-0,0030	15
3	0,140	2,149	2,914	-1,157	0,157	10
4	0,955	4,592	0,210	-0,251	4,0539	10
5	1,543	5,084	2,773	5,589	-94,33	10
6	1,780	5,319	-1,386	0,791	-0,2949	10
7	18,5	2,629	-2,529	-1,280	-0,2949	20

Table 4.7

Brief data content of references used in the evaluation of the ${}^6\text{Li}(d,n){}^7\text{Be}$ integral reaction cross-section

Energy range in MeV	Range of angles in deg	Type of data	Uncertainty in %		Ref.
			random	system.	
0,1-0,18	4 π	UND/EXC, SIG	10	30	[166]
0,2-1,0	30-150	AND, DA, n_0, n_1	8	15	[167]
0,5-3,0	100	EXC, DA, $n_1 + \gamma$	10	20	[168]
1,3-12,0	4 π	EXC, SIG, $n_0 + n_1$	10	20	[169]
12-19,0	57	EXC, DA, $n_0 + n_1$	20	40	[170]
2,9-11,0	55	EXC, DA, n_1	10	15	[171]
3,0-11	20-160	UND/EXC, DA	10	15	[172]
0,1-2,2	90	UND/EXC, DA	20	30	[173]
0,6-4,9	0	UND/EXC, DA	20	50	[174]

Table 4.8

Spline fit coefficients for the description of the ${}^6\text{Li}(d,n){}^7\text{Be}$ integral reaction cross-section
(The cross-section can be calculated using Eq. (2.13)) -

Knot no.	Knot energy in MeV	Spline fit coefficients				Cross section uncert., %
		λ_0	λ_1	λ_2	λ_3	
1	0,016	-18,01	14,20	-2,931	0,1954	10
2	0,163	1,611	3,749	-1,569	0,2134	6
3	1,666	4,526	-0,088	-0,083	-0,059	4
4	17,0	3,138	0	0	0	8

Table 4.9

Total integral neutron production cross-sections for the ${}^6\text{Li}+d$ interaction

Energy in MeV	Cross section in mb	Energy in MeV	Cross section in mb
3,0	319	5,6	321
2,2	320	5,8	322
3,4	321	6,0	328
3,6	322	6,5	338
3,8	321	7,0	344
4,0	322	7,5	349
4,2	325	8,0	350
4,4	324	8,5	358
4,6	323	9,0	352
4,8	322	9,5	344
5,0	322	10	340
5,2	321	10,5	331
5,4	320	11	322

Table 4.10

Brief data content of references used in the evaluation of the ${}^6\text{Li}(d,p){}^7\text{Li}$ reaction cross-section

Energy range in MeV	Range of angles in deg	Type of data	Uncertainty in %		Ref.
			random	system.	
0,1-1,0	20-160	AND, DA, p_0, p_1	3	8	[167]
0,3-1,0	20-160	AND, DA, p_0, p_1	5	20	[160]
0,5-3,4	25-160	AND, DA, p_0, p_1	5	10	[168]
0,03-0,2	90	EXC, DA, p_0, p_1	20	20	[155]
4,5-5,5	15-165	AND, DA, p_0, p_1	10	20	[176]
12	10-160	AND, DA, p_0, p_1	-	15	[177]
0,1-0,18	45-165	EXC, SIG, $p_0 + p_1$	10	20	[178]
2,9-11,0	55	EXC, DA, p_1	10	15	[171]

Table 4.11

Spline fit coefficients for the description of the recommended ${}^6\text{Li}(d,p){}^7\text{Li}$ partial reaction cross-section
(The cross-section can be calculated using Eq. (2.13))

Reaction channel	Knot no.	Knot energy in MeV	Spline fit coefficients				Cross-section uncert., %
			λ_0	λ_1	λ_2	λ_3	
$d p_0$	I	0,028	-10,84	9,804	-1,924	0,090	2I
	2	0,211	1,854	3,133	-1,379	0,182	6
	3	1,592	4,055	-0,214	-0,278	0,085	3,3
	4	12,00	3,187	0,000	0,000	0,000	14
$d p_1$	I	0,027	-13,97	12,06	-3,263	0,378	7
	2	0,206	0,241	3,488	-0,955	0,038	7
	3	1,572	3,699	0,070	-0,726	0,215	4
	4	12,00	2,643	0,000	0,000	0,000	10

Table 4.12

Ratio of partial integral cross-sections for the ${}^6\text{Li}(d,p){}^7\text{Li}$ reaction corresponding to the ground and first excited states of the lithium-7 nucleus

Energy in MeV	$\sigma_{d p_0} / \sigma_{d p_1}$
0,030	12,95
0,100	5,11
0,200	4,70
0,600	2,48
1,000	1,75
1,500	1,45
5,000	1,54
12,00	1,72

Table 4.13

Values of the t and γ parameters of Eq. (4.1) for different reaction channels of the ${}^6\text{Li}+d$ interaction
(Note: these parameters were calculated using the values $B_c=0$ and $r=4.3$ fm)

Channel	t (in MeV.b)	γ
${}^6\text{Li}(d,p_0){}^7\text{Li}$	82 ± 9	$-0,43 \pm 0,04$
${}^6\text{Li}(d,p_1){}^7\text{Li}$	42 ± 8	$-0,02 \pm 0,12$
${}^6\text{Li}(d,n_0){}^7\text{Be}$	63 ± 7	$-0,52 \pm 0,05$
${}^6\text{Li}(d,n_1){}^7\text{Be}$	37 ± 7	$-0,17 \pm 0,11$
${}^6\text{Li}(d,n){}^3\text{He}+{}^4\text{He}$	63 ± 16	$-0,35 \pm 0,12$
${}^6\text{Li}(d,\alpha){}^4\text{He}$	43 ± 4	$-0,58 \pm 0,03$

Table 4.14

Spline fit coefficients to describe the integral cross-section for total tritium yield in the ${}^6\text{Li}(d,t){}^3\text{Li}$ reaction
(The cross-section can be calculated using Eq. (2.13))

Knot no.	Knot energy in MeV	Spline fit coefficients				Cross section uncert., %
		λ_0	λ_1	λ_2	λ_3	
I	0,1135	0,0454	4,006	-0,1797	-0,2987	4,7
2	0,4176	4,298	2,018	-1,347	0,321	1,5
3	3,909	5,663	0	0	0	1,5

Table 4.15

Legendre polynomial coefficients to calculate the angular distribution of neutrons from the ${}^6\text{Li}(d,n+\tau){}^4\text{He}$ reaction

Energy in MeV	B_0	B_1	B_2	B_3	B_4	Cross-section in mb
	mb/sr					
0,204	0,586	0,052	-	-	-	$7,36 \pm 1,1$
0,238	0,779	-0,028	0,119	-	-	$9,79 \pm 1,6$
0,375	2,217	0,516	0,020	-	-	$27,9 \pm 4,2$
0,578	3,984	1,485	0,439	-	-	$50,1 \pm 7,5$
0,779	5,883	2,628	0,455	0,500	0,669	$73,9 \pm 10,4$

Table 4.16

Brief data content of references used in the evaluation of the ${}^6\text{Li}(d,\alpha){}^4\text{He}$ reaction cross-section

Energy range in MeV	Range of angles in deg	Type of data	Uncertainty in %		Ref.
			random	system.	
0,1-0,180	2°	EXC, SIG	8	10	[182]
0,05-0,300	2°	EXC, SIG	5	30	[183]
0,3-1,2	20-160	AND, DA	3	8	[167]
0,07-0,45	90	EXC, DA	7	20	[184]
0,03-0,25	90	EXC, DA	15	25	[155]
0,5-10	80-165	AND, DA	20	25	[185]
0,3-1,0	10-160	AND, DA	5	20	[160]
1,0-11,5	3,5-90	AND, DA	5	20	[186]
0,96-5,0	10-90	AND, DA	3	10	[168]
14,8	15-100	AND, DA	20	30	[181]
2,1-10,9	20-80	AND, DA	10	25	[187]
2,16-5,87	20-160	AND, DA	5	15	[188]

Table 4.17

Spline fit coefficients for the description of the recommended ${}^6\text{Li}(d,\alpha){}^4\text{He}$ integral reaction cross-section (The cross section can be calculated using Eq. (2.13))

Knot no.	Knot energy in MeV	Spline fit coefficients				Cross-section uncert., %
		λ_0	λ_1	λ_2	λ_3	
I	0,029	-10,35	9,114	-1,116	-0,178	23,0
2	0,285	2,514	1,231	0,840	-1,173	4,9
3	0,623	3,431	0,384	-1,920	0,986	3,0
4	3,604	3,521	2,755	-32,966	67,91	3,1
5	4,220	3,402	-2,576	-0,837	1,206	2,6
6	14,80	1,234	0	0	0	11,0

Table 4.18

Brief data content of references used in the evaluation of the ${}^6\text{Li}(t,x)n$ and ${}^6\text{Li}(t,2n){}^7\text{Be}$ reaction cross-sections

Energy range in MeV	Range of angles in deg	Type of data	Uncertainty in %		Ref.
			random	system.	
0,14-1,4	0	EXC, DA	5	10	[192]
0,1-0,3	90	EXC, DA	10	30	[193]
3,8-11,4	30-150	UND/EXC, SIG	5	15	[172]
0,18-2,4	30-150	UND/AND, DA	10	20	[194]
5,4-10	55	EXC, DA	10	15	[171]
4,4-12	4°	UND/EXC, SIG	10	15	[169]

Table 4.19

Spline fit coefficients for the description of the evaluated total neutron production ${}^6\text{Li}+t$ interaction cross-section
(The cross-section can be calculated using Eq. (2.13))

Knot no.	Knot energy in MeV	Spline fit coefficients				Cross-section uncert., %
		λ_0	λ_1	λ_2	λ_3	
I	0,100	-3,753	7,124	-1,963	0,203	0
2	0,708	4,191	1,77	-0,772	0,180	20
3	5,675	6,153	0,896	-2,031	0,762	11
4	11,42	6,047	-0,827	0	0	19

Table 4.20

Spline fit coefficients for the description of the recommended ${}^6\text{Li}(t,2n){}^7\text{Be}$ total cross-section for the production of beryllium-7 in the ground and first excited states (The cross-section can be calculated using Eq. (2.10))

State of ${}^7\text{Be}$	Knot no.	Knot Energy in MeV	Spline fit coefficients				Cross section uncert., %
			A_0	A_1	A_2	A_3	
Ground + first excited	I	4,810	10,20	21,33	-1,97	0,008	0,7
	2	12,00	64,77	-5,72	0	0	1,2
First excited	I	5,43	2,19	3,80	-0,297	-0,0008	0,6
	2	9,95	13,25	1,07	0	0	0,7

Table 4.21

Brief data content of references used in the evaluation of the ${}^6\text{Li}(t,p){}^8\text{Li}$ reaction cross-section

Energy range in MeV	Range of angles in deg	Type of data	Uncertainty in %		Ref.
			random	system.	
2,0-10	4%	WHD/EXC, SIG	5	5	[195]
0,3-1,0	4%	EXC, SIG	10	-	[196]
3,0-9,5	55	EXC, DA	10	15	[171]

Table 4.22

Spline fit coefficients for the description of the ${}^6\text{Li}(t,p){}^8\text{Li}$ excitation function for the production of lithium-8 (The cross section can be calculated using Eq. (2.13))

Knot no.	Knot energy in MeV	Spline fit coefficients				Cross section uncert., %
		A_0	A_1	A_2	A_3	
I	0,100	-5,427	7,124	-2,360	0,553	30
2	0,273	-0,0856	4,054	-0,691	-0,196	34
3	2,180	3,599	-1,350	-1,912	26,68	20
4	2,433	3,463	-0,808	6,855	-7,492	18
5	4,071	3,842	0,294	-4,714	4,504	18
6	5,682	3,583	-1,347	-0,208	0,381	18
7	20,00	2,318	0	0	0	29

Table 4.23

Values of the partial differential cross-sections for the ${}^6\text{Li}(t,p){}^8\text{Li}$ reaction at an angle of 55°

Energy in MeV	Cross section in mb/sr	Energy in MeV	Cross section in mb/sr
2,89	0,832	6,44	0,886
3,40	1,018	6,94	0,855
3,91	0,884	7,44	0,937
4,42	0,767	7,95	0,663
4,92	0,928	8,45	0,641
5,43	0,974	9,45	0,673
5,93	1,097		

Table 4.24

Spline fit coefficients for the description of the recommended ${}^6\text{Li}(t,d){}^7\text{Li}$ reaction cross-section (The cross-section can be calculated using Eq. (2.10))

State	Knot no.	Knot Energy in MeV	Spline fit coefficients				Cross section uncert., mb
			A_0	A_1	A_2	A_3	
Ground state	I	0,088	3,333	-20,40	718,5	-419,0	0,3
	2	1,200	292,9	23,15	109,6	-120,6	15
	3	1,726	317,9	38,34	-80,78	126,5	16
	4	2,252	334,1	58,40	118,9	-193,2	17
	5	2,779	369,4	23,03	-186,1	190,6	18
	6	3,305	358,0	-14,52	-11,77	6,359	18
	7	4,150	341,2	-20,79	4,348	-4,033	17
	8	5,600	307,8	-33,62	-13,20	8,979	16
	9	7,050	258,7	-15,26	25,86	-9,998	15
	10	8,500	260,5	-3,308	-17,62	7,347	16
	11	9,950	241,1	0	0	0	18
First excited state	I	0,100	0,0079	0,563	60,79	-15,49	0,05
	2	2,700	140,2	2,605	-9,055	2,470	1,8
	3	4,150	132,5	-8,076	1,689	-1,566	1,7
	4	5,600	119,6	-13,06	-5,125	3,487	1,6
	5	7,050	100,5	-5,925	10,04	-3,883	1,6
	6	8,500	101,2	-1,285	-6,845	2,853	1,6
	7	9,950	93,62	0	0	0	2,0

Table 4.25

Spline fit coefficients for the description of the recommended ${}^6\text{Li}(t,n){}^8\text{B}$ integral reaction cross-section (The cross section can be calculated using Eq. (2.13))

Knot no.	Knot energy in MeV	Spline fit coefficients				Cross section uncert., %
		A_0	A_1	A_2	A_3	
I	2,998	0,387	22,56	-129,9	278,9	9,2
2	3,710	1,997	5,225	-7,897	2,814	7,1
3	12,686	1,714	-1,432	2,482	-4,341	1,3
4	21,680	0,992	0	0	0	2,0

Table 4.26

Brief data content of references used in the evaluation of the ${}^6\text{Li}(t,p)$ interaction cross-section

Energy range in MeV	Range of angles in deg	Type of data	Channel	Uncertainty in %		Ref.
				random	system.	
0,5-1,85	0-155	AND, DA	(τ, p)	3	5	[200]
0,5-1,85	0-155	AND, DA	($\tau, 2\alpha$)	10	15	[200]
3-6	20-150	AND, DA	(τ, p)	10	15	[203]
3-6	20-150	AND, DA	($\tau, 2\alpha$)	15	25	[203]
5-17	10-170	AND, DA	(τ, p)	20	-	[202]
14	20-100	AND, DA	(τ, p)	10	25	[204]
1-5	10-150	AND, DA	(τ, p)	20	-	[201]

Table 4.27

Spline fit coefficients for the description of the recommended ${}^6\text{Li}(t,p){}^8\text{Be}$ partial reaction cross-section (The cross-section can be calculated using Eq. (2.13))

Channel	Knot no.	Knot energy in MeV	Spline fit coefficients				Cross section uncert., %
			A_0	A_1	A_2	A_3	
p_0	I	0,461	-3,928	11,68	-7,682	1,729	18
	2	1,900	2,112	0,320	-0,339	-0,0549	5
	3	10,00	1,458	0	0	0	5
p_1	I	0,657	-0,0117	9,314	-9,206	3,204	9
	2	1,744	3,289	0,501	0,181	-0,3568	5
	3	10,00	2,817	0	0	0	7

Table 4.28

Integral proton production cross-sections of the ${}^6\text{Li}(\tau, p){}^8\text{Be}$ reaction corresponding to the 16.63 and 16.92 MeV excited levels and to the multi-particle ${}^6\text{Li}+\tau$ interaction channels

Energy in MeV	Cross section in mb		
	Continuous spectrum	16.63 level	16.92 level
0,660	5,98	-	-
0,755	18,1	-	-
0,849	34,2	8,55	-
0,949	46,2	7,92	1,01
1,063	63,8	8,67	3,02
1,163	70,0	9,30	4,78
1,271	80,4	11,8	6,41
1,370	82,2	13,5	7,54
1,470	80,4	15,0	8,42
1,568	90,9	15,1	12,2
1,648	82,8	15,8	9,05
1,745	80,2	15,8	8,80
1,847	88,0	18,7	10,7

Table 4.29

Brief data content of references used in the evaluation of the ${}^6\text{Li}(\tau, d){}^7\text{Be}$ interaction cross-section

Energy range in MeV	Range of angles in deg	Type of data	Uncertainty in %		Ref.
			random	system.	
I,3-I,6	10-170	PAR/AND, DA	10	25	[200]
I,3-I,6	10-170	PAR/AND, DA	10	25	[206]
I,0-2,0	90	PAR/EXC, DA	5	20	[207]
I,7-5,9	4%	UND/EXC, SIG	5	7	[205]
8,0-20	10-160	PAR/AND, DA	5	12	[208]
I,8-6,8	4%	UND/EXC, SIG	5	15	[209]

Table 4.30

Spline fit coefficients for the description of the recommended ${}^6\text{Li}(\tau, d){}^7\text{Be}$ integral reaction cross-section (The cross section can be calculated using Eq. (2.13))

Knot no.	Knot energy in MeV	Spline fit coefficients				Cross section uncert., %
		A_0	A_1	A_2	A_3	
1	0,4090	-0,28702	5,5994	0	0	10
2	0,8687	3,93092	5,5944	-3,9408	-4,7839	6
3	1,122	5,026	2,637	-3,648	2,220	4,4
4	1,868	5,717	0,649	-0,256	-0,177	3,7
5	6,890	5,732	0	0	0	8,9

Table 4.31

Brief data content of references used in the evaluation of the integral gamma ray yield ${}^7\text{Li}(p, \gamma){}^8\text{Be}$ cross-section

Energy range in MeV	Range of angles in deg	Type of data, channel	Uncertainty in %		Ref.
			random	system.	
0,08-0,226	4%	UND/EXC, SIG	20	30	[210]
0,3-0,64	4%	UND/EXC, SIG	20	30	[211]
0,9-1,24	4%	UND/EXC, SIG	7	15	[212]
I,7-16,1	90	PAR/EXC, DA, τ, τ	5	10	[213]
I,7-16,1	0-140	PAR/AND, DA, τ, τ	5	10	[213]
0,8-1,7	0-135	PAR/AND, DA, τ, τ	5	-	[214]
0,43-1,95	90;120	PAR/EXC, DA, τ, τ	7	13	[215]

Table 4.32

Spline fit coefficients for the description of the ${}^7\text{Li}(p, \gamma){}^8\text{Be}$ gamma-ray production integral reaction cross-section (The cross-section can be calculated using Eq. (2.13))

Knot no.	Knot energy in MeV	Spline fit coefficients				Cross section uncert., %
		A_0	A_1	A_2	A_3	
1	0,0900	-9,675	11,765	-9,743	3,321	10
2	0,3790	-3,029	4,346	4,583	1944,2	7
3	0,4182	-0,708	-23,14	4981,9	-77947,	10
4	0,4313	1,033	61,59	-2237,5	14276,2	4
5	0,4830	0,054	-15906	4,89 $\cdot 10^7$	-5,02 $\cdot 10^{10}$	38
6	0,4832	-1,669	-3,608	4,798	-0,2244	9
7	1,0090	-1,814	-2,205	3,021	0,407	3
8	2,0590	-1,702	-2,747	6,275	-3,201	3
9	4,680	-1,500	1,082	-1,560	-0,1237	2
10	18,000	-2,570	0	0	0	4

Table 4.33

Brief data content of references (supplementing information given in [216]) used in the evaluation of the ${}^7\text{Li}(p, n){}^7\text{Be}$ reaction

Energy range in MeV	Range of angles in deg	Type of data	Uncertainty in %		Ref.
			random	system.	
I,8-4,2	4%	EXC, SIG	4	7	[217]
4,2-26	3-159	AND, DA	4	15	[218]
3-8	55	EXC, DA	10	10	[171]
I,8-6,0	90	EXC, DA	10	10	[219]
4-14	4%	EXC, SIG	20	-	[151]

Table 4.34

Values of integral cross-sections and Legendre coefficients for the ${}^7\text{Li}(p, n){}^7\text{Be}$ reaction (ground state)

Energy in MeV	$4\pi B_0$ in mb	B_1/B_0	B_2/B_0	B_3/B_0	B_4/B_0	B_5/B_0
I,8876	50	-	-	-	-	-
I,890	220	-	-	-	-	-
I,895	270	-	-	-	-	-
I,905	285	-	-	-	-	-
I,925	275	-	-	-	-	-
I,950	270	-0,100	0,000	-	-	-
2,000	269	-0,210	0,001	-	-	-
2,050	275	-0,457	0,010	-	-	-
2,100	300	-0,467	0,020	-	-	-
2,150	390	-0,315	0,039	-	-	-
2,200	490	0,136	0,092	-	-	-
2,250	590	0,664	0,145	-	-	-
2,300	508	0,905	0,200	-	-	-
2,350	420	0,956	0,217	-	-	-
2,400	380	1,000	0,250	-	-	-
2,450	315	0,903	0,243	-	-	-
2,500	300	0,816	0,224	-	-	-
2,600	285	0,642	0,193	-	-	-
2,700	280	0,547	0,162	-	-	-
2,800	270	0,559	0,136	-	-	-
2,900	260	0,603	0,120	-	-	-
3,000	251	0,635	0,103	-	-	-
3,200	245	0,607	0,103	-	-	-
3,400	242	0,550	0,110	-	-	-
3,600	242	0,461	0,125	-0,0023	-	-
3,800	244	0,401	0,153	-0,100	-	-
4,000	250	0,308	0,198	-0,136	-0,100	-
4,200	268	0,270	0,28	-0,20	0,000	-0,200
4,400	300	0,260	0,418	-0,26	-	-
4,600	330	0,235	0,515	-0,235	-	-
4,800	355	0,215	0,595	-0,157	-	-
5,000	376	0,152	0,610	-0,076	0,200	-0,19
5,200	352	0,057	0,593	-0,024	-	-
5,400	326	-0,038	0,542	0,023	-	-
5,600	285	-0,122	0,489	0,072	-	-
5,800	264	-0,186	0,455	0,110	-	-
6,000	233	-0,237	0,421	0,132	0,200	-0,18
6,200	207	-0,282	0,391	0,159	-	-
6,400	185	-0,315	0,316	0,173	-	-
6,600	162	-0,331	0,355	0,181	-	-
6,800	140	-0,341	0,335	0,188	-	-
7,000	121	-0,356	0,327	0,199	-	-
7,500	92	-	-	-	-	-
8,000	74	-	-	-	-	-

Table 4.34 (continued)

Energy in MeV	$4\pi B_0$ in mb	B_1/B_0	B_2/B_0	B_3/B_0	B_4/B_0	B_5/B_0
8,500	63	-	-	-	-	-
9,000	55	-	-	-	-	-
9,500	49	-	-	-	-	-
10,00	45	-	-	-	-	-
11,00	38	-	-	-	-	-
12,00	34	-	-	-	-	-
13,00	30	-	-	-	-	-
14,00	28	-	-	-	-	-
15,00	26	-	-	-	-	-
16,00	24	-	-	-	-	-
17,00	23	-	-	-	-	-
18,00	22	-	-	-	-	-
19,00	21	-	-	-	-	-
20,00	20	-	-	-	-	-

Table 4.35

Values of integral cross-sections and Legendre coefficients for the ${}^7\text{Li}(p,n){}^7\text{Be}$ reaction (first excited state)

Energy in MeV	$4\pi B_0$ in mb	B_1/B_0	B_2/B_0	B_3/B_0
2,4	3,41	0	-	-
2,5	7,62	0	-0,005	-0,005
2,6	14,1	-0,023	-0,018	-0,046
2,7	22,8	0	0	-0,114
2,8	32,4	-0,143	-0,075	-0,133
2,9	41,9	-0,177	-0,125	-0,128
3,0	50,0	-0,188	-0,167	-0,114
3,1	55,9	-0,210	-0,186	-0,079
3,2	59,0	-0,223	-0,185	-0,056
3,3	61,2	-0,247	-0,154	-0,037
3,4	61,0	-0,276	-0,124	-0,012
3,5	59,7	-0,309	-0,073	+0,013
4,0	49,4	-0,457	0,328	-0,090
4,5	43,2	-0,481	0,477	-0,221
5,0	39,8	-0,447	0,537	-0,276
5,5	37,8	-0,060	0,738	-0,336
6,0	36,7	0,252	0,777	-0,087
6,5	36,0	0,312	0,411	0,062
7,0	35,3	0,296	0,119	0,067
8,0	32,2	-	-	-
9,0	29,7	-	-	-
10,0	23,8	-	-	-

Table 4.35 (continued)

Energy in MeV	$4\pi B_0$ in mb	B_1/B_0	B_2/B_0	B_3/B_0
11,0	18,5	-	-	-
12,0	14,3	-	-	-
13,0	11,4	-	-	-
14,0	9,6	-	-	-
15,0	8,6	-	-	-
16,0	8,2	-	-	-
17,0	8,2	-	-	-
18,0	8,4	-	-	-
19,0	8,6	-	-	-
20,0	8,8	-	-	-

Table 4.36

Total integral neutron production cross-sections of the ${}^7\text{Li}-p$ interaction

Energy in MeV	Cross section in mb	Energy in MeV	Cross section in mb
4,0	300	5,0	500
4,2	325	5,2	460
4,4	350	5,4	420
4,6	425	5,6	380
4,8	450	5,8	360
6,0	325	9,5	200
6,2	320	10,0	180
6,4	290	10,5	200
6,6	270	12,0	185
6,8	265	12,5	195
7,0	255	13,0	180
7,5	255	13,5	190
8,0	240	14,0	200
8,5	220		
9,0	210		

Table 4.37

Brief data content of references used in the evaluation of the ${}^7\text{Li}(p,\alpha){}^4\text{He}$ reaction cross-section

Energy range in MeV	Range of angles in deg	Type of data	Uncertainty in %		Ref.
			random	system.	
0,05-0,9	30-90	AND, DA	8	10	[223]
0,023-0,05	2 π	EXC, SIG	12	20	[154]
0,13-0,56	20-90	AND, DA	7	15	[159]
0,025-0,236	2 π	EXC, SIG	15	25	[155]
1,01-1,47	90;120	EXC, DA	10	15	[220]
1,3-11,8	80-165	AND, DA	10	15	[221]
2,7-10,3	90-170	AND, DA	10	15	[228]
0,4-2,4	125;90	EXC, DA	5	8	[215]
0,075-0,6	90	EXC, DA	10	20	[226]
4-12	80-165	AND, DA	10	-	[227]

Table 4.38

Spline fit coefficients for the description of the recommended ${}^7\text{Li}(p,\alpha){}^4\text{He}$ integral reaction cross-section (The cross section can be calculated using Eq. (2.13))

Knot no.	Knot energy in MeV	Spline fit coefficients				Cross section uncert., %
		λ_0	λ_1	λ_2	λ_3	
I	0,020	-13,208	14,140	-10,453	4,669	20
2	0,035	-7,7505	6,8267	-2,6140	0,5652	I3
3	0,0675	-4,2368	4,1264	-1,5014	0,4991	I4
4	0,2664	-0,1082	2,8267	-1,7242	0,5442	I4
5	2,548	3,7495	3,3653	2,1621	-49,34	I4
6	3,416	3,6805	-8,0709	-0,3650	9,4684	I4
7	4,429	1,7246	-6,3422	7,0168	414,20	I4
8	5,175	2,4667	25,906	-202,45	435,93	I4
9	6,061	3,2249	-5,4209	4,2600	7,3228	I4
10	8,406	2,1638	-0,2846	11,445	-36,403	I4
II	11,84	1,9458	0	0	0	20

Table 4.39

Brief data content of references used in the evaluation of the total integral neutron and beryllium-7 production cross-sections in ${}^7\text{Li}+d$ interactions

Energy range in MeV	Range of angles in deg	Type of data	Uncertainty in %		Ref.
			random	system.	
0,64	0-160	PAR/AND, DA; n_0	10	-	[231]
0,2-2,0	90	UND/EXC, DA;	10	50	[173]
1,62-2,97	4-160	PAR/AND, DA; n_0, n_1	10	15	[232]
I, I-4, I	I20	PAR/EXC, DA; n_0, n_1	-	-	[232]
I, 0	0-I40	PAR/AND, DA; n_0, n_1	20	-	[233]
2,8-II	0-160	UND/EXC, SIG	5	15	[172]
2,9-II	55	UND/EXC, DA; $2n$	10	15	[171]
I,3-I2	4 π	UND/EXC, SIG	10	10	[169]

Table 4.40

Spline fit coefficients for the description of the evaluated total neutron production cross-sections in ${}^7\text{Li}+d$ interaction channels (The cross-section can be calculated using Eq. (2.11))

Knot no.	Knot energy in MeV	Spline fit coefficients				Cross section uncert., mb
		A_0	A_1	A_2	A_3	
I	0,134	6,722	-14,60	140,26	-54,82	0,669
2	0,283	51,65	103,3	16,75	541,9	2,266
3	0,599	368,2	1045,4	12111	-94308	0,238
4	0,664	500,2	604,9	-16471	68790	0,318
5	0,734	464,1	-616,9	4376,9	-21921	0,292
6	0,812	423,9	-403,7	-226,7	51996	0,277
7	0,898	413,6	730,3	13492	142090	0,264
8	0,994	478,6	-89,40	-29570	204890	0,281
9	I,1	297,7	-595,6	10,79	1370,3	0,118
10	I,473	252,7	417,3	2308,6	-4488,2	0,170
11	2,0	463,9	-594,3	-592,7	-444,0	0,478
12	2,809	579,9	36,83	-1045,9	1454,9	0,204
13	3,951	528,7	-169,6	439,1	85,45	8,979
14	5,551	525,2	158,8	526,3	-1638,6	9,507
15	7,799	575,7	-52,06	-1146,1	4754,4	10,71
16	10,957	612,3	0	0	0	22,99

Table 4.41

Beryllium-7 production cross-sections in ${}^7\text{Li}+d$ interactions (The uncertainties given in parentheses are expressed in last significant figures of the cross-section values)

${}^7\text{Li}(d,2n){}^7\text{Be}$		${}^7\text{Li}(d,2n){}^7\text{Be}$ ($E_x=0,43$)	
Energy in MeV	Total cross-section in mb	Energy in MeV	Partial cross-section in mb
5,38	12,90(37)	6,20	2,0(11)
5,89	22,30(60)	6,70	2,76(28)
6,40	22,10(77)	6,96	3,39(28)
6,90	34,40(90)	7,21	4,14(62)
7,41	39,6(14)	7,46	3,01(28)
7,91	42,6(14)	7,96	4,27(75)
8,42	47,9(16)	8,46	6,66(38)
9,18	53,9(18)	8,96	8,66(176)
9,43	55,5(23)	9,22	9,67(75)
9,93	58,4(22)	9,72	8,79(151)
10,43	60,9(24)	9,97	10,2(10)
10,93	63,2(24)	10,22	9,29(163)
11,44	61,8(25)	10,72	10,17(62)
11,94	62,1(25)	10,97	10,80(75)

Table 4.42

Brief data content of references used in the evaluation of the ${}^7\text{Li}(d,p){}^6\text{Li}$ reaction cross-section

Energy range in MeV	Range of angles in deg	Type of data	Uncertainty in %		Ref.
			random	system.	
0,3-4,0	4 π	EXC, SIG	10	20	[168]
0,6-I,6	4 π	EXC, SIG	10	15	[234]
0,6-I,9	4 π	EXC, SIG	5	50	[235]
2,0-10	4 π	EXC, SIG	10	20	[236]
0,6-I,2	4 π	EXC, SIG	5	10	[237]
0,76-0,79	75-135	AND, DA	5	9	[238]
0,68-0,90	50	EXC, DA	5	9	[238]
2,9-II	55	EXC, DA	10	15	[171]

Table 4.43

Spline fit coefficients for the description of the evaluated ${}^7\text{Li}(d,p){}^6\text{Li}$ integral reaction cross-section

Knot no.	Knot energy in MeV	Spline fit coefficients				Cross section uncert., mb
		A_0	A_1	A_2	A_3	
I	0,405	1,839	110,61	-609,97	1464,3	14,84
2	0,675	113,39	728,56	-4328,9	4373,2	6,0
3	0,768	147,33	-6,289	-3016,3	11732	5,5
4	0,849	128,26	-257,54	504,91	8453,3	5,9
5	0,938	116,02	97,314	3042,0	-25032	6,0
6	1,037	131,13	-45,657	-4471,1	29263	5,9
7	1,146	111,12	-61,583	4311,9	-18063	6,0
8	1,266	130,04	259,11	-1106,4	2580,8	7,5
9	1,400	147,47	115,22	-331,83	496,67	6,7
10	1,962	167,66	60,977	171,14	-484,68	6,5
11	2,750	189,10	10,833	2829,5	-10845	6,4
12	3,317	219,13	-70,895	-3265,7	12010	6,8
13	4,000	170,19	-29,953	-756,69	1241,2	6,9
14	4,968	129,09	-159,43	300,81	-390,66	6,9
15	7,059	99,125	0	0	0	10,7

Table 4.44

Total integral neutron production cross-sections of the ${}^7\text{Li}(d,t){}^6\text{Li}$ reaction

Energy in MeV	Cross section in mb	Energy in MeV	Cross section in mb	Energy in MeV	Cross section in mb
I,36	0,1	I,98	48,1	2,98	117,6
I,45	1,0	2,07	57,2	3,15	137,0
I,49	1,8	2,20	67,5	3,31	133,6
I,54	2,5	2,18	74,3	3,47	141,6
I,63	7,7	2,27	83,4	3,60	157,5
I,65	9,5	2,47	91,4	3,78	158,7
I,69	14,0	2,35	95,9	3,84	154,2
I,76	19,7	2,49	105,0	4,11	158,8
I,83	26,6	2,64	103,9	-	-
I,87	35,6	2,84	110,8	12,0	200

Table 4.45

Brief data content of references used in the evaluation of the ${}^7\text{Li}(t,p){}^9\text{Li}$ reaction cross-section

Energy range in MeV	Range of angles in deg	Type of data	Uncertainty in %		Ref.
			random	system.	
3,5-10,0	4 \pm	EXC,SIG	3	7	[195]
23,0	35	AND,DA	3	-	[242]
15,0	9-115	AND,DA	3	7	[243]

Table 4.46

Spline fit coefficients for the description of the ${}^7\text{Li}(t,p){}^9\text{Li}$ excitation function of the total cross-section for the production of lithium-9 (The cross-section can be calculated using Eq. (2.10))

Knot no.	Knot energy in MeV	Spline fit coefficients				Cross section uncert., mb
		A_0	A_1	A_2	A_3	
I	0,50	-0,485	15,41	7,517	-4,271	0,6
2	5,487	26,31	-5,304	-17,94	-546,8	0,6
3	5,70	19,09	18,06	-13,56	3,163	0,6
4	6,851	26,73	0,584	-2,645	6,502	0,6
5	8,00	32,44	19,10	-40,91	15,00	0,6
6	9,061	24,56	-17,06	6,826	0,178	0,6
7	9,67	16,74	-8,551	7,979	-1,015	0,6
8	10,57	14,77	3,353	5,237	-2,278	0,6
9	11,81	22,65	5,825	-22,14	59,12	0,6
10	11,93	23,13	3,063	-0,736	0,056	0,6
II	14,89	27,20	0	0	0	0,6

Table 4.47

Spline fit coefficients for the description of the ${}^7\text{Li}(t,d){}^8\text{Li}$ excitation function of the total cross-section for the production of lithium-8 (The cross-section can be calculated using Eq. (2.10))

Knot no.	Knot energy in MeV	Spline fit coefficients				Cross section uncert., mb
		A_0	A_1	A_2	A_3	
I	6,1	0,139	-11,14	83,56	-36,68	2,426
2	7,267	42,32	33,20	-45,56	27,91	1,732
3	7,984	53,00	10,93	14,50	-9,972	1,709
4	9,013	68,74	9,092	-16,29	27,71	1,679
5	9,414	71,55	9,393	17,04	30,51	1,888
6	10,200	74,65	0	0	0	2,553

Table 4.48

Brief data content of references used in the evaluation of the total integral neutron and helium-7 production cross-section in ${}^7\text{Li}+$ interactions (The information given in parentheses indicates which level (ground (0) or first excited (1) state) is considered in the reference.)

Energy range in MeV	Range of angles in deg	Type of data	Uncertainty in %		Ref.
			random	system.	
0,06-0,11	150	EXC,DA(0,1)	5	15	[244]
0,24	41-139	AND,DA,REL(0,1)	5	-	[245]
3,0-10,0	-	EXC,SIG(0)	20	30	[195]
I,15-I,95	15-170	AND,DA(0,1)	5	10	[246]
22	15-80	AND,DA(0,1)	5	10	[247]
13	5-175	AND,DA,REL(0,1)	20	-	[248]
0,08-0,49	90	EXC,DA(0,1)	3	7	[249]

Table 4.49

Spline fit coefficients for the description of ${}^7\text{Li}(t,\alpha){}^6\text{He}$ partial reaction cross-sections (The cross-section can be calculated using Eq. (2.13))

State	Knot no.	Knot Energy in MeV	Spline fit coefficients				Cross section uncert., %
			A_0	A_1	A_2	A_3	
Ground state	I	0,055	-10,48	8,047	-17,39	0,156	35
	2	0,272	-1,426	3,682	-0,989	0,051	25
	3	1,350	2,144	0,911	-0,743	0,149	14
	4	22,00	2,112	0	0	0	10
First excited state	I	0,055	-8,753	9,295	0,029	-1,096	8
	2	0,150	-0,505	6,043	-3,706	0,795	3
	3	0,520	2,806	0,513	-0,745	0,254	4
	4	1,800	2,781	-0,161	0,203	-0,068	5
	5	22,00	2,587	0	0	0	10

Table 4.50

Brief data content of references used in the evaluation of the excitation function for the total integral neutron production cross-section in ${}^7\text{Li}+$ interactions

Energy range in MeV	Range of angles in deg	Type of data	Uncertainty in %		Ref.
			random	system.	
0,25-2,0	0	EXC,DA	5	20	[250]
0,1-0,3	90	EXC,DA	20	50	[193]
3,0-12,1	0-160	AND,DA	5	10	[172]
0,13-0,33	0	EXC,DA	5	10	[251]
0,36-2,12	0	AND,DA	10	20	[194]
0,14-1,38	0	EXC,DA	5	10	[192]

Table 4.51

Spline fit coefficients for the description of the total neutron production cross-sections in ${}^7\text{Li}+$ interaction channels (The cross-section can be calculated using Eq. (2.13))

Knot no.	Knot energy in MeV	Spline fit coefficients				Cross section uncert., %
		A_0	A_1	A_2	A_3	
I	0,133	1,569	6,331	-4,560	1,606	10
2	0,350	4,888	2,017	1,359	-1,387	10
3	0,702	6,482	1,895	-1,535	-98,18	10
4	0,740	6,563	0,901	-17,17	36,70	10
5	0,934	6,305	-1,123	8,493	-7,736	10
6	1,932	7,005	-1,031	1,790	-0,755	10
7	12,120	6,474	0	0	0	10

Table 4.52

Brief data content of references used in the evaluation of the ${}^7\text{Li}(t,n){}^9\text{B}$ reaction cross-section

Energy range in MeV	Range of angles in deg	Type of data	Uncertainty in %		Ref.
			random	system.	
I,5-5,5	10-160	PAR/AND,DA	5	30	[252]
I,2-2,7	0	PAR/EXC,DA	7	50	[253]
2,I	20-150	AND,DA	-	-	-
0,5-I,4	0	UND/EXC,DA	10	25	[192]

Table 4.53

Values of the differential total neutron yield cross-section in the ${}^7\text{Li}(t,n){}^9\text{B}$ reaction at an angle of 0°

Energy in MeV	Cross section in mb/sr	Energy in MeV	Cross section in mb/sr	Energy in MeV	Cross section in mb/sr
0,46	0,17	0,72	4,4	0,95	20,0
0,49	0,23	0,75	6,2	0,98	21,0
0,52	0,33	0,78	8,0	1,03	21,5
0,55	0,52	0,81	10,0	1,05	22,5
0,58	0,80	0,85	12,2	1,10	23,0
0,62	1,4	0,87	14,0	1,20	23,8
0,65	2,2	0,90	16,0	1,30	24,0
0,68	3,0	0,93	18,0	1,40	24,3

Table 4.54

Normalized values of Legendre coefficients for the description of the angular differential cross-section of the ${}^7\text{Li}(\tau, n_0){}^9\text{Be}$ reaction (20% uncertainty)

Energy in MeV	$4\pi B_0$, mb	B_1/B_0	B_2/B_0	B_3/B_0	B_4/B_0	B_5/B_0	B_6/B_0
1,559	8,2	-0,106	0,242	0,068	-0,045	0,0	0,0
1,966	7,9	0,123	0,632	0,123	0,088	0,0	0,0
2,232	10,7	0,239	0,639	0,048	0,061	0,0	0,0
2,589	12,0	0,259	0,333	-0,045	-0,067	0,0	0,0
2,966	9,8	0,358	0,449	-0,003	-0,103	0,032	0,0
3,308	10,0	0,247	0,552	0,139	-0,078	0,056	0,06
3,650	9,2	0,163	0,537	0,133	-0,045	0,020	0,05
4,008	7,0	0,036	0,575	0,162	-0,077	0,070	0,057
4,396	7,5	-0,014	0,390	0,064	-0,040	0,099	0,129
4,903	6,5	-0,038	0,301	0,106	0,014	0,092	0,036
5,312	6,7	-0,126	0,243	0,047	-0,148	0,104	0,052

Table 4.55

Brief data content of references used in the evaluation of the ${}^7\text{Li}(\tau, p){}^9\text{Be}$ reaction cross-section

Energy range in MeV	Range of angles in deg	Type of data	Uncertainty in %		Ref.
			random	system.	
1,0-2,5	70;130	PAR/EXC, DA, P_0, P_2	5	25	[255]
1,7-4,8	20;165	PAR/EXC, P_0	15	30	[256]
10	5-160	PAR/AND	3	12	[254]

Table 4.57

Brief data content of references used in the evaluation of the ${}^7\text{Li}(\tau, t){}^9\text{Be}$ reaction cross-section

Energy range in MeV	Range of angles in deg	Type of data	Uncertainty in %		Ref.
			random	system.	
1,8-7,9	4 π	UND/EXC, SIG	3	10	[209]
1,7-5,9	4 π	UND/EXC, SIG	5	10	[205]
3,0-4,0	20-90	AND, DA	1	12	[259]
3,0;3,5;4,0	30-150	PAR/AND, DA	5	13	[260]
2,0-4,2	30;40	EXC, DA	5	13	[260]

Table 4.56

Partial differential cross-sections of the ${}^7\text{Li}(\tau, p){}^9\text{Be}$ reaction for a few angles and reaction channels

$20^\circ, P_0$		$70^\circ, P_0$		$70^\circ, P_2$	
Energy in MeV	Cross section, mb/sr	Energy in MeV	Cross section, mb/sr	Energy in MeV	Cross section, mb/sr
2,02	0,48	I,0	0,20	I,0	0,42
2,26	0,55	I,II	0,26	I,II	0,44
2,52	0,67	I,20	0,31	I,20	0,52
2,71	0,76	I,31	0,42	I,32	0,64
3,01	0,88	I,41	0,39	I,41	0,86
3,22	0,94	I,50	0,46	I,50	0,85
3,33	0,96	I,60	0,48	I,61	0,95
3,44	0,98	I,70	0,52	I,72	0,90
3,54	0,95	I,81	0,62	I,82	0,87
3,75	0,69	I,91	0,68	I,91	0,95
4,03	0,62	2,02	0,69	2,01	0,84
4,33	0,65	2,10	0,86	2,10	1,08
4,61	0,68	2,31	0,97	2,31	1,31
4,80	0,73	2,50	0,91	2,48	1,19
10	0,33	10	0,65	10	0,8

Table 4.58

Spline fit coefficients for the description of the evaluated ${}^7\text{Li}(\tau, t){}^9\text{Be}$ integral reaction cross-section. The cross section can be calculated using Eq. (2.10).

Knot no.	Knot energy in MeV	Spline fit coefficients				Cross section, mb
		λ_0	λ_1	λ_2	λ_3	
1	1,700	3,772	20,15	78,15	-22,99	1,9
2	2,950	106,18	107,79	-8,044	-33,16	2,8
3	4,200	163,58	-67,77	100,45	-24,25	2,0
4	6,065	229,25	53,84	-35,25	9,084	3,0
5	7,930	265,98	0	0	0	4,0

Table 4.59

Brief data content of references used in the evaluation of the ${}^7\text{Li}(\tau, \alpha){}^6\text{Li}$ reaction cross-section

Energy range in MeV	Range of angles in deg	Type of data, channel	Uncertainty in %		Ref.
			random	system.	
1,3-5,5	8;90;125	PAR/EXC, DA, α_0, α_1	10	15	[261]
1,8-5,1	10-165	PAR/AND, DA, α_0, α_1	10	15	[261]
1,3-5,0	90	PAR/EXC, DA, α_2	10	15	[261]
2,0-4,2	30	PAR/EXC, DA, α_0, α_2	5	13	[260]
6,0-7,5	10-170	PAR/AND, DA, α_0, α_2	8	15	[262]
5,0-8,0	20;160	PAR/EXC, DA, α_0, α_2	8	15	[262]
5,1-9,0	20-170	PAR/EXC, DA, α_0, α_2	15	20	[263]
0,8-3,0	40-150	PAR/AND, α_0, α_2	20	25	[264]

Table 4.60

Spline fit coefficients for the description of the ${}^7\text{Li}(\tau, \alpha){}^6\text{Li}$ integral reaction cross-section. (The cross-section can be calculated using Eq. (2.10)).

Knot no.	Knot energy in MeV	Spline fit coefficients				Cross section, mb
		λ_0	λ_1	λ_2	λ_3	
1	0,8562	0,8542	12,48	5,713	-1,838	0,4
2	3,675	40,27	0,8762	-9,830	3,155	1,0
3	4,900	32,39	-9,003	1,768	-0,1199	1,0
4	9,00	16,93	0	0	0	1,3

Table 4.61

Ratio of partial cross-sections to the total ${}^7\text{Li}(\tau, \alpha){}^6\text{Li}$ reaction cross-section

Energy in MeV	Summed integral cross-section in mb	Ratios		
		0	I	2
0,86	0,85	0,13	0,60	0,26
1,36	8,29	0,33	0,25	0,41
1,86	17,2	0,44	0,29	0,26
2,36	26,2	0,51	0,35	0,13
2,86	34,0	0,47	0,33	0,21
3,36	39,1	0,47	0,34	0,19
3,86	40,1	0,49	0,35	0,15
4,36	37,3	0,51	0,37	0,11
4,86	32,8	0,54	0,38	0,09
5,36	28,6	0,56	0,39	0,08
5,86	25,3	0,57	0,37	0,07
6,36	22,7	0,55	0,34	0,09
6,86	20,6	0,45	0,42	0,11
7,36	19,2	0,44	0,44	0,12
7,86	18,1	0,50	0,40	0,10
8,36	17,4	0,49	0,41	0,10
8,86	17,0	0,49	0,41	0,08

Table 4.62

Evaluated total integral cross-section values for the ${}^7\text{Li}(\alpha, n){}^{10}\text{B}$ reaction

Energy in MeV	Cross-section in mb	Energy in MeV	Cross-section in mb	Energy in MeV	Cross-section in mb
4,38	0,95	5,10	38,0	6,95	243,5
4,41	2,91	5,22	34,2	7,13	255,5
4,45	3,54	5,38	31,6	7,32	257,8
4,50	4,84	5,56	40,0	7,49	240,5
4,55	5,42	5,64	46,0	7,65	183,0
4,60	8,13	5,73	52,0	7,83	143,8
4,70	12,1	5,87	60,4	8,02	143,6
4,80	14,8	6,07	80,9	8,22	148,3
4,90	17,8	6,22	99,1		
4,95	21,0	6,40	119,6		
5,00	25,9	6,58	141,4		
5,05	30,0	6,76	190,0		

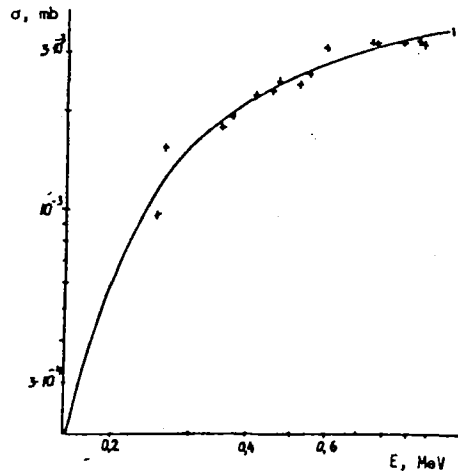


Fig. 4.1. Energy dependence of the integral proton radiative capture cross-section of lithium-6. Spline fit given by continuous curve. Experimental data: + - [149].

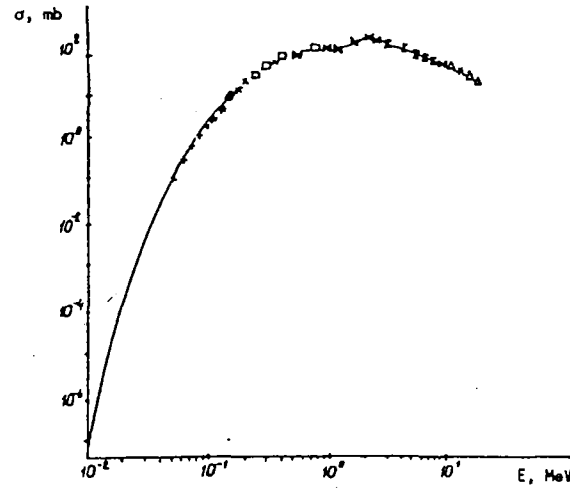


Fig. 4.2. Energy dependence of the integral ${}^6\text{Li}(p,t){}^4\text{He}$ reaction cross-section. Spline fit given by continuous curve. Experimental data: + - [156], \square - [157], \square - [158], \blacklozenge - [159], \circ - [162], \times - [163], Σ - [164], Δ - [165].

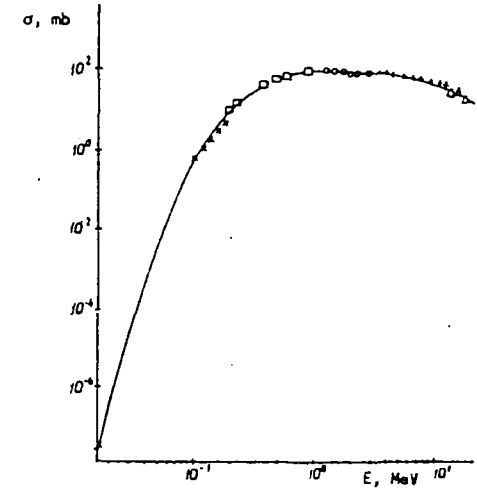


Fig. 4.3. Energy dependence of the integral ${}^6\text{Li}(d,n){}^7\text{Be}$ reaction cross-section. Spline fit given by continuous curve. Experimental data: \times - [166], \square - [167], \circ - [168], + - [169], Δ - [170].

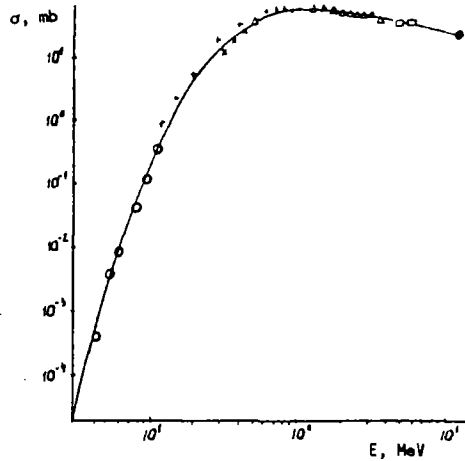


Fig. 4.4. Energy dependence of the integral ${}^6\text{Li}(d,pp){}^7\text{Li}$ reaction cross-section. Spline fit given by continuous curve. Experimental data: \circ - [155], \times - [160], + - [167], Δ - [168], \square - [176], \bullet - [177].

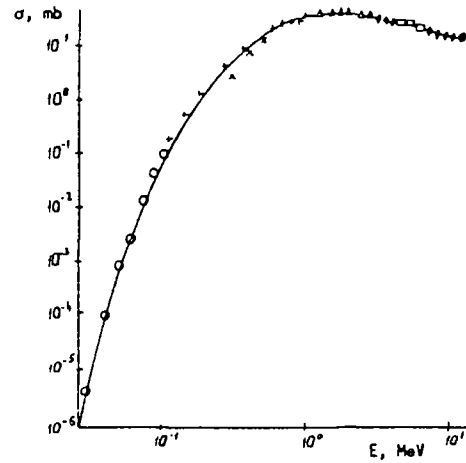


Fig. 4.5. Energy dependence of the integral ${}^6\text{Li}(d,p){}^7\text{Li}$ reaction cross-section. Spline fit given by continuous curve. Experimental data: \circ - [155], \times - [160], + - [167], Δ - [168], \square - [176], \blacklozenge - [171], \bullet - [177].

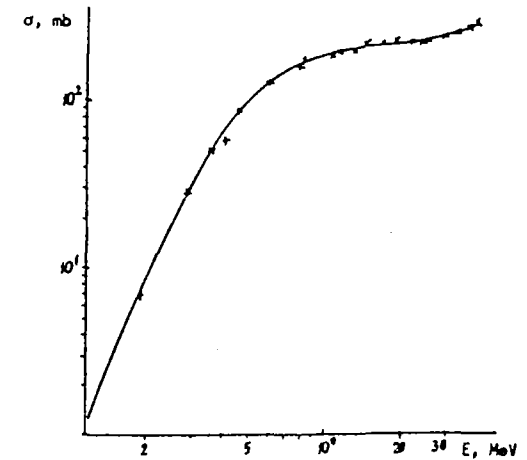


Fig. 4.6. Energy dependence of the integral ${}^6\text{Li}(d,p+t){}^4\text{He}$ reaction cross-section. Spline fit given by continuous curve. Experimental data: \times - [179], + - [180].

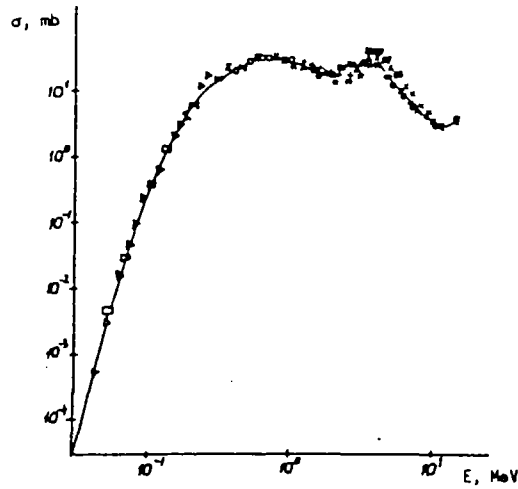


Fig. 4.7. Energy dependence of the integral ${}^6\text{Li}(d,\alpha){}^4\text{He}$ reaction cross-section. Spline fit given by continuous curve. Experimental data: \triangleright - [155], \circ - [160], $\bar{\Delta}$ - [167], Δ - [168], ∇ - [181], \square - [183], \equiv - [184], $*$ - [186], \ominus - [187], \blacksquare - [188], $+$ - [189], \times - [190].

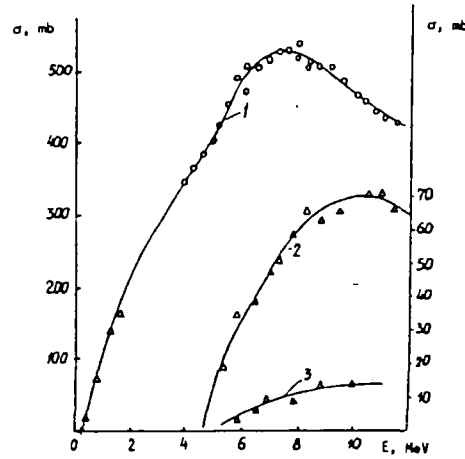


Fig. 4.8. Energy dependence of the following integral cross-sections: (1) ${}^6\text{Li}(t,x)n$ (left-hand scale), (2) ${}^6\text{Li}(t,2n){}^7\text{Be}$ and (3) ${}^6\text{Li}(t,2n){}^7\text{Be}$ (first excited state) (right-hand scale). Spline fit given by the continuous curve. Experimental data: Δ - [172], $+$ - [192], \circ - [194].

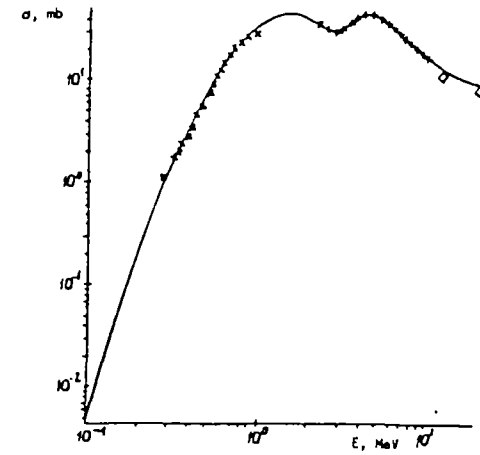


Fig. 4.9. Energy dependence of the integral ${}^6\text{Li}(t,p){}^8\text{Li}$ reaction cross-section. Spline fit given by continuous curve. Experimental data: $+$ - [195], \times - [196], \diamond - calculated value.

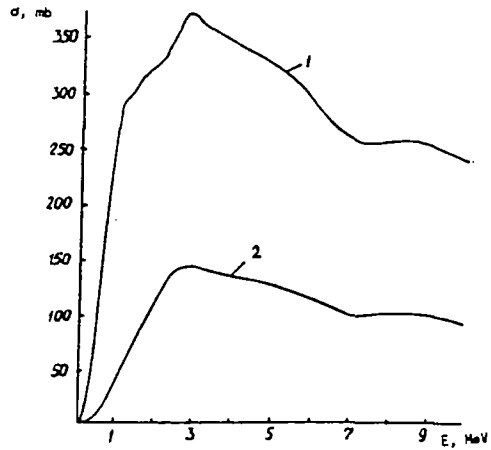


Fig. 4.10. Energy dependence of the (1) ${}^6\text{Li}(t,d){}^7\text{Li}$ and (2) ${}^6\text{Li}(t,d){}^7\text{Li}$ integral reaction cross-sections.

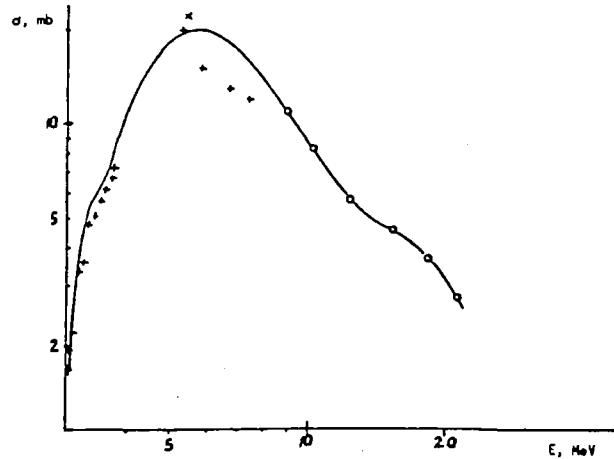


Fig. 4.11. Energy dependence of the integral ${}^6\text{Li}(t,n){}^8\text{B}$ boron-8 production cross-section. Spline fit given by continuous curve. Experimental data: $+$ - [168], \times - [197], \circ - [198].

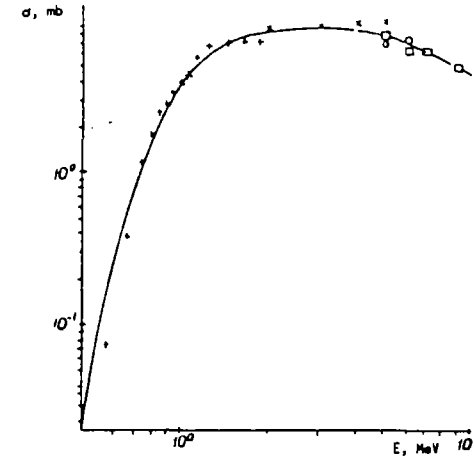


Fig. 4.12. Energy dependence of the integral ${}^6\text{Li}(t,p){}^8\text{Be}$ reaction cross-section. Spline fit given by continuous curve. Experimental data: $+$ - [200], \times - [201], \square - [202], \circ - [203].

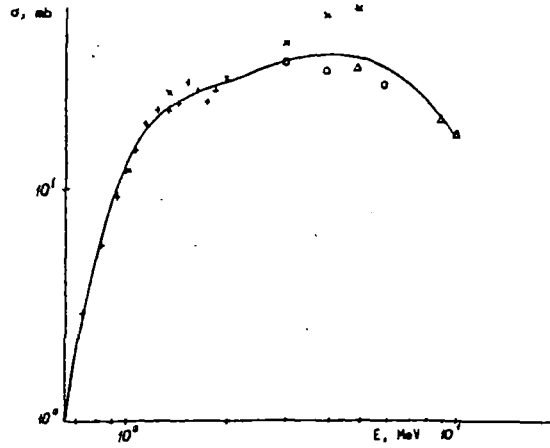


Fig. 4.13. Energy dependence of the integral ${}^6\text{Li}(\alpha, p){}^8\text{Be}$ reaction cross-section. Spline fit given by continuous curve. Experimental data: + - [200], x - [201], Δ - [202], o - [203].

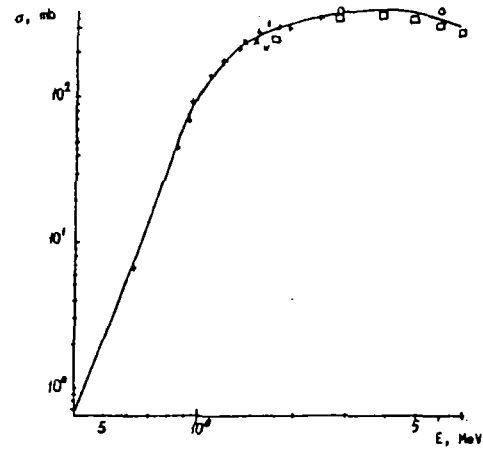


Fig. 4.14. Energy dependence of the integral ${}^6\text{Li}(\alpha, d){}^7\text{Be}$ reaction cross-section. Spline fit given by continuous curve. Experimental data: + - [200], o - [205], x - [206], \square - [209].

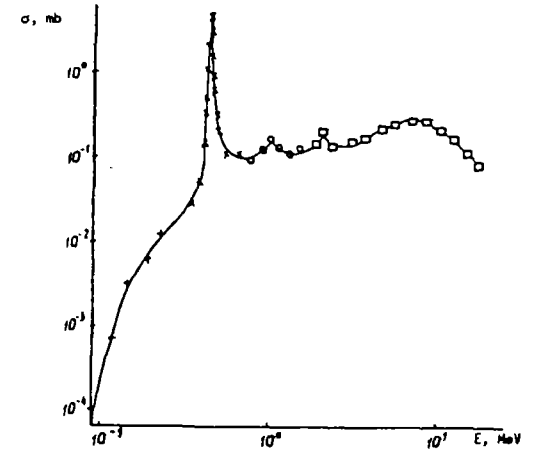


Fig. 4.15. Energy dependence of the integral proton radiative capture cross-section of lithium-7 in the ${}^7\text{Li}(p, \gamma){}^8\text{Be}$ reaction. Spline fit given by continuous curve. Experimental data: + - [210], x - [211], o - [212], \square - [213].

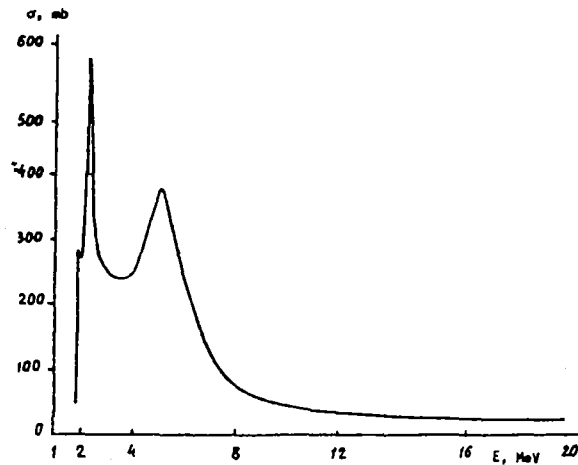


Fig. 4.16. Energy dependence of the integral ${}^7\text{Li}(p, n){}^7\text{Be}$ reaction cross-section (ground state).

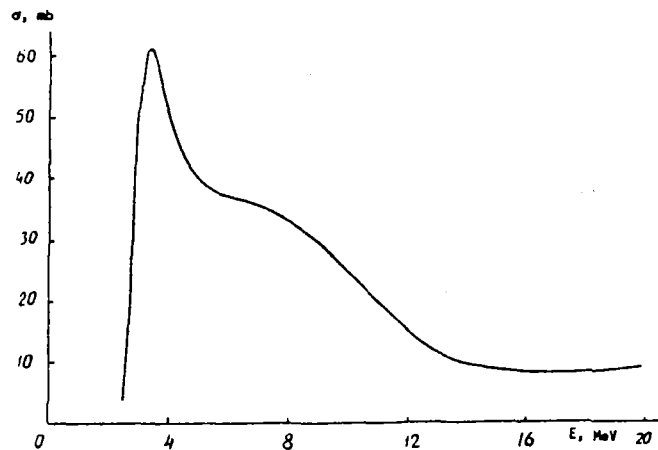


Fig. 4.17. Energy dependence of the integral ${}^7\text{Li}(p, n){}^7\text{Be}$ reaction cross-section (first excited state).

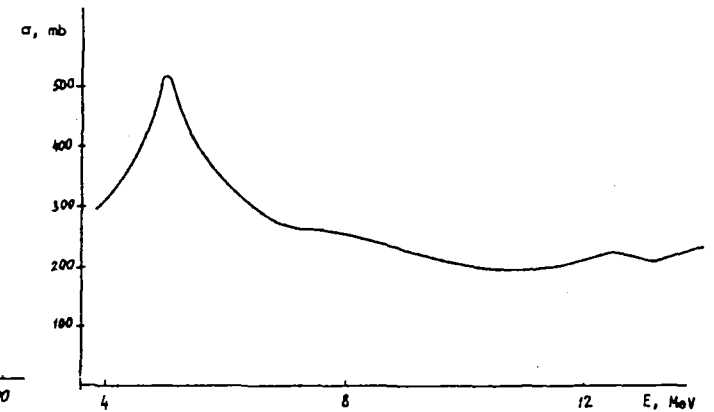


Fig. 4.18. Energy dependence of the total integral ${}^7\text{Li}(p, n){}^7\text{Be}$ neutron production cross-section.

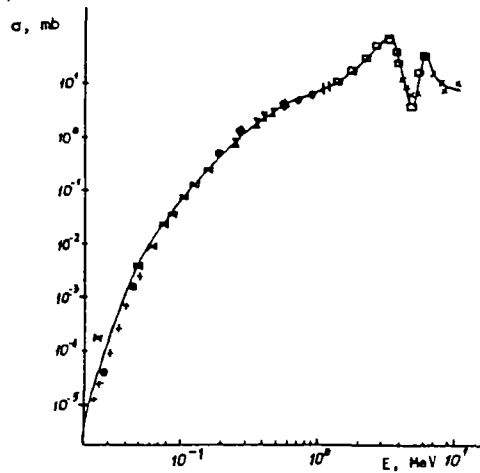


Fig. 4.19. Energy dependence of the integral ${}^7\text{Li}(p,\alpha){}^4\text{He}$ reaction cross-section. Spline fit given by continuous curve. Experimental data: + - [154], * - [155], ◆ - [159], | - [215], □ - [221], ● - [223], ⌘ - [226], x - [228].

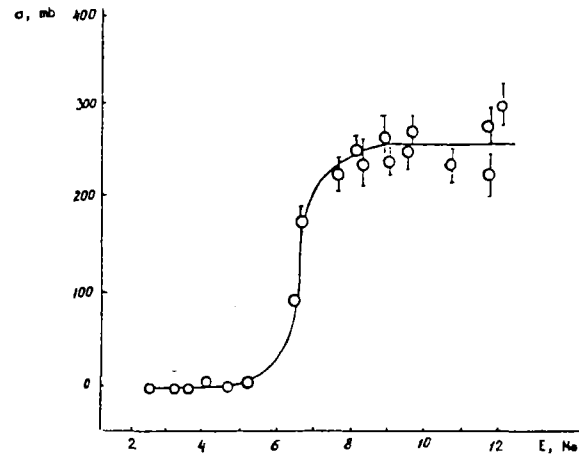


Fig. 4.20. Energy dependence of the total integral ${}^7\text{Li}(p,x){}^3\text{H}$ tritium production cross-section. Approximate fit given by continuous curve (see description in text). Experimental data: o - [229].

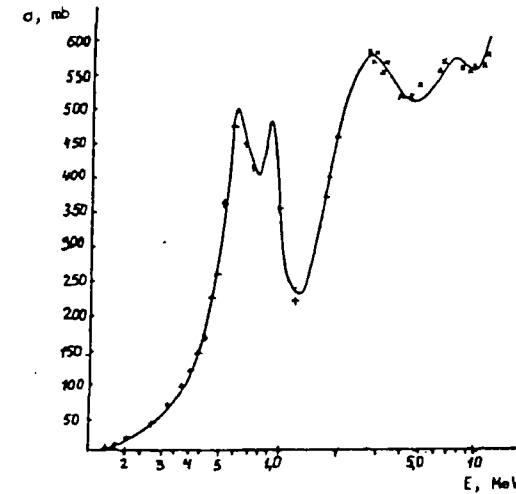


Fig. 4.21. Energy dependence of the total integral ${}^7\text{Li}(d,x)n$ neutron production cross-section. Spline fit given by continuous curve. Experimental data: x - [172], + - [173].

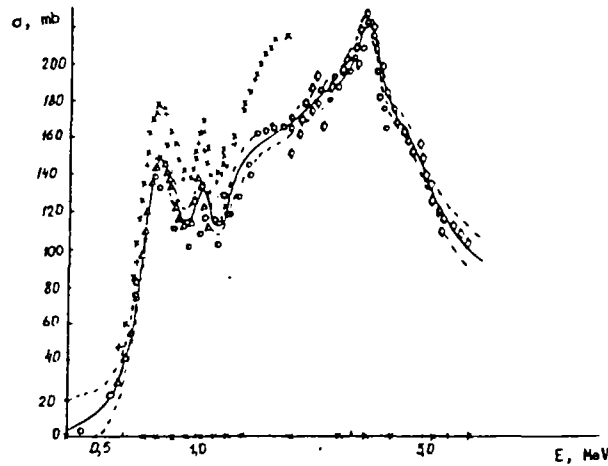


Fig. 4.22. Energy dependence of the total integral ${}^7\text{Li}(d,p){}^8\text{Li}$ lithium-8 production cross-section. Spline fit given by continuous curve. Experimental data: o - [168], + - [234], x - [235], □ - [236], * - [238], Δ - [237].

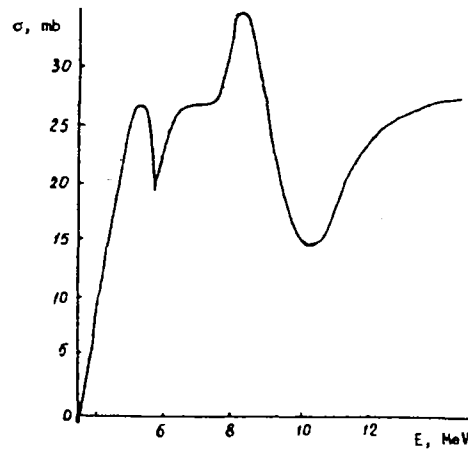


Fig. 4.23. Energy dependence of the total integral ${}^7\text{Li}(t,p){}^9\text{Li}$ lithium-9 production cross-section. Spline fit given by continuous curve.

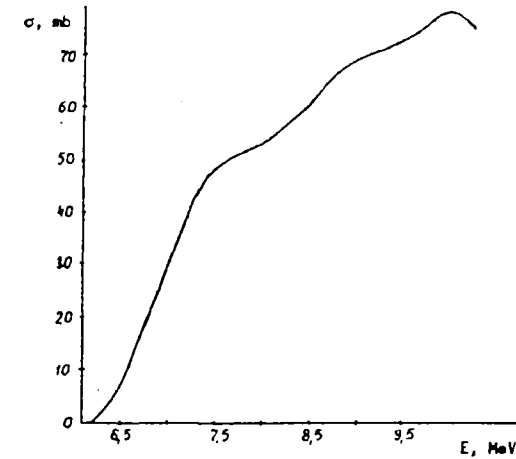


Fig. 4.24. Energy dependence of the total integral ${}^7\text{Li}(t,d){}^8\text{Li}$ lithium-8 production cross-section. Spline fit given by continuous curve.

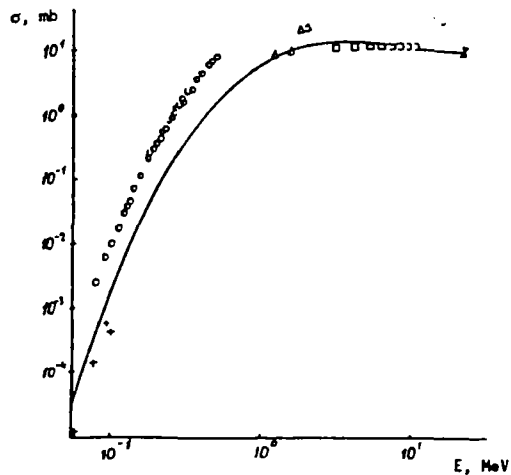


Fig. 4.25. Energy dependence of the integral ${}^7\text{Li}(t, \alpha){}^6\text{He}$ reaction cross-section (ground state). Spline fit given by continuous curve. Experimental data: \square - [195], $+ -$ [244], Δ - [246], ∇ - [247], \circ - [249].

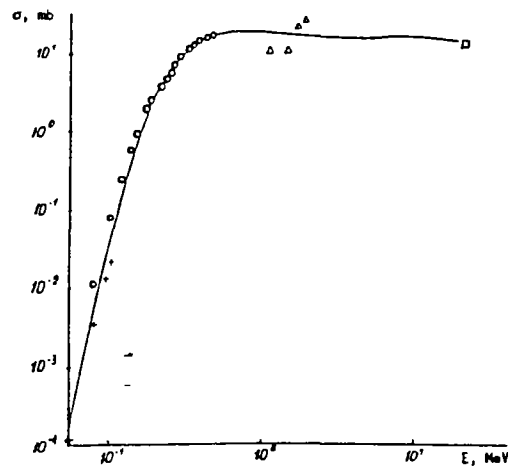


Fig. 4.26. Energy dependence of the integral ${}^7\text{Li}(t, \alpha){}^6\text{He}$ reaction cross-section (first excited state). Spline fit given by continuous curve. Experimental data: $+ -$ [224], Δ - [246], \square - [247], \circ - [249].

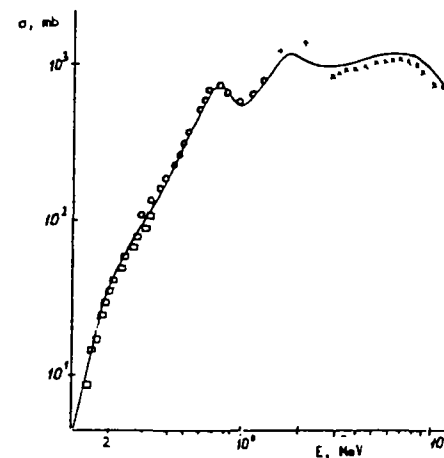


Fig. 4.27. Energy dependence of the total integral ${}^7\text{Li}(t, x)n$ neutron production cross-section. Spline fit given by continuous curve. Experimental data: $x -$ [172], $\circ -$ [193], $+ -$ [194], $\square -$ [251].

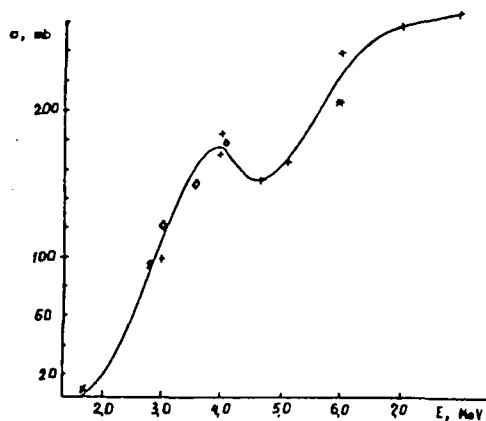


Fig. 4.28. Energy dependence of the total integral ${}^7\text{Li}(t, t){}^7\text{Be}$ beryllium-7 production cross-section. Spline fit given by continuous curve. Experimental data: $\circ -$ [206], $+ -$ [209], $\diamond -$ [260].

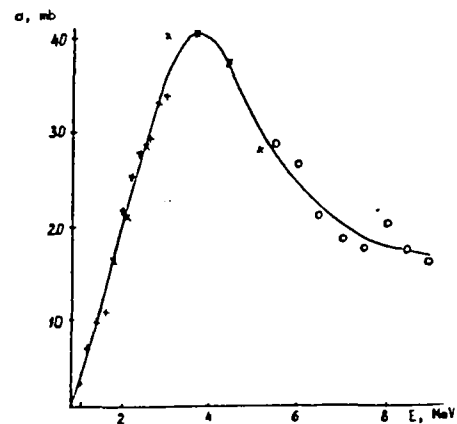


Fig. 4.29. Energy dependence of the integral ${}^7\text{Li}(t, \alpha){}^6\text{Li}$ reaction cross-section (for the ground and first excited states). Spline fit given by continuous curve. Experimental data: $x -$ [261], $\circ -$ [262], $+ -$ [264].

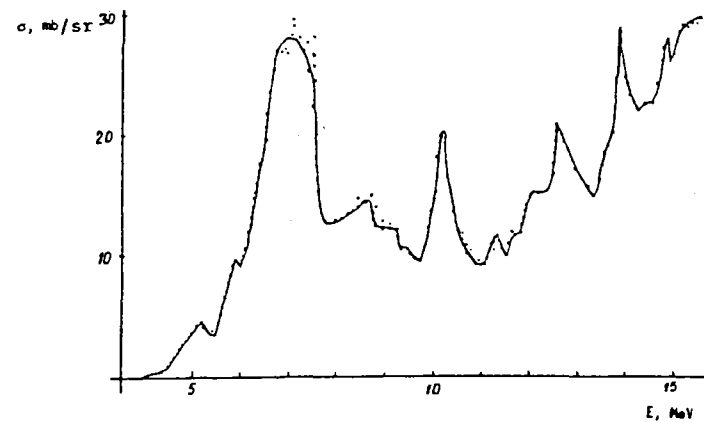


Fig. 4.30. Energy dependence of the total differential ${}^7\text{Li}(\alpha, n){}^{10}\text{B}$ neutron production cross-section at an angle of zero degrees. Spline fit given by continuous curve. Experimental data from Ref. [265].

5. CROSS-SECTIONS FOR THE INTERACTION OF BERYLLIUM NUCLEI WITH ISOTOPES OF HYDROGEN AND HELIUM

5.1. Basic data

Beryllium: atomic number - 4

atomic mass - 9.0122

Isotopic composition: beryllium-9 100%

Density: 1.848 g/cm³

Melting temperature: 1284°C

Thermal neutron capture cross-section: 0.009 b.

Fields of application: in nuclear technology, as a neutron moderating and reflecting medium in nuclear reactors. Beryllium is widely used as a neutron source through the ${}^9\text{Be} + \alpha = n + {}^{12}\text{C}$ reaction, and is considered as a potential nuclear fuel in thermonuclear reactors through reactions such as ${}^9\text{Be}(p,d){}^4\text{He}$ or ${}^9\text{Be}(p,\alpha){}^6\text{Li}$. Beryllium is also used in metallurgy and in the silicon industry.

Nuclear properties of reactions between beryllium nuclei and isotopes of hydrogen and helium are listed in Table 5.1.

5.2. The ${}^9\text{Be}(p,\gamma){}^{10}\text{B}$ reaction

This reaction is primarily of astrophysical interest, which explains the small number of measurements listed in Table 5.2.

At proton energies below 0.2 MeV the total gamma-ray production cross-section can be estimated with the use of Eq. (2.14) and the following (centre of mass) parameters: $S(E_{c.m.}) = (2.9 \pm 0.3) \cdot 10^{-3} \text{ b} \cdot \text{MeV}$ and $E_g = 14.1 \text{ MeV}$. At energies above 0.2 MeV the excitation function is influenced by resonances corresponding to the states of the compound nucleus of boron-10 which manifest themselves at incident proton energies of 0.330 and 1.0 MeV.

The evaluation of the integral cross-section for this reaction was performed on the assumption of moderate angular anisotropy, which was inferred from the measured [269] partial differential cross-sections of the ${}^9\text{Be}(p,\gamma){}^{10}\text{B}$ reaction at 90°. The coefficients for a spline curve describing the total integral gamma-ray yield from the ${}^9\text{Be}(p,\gamma){}^{10}\text{B}$ reaction are listed in Table 5.3. Figure 5.1 shows the excitation function of the total integral gamma-ray yield summed over all partial cross-sections.

The results given in Ref. [269] were normalized to the data published in [272]. There is only one set of data [270], giving the total gamma-ray yield at 0.33 MeV and 0.5 MeV, which can be used to check the normalized data given in Ref. [269]. The agreement between these two sets of data is very good at 0.5 MeV, but the data diverge by a factor of two at 0.35 MeV.

In our evaluation, preference was given to the data from Ref. [269] because other independent data [147] seem to indicate that there is a resonance at $E_p = 0.33 \text{ MeV}$, and its absence in the Ref. [270] data casts doubt on their reliability at 0.33 MeV.

5.3. The ${}^9\text{Be}(p,n){}^9\text{B}$ reaction

Measurements of this reaction, which were first performed in the 1950s, were devoted initially to the development of nuclear spectroscopy and are well documented in Ref. [273]. It was not until the early sixties that the cross-section for this reaction was measured with the intention of using it as a neutron source. The excitation function of the total neutron production cross-section of this reaction for the energy range from threshold to 13 MeV, as well as the partial integral and differential neutron production cross-sections corresponding to the ground state of the resultant boron-9 nucleus, were evaluated on the basis of the existing data, listed in Table 5.4.

The integral neutron production cross-section was evaluated from data published in Refs [21] and [280]; these data were then used to normalize the

relative measurements given in Ref. [151]. The cross-section data presented in Ref. [274] were multiplied by a factor of 1.7 in order to obtain better agreement with the data given in Ref. [21]. The spline coefficients for the evaluated curve of the total neutron yield cross-section are listed in Table 5.5. The evaluated curve is compared with the experimental data in Fig. 5.2.

The partial integral cross-section for the ${}^9\text{Be}(p,n_0){}^9\text{B}$ reaction corresponding to the ground state of boron-9, based on data published in Ref. [279], is plotted in Fig. 5.3. The differential partial cross-sections for this reaction can be calculated from the Legendre coefficients listed in Table 5.6 by means of the following expression:

$$\sigma(\theta, E) = \frac{\sigma(E)}{4\pi} \left[1 + \sum B_n P_n(\cos\theta) \right] \text{ mb}$$

The energies in Table 5.6 are given in the laboratory system, and the differential cross-sections in the centre of mass.

5.4. The ${}^9\text{Be}(p,d){}^8\text{Be}$ reaction

An interesting feature of this reaction lies in the fact that it leads to a quasi-stable state of beryllium-8 which in turn decays into two alpha particles. From a practical point of view, the interest in this reaction lies in the integral cross-section for the production of deuterons as well as in the partial cross-sections of the separate reaction channels. The most extensively studied reaction channel is the one leading to the ground state of beryllium-8. This channel predominates up to an energy of $E_p = 3.3$ MeV. At higher energies, the charged particle spectrum resulting from ${}^9\text{Be} + p$ interactions reveals a broad resonance [281] which corresponds to the 3.04 MeV state of the resultant beryllium-8 nucleus. At a proton energy of 14.26 MeV, the integral partial cross-sections of the ${}^9\text{Be}(p,d){}^8\text{Be}$ reaction leading to the ground state and to the first excited state are practically equal [282].

Since the only available data, listed in Table 5.7, consist of differential data, a more or less complete description of the energy dependence and angular distributions is possible only for the partial cross-section corresponding to the ground state of the resultant beryllium-8 nucleus.

At low energies, the energy dependence of the ${}^9\text{Be}(p,d_0){}^8\text{Be}$ cross-section can be approximated by Eq. (2.14) with the following parameters: $S(0) = 35$ MeV·b and $E_g = 14.1$ MeV (in the centre-of-mass system).

This s-factor value was derived in Ref. [283] as a result of interpreting the measured reaction cross-section values in the framework of the R-matrix theory. According to the analysis performed in Ref. [283], the character of the angular distribution and of the energy dependence of the partial cross-section for the ${}^9\text{Be}(p,d_0){}^8\text{Be}$ reaction at proton energies smaller than 0.70 MeV can be explained on the basis of the mechanism for the formation of the compound nucleus. At higher energies it is necessary to take the mechanisms of direct reactions into account [281].

The spline curve describing the excitation function of the evaluated integral cross-section of the ${}^9\text{Be}(p,d){}^8\text{Be}$ reaction in the low part of the energy range, shown in Fig. 5.4, was determined from data given in Ref. [283].

The evaluation in the upper part of the energy range was based on data given in Ref. [287]. The coefficients which define the spline curve, as well as the cross-section uncertainty range having a statistical probability level of 67%, are listed in Table 5.8.

5.5. The ${}^9\text{Be}(p,\alpha){}^6\text{Li}$ reaction

This reaction has been investigated in numerous experiments, some of which, listed in Table 5.9, are used here in the evaluation of its cross-section. This strong interest in the exothermic ${}^9\text{Be}(p,\alpha){}^6\text{Li}$ reaction is due to a large cross-section at low proton energies which makes it

usable in a fusion fuel cycle. In addition, this reaction could be used advantageously in the production of lithium-6 which is a potential fuel in thermonuclear fusion.

At low incident proton energies ($E_p < 0.2$ MeV), the integral cross-section for the ${}^9\text{Be}(p,\alpha_0){}^6\text{Li}$ reaction channel behaves practically identically to the ${}^9\text{Be}(p,d_0)$ cross-section and can be described by Eq. (2.14) with the same parameters that were used in the case of the ${}^9\text{Be}(p,d_0)$ reaction.

The angular distribution of the alpha particles up to an energy of 0.7 MeV has been measured by Sierk and Tombrello [283]. The integral cross-section at $E_p = 0.33$ MeV, determined to an accuracy of 3%, is in good agreement with the value given in Ref. [285].

Data from Refs [284] and [286] were used to obtain the evaluated curve in the energy range $E_p = 1$ to 4 MeV. The data from these two references show fairly good agreement (within the limits of their uncertainties) only between 1.5 and 4.5 MeV. In the range $1 < E_p < 1.5$ MeV the data from [286] are higher than those from [284] by a factor of 1.25. The integral cross-section of the ${}^9\text{Be}(p,\alpha_0){}^6\text{Li}$ reaction was derived from the data of Ref. [286] after they had been normalized at $E_p = 1.0$ MeV and $E_p = 1.25$ MeV.

Above 4 MeV the evaluation was based on the data from Ref. [288] which contain α -particle angular distributions for the ground state and first excited state in the energy range $E_p = 6$ to 12 MeV. The same reference also gives the excitation functions of the differential cross-section for both channels of this reaction. The differential cross-sections given in Refs [286] and [292] agree within the limits of their uncertainties. Furthermore, our analysis shows that the error introduced in the normalization of the data in [288], which is estimated by the authors to be $\geq 40\%$, is

actually less than 20% if one takes the additional comparison with the data from Ref. [289] into account.

A spline curve reflecting the evaluation of the integral partial cross-section for the ${}^9\text{Be}(p,\alpha){}^6\text{Li}$ reaction was constructed in the light of the above considerations and is shown in Fig. 5.5 together with the experimental data used in the evaluation. The spline coefficients are listed in Table 5.10.

Angular distributions for the (p,α_1) channel corresponding to the excited state of the resultant nucleus with $E_x = 2.18$ MeV are given only in Ref. [288], for the energy range $E_p = 9.0$ to 11.5 MeV. The excitation function for this reaction channel is also given in the same reference, but for a broader energy range, namely $E_p = 5$ to 12 MeV. Analysis of these angular distributions suggests that, within the limits of the errors in the measured data, the cross-section can be approximated by $\sigma(E) = \sigma(90^\circ, E)4\pi$ (see Fig. 5.6).

Spline curve coefficients for evaluation of the integral partial cross-section for this reaction channel are given in Table 5.11.

5.6. The ${}^9\text{Be}(d,\gamma){}^{11}\text{B}$ reaction

Experimental data for this reaction, which are summarized in Table 5.12, are sparse and conflicting. The measurements consist primarily in a study of the (d,γ_0) reaction channel with the objective of obtaining information on the inverse ${}^{11}\text{B}(\gamma,d){}^9\text{Be}$ reaction.

The evaluation of the integral cross-section for the ${}^9\text{Be}(d,\gamma_0){}^{11}\text{B}$ reaction was based mainly on the data in Ref. [295], which contains values of the excitation function of the differential cross-section measured at 90° for energies ranging from 2.9 to 11.9 MeV at energy increments of 0.25 MeV. From an analysis of the angular distribution data, it is clear that the integral

cross-section can be represented with an accuracy of $\leq 5\%$ by the expression:

$$\sigma(E) = \sigma(E, 90^\circ) 4\pi / (1 - 0.5 \cdot A_2 / A_0),$$

where A_0 and A_2 are the corresponding Legendre coefficients.

The experimental data for the ${}^9\text{Be}(d, \gamma_0){}^{11}\text{B}$ reaction channel are plotted in Fig. 5.7.

The excitation function for the integral ${}^9\text{Be}(d, \gamma_0){}^{11}\text{B}$ reaction cross-section can be described by the expression

$$\sigma(E) = \exp \left[A_0 + \sum_{k=1}^3 A_k \left\{ \ln \left(\frac{E}{0.399} \right) \right\}^k \right] \cdot 10^{-3}$$

where $A_0 = -6.499$, $A_1 = 2.465$, $A_2 = -0.987$, $A_3 = 0.0609$, and E ranges from 0.399 MeV to 12 MeV.

For energies $E_d < 0.4$ MeV, this excitation function can be represented by Eq. (2.14) with the following parameters: $S(0) = 3.46$ mb·MeV and $E_g = 25.63$ MeV in the centre-of-mass system.

Without taking the weak resonance structure into account, the energy dependence of the integral partial cross-sections for the ${}^9\text{Be}(d, \gamma_1){}^{11}\text{B}$ and ${}^9\text{Be}(d, \gamma_2 + \gamma_3){}^{11}\text{B}$ reaction channels, which are qualitatively and quantitatively similar to the dependence of the (d, γ_0) channel, can be represented by

$$\sigma(E) = A \cdot E^2 + B \cdot E + C \text{ mb}$$

if one takes $A = -1.33$, $B = 5.94$ and $C = -1.32$ for the γ_1 channel, and $A = -5.531$, $B = 17.12$ and $C = -4.29$ for the $\gamma_2 + \gamma_3$ channels.

5.7. The ${}^9\text{Be}(d, n){}^{10}\text{B}$ reaction

The majority of publications dealing with this reaction have reported data in the form of relative measurements because most of the measurements were made with the objective of checking the applicability of the distorted wave method to low mass nuclei. The relative data reported in Refs [296, 297], listed in Table 5.13, were normalized to absolute data at a

deuteron energy of 1.4 MeV taken from Ref. [298], as well as data from Refs [270] and [299].

The neutron spectrum consists of individual peaks with particularly well-defined peaks corresponding to the excited states of the resultant boron-10 nucleus. Only at energies of $E_d = 15$ MeV and above does one detect a small background caused by the continuous neutron spectrum. Up to a deuteron energy of 1.5 MeV, the main contribution to the cross-section is due to the reaction channels corresponding to the ground and first excited states of boron-10.

The evaluated values of the partial cross-sections for the ground and the first four excited states are listed in Table 5.14.

The integral cross-sections at low energies can be obtained from Eq. (2.14) using $E_g = 25.63$ MeV and the following $S(0)$ values for the states of boron-10: 12320 MeV·mb for n_0 , 33610 MeV·mb for n_1 , 3360 MeV·mb for n_2 , 8960 MeV·mb for n_3 and 5600 MeV·mb for n_4 .

These five levels determine the neutron yield in this reaction up to a deuteron energy of 0.5 MeV, at which point the next level at $E_x = 4.774$ comes into play. However, as shown by the relative dependence of the excitation function of the total neutron yield [297], the influence of this and above-lying levels is small ($\leq 10\%$) up to an energy of $E_d = 1.54$ MeV. Unfortunately, data on the contribution of levels with excitation energies higher than 3.587 MeV are missing completely up to a deuteron energy of 12 MeV.

As shown by the data in Ref. [301], the contributions of high-lying states, at energies of 12, 15 and 16 MeV, are comparable to the contributions of the first five states. Moreover, it must be noted that a contribution to the total neutron yield cross-section is made - at deuteron energies of 2.7 MeV and above - by three-particle channels, notably the ${}^9\text{Be}(d, n + p){}^9\text{Be}$ reaction.

5.8. The ${}^9\text{Be}(d,p){}^{10}\text{Be}$ reaction

The total as well as the partial proton yield from this reaction has been measured over a broad energy range, viz. $E_d = 0.03$ to 21 MeV. The references used in the evaluation of the reaction are listed in Table 5.15.

From the point of view of practical applications, evaluation of the total integral beryllium-10 production cross-section is the most interesting task. The basic data used for this evaluation have been taken from Ref. [314]. The values of the total integral beryllium-10 production cross-section given in [314] can be checked against later measurements - ten partial cross-section values measured at a deuteron energy of 15 MeV [281]. This same reference reports on the measured values of proton spectra. A summation of all of the partial cross-section values given in Ref. [281] yields an integral cross-section of 40 mb, which is 2.5 times smaller than the total cross-section value given in Ref. [314]. On the other hand, the integral cross-sections at $E_d < 1.6$ MeV (which take into account only the contributions of the ground and first excited states) reported in Ref. [314] are 2.7 times larger than the values derived from an analysis of the data in Ref. [307]. A comparison of the summation of the integral partial cross-sections for all low-lying stable states of beryllium-10, reported in Ref. [313], with the summed yield value given in [314] reveals a discrepancy of 2.3. The data reported in [314], renormalized on the basis of the above considerations (i.e. their values were reduced by a factor of 2.5), were used in the evaluation of the recommended spline curve for the total integral beryllium-10 yield cross-section for the ${}^9\text{Be}(d,p){}^{10}\text{Be}$ reaction (see Table 5.16). The curve representing the total beryllium-10 yield can be used to derive evaluated values of the integral total proton yield from the same reaction. In this operation, it is important to take into account that the latter conforms to the integral beryllium-10 production cross-section up to $E_d = 2.7$ MeV, and is then enhanced by the

contribution of protons from three-particle reactions of the ${}^9\text{Be}(d,n+p){}^9\text{Be}$ type.

As mentioned above, at $E_d < 2.7$ MeV, the total proton yield cross-section can be derived from the excitation functions of the partial cross-sections for the (d,p_0) and (d,p_1) reaction channels. In view of the number of existing measurements (see Table 5.15), it is possible to solve this problem to a high degree of accuracy. At low energies, data from Ref. [210] were used to derive the following input parameters for the approximating curve described by Eq. (2.14): $E_g = 25.634$ MeV; and
for p_0 $S(E_{c.m.}) = 23.8 - (115.6 \cdot E_{c.m.}) + (119 \cdot E_{c.m.}^2)$ MeV·mb, and
for p_1 $S(E_{c.m.}) = 15.4 - (20 \cdot E_{c.m.}) - (172 \cdot E_{c.m.}^2)$ MeV·mb
(for $E_d < 0.1$ MeV).

At higher energies, there are two groups of data which differ in their cross-section values by a factor of two. The first group [304, 308] was excluded on the basis of an analysis of other reaction channels, e.g. (d,t) and (d,α) . Angular distributions and integral partial cross-sections were obtained from the other references. The excitation functions of the integral partial cross-sections for the ${}^9\text{Be}(d,p_0){}^{10}\text{Be}$ and ${}^9\text{Be}(d,p_1){}^{10}\text{Be}$ reactions and the experimental data used in their evaluations are shown in Fig. 5.8 and Fig. 5.9 respectively. The spline curve coefficients for the recommended partial cross-sections are listed in Tables 5.17 and 5.18.

5.9. The ${}^9\text{Be}(d,t_0){}^8\text{Be}$ and ${}^9\text{Be}(d,t){}^8\text{Be}$ reactions

Two different types of data are investigated in this section: the first deals with the integral partial cross-section for the generation of monoenergetic tritons corresponding to the ground state of the resultant beryllium-8 nucleus, and the second is concerned with the total integral triton production cross-section in this reaction.

The references used in this evaluation are described in Table 5.19. In our analysis of the literature, references which did not include absolute values or those which presented results of relative measurements with uncertainties exceeding 20% were not taken into account. The evaluation of the total triton production cross-section is based primarily on the data reported in Refs [302, 314, 315]. The limited amount of data from the different authors precludes a thorough intercomparison of results. In addition, the sparse distribution of data points prevents the construction of a reliable approximating cross-section curve (see Fig. 5.10).

The proposed spline curve to represent the triton generation cross-section of this reaction must therefore be considered only as a rough approximation (the errors inherent in the relative measurements and the normalization errors are estimated to give a combined uncertainty of 30%). Spline curve coefficients describing the excitation function of the reaction cross-section of interest in the energy range $E_d > 1.4$ MeV are tabulated in Table 5.20. At lower energies the cross-section can be calculated with the aid of Eq. (2.14) and with the following parameters (given in the centre-of-mass system): $E_g = 25.634$ MeV and $S(0) = 13.86$ MeV·b.

In view of the large number of studies that have been made of the ${}^9\text{Be}(d,t){}^8\text{Be}$ reaction, it has been possible to perform a more detailed analysis. A comparison of the experimental data with the evaluated cross-section curve is shown in Fig. 5.11, and the spline curve coefficients are tabulated in Table 5.21. Equation (2.14) can be used to obtain cross-section values at deuteron energies below 0.5 MeV, with the following parameters in the centre-of-mass system: $E_g = 25.634$ MeV and $S(0) = 2590$ MeV·mb.

5.10. The ${}^9\text{Be}(d,\alpha){}^7\text{Li}$ reaction

The evaluation of the integral cross-sections for this reaction is based on papers that appeared between 1957 and 1987 (see Table 5.22).

The large cross-section of this reaction and its large energy yield make it interesting for the study of fusion as well as for astrophysics applications. The lithium-7 nucleus has two excited levels which are stable against decay to $(\alpha + t)$ states, and this allows two two-particle channels leading to the ground and first excited states of the resultant lithium-7 nucleus.

At low energies, the partial cross-section for the ${}^9\text{Be}(d,\alpha){}^7\text{Li}$ reaction can be described by Eq. (2.14) with the following parameters (in the centre-of-mass system): $E_g = 25.634$ MeV and $S(0) = 16.606$ MeV·b for α_0 , and $S(0) = 20.058$ MeV·b for α_1 . The evaluated partial cross-sections for deuteron energies larger than 0.2 MeV are listed in Table 5.23.

The summation of the partial integral cross-sections for the reactions leading to the ground and first excited states of the lithium-7 nucleus was evaluated and described by a spline curve, whose coefficients are listed in Table 5.24. Figure 5.12 shows the evaluated spline curve and the experimental data used in the evaluation.

5.11. The ${}^9\text{Be}(t,n){}^{11}\text{B}$ reaction

The total neutron yield from the interaction of tritium with beryllium-9 nuclei in the energy range from 0.3 to 2.3 MeV has been reported in Ref. [323]. A significant number of resonances were discovered in the excitation function of the differential cross-section for the total neutron yield at an angle of 0° by the authors of this report. The neutron angular distributions in Ref. [323] for energies larger than 1 MeV are anisotropic and exhibit a sharp forward peaking. In Ref. [192] the differential cross-section for the total neutron yield at an angle of 0° was measured from 0.3 to 1.4 MeV.

The presence of resonances in the excitation function of the differential cross-section has been confirmed by the data published in Ref. [192]. Furthermore, the absolute values reported in Ref. [190] are twice as large as the analogous values reported in Ref. [323]. The data reported in Ref. [324] do not help to clarify the situation. This paper reports partial ${}^9\text{Be}(t,n){}^{11}\text{B}$ cross-sections corresponding to the ground state as well as to the first, second, sixth, eighth and ninth excited states of the boron-11 nucleus, which when added together to obtain the integral partial cross-section yield a value of 98 mb at $E = 1.3$ MeV which is four times lower than the corresponding value given in Ref. [323]. Also, Ref. [324] reports a distinctive peak in the angular distributions at angles $> 160^\circ$.

In view of the discrepancies in the data, it was decided to represent the integral neutron production cross-section for this reaction in the form of a smooth curve drawn through the data reported in Ref. [323]. The recommended cross-section values for the total neutron yield in the ${}^9\text{Be}(t,n){}^{11}\text{B}$ reaction are listed in Table 5.25.

5.12. The ${}^9\text{Be}(\tau,n){}^{11}\text{C}$ reaction

This reaction has been studied in a relatively large number of papers (see Table 5.26). Their prime objective has been to investigate the mechanism of the (τ,n) process, which provides the means to obtain and study proton-emitting nuclei that are otherwise difficult to produce.

The evaluation of the total cross-section for the production of the radioactive carbon-11 nucleus was based on measurements reported in Refs [325-327]. The good agreement among the data reported in these three independent measurements made it possible to derive recommended values with an uncertainty of $\leq 5\%$.

In order to obtain a reliable extrapolation to low energies, the above-mentioned data were supplemented by the excitation function for the

total differential cross-section at 0° , taken from Ref. [192]. The normalizing factor was chosen so as to guarantee a smooth transition from the data given in Ref. [192] to the data derived from Refs [325-327].

Spline coefficients describing the total integral carbon-11 production cross-section are listed in Table 5.27. Expression (2.11) can be used to calculate the cross-section. A comparison of the evaluated curve with the experimental data will be found in Fig. 5.13.

Extrapolation of the cross-section to energies lower than 0.8 MeV can rely on Eq. (2.14) with the following parameters (in the centre-of-mass system): $E_g = 140.98$ MeV and $S(0) = 5.78$ MeV·b.

The partial differential cross-sections of the ${}^9\text{Be}(\tau,n){}^{11}\text{C}$ reaction leading to the ground and first excited states of carbon-11 have been studied in detail in the measurements reported in Refs [328-330]. As indicated in Ref. [328], the shape of the neutron angular distributions changes considerably with increasing energy. For neutrons emitted in the reaction channel corresponding to the ground state, the angular distribution changes from a near-symmetrical distribution with respect to 90° at low energies [328] to one that is highly asymmetrical, and has a pronounced forward peak at energies larger than 4 MeV.

In contrast to the shape of the integral cross-section, the excitation function of the partial differential cross-section at 0° for the ${}^9\text{Be}(\tau,n){}^{11}\text{C}$ reaction corresponding to the ground state of the resultant nucleus (shown in Fig. 5.14) displays a rather irregular behaviour characterized by depressions at 2.4 and 5.5 MeV.

The evaluated spline curve for the partial differential cross-section of the ${}^9\text{Be}(\tau,n_0){}^{11}\text{C}$ reaction, which was derived from the results published in [328] and [330], is plotted in Fig. 5.14, and the spline coefficients are listed in Table 5.28.

The angular distribution of neutrons emitted in the reaction channel corresponding to the ground state of carbon-11 can be calculated using the Legendre polynomial coefficients listed in Table 5.29. The differential cross-section in the centre-of-mass system can be derived from the following equation:

$$\sigma(\theta, E) = \sigma(0^\circ, E) \sum_{k=0}^n B_k(E) P_k(\cos\theta)$$

where B_k are the Legendre coefficients for the k -th term of the polynomial, and $\sigma(0^\circ, E)$ is the differential cross-section at zero degrees.

The partial cross-section corresponding to the ground state of carbon-11 has been reviewed here. Information on the partial cross-section corresponding to the first excited state is available from only one paper [328]. The excitation function for the integral partial cross-section of the ${}^9\text{Be}(\tau, n){}^{11}\text{C}$ reaction taken from that paper is reproduced in Fig. 5.15.

5.13. The ${}^9\text{Be}(\tau, p){}^{11}\text{B}$ reaction

The partial differential cross-sections of this reaction have been studied in the energy range 1.0 to 14 MeV (see Table 5.30).

The principal interest in this reaction was stimulated by the opportunity of studying the double nucleon transfer mechanism. The most complete data are reported in Ref. [331], which includes measurements of angular distributions and excitation functions of the partial differential cross-sections for the first seven levels of the residual nucleus. With reference to the shape of the angular distributions associated with these partial ${}^9\text{Be}(\tau, p){}^{11}\text{B}$ reaction cross-sections, the authors of Ref. [331] conclude that the direct double nucleon transfer mechanism plays a dominant role in most of the partial cross-sections of this reaction.

Reference [332] reports on an investigation of this reaction in the energy range from 1.8 to 4.8 MeV, which includes measurements of the

differential cross-section over a broad range of angles for channels corresponding to the ground and first excited states of the boron-11 nucleus. The data from Ref. [332] are in good agreement with Ref. [335]. In our own paper we have used a linear extrapolation of the excitation functions of the partial integral cross-sections reported in Ref. [332] up to 5.8 MeV to normalize the measurements reported in Ref. [331]. An analysis of the [331] data shows that the shapes of the angular distributions do not change significantly with increasing energy; as a result, the excitation function of the integral cross-section can be described to a high degree of accuracy by the excitation function of this cross-section at an angle of 90° . In most cases, the angular distributions reported in Ref. [331] are characterized by prominent forward peaking, which confirms the conclusion that the direct reaction mechanism plays a dominant role in these reactions.

Excitation functions of the integral partial cross-sections corresponding to the reaction channels leading to the ground and first excited states of the boron-11 nucleus are shown in Figs 5.16 and 5.17 respectively. The spline coefficients for these evaluated curves are listed in Table 5.31.

5.14. The ${}^9\text{Be}(\alpha, n){}^{12}\text{C}$ reaction

The interaction of α -particles with beryllium-9 nuclei has been thoroughly studied because of the extensive use of the ${}^9\text{Be}(\alpha, n){}^{12}\text{C}$ reaction as a neutron source. Most of these measurements concentrated on thick-target yields of neutrons from beryllium targets rather than on detailed studies of angle and energy characteristics of this reaction. The available data on the interaction of α -particles with beryllium-9 nuclei lead to the conclusion that the compound nucleus process plays a prevalent role in determining the shape of the ${}^9\text{Be}(\alpha, n){}^{12}\text{C}$ reaction cross-section.

Both partial as well as total neutron production cross-sections, measured over a broad energy range (0.4 to 20 MeV), are described in the literature (see Table 5.32).

Direct measurements of the total cross-section are reported only in one paper [337]. The resulting data were compared with the summed partial integral cross-sections from Refs [338] and [339], taking into account the continuous neutron spectrum reported in [340].

The data recommended in our evaluation are based on the evaluated results published in Ref. [339], which emerged from an analysis of more than 127 angular distributions taken from measurements reported in Refs [338, 340-344].

Table 5.33 lists recommended integral cross-section data for separate reaction channels, as well as for the total neutron yield. Graphical representations of the excitation functions for the partial and total neutron production cross-sections are shown in Fig. 5.18.

The difference between the summed partial cross-sections for individual reaction channels and the total cross-section is due to the contribution of the continuous neutron spectrum which results from the three-particle reaction channel.

Table 5.1

Energy characteristics of interactions between hydrogen and helium isotopes and beryllium nuclei

Input channel	Output channel	Energy MeV	Reaction Product Decay	Decay Energy, MeV
$^9\text{Be}+p$	$^{10}\text{B}+\gamma$	6,586	-	-
$^9\text{Be}+p$	$^9\text{B}+n$	-1,851	$^9\text{B} \rightarrow ^8\text{Be}+p$	0,158
$^9\text{Be}+p$	$^8\text{Be}+d$	0,559	$^8\text{Be} \rightarrow 2\alpha$	0,092
$^9\text{Be}+p$	$^6\text{Li}+\alpha$	2,126	-	-
$^9\text{Be}+p$	$^7\text{Be}+t$	-12,082	$^7\text{Be}(\epsilon) \rightarrow ^7\text{Li}$	0,862
$^9\text{Be}+d$	$^{11}\text{B}+\gamma$	15,816	-	-
$^9\text{Be}+d$	$^{10}\text{B}+n$	4,362	-	-
$^9\text{Be}+d$	$^{10}\text{B}+p$	4,588	$^{10}\text{B}(\beta) \rightarrow ^{10}\text{B}$	0,557
$^9\text{Be}+d$	$^8\text{Be}+t$	4,592	$^8\text{Be} \rightarrow 2\alpha$	0,092
$^9\text{Be}+d$	$^7\text{Li}+\alpha$	7,152	-	-
$^9\text{Be}+t$	$n+^{11}\text{B}$	9,559	-	-
$^9\text{Be}+t$	$^8\text{Li}+\alpha$	2,926	$^8\text{Li}(\beta) \rightarrow ^8\text{Be}$	16,006
$^9\text{Be}+t$	$^{10}\text{B}+d$	0,555	$^{10}\text{B}(\beta) \rightarrow ^{10}\text{B}$	0,557
$^9\text{Be}+t$	$^{12}\text{C}+\gamma$	26,279	-	-
$^9\text{Be}+t$	$n+^{11}\text{C}$	7,558	$^{11}\text{C}(\beta) \rightarrow ^{11}\text{B}$	1,982
$^9\text{Be}+t$	$p+^{11}\text{B}$	10,323	-	-
$^9\text{Be}+t$	$d+^{10}\text{B}$	1,092	-	-
$^9\text{Be}+t$	$t+^9\text{B}$	-1,087	$^9\text{B} \rightarrow ^8\text{Be}+p$	0,158
$^9\text{Be}+t$	$\alpha+^8\text{Be}$	18,912	$^8\text{Be} \rightarrow 2\alpha$	0,092
$^9\text{Be}+\alpha$	$^{13}\text{C}+\gamma$	10,648	-	-
$^9\text{Be}+\alpha$	$^{12}\text{C}+n$	5,702	-	-

Table 5.2

Brief data content of references used in the evaluation of the $^9\text{Be}(p,\gamma)^{10}\text{B}$ integral gamma ray production cross-section

Energy range in MeV	Range of angles in deg	Type of data	Uncertainty in %		Ref.
			random	system.	
0,1-0,22	90	UND/EXC, DA	5	20	[210]
0,27-1,2	90	PAR/EXC, DA	15	20	[269]
0,33;0,50	90	UND/EXC, DA	10	20	[270]
1,2-1,9	0-120	PAR/AND, DA	25	30	[271]

Table 5.3

Spline fit coefficients for the description of the ${}^9\text{Be}(p,\gamma){}^{10}\text{B}$ gamma ray production cross-section
(The cross-section can be calculated using Eq. (2.13))

Knot No.	Knot energy in MeV	Spline fit coefficients				Cross-section uncart., %
		A ₀	A ₁	A ₂	A ₃	
I	0,102	-7,858	4,644	-0,992	0,231	12,86
2	0,335	-3,354	0,570	-45,34	167,8	4,932
3	0,403	-3,735	1,248	48,96	-1262,8	4,156
4	0,420	-3,688	-0,928	-103,2	3593,5	6,210
5	0,424	-3,703	-1,914	-0,846	8,907	5,576
6	0,686	-3,434	2,399	-15,73	80,97	4,632
7	0,808	-3,101	3,837	24,26	170,8	4,530
8	0,952	-1,077	25,48	-582,4	2648,4	3,370
9	1,037	-1,502	-16,00	97,87	-71,74	4,574
10	1,130	-2,200	-82,36	79,44	-1501,5	2,580
II	1,194	-2,256	0,000	0,000	0,000	4,678

Table 5.6

Legendre polynomial coefficients to calculate the ${}^9\text{Be}(p,n){}^9\text{B}$ differential cross-section

Energy in MeV	σ_p in mb	B ₁	B ₂	B ₃	B ₄	B ₅	B ₆
2,06	1,09	-0,04	0,095	0,048	-0,038	-0,01	-
2,12	3,71	-0,08	0,220	0,085	-0,058	0,318	-
2,30	18,1	-0,33	0,506	0,202	-0,084	0,073	-
2,40	44,9	-0,37	0,506	0,209	-0,113	0,086	-
2,50	93,6	-0,22	0,310	0,138	-0,172	0,122	-
2,56	130,2	0,02	0,140	0,056	-0,218	0,151	-
2,58	137,8	0,04	0,092	0,028	-0,230	0,160	-
2,60	102,1	0,08	0,045	0,002	-0,240	0,170	-
2,70	88,1	0,063	-0,123	-0,048	-0,247	0,182	-
2,76	85,6	-0,013	-0,186	0,03	-0,228	0,160	-
2,80	86,2	-0,016	-0,217	0,143	-0,210	0,122	-
2,90	91,2	-0,083	-0,254	0,283	-0,156	0,065	-
3,00	95,4	-0,141	-0,249	0,285	-0,108	0,048	-
3,10	95,8	-0,191	-0,215	0,243	-0,082	0,035	-
3,5	87,2	-0,328	0,023	0,187	0,062	0,008	-
4,0	121,3	-0,396	0,561	0,329	0,159	0,047	-
4,5	160,0	-0,392	0,942	0,814	-0,024	0,028	-
5,0	119,5	-0,344	0,691	0,401	-0,420	-0,014	-0,035
5,5	114,0	-0,266	0,43	-0,075	-0,512	-0,019	-0,035
6,0	94,8	-0,172	0,334	-0,201	-0,440	-0,009	-0,031
7,0	79,5	0,045	0,356	-0,365	-0,182	0,009	-0,014
8,0	53,2	0,275	0,465	-0,374	0,012	-0,0015	0,011
9,0	46,2	0,469	0,529	-0,251	0,088	-0,079	0,041
10,0	44,1	0,381	0,511	-0,308	0,060	-0,150	0,080
12,0	37,9	0,435	0,416	-0,423	-0,016	-0,243	0,204
14,0	33,2	0,597	0,421	-0,412	-0,210	-0,088	0,392

Table 5.4

Brief data content of references used in the evaluation of the ${}^9\text{Be}(p,n){}^9\text{B}$ neutron production cross-section

Energy range in MeV	Range of angles in deg	Type of data	Uncertainty in %		Ref.
			random	system.	
2,1-5,1	0-150	UND/AND, DA	7-10		[274]
2,1-2,8	4 π	UND/EXC, SIG	7-10		[274]
2,3-5,6	0; 90	EXC, DA	10		[275]
2,1-5,4	4 π	UND/EXC, SIG	3		[21]
2,5-4,1	0-150	AND, DA	30		[276]
3,5-10,9	0-150	AND, DA	10		[277]
18,5	0-150	AND, DA	10		[278]
4-14,3	4 π	UND/EXC, SIG	5-20		[151]
8,2-15,7	0-150	AND, DA	5		[279]

Table 5.7

Brief data content of references used in the evaluation of the ${}^9\text{Be}(p,d){}^8\text{Be}$ reaction cross-section (angular distribution data, ground state)

Energy range in MeV	Range of angles in deg	Uncertainty in %		Ref.
		random	system.	
0,03-0,7	60-160	3	6	[283]
0,8-3,0	30-150	5	10	[284]
0,3	40-150	3	6	[285]
2,1-3,3	20-160	5	10	[286]
5-11	15-165	3	5	[287]
6,0	24-164	5	10	[288]
7,0	40-160	7	15	[289]
10	20-165	12	30	[290]
12	20-166	10	20	[291]
15	10-150	20	20	[281]
14;26	10-100	10	20	[282]

Table 5.5

Spline fit coefficients for the description of the ${}^9\text{Be}(p,n){}^9\text{B}$ neutron production cross-section. (The cross-section can be calculated using Eq. (2.13))

Knot no.	Knot energy in MeV	Spline fit coefficients				Cross section uncart., %
		A ₀	A ₁	A ₂	A ₃	
I	2,053	0,827	98,35	-2092	21262	6,8
2	2,101	2,242	35,83	-622,5	4970,5	4,2
3	2,187	3,001	9,873	-21,04	230,04	4,5
4	2,430	4,075	13,08	51,56	1235	3,0
5	2,537	4,834	24,43	211,3	-37703	4,0
6	2,562	5,063	17,18	-929,7	-399164	4,2
7	2,573	5,069	-12,58	145,6	-415,8	4,5
8	2,933	5,003	2,720	-3,082	2,369	5,0
9	4,049	5,639	1,471	17,06	36,23	5,0
10	4,466	5,981	5,856	-41,74	18,65	6,0
II	4,904	6,179	-1,471	-36,51	459,8	7,0
12	5,315	6,064	1,587	-17,07	52,21	8,0
13	6,749	6,180	2,364	-2295	427407	9,0
14	6,761	6,179	-1,743	28,57	-109,8	10,0
15	7,489	6,182	0,656	-5,113	17,39	12,0
16	8,988	6,238	0,528	-2,664	3,729	15,0
17	11,38	6,263	-0,107	1,618	-12,01	20,0
18	14,22	6,186	0	0	0	20,0

Table 5.8

Spline fit coefficients for the description of the ${}^9\text{Be}(p,d){}^8\text{Be}$ partial reaction cross-section. (The cross-section can be calculated using Eq. (2.13))

Knot no.	Knot Energy in MeV	Spline fit coefficients				Cross section uncart., %
		A ₀	A ₁	A ₂	A ₃	
I	0,0280	-9,040	5,700	2,781	-1,300	10
2	0,115	0,878	5,699	-2,762	2,444	6
3	0,210	3,824	5,019	11,24	-24,91	6
4	0,311	6,022	2,284	-18,19	23,95	6
5	0,405	5,800	-2,313	207,72	-6402,9	6
6	0,409	5,792	-0,0665	-1,719	1,448	5
7	0,629	5,561	-0,742	0,144	6,885	5
8	0,953	5,774	-10,86	81,86	-104,91	6
9	1,272	5,269	-1,370	8,540	-17,87	10
10	1,512	5,195	-0,020	-0,742	-0,970	10
11	2,489	4,881	-1,481	2,035	-1,067	10
12	7,696	4,268	-0,966	-1,579	-0,848	10
13	26,20	2,273	0	0	0	15

Table 5.9

Brief data content of references used in the evaluation of the ${}^9\text{Be}(p,\alpha){}^6\text{Li}$ cross-section

Energy range in MeV	Range of angles in deg	Type of data	Uncertainty in %		Ref.
			random	system.	
0,03-0,7	60-160	AND, DA, α_0	3	6	[283]
0,3	40-150	AND, DA, α_0	5	10	[285]
0,8-3,0	90	EXC, DA, α_0	5	10	[284]
I-4,5	20-160	AND, DA, α_0	12	20	[286]
2,2-4,5	35;80	EXC, DA, α_0	12	20	[286]
2,2-3,2	35	EXC, DA, α_1	12	20	[286]
6,0-II,5	24-164	AND, DA, α_0	10	20	[288]
9,0-II,5	24-164	AND, DA, α_1	10	20	[288]
3,7-12,1	90	EXC, DA, α_0	10	20	[288]
5,1-12,0	90	EXC, DA, α_1	10	20	[288]
5,9;7,0	40-160	AND, DA, α_0, α_1	7	15	[289]

Table 5.10

Spline fit coefficients for the description of the ${}^9\text{Be}(p,\alpha){}^6\text{Li}$ partial reaction cross-section. (The cross-section can be calculated using Eq. (2.13))

Knot No.	Knot Energy in MeV	Spline fit coefficients				Cross section uncert., %
		A_0	A_1	A_2	A_3	
I	0,0280	-9,853	9,28	-1,403	0,099	II
2	0,2640	5,031	4,492	-0,731	-14,96	4
3	0,3826	5,832	-2,240	4,593	-2,468	4,5
4	I,5942	4,816	-4,211	$3,29 \cdot 10^5$	$-5,23 \cdot 10^9$	7
5	I,5942	4,816	2,697	-4,044	I,117	5,5
6	8,3002	3,275	-1,524	1,485	-6,209	3,5
7	II,586	2,704	0	0	0	6

Table 5.11

Spline fit coefficients for the description of the ${}^9\text{Be}(p,\alpha){}^6\text{Li}$ partial reaction cross-section. (The cross-section can be calculated using Eq. (2.10))

Knot No.	Knot Energy in MeV	Spline fit coefficients				Cross section uncert., %
		A_0	A_1	A_2	A_3	
I	4,940	85,29	-29,36	19,36	-6,402	I,5
2	5,823	70,05	-10,15	2,40	-0,416	I,0
3	9,652	42,94	-10,11	-2,38	1,525	2,0
4	II,93	25,56	0	0	0	2,5

Table 5.12

Brief data content of references used in the evaluation of the ${}^9\text{Be}(d,\gamma){}^{11}\text{B}$ cross-section

Energy range in MeV	Range of angles in deg	Type of data	Systematic uncertainty in %		Ref.
			random	system.	
0,5-5,5	90; 0-130	AND, DA, γ_0	30		[293]
0,56-3,56	0-130	AND, γ_1, γ_3	35		[294]
2,9-II,9	90; 0-160	AND, DA, γ_0	30		[295]

Table 5.13

Brief data content of references used in the evaluation of the ${}^9\text{Be}(d,n){}^{10}\text{B}$ reaction cross-section

Energy range in MeV	Range of angles in deg	Type of data	Uncertainty in %		Ref.
			random	system.	
0,06-0,16	4 \times	PAR/EXC, SIG, n_0-n_4	10	20	[299]
0,3-0,7	4 \times	PAR/EXC, SIG, n_1	10	30	[270]
0,8-2,4	30	PAR/EXC, DA, n_0, n_1	3	10	[298]
I,4;I,9;2,4	10-150	PAR/AND, DA, n_0, n_1	3	10	[298]
0,5-1,6	5-150	PAR/AND, DA, n_0-n_4	15	-	[296]
0,5-1,5	4 \times	EXC, SIG	10	-	[297]
I,1-3,2	0-150	PAR/AND, DA, n_0-n_2	5	-	[300]
7;12;15;16	10-150	PAR/AND, DA, n_0-n_8	10	15	[301]

Table 5.14

Evaluated partial differential cross-section values for the ${}^9\text{Be}(d,n){}^{10}\text{B}$ reaction

Energy in MeV	Partial cross-section in mb (uncertainty given in %)				
	0(± 20)	0,72(± 20)	1,74(± 30)	2,15(± 25)	3,59(± 30)
0,5	11	30	3	8	5
0,6	19	41	5	11	10
0,7	31	54	7	14	13
0,8	46	72	9	21	19
0,9	58	84	11	29	32
I,0	73	96	13	42	56
I,1	64	78	10	40	48
I,2	55	70	13	27	36
I,3	47	65	11	23	33
I,4	43	65	8	22	47
I,5	55	73	7	26	51
I,8	87	110	11	54	65
3,0	68	78	11	38	58
3,5	63	68	10	32	52
5,0	51	45	8	21	41
7,0	40	24	6	10	29
10,0	28	10	4	3	17
12,0	22	6	3	2	10

Table 5.15

Brief data content of references used in the evaluation of the ${}^9\text{Be}(d,p){}^{10}\text{Be}$ reaction cross-section

Energy range in MeV	Range of angles in deg	Type of data	Uncertainty in %		Ref.
			random	system.	
0,3-0,6	5-170	PAR/AND, DA, p_0	10	30	[302]
0,6-1,4	0-170	PAR/AND, DA, p_0	10	20	[303]
0,6-2,7	10-150	PAR/AND, DA, p_0, p_1	20	70	[304]
0,09-0,24	90	PAR/EXC, DA, p_0, p_1	10	15	[210]
0,9-2,5	30-160	PAR/AND, DA, p_0, p_1	7	15	[305]
0,85-2,0	-	EXC, SIG, p_0	5	10	[306]
0,9-3,1	-	PAR/EXC, SIG, p_0, p_1	5	10	[307]
I,7-3,1	0-170	AND, DA, p_0	5	20	[308]
2,0-2,8	30-150	AND, DA, p_0	3	10	[309]
3,4; 3,9	20-100	PAR/AND, DA, p_0-p_2	10	-	[310]
3,6	20-160	PAR/AND, DA, p_0, p_1	15	20	[311]
3,8-6,3	40	PAR/EXC, DA, p_0, p_1	7	30	[312]
4,5-5,2	20-160	PAR/AND, DA, p_0-p_4	10	20	[176]
II,8	20-160	PAR/AND, DA, p_0-p_9	7	15	[313]
I-2I	4 \times	EXC, SIG, ACT	20	30	[314]
15	15-140	PAR/AND, DA, p_0-p_9	5	18	[281]

Table 5.16

Integral proton production cross-sections of the ${}^9\text{Be}(d,p){}^{10}\text{Be}$ reaction

Energy in MeV	Cross-section in mb	Energy in MeV	Cross-section in mb	Energy in MeV	Cross-section in mb
0,045	0,09	3,645	119,2	9,968	73,3
0,605	0,941	3,652	125,4	10,41	69,7
0,945	5,37	3,768	129,9	10,96	64,4
1,064	11,6	3,995	132,6	11,41	59,9
I,292	16,0	4,221	134,3	11,74	58,9
I,413	23,2	4,557	135,2	12,41	52,7
I,533	31,2	5,000	131,6	13,18	49,1
I,763	36,5	5,444	128,0	13,85	45,4
I,995	43,6	5,552	124,4	14,63	43,6
2,114	50,7	5,992	118,2	15,20	41,8
2,235	58,7	6,322	112,8	15,86	40,0
2,354	65,0	6,764	108,3	16,75	37,2
2,473	71,2	7,094	102,9	17,53	36,3
2,592	78,3	7,425	99,3	18,20	35,3
2,712	85,4	7,867	94,9	19,21	33,5
2,830	90,8	8,310	90,4	19,99	31,6
3,063	98,8	8,752	85,9	20,77	30,7
3,182	105,9	8,972	82,3	21,3	30,7
3,412	111,2	9,302	77,8	22,0	30,0

Table 5.17

Spline fit coefficients for the description of the recommended ${}^9\text{Be}(d,pq){}^{10}\text{Be}$ integral reaction cross-section. (The cross-section can be calculated using Eq. (2.13))

Knot No.	Knot Energy in MeV	Spline fit coefficients				Cross section uncert., %
		A_0	A_1	A_2	A_3	
I	0,0857	-6,6155	6,5678	-1,1903	0,0403	9
2	0,7356	2,4031	2,0086	-20,998	93,138	4,5
3	0,7928	2,4749	0,4307	-0,0859	-0,057	20
4	11,181	1,9567	-1,2212	-0,5383	-1112,6	18
5	11,8	1,7156	0	0	0	10

Table 5.18

Spline fit coefficients for the description of the recommended ${}^9\text{Be}(d,p_1){}^{10}\text{Be}$ integral reaction cross-section. (The cross-section can be calculated using Eq. (2.13))

Knot No.	Knot Energy in MeV	Spline fit coefficients				Cross section uncert., %
		A_0	A_1	A_2	A_3	
I	0,09	-6,6540	8,3144	-4,1220	1,0023	25
2	0,789	2,2187	4,5829	-1,0331	9,1825	20
3	1,521	3,3736	2,8941	-8,0214	5,6273	20
4	2,714	3,4522	-0,7341	0,7063	-0,4968	20
5	11,9	2,306	0	0	0	25

Table 5.19

Brief data content of references used in the evaluation of the ${}^9\text{Be}(d,t_0){}^8\text{Be}$ and ${}^9\text{Be}(d,t){}^8\text{Be}$ reaction cross-sections

Energy range in MeV	Range of angles in deg	Type of data	Uncertainty in %		Ref.
			random	system.	
15	25-125	PAR/AND, DA, α_0, α_1	10	20	[281]
0,295-0,62	5-170	AND, DA, t_0	10	30	[302]
15,1	25-110	AND, DA, t_0	20	30	[316]
0,9-2,5	30-160	AND, DA, t_0	20	20	[317]
1,5-13,5	4 π	UND/EXC, SIG	5	25	[314]
0,86-2,2	25-160	AND, DA, t_0	5	10	[306]
3,8-6,3	40	EXC, DA, t_0	15	25	[312]
0,6-2,7	30-160	AND, DA, t_0	20	70	[304]
2,3;2,5;2,8	30-160	AND, DA, t_0	5	10	[309]
12,2-14,4	85	PAR/EXC, DA, t_0, t_1	10	20	[318]
12,4;14,1	20-170	PAR/AND, DA, t_0, t_1	10	20	[318]
0,9-3,1	30-160	AND, DA, t_0	5	15	[307]
0,35-7,7	4 π	UND/EXC, SIG	5	15	[315]

Table 5.20

Spline fit coefficients for the description of the tritium production ${}^9\text{Be}(d,t){}^8\text{Be}$ reaction cross-section. (The cross-section can be calculated using Eq. (2.11))

Knot No.	Knot Energy in MeV	Spline fit coefficients				Cross section uncert., %
		A_0	A_1	A_2	A_3	
I	1,440	108,84	388,90	-397,7	126,14	30
2	8,049	243,16	-891,1	1332,9	-557,9	20
3	18,42	102,5	0	0	0	20

Table 5.21

Spline fit coefficients for the description of the ${}^9\text{Be}(d,t_0){}^8\text{Be}$ integral reaction cross-section. (The cross-section can be calculated using Eq. (2.11))

Knot No.	Knot Energy in MeV	Spline fit coefficients				Cross section uncert., %
		A_0	A_1	A_2	A_3	
I	0,295	0,871	-3,18	14,88	-3,46	30
2	0,825	9,58	16,45	4,204	7,444	30
3	1,384	20,24	26,77	15,75	-35,32	30
4	2,347	33,57	13,88	-40,18	13,64	30
5	15,0	8,11	0	0	0	30

Table 5.22

Brief data content of references used in the evaluation of the ${}^9\text{Be}(d,\alpha_0){}^7\text{Li}$ and ${}^9\text{Be}(d,\alpha_1){}^7\text{Li}$ reaction cross-sections

Energy range in MeV	Range of angles in deg	Type of data	Uncertainty in %		Ref.
			random	system.	
0,5-0,9	-	PAR/EXC, SIG, α_0, α_1	5	10	[319]
0,09-0,24	90	EXC, DA, α_0	10	30	[210]
13,6	8-143	PAR/AND, DA, α_0, α_1	10	20	[320]
0,3-1,0	10-170	PAR/AND, DA, α_0, α_1	5	15	[321]
0,2-0,5	50-170	PAR/AND, DA, α_0, α_1	10	30	[270]
14,1	30-170	PAR/AND, DA, α_0, α_1	8	15	[289]
0,9-2,2	15-165	PAR/AND, DA, α_0, α_1	5	10	[322]
0,4-2,4	25-170	PAR/AND, DA, α_0, α_1	4	10	[306]
0,4-2,4	90; 165	PAR/EXC, DA, α_0, α_1	6	10	[306]
0,6-2,0	25-170	PAR/AND, DA, α_0, α_1	40	70	[304]
0,6-2,0	160	PAR/EXC, DA, α_0, α_1	-	-	[304]
12,7-14,4	25-170	PAR/AND, DA, α_0, α_1	8	10	[318]
12,7-14,4	35	PAR/EXC, DA, α_0, α_1	8	10	[318]

Table 5.23

Partial cross-sections for the ${}^9\text{Be}(d,\alpha_0){}^7\text{Li}$ and ${}^9\text{Be}(d,\alpha_1){}^7\text{Li}$ reactions (Data uncertainty is $\pm 10\%$)

Energy in MeV	Reaction channel cross-sections in mb	
	d,α_0	d,α_1
0,2	0,35	0,50
0,3	2,3	3,2
0,4	5,5	7,2
0,5	9,1	10,9
0,6	12,5	14,5
0,7	16,5	17
0,8	19,5	19
0,9	23	22,7
1,0	27,9	26,2
1,5	45	37
2,0	41	39,7
2,5	42,1	33,2
3,0	36	35
3,5	31	29
4,0	28	24
4,5	25	21
5,0	22	20
5,5	20	18
6,0	19	17
7,0	18	14
8,0	15	12
9,0	13	10,5
10,0	12,7	8,0
11,0	11,1	7,2
12,0	10,0	6,1
13,0	7,6	5,6
14,0	7,3	5,1

Table 5.24

Spline fit coefficients for the description of the evaluated ${}^9\text{Be}(d,\alpha){}^{11}\text{C}$ integral reaction cross-section. (The cross-section can be calculated using Eq. (2.13))

Knot No.	Knot Energy in MeV	Spline fit coefficients				Cross section uncert., %
		A ₀	A ₁	A ₂	A ₃	
1	0,087	-4,662	4,568	2,089	-1,309	15
2	0,363	2,313	2,525	-1,149	0,120	10
3	0,833	3,686	0,865	-0,885	28332	10
4	0,836	3,690	1,888	-1,121	-0,140	10
5	2,043	4,382	-0,452	-1,497	11,243	10
6	2,680	4,374	1,225	-59,225	458,81	10
7	2,800	4,353	-1,323	0,632	-0,322	10
8	14,06	2,518	0	0	0	12

Table 5.25

Integral neutron production cross-sections of the ${}^9\text{Be}(t,n){}^{11}\text{B}$ reaction

Energy in MeV	Cross-section in mb	Energy in MeV	Cross-section in mb
0,58	56	1,23	314
0,78	127	1,43	390
0,88	164	1,48	410
1,03	227	1,54	438
1,13	272	1,584	472
1,182	292	1,975	555

Table 5.26

Brief data content of references used in the evaluation of the ${}^9\text{Be}(t,n){}^{11}\text{C}$ reaction cross-section

Energy range in MeV	Range of angles in deg	Type of data	Uncertainty in %		Ref.
			random	system.	
5-40	4 π	UND/EXC, SIG	10	15	[325]
3,2-9,6	4 π	UND/EXC, SIG	10	15	[326]
2,0-6,2	4 π	UND/EXC, SIG	5	8	[327]
1,5-5,0	0-170	PAR/AND, DA	10	20	[328]
0,9-1,4	0-160	PAR/AND, DA	5	20	[329]
3,5-5,8	0-160	PAR/AND, DA	10	25	[380]
0,6-1,3	0	UND/EXC, DA	10	25	[192]

Table 5.27

Spline fit coefficients for the description of the ${}^9\text{Be}(t,n){}^{11}\text{C}$ carbon-11 production cross-section.

Knot No.	Knot Energy in MeV	Spline fit coefficients				Cross section uncert., %
		A ₀	A ₁	A ₂	A ₃	
1	0,652	0,337	8,368	-18,81	103,0	0,03
2	1,151	17,95	86,89	156,93	-163,9	0,47
3	1,916	81,30	119,1	-93,75	4,474	2,94
4	7,991	73,23	-121,3	-82,13	7,22·10 ⁶	3,55
5	8,002	73,08	-79,85	41,80	-12,16	3,55
6	24,18	19,46	-32,00	1,480	22,91	0,8
7	40,70	6,433	0	0	0	0,5

Table 5.28

Spline fit coefficients for the description of the partial differential ${}^9\text{Be}(t,n){}^{11}\text{C}$ (ground state) cross-section at 0°. (The cross-section can be calculated using Eq. (2.10))

Knot No.	Knot energy in MeV	Spline fit coefficients				Cross section uncert., %
		A ₀	A ₁	A ₂	A ₃	
1	1,330	0,613	1,480	6,831	-9,714	0,11
2	1,732	1,681	2,265	-4,878	4,167	0,08
3	2,561	2,582	2,776	5,495	-4,594	0,09
4	3,312	5,819	3,256	-4,857	1,837	0,09
5	4,867	6,045	1,473	3,710	-5,243	0,1
6	5,719	6,750	0,0	0,0	0,0	0,24

Table 5.29

Legendre polynomial coefficients for calculating partial angular differential cross-sections for the ${}^9\text{Be}(t,n_0){}^{11}\text{C}$ reaction corresponding to the ground state of the residual C nucleus

Energy in MeV	Cross-section in mb/r	B ₀	B ₁	B ₂	B ₃	B ₄	B ₅
0,9	0,217	0,635	-0,177	0,488	0,020	0,014	-0,005
1,0	0,223	0,607	-0,093	0,469	0,002	0,033	-0,032
1,2	0,315	0,633	-0,097	0,456	0,083	-0,059	0,018
1,4	0,642	0,728	-0,227	0,487	-0,04	-0,075	-0,007
1,59	1,10	0,704	-0,141	0,445	0,03	-0,027	-0,014
1,77	1,55	0,729	-0,088	0,298	-0,039	0,031	0,052
1,97	1,71	0,779	-0,073	0,236	-0,049	0,054	0,001
2,19	1,76	0,854	-0,094	0,214	-0,050	0,031	0,031
2,48	2,02	0,938	-0,121	0,236	-0,029	0,09	0,009
2,80	2,68	0,831	-0,012	0,182	0,056	0,082	-0,016
3,11	3,98	0,594	0,055	0,230	0,141	-0,034	-0,032
3,46	5,11	0,502	0,096	0,215	0,182	-0,031	-0,000

Table 5.29 (cont.)

Energy in MeV	Cross-section in mb/r	B ₀	B ₁	B ₂	B ₃	B ₄	B ₅
3,81	5,26	0,489	0,136	0,242	0,156	-0,067	0,040
4,12	5,07	0,427	0,152	0,248	0,124	-0,046	0,049
4,52	4,59	0,432	0,152	0,245	0,086	-0,018	0,074
4,90	4,92	0,388	0,156	0,226	0,103	0,055	0,051
5,16	4,83	0,379	0,153	0,193	0,123	0,080	0,012

Table 5.30

Brief data content of references used in the evaluation of the ${}^9\text{Be}(t,p){}^{11}\text{B}$ reaction cross-section

Energy range in MeV	Range of angles in deg	Type of data	Uncertainty in %		Ref.
			random	system.	
1,8-4,8	10-150	PAR/EXC, DA	5	20	[332]
5,7-10,2	10-130	PAR/AND, DA	7	-	[331]
5,7-10,2	10	PAR/EXC, DA	7	-	[331]
2,0	30-160	PAR/AND, DA	5	20	[333]
13-14,2	30-60	PAR/AND, DA	5	9	[334]
14,0	20-150	PAR/AND, DA	5	20	[204]
2,0	5-170	PAR/AND, DA	5	20	[335]
1-3	10-160	PAR/AND, DA	10	25	[336]

Table 5.31

Spline fit coefficients for the description of the partial cross section for the ${}^9\text{Be}(t,p){}^{11}\text{B}$ reaction. (The cross-section can be calculated using Eq. (2.10))

Channel	Knot No.	Knot energy in MeV	Spline fit coefficients				Cross section uncert., %
			A ₀	A ₁	A ₂	A ₃	
P ₀	1	1,806	12,141	14,152	-13,725	-5,598	0,6
	2	2,327	14,994	-4,733	6,660	-3,430	0,4
	3	3,662	12,384	-5,292	8,351	-4,030	0,3
	4	4,423	11,416	0,417	-0,841	0,076	0,3
P ₀	5	6,789	8,702	-2,285	0,322	-0,019	1,2
	6	14,0	1,660	0	0	0	0,8
P ₁	1	1,815	6,433	2,268	-3,613	1,871	0,4
	2	3,152	7,612	2,740	3,892	-16,12	0,3
	3	3,516	8,348	-0,813	-0,025	0,052	0,4
	4	5,157	7,173	-0,479	0,229	-5,403	0,4
	5	5,493	6,833	-2,157	-5,220	8,233	0,5
	6	5,981	5,494	-1,378	0,171	-0,0075	1,1
	7	14,0	1,610	0	0	0	0,2

Table 5.32

Brief data content of references used in the evaluation of the ${}^9\text{Be}(\alpha, n){}^{12}\text{C}$ reaction cross-section

Energy range in MeV	Range of angles in deg	Type of data	Uncertainty in %		Ref.
			random	system.	
0,48-0,70	0-140	AND, DA, n_0, n_1	5	15	[344]
0,56-1,32	0-160	AND, DA, n_0, n_1	5	25	[343]
0,56-1,32	0	EXC, DA, n_0, n_1	5	25	[343]
1,5-7,8	0-160	AND, DA, n_0-n_3	10	15	[338]
1,5-7,8	0	EXC, DA, n_0-n_3	10	15	[338]
-3,6-7,6	0; 90	EXC, DA, n_1	10	25	[345]
1,8-5,3	0; 90	EXC, DA, n_0, n_1	15	25	[346]
1,8;2,0	0-165	AND, DA, n_0	5	20	[347]
1,7-6,4	0	EXC, DA, n_0-n_3	5	10	[340]
1,7-6,4	0-70	AND, DA, n_0, n_1	3	-	[342]
6,8-9,9	0-170	AND, DA, n_0-n_2	5	10	[341]
13-14	10-160	AND, DA, n_0-n_4	5	15	[348]
17-22	12-165	AND, DA, n_0-n_3	15	30	[349]
14-23	0-165	AND, DA, n_0, n_1	5	20	[350]
1,7-10,5	4 π	UND/EXC, SIG	5	6	[337]

Table 5.33

Total and partial neutron production cross-sections for the ${}^9\text{Be}(\alpha, n){}^{12}\text{C}$ reaction.

Energy in MeV	Partial cross-section in mb				Total cross-section in mb
	n_0	n_1	n_2	n_3	
1,4	5,8	0	-	-	5,8
1,5	8,1	0	-	-	8,5
1,6	9,0	8,8	-	-	17,8
1,7	12,6	39,9	-	-	52,5
1,8	39,9	185,3	-	-	225,2
1,9	59,3	236,7	-	-	296,0
2,0	72,0	167,2	-	-	239,2
2,1	81,8	90,7	-	-	172,5
2,2	107,4	74,3	-	-	181,7
2,3	115,0	55,3	-	-	170,3
2,4	111,7	53,6	-	-	165,3
2,5	111,0	74,6	-	-	185,6
2,6	95,6	97,6	-	-	193,2
2,7	71,5	100,8	-	-	172,3
2,8	59,7	80,9	-	-	140,6
2,9	58,9	63,1	-	-	122,0
3,0	49,1	51,7	-	-	101,0

Table 5.33 (contd.)

Energy in MeV	Partial cross-section in mb				Total cross-section in mb
	n_0	n_1	n_2	n_3	
3,1	42,5	48,5	-	-	91,1
3,2	35,1	53,5	-	-	88,6
3,3	32,4	54,4	-	-	86,8
3,4	36,4	55,4	-	-	92,1
3,5	47,1	62,6	-	-	110,0
3,6	75,6	72,0	-	-	148,0
3,7	98,6	73,6	-	-	174,1
3,8	113,5	74,6	13,8	-	202,0
3,9	130,2	84,5	33,4	-	250,0
4,0	140,2	339,8	58,4	-	541,0
4,1	148,0	236,0	70,5	-	462,0
4,2	139,2	202,8	71,6	-	430,0
4,3	119,9	232,2	65,8	-	438,0
4,4	109,6	250,0	57,5	-	442,0
4,5	110,0	257,8	51,7	-	448,0
4,6	84,1	256,0	46,8	-	435,0
4,7	76,4	244,4	45,9	-	407,0
4,8	70,6	255,0	44,6	-	431,0
4,9	75,6	296,9	47,6	-	475,0
5,0	79,	330,3	37,9	-	522,0
5,1	60,1	340,0	32,7	-	536,0
5,2	65,9	325,0	38,4	-	549,0
5,3	63,8	335,1	41,8	-	580,0
5,4	54,7	320,2	36,4	-	580,0
5,5	49,3	316,8	35,6	-	590,0
5,6	45,3	320,0	28,4	-	613,0
5,7	42,1	325,8	22,8	-	637,0
5,8	36,1	323,0	21,5	-	657,0
5,9	48,6	257,2	21,4	-	626,0
6,0	43,7	244,9	18,6	-	606,0
6,1	34,9	217,1	18,0	-	592,0
6,2	34,8	195,5	19,3	0,1	592,0
6,3	34,8	168,9	18,4	4,2	592,0
6,4	32,3	152,2	23,3	8,2	588,0
6,5	31,2	139,3	32,5	10,9	592,0
6,6	30,4	128,7	38,0	13,0	595,0
6,7	26,4	117,8	34,5	16,4	590,0
6,8	22,4	109,4	28,7	17,5	585,0
6,9	20,8	105,6	30,2	21,3	584,0
7,0	28,0	103,7	34,6	22,5	598,0
7,1	33,5	95,0	37,1	25,6	610,0
7,2	29,9	89,5	37,6	27,4	621,0
7,3	24,9	81,8	36,2	34,0	618,0
7,4	23,9	87,1	32,8	38,1	618,0

Table 5.33 (contd.)

Energy in MeV	Partial cross-section in mb				Total cross-section in mb
	n_0	n_1	n_2	n_3	
7,5	27,7	104,4	31,5	40,8	648,0
7,6	33,3	113,1	34,9	37,1	678,0
7,7	37,3	122,1	38,6	33,9	688,0
7,8	37,3	118,7	42,9	33,9	696,0
7,9	29,8	120,2	42,0	33,8	698,0

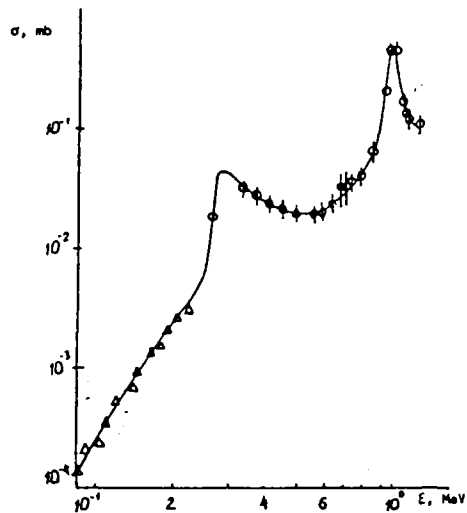


Figure 5.1. Energy dependence of the total integral proton radiative capture cross-section of beryllium-9 in the ${}^9\text{Be}(p,\gamma){}^{10}\text{B}$ reaction. Spline fit given by continuous curve. Experimental data: Δ - [210], ϕ - [269].

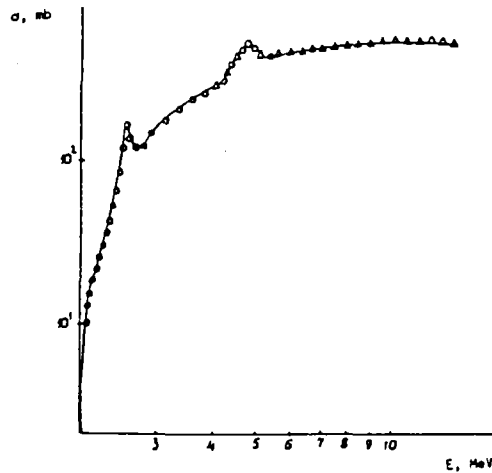


Figure 5.2. Energy dependence of the total integral ${}^9\text{Be}(p,n){}^9\text{B}$ reaction cross-section. Spline fit given by continuous curve. Experimental data: \circ - [21], Δ - [151].

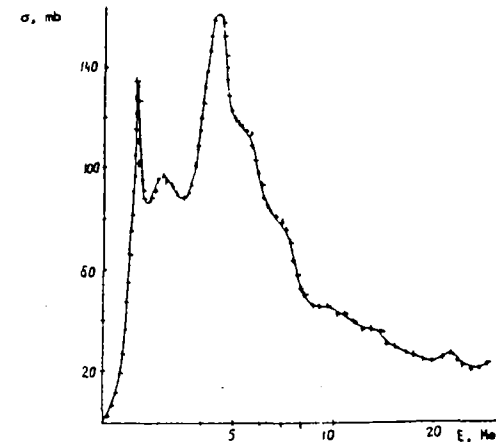


Figure 5.3. Energy dependence of the total integral ${}^9\text{Be}(p,n){}^9\text{B}$ reaction cross-section (for the ground state). The $+$ indicates evaluated data used for the spline fit.

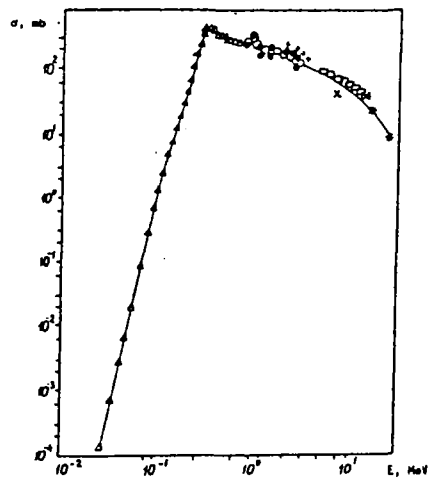


Figure 5.4. Energy dependence of the partial ${}^9\text{Be}(p,d){}^8\text{Be}$ reaction cross-section (for the ground state). Spline fit given by continuous curve. Experimental data: \circ - [281], \ast - [282], Δ - [283], \bullet - [284], $+$ - [286], \square - [287], \times - [289], \boxtimes - [291].

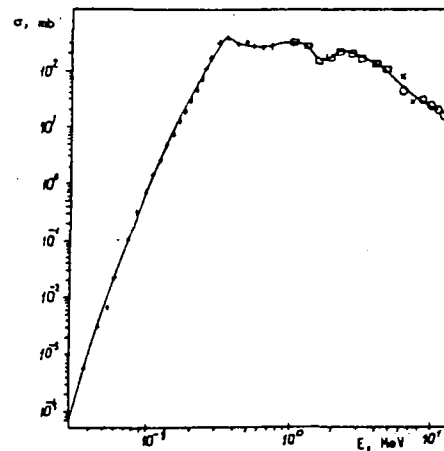


Figure 5.5. Energy dependence of the partial ${}^9\text{Be}(p,\alpha){}^6\text{Li}$ reaction cross-section (for the ground state). Spline fit given by continuous curve. Experimental data: $+$ - [285], \circ - [288], \times - [289].

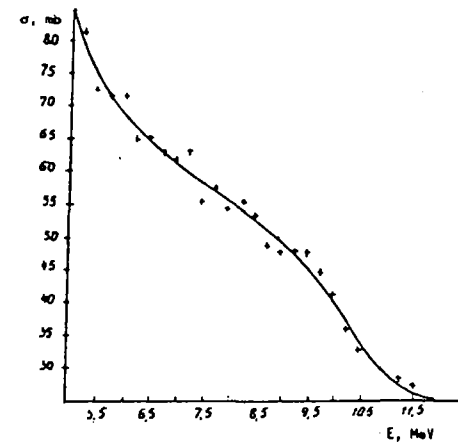


Figure 5.6. Energy dependence of the partial ${}^9\text{Be}(p,\alpha){}^6\text{Li}$ reaction cross-section (for the first excited state). Spline fit given by continuous curve based on experimental data [283] indicated by $+$.

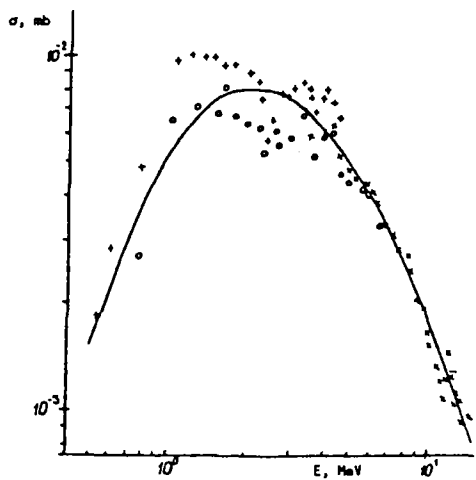


Figure 5.7. Energy dependence of the partial ${}^9\text{Be}(d,\gamma){}^{11}\text{B}$ reaction cross-section (for the ground state). Spline fit given by continuous curve. Experimental data: o - [293], + - [294], x - [295].

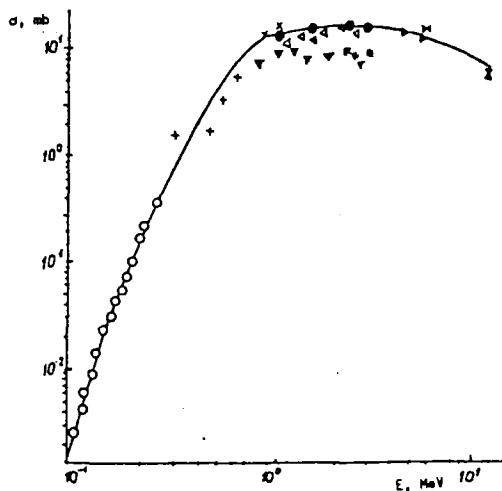


Figure 5.8. Energy dependence of the partial ${}^9\text{Be}(d,pp){}^{10}\text{Be}$ reaction cross-section. Spline fit given by continuous curve. Experimental data: - [176], o - [210], + - [302], ▽ - [304], Δ - [305], x - [306], * - [307], * - [308], ◀ - [312], ⌘ - [313].

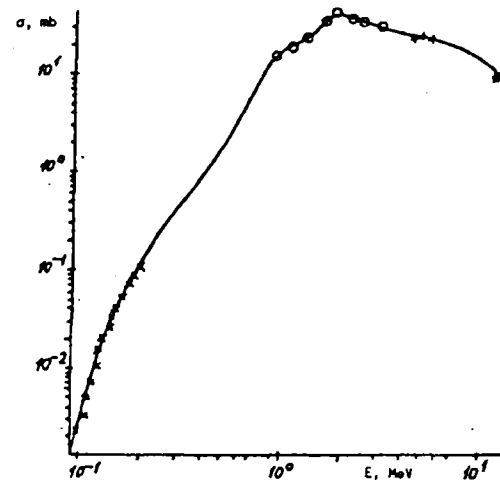


Figure 5.9. Energy dependence of the partial ${}^9\text{Be}(d,p){}^{10}\text{Be}$ reaction cross-section. Spline fit given by continuous curve. Experimental data: + - [176], x - [210], o - [307], * - [313].

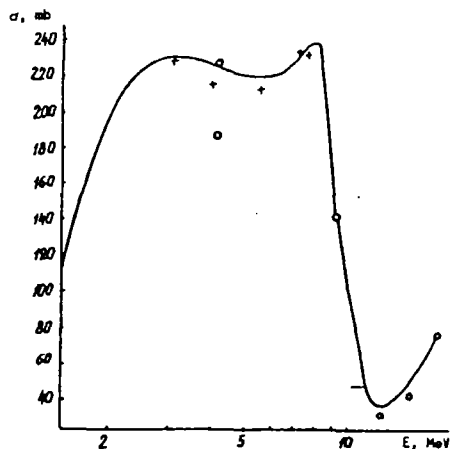


Figure 5.10. Energy dependence of the total integral ${}^9\text{Be}(d,t){}^8\text{Be}$ reaction cross-section. Spline fit given by continuous curve. Experimental data: o - [314], + - [315].

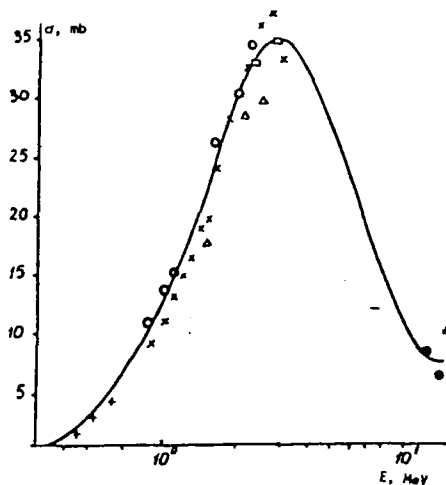


Figure 5.11. Energy dependence of the partial ${}^9\text{Be}(d,t){}^8\text{Be}$ reaction cross-section. Spline fit given by continuous curve. Experimental data: * - [281], o - [306], x - [307], □ - [309], Δ - [317], * - [318].

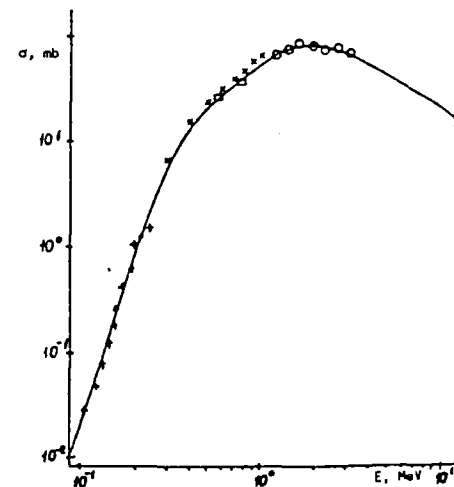


Figure 5.12. Energy dependence of the total integral ${}^9\text{Be}(d,\alpha){}^7\text{Li}$ reaction cross-section. Spline fit given by continuous curve. Experimental data: + - [210], ⌘ - [318], □ - [319], x - [321], o - [322].

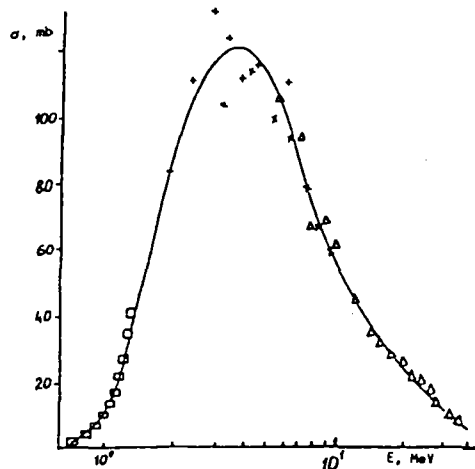


Figure 5.13. Energy dependence of the total integral ${}^9\text{Be}(\tau, n){}^{11}\text{C}$ neutron production cross-section. Spline fit given by continuous curve. Experimental data: \square - [192], Δ - [325], \times - [326], $+$ - [327].

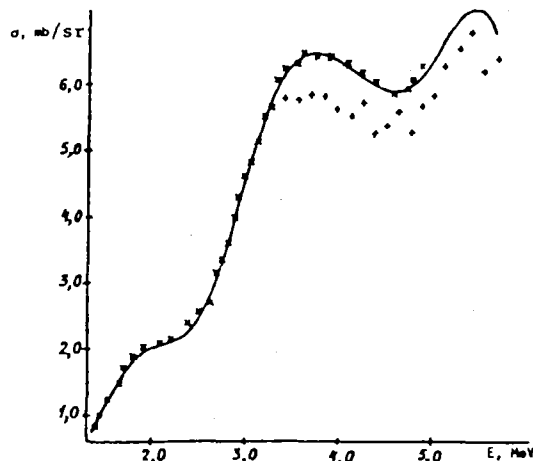


Figure 5.14. Energy dependence of the partial differential ${}^9\text{Be}(\tau, n_0){}^{11}\text{C}$ reaction cross-section (for the first excited state) at an angle of zero degrees in the laboratory system. Spline fit given by continuous curve. Experimental data: \times - [328], $+$ - [330].

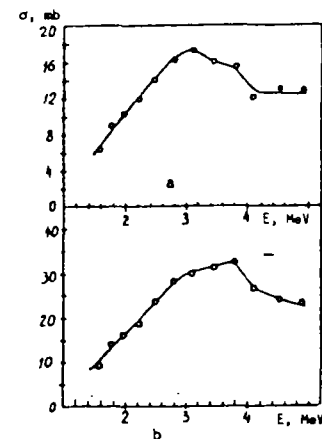


Figure 5.15. Energy dependence of the partial ${}^9\text{Be}(\tau, n){}^{11}\text{C}$ reaction cross-section: for the first excited state (curve a) and for the ground state (curve b) of carbon-11. Experimental data: \circ - [328].

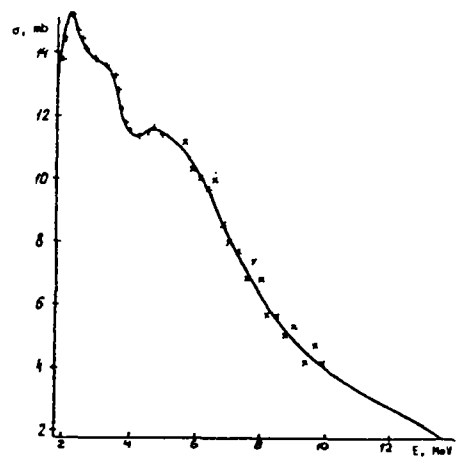


Figure 5.16. Energy dependence of the partial ${}^9\text{Be}(\tau, p_0){}^{11}\text{B}$ reaction cross-section for the ground state. Spline fit given by continuous curve. Experimental data: \times - [331], $+$ - [332].

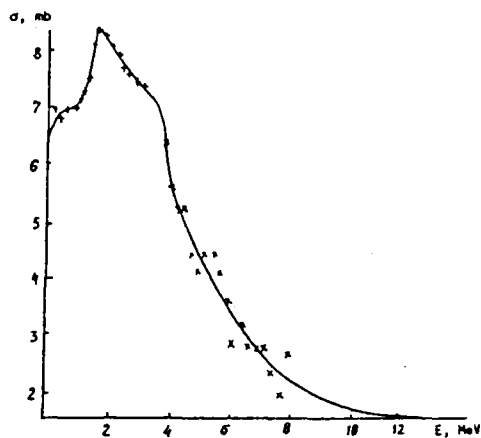


Figure 5.17. Energy dependence of the partial ${}^9\text{Be}(\tau, p_1){}^{11}\text{B}$ reaction cross-section for the first excited state. Spline fit given by continuous curve. Experimental data: \times - [331], $+$ - [332].

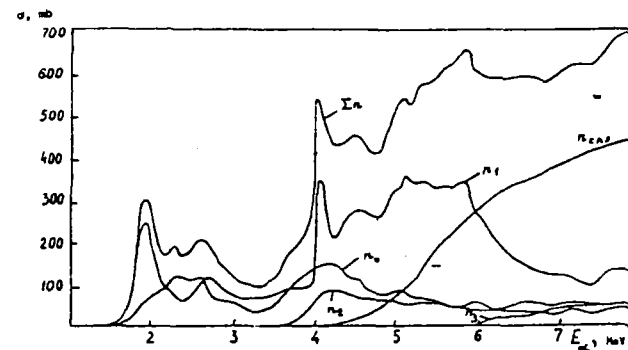


Figure 5.18. Energy dependence of the partial (n_0, n_1, n_2, n_3) and summed (I_n) cross-sections of the ${}^9\text{Be}(\alpha, n){}^{12}\text{C}$ reaction, and of the total neutron production spectrum (n_{TOT}).

6. CHARACTERISTIC LEVELS OF INDIVIDUAL NUCLEI [108, 199]

(Estimated values are given in parentheses)

Table 6.1

Characteristic levels of helium-5

E_x , MeV	J^π , (T = 1/2)	$\Gamma_{c.m.}$, MeV	Decay channel
0	3/2-	0,60±0,02	n, α
4±1	1/2-	4±1	n, α
16,76±0,13	3/2+	0,10±0,05	γ , n, d, t, α

Table 6.2

Characteristic levels of lithium-5

E_x , MeV	J^π , (T = 1/2)	$\Gamma_{c.m.}$, MeV	Decay channel
0	3/2-	1,5	p, α
4-10	1/2-	5±2	p, α
16,66±0,07	3/2+	0,3	γ , p, d, α

Table 6.3

Characteristic levels of helium-6

E_x , MeV	J^π , T	τ or $\Gamma_{c.m.}$, keV	Decay channel
0	0+; 1	$\tau_{1/2} = 806,7 \pm 1,5$ MC	β^-
1,797±0,025	(2)+; 1	$r = 11,7 \pm 2,0$	n, α
13,6±0,5	- -	-	-
15,5±0,4	- -	-	γ
23,2±0,7	- -	-	γ

Table 6.4

Characteristic levels of lithium-6

E_x , MeV	J^π , T	$\Gamma_{c.m.}$, MeV	Decay channel
0	1+; 0	0	-
2,186±0,002	3+; 0	0,024±0,002	γ , d, α
3,563±0,1	0+; 1	(8,2±0,2) · 10 ⁻⁶	γ
4,31±0,022	2+; 0	1,7±0,2	γ , d, α
5,366±0,015	2+; 1	0,540±0,020	γ , n, p, α
5,65±0,05	1+; 0	1,5±0,2	d, α

Table 6.5

Characteristic levels of beryllium-6

E_x , MeV	J^π , T	$\Gamma_{c.m.}$, keV	Decay channel
0	0+; 1	92±6	p, α
1,67±0,05	(2)+; 1	1160±60	p, α
23	4-; -	-	γ , π

Table 6.6

Characteristic levels of lithium-7

E_x , MeV	J^π , T	τ or $\Gamma_{c.m.}$, keV	Decay channel
0	3/2-; 1/2	0	
0,4776±3 · 10 ⁻⁶	1/2-; 1/2	$\tau_m = 105 \pm 5$ ϕ c	γ
4,630±0,009	7/2-; 1/2	$r = 93 \pm 8$ kaB	t, α
6,68±0,05	5/2-; 1/2	$r = 875^{+200}_{-100}$	t, α
7,460±0,001	5/2-; 1/2	$r = 89 \pm 7$	n, t, α
9,67±0,1	7/2-; 1/2	$r = 400$	n, t, α
9,85	3/2-; 1/2	$r = 1200$	n, α
11,24±0,03	3/2-; 3/2	$r = 260 \pm 35$	n, p

Table 6.7

Characteristic levels of beryllium-7

E_x , MeV	J^π , T	τ or $\Gamma_{c.m.}$, keV	Decay channel
0	3/2-; 1/2	$\tau_{1/2} = 53,29$ cyt	ϵ
0,42908±0,0001	1/2-; 1/2	$\tau_m = 192$ ϕ c	γ
4,57±0,05	7/2-; 1/2	$r = 175 \pm 7$	t, α
6,73±0,1	5/2-; 1/2	$r = 1200$	t, α
7,21±0,06	5/2-; 1/2	$r = 500$	p, t, α
9,27±0,1	7/2-; 1/2	-	p, t, α
9,9	3/2-; 1/2	$r = 1800$	p, t, α
11,01±0,03	3/2-; 3/2	$r = 320 \pm 30$	p, t, α

Table 6.8

Characteristic levels of lithium-8

E_x , MeV	J^π , T	τ or $\Gamma_{c.m.}$, keV	Decay channel
0	2+; 1	$\tau_{1/2} = 838 \pm 6$ MC	β^-
0,9808±0,0001	1+; 1	$\tau_m = 12 \pm 4$ ϕ c	γ
2,255±0,003	3+; 1	$r = 33 \pm 6$	γ , n
3,21	1+; 1	$r = 1000$	n
5,4	(0,1)+; 1	$r = 650$	n
6,1±0,1	(3); 1	$r = 1000$	n
6,53±0,02	4+; 1	$r = 35 \pm 15$	n
7,1±0,1	- -	$r = 400$	n

Table 6.9

Characteristic levels of beryllium-8

E_x , MeV	J^π , T	$\Gamma_{c.m.}$, keV	Decay channel
0	0+; 0	(6,8±1,7) · 10 ⁻³	α
3,04±0,03	2+; 0	1500±0,02	α
11,4±0,3	4+; 0	3500	α
16,626±0,003	2+; 0+1	108,1±0,5	γ , α
16,922±0,003	2+; 0+1	74,0±0,4	γ , α
17,640±0,001	1+; 1	10,7±0,5	γ , p
18,150±0,004	1+; 0	138±6	γ , p
18,91	2-; -	48±20	γ , n, p
19,07±0,03	3+; (1)	270±20	γ , p
19,24±0,03	3+; (0)	230±30	n, p
19,4	1- -	650	n, p
19,86±0,05	4+; 0	700±100	p, α

Table 6.10

Characteristic levels of boron-8

E_x , MeV	J^π , T	τ or $\Gamma_{c.m.}$, keV	Decay channel
0	2+; 1	$\tau_{1/2} = 770 \pm 3$ MC	β^+
0,778±0,007	-	$r = 40 \pm 10$	γ , p
2,32±0,03	3+; 1	$r = 350 \pm 40$	-
10,619±0,009	0+; 2	$r \leq 60$	-

Table 6.11

Characteristic levels of lithium-9

E_x , MeV	J^π , T	τ or $\Gamma_{c.m.}$, keV	Decay channel
0	3/2-; 3/2	$\tau_{1/2} = 178,3 \pm 0,4$ MC	β^-
2,691 \pm 0,005	(1/2-)	-	γ
4,31 \pm 0,02	-	$r = 100 \pm 30$	-
5,38 \pm 0,06	-	$r = 600 \pm 100$	-
6,43 \pm 0,015	$\geq 9/2$	$r = 40 \pm 20$	-

Table 6.12

Characteristic levels of beryllium-9

E_x , MeV	J^π , T	$\Gamma_{c.m.}$, keV	Decay channel
U	3/2-; 1/2	0	-
1,685 \pm 0,015	1/2+; -	-150	γ, α
2,4294 \pm 0,0013	5/2-; -	0,77 \pm 0,15	γ, α, α
2,78 \pm 0,12	1/2-; -	1080 \pm 110	γ, α
3,049 \pm 0,009	5/2+; -	282 \pm 11	γ, α
4,704 \pm 0,025	(3/2+); -	743 \pm 55	γ, α
6,76 \pm 0,06	7/2-; -	1540 \pm 200	γ, α
7,94 \pm 0,08	(1/2-); -	1000	-
11,283 \pm 0,024	(3/2-); -	575 \pm 50	α
11,81 \pm 0,02	-; 1/2	400 \pm 30	γ, α
13,79 \pm 0,03	-; 1/2	590 \pm 60	γ, α
14,3929 \pm 0,0018	3/2-; 3/2	0,381 \pm 0,033	γ, α, α
14,4 \pm 0,3	-	800	-
15,10 \pm 0,05	-	-	γ
15,97 \pm 0,03	-; 1/2	300	γ
16,671 \pm 0,01	-	41 \pm 4	γ

Table 6.13

Characteristic levels of boron-9

E_x , MeV	J^π , T	$\Gamma_{c.m.}$, keV	Decay channel
0	3/2-; 1/2	0,54 \pm 0,21	p, α
(1,6)	-	700	(p, α)
2,361 \pm 0,005	5/2-; 1/2	81 \pm 5	α
2,788 \pm 0,03	(3/2, 5/2)+; 1/2	550 \pm 40	α
(4,8 \pm 0,1)	-	1000 \pm 200	-
6,97 \pm 0,06	7/2-; 1/2	2000 \pm 200	p
11,70 \pm 0,07	(7/2)-; 1/2	800 \pm 50	p
12,06 \pm 0,06	-; 1/2	800 \pm 200	p
14,0 \pm 0,07	-; 1/2	390 \pm 110	-
14,655 \pm 0,002	3/2-; 3/2	0,395 \pm 0,042	γ, p

Table 6.14

Characteristic levels of beryllium-10

E_x , MeV	J^π (T = 1)	τ or $\Gamma_{c.m.}$, keV	Decay channel
0	0+	$\tau_{1/2} = (1,6 \pm 0,2) \cdot 10^6$ года	β^-
3,3680 \pm 0,0002	2+	$\tau_{1/2} = 180 \pm 17$ фс	γ
5,9583 \pm 0,0003	2+	$\tau_m = 80$ фс	γ
5,9599 \pm 0,0006	1-	-	-
6,1793 \pm 0,0007	0+	$\tau_m = 1,1 \pm 0,4$ пс	γ
6,2633 \pm 0,005	2-	-	-
7,371 \pm 0,001	3-	$r = 15,7 \pm 0,5$	α
7,542 \pm 0,001	2+	$r = 6,3 \pm 0,8$	α
9,27	(4-)	$r = 150 \pm 20$	α
9,4	(2)+	$r = 291 \pm 20$	α

Table 6.15

Characteristic levels of boron-10

E_x , MeV	J^π , T	τ or $\Gamma_{c.m.}$, keV	Decay channel
0	3+; 0	0	-
0,71835 \pm 0,00004	1+; 0	$\tau_m = 1,020 \pm 0,005$ нс	γ
1,74015 \pm 0,00017	0+; 1	$\tau_m = 7 \pm 3$ фс	γ
2,1543 \pm 0,0005	1+; 0	$\tau_m = 2,13 \pm 0,2$ пс	γ
3,5871 \pm 0,0005	2+; 0	$\tau_m = 153 \pm 12$ фс	γ
4,7740 \pm 0,0005	3+; 0	$r = (8,7 \pm 2,2) \cdot 10^{-8}$	γ, α
5,1103 \pm 0,0006	2-; 0	$r = 0,98 \pm 0,07$	γ, α
5,1639 \pm 0,0006	2+; 1	$\tau_m = 6$ фс	γ, α
5,180 \pm 0,01	1+; 0	$r = 110 \pm 10$	γ, α
5,9195 \pm 0,0006	2+; 0	$r = 6 \pm 1$	γ, α
6,025 \pm 0,0006	4+; -	$r = 0,05 \pm 0,03$	γ, α
6,1272 \pm 0,0007	3-; -	$r = 2,36 \pm 0,03$	γ, α
6,561 \pm 0,002	(4)-; -	$r = 25,1 \pm 1,1$	α
6,873 \pm 0,005	1-; 0+1	$r = 120 \pm 50$	γ, p, d, α
7,002 \pm 0,006	(1,2)+; (0)	$r = 100 \pm 10$	p, d, α
7,430 \pm 0,010	2(-); 0+1	$r = 100 \pm 10$	γ, p, d, α
7,467 \pm 0,010	1+; -	$r = 65 \pm 10$	p
7,479 \pm 0,002	2+; 1	$r = 74 \pm 4$	γ, p
7,561 \pm 0,001	0+; 1	$r = 2,65 \pm 0,2$	γ, p
(7,67 \pm 0,030)	(1+; 0)	$r = 250 \pm 20$	p, d
7,819 \pm 0,02	1-; -	$r = 260 \pm 30$	p
8,07	2+; -	$r = 800 \pm 200$	γ, p, d
(8,7)	(1+, 2+); -	$r = (200)$	p
8,889 \pm 0,006	3-; 1	$r = 84 \pm 7$	$\gamma, \alpha, p, \alpha$
8,895 \pm 0,002	2+; 1	$r = 40 \pm 1$	γ, p, α

Table 6.16

Characteristic levels of carbon-10

E_x , MeV	J^π , T	τ or $\Gamma_{c.m.}$, keV	Decay channel
0	0+; 1	$\tau_{1/2} = 19,255 \pm 0,05$ с	β^-
3,3536 \pm 0,0009	2+; -	$\tau_m = 155 \pm 25$ фс	γ
5,22 \pm 0,04	-	$r = 225 \pm 45$	-
5,38 \pm 0,07	-	$r = 300 \pm 60$	-
6,58 \pm 0,02	-	$r = 200 \pm 40$	-

Table 6.17

Characteristic levels of beryllium-11

E_x , MeV	J^π , T	τ or $\Gamma_{c.m.}$, keV	Decay channel
U	1/2; 3/2	$\tau_{1/2} = 13,81 \pm 0,08$ с	β^-
0,320 \pm 0,000	1/2-; -	$\tau_m = 166 \pm 15$ фс	γ
1,778 \pm 0,012	(5/2, 3/2)+; -	$r = 100 \pm 20$	(α)
2,69 \pm 0,02	(1/2+, 3/2+, 5/2+)	$r = 200 \pm 20$	(α)
3,41 \pm 0,02	(1/2+, 3/2+, 5/2+)	$r = 125 \pm 20$	(α)
3,887 \pm 0,015	$> 7/2$; -	$r = 10$	(α)
3,956 \pm 0,015	3/2-; -	$r = 15 \pm 5$	(α)

Table 6.18

Characteristic levels of boron-11

E_x , MeV	J^π , T	$\Gamma_{c.m.}$, keV	Decay channel
0	3/2-; 1/2	0	-
2,1247±0,00003	1/2-; -	(0,12±0,01)10 ⁻³	γ
4,4449±0,0005	5/2-; -	(0,56±0,02)10 ⁻³	γ
5,0203±0,0003	3/2-; -	(1,963±0,07)10 ⁻³	γ
6,7429±0,0018	7/2-; -	(0,03±0,007)10 ⁻³	γ
6,7918±0,0003	1/2-; -	(0,385±0,044)10 ⁻³	γ
7,2855±0,0004	5/2+; -	(1,149±0,08)10 ⁻³	γ
7,9778±0,0004	3/2+; -	(1,15±0,15)10 ⁻³	γ
8,560±0,002	5/2+; -	(0,946±0,09)10 ⁻³	γ
8,920±0,002	5/2-; -	(4,37±0,02)10 ⁻³	γ, α
9,1850±0,002	7/2+; -	(1,9±1,5)10 ⁻³	γ, α
9,2744±0,002	5/2+; -	(7)	γ, α
9,876±0,008	3/2+; -	110±15	γ, α
10,26±0,015	3/2-; -	165±25	α
10,33±0,011	5/2-; -	110±20	γ, α
10,597±0,009	7/2+; -	100±20	γ, α
10,96±0,05	5/2-; -	4500	α
11,265±0,017	9/2+; -	110±20	α
11,444±0,019	-	103±20	α
11,589±0,026	5/2+; -	170±30	n, α
11,886±0,017	5/2-; -	200±20	n, α
12,0±0,2	7/2+; -	1000	n, α
12,557±0,016	1/2+; 3/2	210±20	γ, p, α
12,916±0,012	1/2-; 3/2	155±20	γ, p, α
13,137±0,04	9/2-; -	426±40	n, α, t

Table 6.19

Characteristic levels of carbon-11

E_x , MeV	J^π , T	τ or $\Gamma_{c.m.}$, keV	Decay channel
0	3/2-; 1/2	$\tau_{1/2} = 20,39 \pm 0,02$ мин	β^+
2,0000±0,0005	1/2-; -	$\tau_m = 10,3 \pm 0,7$ фс	γ
4,3188±0,0011	5/2-; -	$\tau_m < 12$ фс	γ
4,8042±0,001	3/2-; -	$\tau_m < 11$ фс	γ
6,3392±0,001	1/2+; -	$\tau_m < 110$ фс	γ
6,4782±0,001	7/2-; -	$\tau_m < 8$ фс	γ
6,9048±0,001	5/2+; -	$\tau_m < 69$ фс	γ
7,4797±0,002	3/2-; -	$\tau_m < 91$ фс	γ
8,1045±0,002	3/2-; -	$\tau_m = 0,06 \pm 0,04$ фс	γ
8,420±0,002	5/2-; -	$\tau_m = 0,043 \pm 0,01$ фс	γ
8,655±0,008	7/2+; -	$r \leq 5$	γ, p
8,701±20	5/2+; -	$r = 15 \pm 1$	γ, p
9,200±0,05	(5/2+); -	$r = 500 \pm 100$	γ, p
9,65±0,05	(3/2-); -	$r = 210 \pm 50$	γ, p, α
9,78±0,05	(5/2-); -	$r = 240 \pm 60$	γ, p
9,97±0,05	7/2-; -	$r = 120 \pm 20$	γ, p
10,083±0,005	7/2+; -	$r = 230$	γ, p, α
10,679±0,005	9/2+; -	$r = 200 \pm 30$	γ, p, α
11,03±30	-	$r = 300 \pm 60$	-
11,44±10	-	$r = 360$	p, α
12,51±30	1/2-; 3/2	$r = 490 \pm 40$	p
12,65±20	7/2+; -	$r = 360$	p, α

Table 6.20

Characteristic levels of carbon-12

E_x , MeV	J^π , T	$\Gamma_{c.m.}$, keV	Decay channel
0	0+; 0	0	-
4,43891±0,00031	2+; 0	(10,8±0,6)10 ⁻⁶	γ
7,6542±0,00015	0+; 0	(8,5±1,0)10 ⁻³	γ, α
9,641±0,005	3-; 0	34±5	γ, α
10,3±0,3	(0+); 0	3000±700	α
10,844±0,016	1-; 0	315±25	α
11,828±0,016	2-; 0	260±25	γ, α
12,710±0,006	1+; 0	(18,1±2,8)10 ⁻³	γ, α
13,352±0,017	(2-); 0	375±40	γ, α
14,083±0,015	4+; 0	258±15	α
15,110±0,003	1+; 1	(43,6±1,3)10 ⁻³	γ, α
15,44±40	2+; 0	1500±200	-
16,1067±0,0005	2+; 1	5,2±0,5	γ, p, α

BIBLIOGRAPHY

(Non-English references only)

- [2] Zvenigorodskij A.G., Agureev V.A., Dunaev I.B., et al., A set of computer programs for the evaluation of nuclear physics data, Problems of Atomic Sciences and Technology, Ser. Nuclear Constants Vol.2 (1983) 61-68 [in Russian]
- [5] Zavalov Yu.S., Kvasov B.N., Miroshnichenko V.A., "Spline function methods", Nauka (1980) [in Russian]
- [6] Brandt Z., "Statistical methods for the analysis of observational data", Mir (1975) [in Russian]
- [7] Gamow, G., Quantum theory of the atomic nucleus. Z.Phys. 51 (1928) 204 [in German]
- [39] Ganeev A.S., Govorov A.M., Ossentinskij G.M., et al., "The d-d reaction in the 100-1000 keV range", Nuclear Reactions of Light Nuclei. Atomizdat, Moscow (1957) 26-47 [in Russian]
- [40] Davidenko V.A., Pogrebov I.S., Saukov A.I., Determination of the excitation function of the $T(d,n)^4\text{He}$ reaction, Atomm.Energ. 2, 4 (1957) 386-388 [in Russian]
- [58] Volkov B.B., Vorotnikov P.E., Koltypin E.A., et al., "Investigation of the d-d reaction in the 0.20-1.75 MeV range", Nuclear Reactions of Light Nuclei. Atomizdat, Moscow (1957) [in Russian]
- [74] Bogdanov G.F., Vlassov N.A., Kalinin S.P., et al., The $T(p,n)^3\text{He}$ reaction for proton energies ranging from 7 to 12 MeV, J.Exp.Theor.Phys. 36, 2 (1959) 633-636 [in Russian]
- [76] Vlassov N.A., Kalinin S.P., Ogloblin A.A., et al., The interaction of protons with tritium and the excited state of ^4He , J.Exp.Theor.Phys. 28, 6 (1955) 639-650 [in Russian]
- [81] Besotosnyj V.M., Zhmajlov V.A., Surov L.M., et al., The 16.7 MeV gamma ray production $T(d,\gamma)^5\text{He}$ cross-section for deuteron energies ranging from 25 to 100 keV, Yad.Fiz. 10, 2 (1969) 225-226 [in Russian]
- [87] Balabanov E.M., Barit I.Ya., Katsurov L.N., et al., "The measurement of the effective $d(t,n)^4\text{He}$ cross-section in the deuteron energy range of 40-730 keV", Nuclear Reactions of Light Nuclei, Atomizdat, Moscow (1957) (in Russian)
- [94] Strel'nikov Yu.V., Abramovich S.N., Morkin L.A., Yur'eva N.D., Excitation function of the $^3\text{He}(t,2n)^4\text{He}$ reaction at an angle of 0° in the energy range of 40 to 200 keV, Izv.Akad.Nauk USSR. Ser.Fiz. 35, 1 (1971) 165-168 [in Russian]
- [95] Serov V.I., Abramovich S.N., Morkin L.A., Measurement of the total cross-section of the $T(t,2n)^4\text{He}$ reaction, Atomm.Energ. 42, 1 (1977) 59-61 [in Russian]
- [96] Govorov A.M., Li Ga Yen, Total cross-section of the T-T reaction in the 60-1140 keV energy range, Preprint P-764 JINR, Dubna (1961) [in Russian]
- [97] Govorov A.M., Li Ga Yen, Ossetinskij G.M., et al., The differential cross-section of the $^3\text{H}(t,2n)^4\text{He}$ reaction at an angle of 90° and the associated alpha particle spectra, J.Exp.Theor.Phys. 41, 3 (1961) 703-707 [in Russian]
- [103] Kraus L., Suffert M., Magnag-Valette D., Study of the $^2\text{H}(^3\text{He},\gamma)^5\text{Li}$ reaction at a ^3He energy of 5.5 MeV, Nucl.Phys. A109,3 (1968) 593-602 [in French]
- [114] Klyutcharov A.P., Yessel'son V.A., Walter A.K., Study of the interaction of ^3He with deuterons, Dokl.Akad.Nauk USSR 109, 4 (1956) 737-739 [in Russian]
- [123] Van Nen-Min, Novatskij B.M., et al., Investigation of the $^3\text{He}+^3\text{He}$ reaction, Yad.Fiz. 3, 6 (1966) 1064-1069 [in Russian]
- [127] Li Ga Yen, Ossetinskij G.M., Sodnom N., et al., Investigation of the $^3\text{He}+^3\text{H}$ reaction J.Exp.Theor.Phys. 39, 2 (1960) 225-229 [in Russian]
- [128] Kim Syn Nam, Ossetinskij G.M., Sergejev V.A. Conservation of the isospin in the $^3\text{He}(t,d)^4\text{He}$ reaction, Yad.Fiz. 10, 4 (1969) 705-712 [in Russian]
- [152] Merchez F., Bouchez R., Hofswell R.A., Yavin R.A., Excitation of the $3.56\text{ MeV } 0^+$ level by (p,p') diffusion from 14 to 16 MeV, J.Physique Vol. 29, 11-12 (1968) 969-972 [in French]
- [154] Fiedler O., Kunze P., Cross-sections of the $^6\text{Li}(p,\alpha)^3\text{He}$ and the $^3\text{Li}(p,\alpha)^4\text{He}$ reactions at very low energies, Nucl.Phys. A96, 3 (1967) 513-520 [in German]
- [156] Gemeinhard W., Kamke D., Reaction channels and cross-section of the $^6\text{Li}(p,\alpha)^3\text{He}$ reaction in the 50 to 190 keV energy range, Z.Phys. 197, 1 (1966) 58-74 [in German]
- [160] Bertrand F., Grenier G., Pomet J., Study of the $^6\text{Li}(p,\alpha)^3\text{He}$, $^6\text{Li}(d,\alpha)^4\text{He}$, $^6\text{Li}(d,p_0)^7\text{Li}$ and $^6\text{Li}(d,p_1)^7\text{Li}$ reactions from 300 to 1000 keV, Rep. CEA-R-3428 (1968) [in French]
- [169] Guzhovskij B.Ya., Abramovich S.N., Zvenigorodskij A.G., et al., Total cross-sections of the $^6\text{Li}(d,n)^7\text{Be}$, $^7\text{Li}(d,2n)^7\text{Be}$ and $^6\text{Li}(t,2n)^7\text{Be}$ reactions, Izv.Akad.Nauk USSR, Ser.Fiz. 44, 9 (1980) 1983-1987 [in Russian]
- [171] Abramovich S.N., Guzhovskij B.Ya., Protopopov V.N. The effect of the partial decay channel properties on the shape of the excitation function of the [? missing in original] reaction, Izv.Akad.Nauk Kazakh.SSR, Ser.Mat-Fiz. 4 (1984) 24-29 [in Russian]
- [172] Guzhovskij B.Ya., Abramovich S.N., Zvenigorodskij A.G., et al., Energy dependence of the total $^6,^7\text{Li}+^2,^3\text{H}$ neutron production reaction cross-sections, Appl.Nucl.Spectr. 13 (1984) 135-143 [in Russian]
- [183] Golovkov M.S., Kulikauskas V.S., Voronchev V.T., et al., Study of the low energy deuteron+ ^6Li reaction cross-sections, Yad.Fiz. 34, 3 (1981) 861-864 [in Russian]

- [187] Durr W., Clausnitzer G., Fick D., et al., Analysis of the vector polarized ${}^6\text{Li}(d,\alpha){}^4\text{He}$ reaction at 2.1 to 10.9 MeV, Nucl.Phys. A120, 3 (1968) 678-690 [in German]
- [192] Serov V.I., Guzhovskij B.Ya., Investigation of the ${}^6\text{Li}(t,n)$, ${}^7\text{Li}(t,n)$, ${}^9\text{Li}({}^3\text{He},n)$, ${}^9\text{Be}(t,n){}^{11}\text{B}$ and ${}^9\text{Be}({}^3\text{He},n){}^{11}\text{C}$ reactions, Atomm.Energ. 12, 1 (1962) 5-11 [in Russian]
- [193] Seltz R., Magnag-Valette D., Excitation functions and cross-sections of the $\text{Li}(t,n)$ reactions from 100 to 300 keV, Compt.Rend. 251, 19 (1960) 2006-2008 [in French]
- [194] Salter A.K., Watset P.I., Kolesnikov L.Ya., et al., Neutron yield from the ${}^6\text{Li}(t,n)$ and ${}^7\text{Li}(t,n)$ reactions, Atomm.Energ. 10, 6 (1961) 577-586 [in Russian]
- [195] Abramovich S.N., Guzhovskij B.Ya., Dunaeva S.A., et al., Shape of the excitation function for the generation of short-lived ${}^6\text{He}$, ${}^8\text{Li}$, ${}^9\text{Li}$ nuclei and for the ${}^7\text{Li}+{}^3\text{H}$ reaction, Problems of Atomic Science and Technology. Ser. Nuclear Constants No.2 (1985) 14-18 [in Russian]
- [207] Byzhin'ski S., Zhupran'ski M., Russek K.I. et al., Measurement of the excitation function of the ${}^6\text{Li}({}^3\text{He},\text{He}){}^6\text{Li}$ and ${}^6\text{Li}({}^3\text{He},d){}^7\text{Be}$ reactions, Izv.Akad.Nauk USSR. Ser.Fiz. 43, 1 (1979) 158-159 [in Russian]
- [209] Abramovich S.N., Guzhovskij B.Ya., Pereshivkin V.A., Measurement of the total cross-sections for the formation of the radioactive ${}^7\text{Be}$ nuclide in the interactions of ${}^6\text{Li}$, ${}^7\text{Li}$, ${}^9\text{Be}$ and ${}^{10}\text{B}$ with ${}^3\text{He}$, Problems of Atomic Science and Technology. Ser. Nuclear Constants No.5 (1982) 21-25 [in Russian]
- [228] Kilian K., Clausnitzer G., Durr W., et al., Investigation of the ${}^7\text{Li}(p,p_0){}^7\text{Li}$, ${}^7\text{Li}(p,p_1){}^7\text{Li}$ and ${}^7\text{Li}(p,\alpha){}^4\text{He}$ reactions with polarized protons with energies of 2.7 to 10.8 MeV, Nucl.Phys. A126, 3 (1969) 529-544 [in German]
- [229] Vlassov N.A., Ogloblin A.A., "The ${}^7\text{Li}(p,t)$ reaction", Nuclear Reactions at Low and Medium Energies (1958) 24 [in Russian]
- [230] Friedland E., Venter I., The ${}^7\text{Li}(d,\alpha){}^5\text{He}$ reaction in the 0.6 to 2.0 MeV energy range, Z.Phys. 243, 2 (1971) 126-131 [in German]
- [232] Ossetinskij G.M., Sikoro B., Fryshyn B., Investigation of the ${}^7\text{Li}(d,n){}^8\text{Be}$ reaction, Preprint 5143 (1970) JINR, Dubna [in Russian]
- [236] Abramovich S.N., Guzhovskij B.Ya., Zvenigorodskij A.G., et al., Investigation of the highly excited states of the ${}^9\text{Be}$ nucleus in the ${}^6\text{Li}(t,p){}^8\text{Li}$ and ${}^7\text{Li}(d,p){}^8\text{Li}$ reactions, Izv.Akad.Nauk USSR. Ser.Fiz. 50, 1 (1986) 65-67 [in Russian]
- [241] Abramovich S.N., Baz' A.I., Guzhovskij B.Ya., Near-threshold anomaly in the ${}^7\text{Li}(p,{}^9\text{Li}){}^4\text{H}$ reaction, Yad.Fiz. 32, 2 (1980) 402-406 [in Russian]
- [249] Serov V.I., Strel'nikov Yu., Abramovich S.N., et al., State of the ${}^{10}\text{Be}$ nucleus with an excitation energy of 17.3 MeV, Izv.Akad.Nauk USSR. Ser.Fiz. 51, 5 (1987) 930-932 [in Russian]
- [251] Serov V.I., Strel'nikov Yu., Abramovich S.N., et al., State of the ${}^{10}\text{Be}$ nucleus with an excitation energy of 17.3 MeV, Izv.Akad.Nauk USSR. Ser.Fiz. 51, 5 (1987) 930-932 [? same as Ref. 249!] [in Russian]
- [293] Linock I., Bilwes R., Kraus L., et al., Study of the first excited states of ${}^6\text{Li}$, J.Physique 30, 1 (1969) 17-28 [in French]
- [296] Shpetnyij A.I., Energy and angular distribution of neutrons in the ${}^9\text{Be}(d,n){}^{10}\text{B}$ reaction, J.Exp.Theor.Fiz. 32, 3 (1957) 423-431 [in Russian]
- [309] Antuf'ev Yu.P., Deinenko A.S., Zalyubovskij I.I., et al., Angular differential cross-sections and vector analysing capacity of the ${}^9\text{Be}(d,p){}^{10}\text{Be}$, ${}^9\text{Be}(d,t){}^8\text{Be}$ and ${}^9\text{Be}(d,\alpha){}^7\text{Li}$ reactions for deuteron energies ranging from 2 to 2.8 MeV, Yad.Fiz. 40, 1 (1984) 53-61 [in Russian]
- [313] Schmidt-Rohr U., Stock R., Turek P., Angular distribution of protons in the ${}^9\text{Be}(d,p){}^{10}\text{Be}$, ${}^{12}\text{C}(d,p){}^{13}\text{C}$, ${}^{16}\text{O}(d,p){}^{17}\text{O}$ and ${}^{40}\text{Ca}(d,p){}^{41}\text{Ca}$ reactions at 11.8 MeV, Nucl.Phys. 53, 1 (1964) 77-76 [in German]
- [320] Ivanits'kij I.G., Alpha particle angular distribution in the ${}^9\text{Be}(d,\alpha){}^7\text{Li}$ reaction, Ukr.Fiz.J. 7, 11 (1962) 1160-1163 [in Russian]
- [321] Bertrand F., Grenier G., Pornat J., Study of the ${}^9\text{Be}(d,\alpha_0){}^7\text{Li}$, ${}^9\text{Be}(d,\alpha_1){}^7\text{Li}$, ${}^9\text{Be}(d,t){}^8\text{Be}$ and ${}^9\text{Be}(d,p_0){}^{10}\text{Be}$ reactions from 300 to 1000 keV, Rep. CEA-R-3504 (1964) [in French]
- [323] Wal'ter A.K., Watset P.I., Kolesnikov L.Ya., et al., Neutron yield in the ${}^9\text{Be}(t,n)$ reaction, Ukr.Fiz.J. 6, 4 (1961) 457-460 [in Russian]
- [324] Palushin'ska K., Nedvedyuk K., Salatskij V.I., Khal'evik I., Investigation of the ${}^9\text{Be}(t,n){}^{11}\text{B}$ reaction in the triton energy range of 1.1 to 1.7 MeV, Preprint P.15-9986. (1976) JINR, Dubna [in Russian]
- [327] Abramovich S.N., Guzhovskij B.Ya., Pereshivkin V.A., Total cross-section for the formation of ${}^{11}\text{C}$ in the ${}^9\text{Be}({}^3\text{He},n)\text{C}$, ${}^{10}\text{B}(d,n){}^{11}\text{C}$ and ${}^{11}\text{B}(d,2n){}^{11}\text{C}$ reactions, Problems of Atomic Science and Technology. Ser. Nuclear Constants No. 2(56) (1984) 55-60 [in Russian]
- [334] Pouliot J., Roy R., Bricault P., Polarization and measurement of the ${}^9\text{Be}({}^3\text{He},p){}^{11}\text{B}$ reaction, Can.J.Phys. 61, 12 (1963) 1609-1612 [in French]
- [347] Klages H.O., Scholermann H., Polarization and neutron angular differential cross-section in the ${}^9\text{Be}(\alpha,n){}^{12}\text{C}$ reaction, Z.Phys. 227, 4 (1969) 344-351 [in German]

Список литературы

1. Caughlan G., Fowler A., Harris M. e.a. Tables of thermonuclear reaction rates for low-mass nuclei// At.Data and Nucl. Data Tables. 1985. Vol. 36, N 2. P.177-233.

2. Звенигородский А.Г., Агуреев В.А., Дунаев И.Б. и др. Аппаратно-программный комплекс для работы по оценке ядерно-физических констант// ВАНТ. Сер. Ядерные константы. 1983. Вып. 2. С. 61-68.

3. Mileu G.H. Charged-particle cross section plasma applications// COO-2218-195, 1980.

4. Horsley A., Parker J.B., Price J.A. Curve fitting and statistical techniques for use in the mechanised evaluation of neutron cross section// Nucl.Instr.Meth. 1968. Vol. 62. P. 29-42.

5. Завьялов Ю.С., Квасов Б.Н., Мирошниченко В.А. Методы сплайн-функций. М.: Наука, 1980.

6. Брандт З. Статистические методы анализа наблюдений. М.: Мир, 1975.

7. Gamov G. Zur quantentheorie des atomkernen// Z.Phys. 1928. Bd. 51. S. 204.

8. Gurney R.W., Condon E.V. Quanten mechanics and radioactive disintegration// Phys. Rev. 1929. Vol. 33. P. 127.

9. Curran S.C., Strothers J. The excitation of γ -radiation in processes of proton capture// Proc. Roy. Soc. 1939. Vol. A172, N 948. P. 72-89.

10. Wilkinson D.H. A source of plane-polarized gamma-ray of variable energy above 5.5 MeV// Phyl. Mag. 1952. Vol. 43, N 341. P. 659-662.

11. Griffiths G.M., Lal M., Scarfe C.D. The reaction $D(p, \gamma)^3\text{He}$ below 50 keV// Can. J. Phys., 1963. Vol. 41, N 5. P. 724-736.

12. Griffiths G.M., Larson E.A., Robertson L.P. The capture of protons by deuterons// Can.J.Phys. 1962. Vol.40, N 4. P. 402-411.

13. Geller K.N., Muirhead E.G., Cohen L.D. The $^2\text{H}(p, \gamma)^3\text{He}$ reaction at the breakup threshold// Nucl.Phys. 1967. Vol. A96, N 2. P.397-400.

14. Skopik D.M., Weller H.R., Robertson N.R., Wender S.A. $^2\text{H}(p, \gamma)^3\text{He}$ reaction using polarized protons// Phys. Rev. 1979. Vol. C19, N 3. P. 601-609.

15. Woude vander A., Halbert M.L., Bingham C.R., Belt B.D. Evidence for a T=1/2 resonance in the ^3He system// Phys. Rev. Lett. 1971. Vol. 26, N 15. P. 909-912.

16. Matthews J.L., Kruse T., Williams M.E. e.a. Radiative capture of protons by deuterons at $E_p=16$ MeV// Nucl. Phys. 1974. Vol. A223, N 2. P P. 221-233.

17. King E.E., Robertson N.R., Weller H.R., Tilley D.R. Polarized and unpolarized proton capture on deuterium// Phys. Rev. 1984. Vol. C30, N 1. P. 21-25.

18. Belt B.D., Bingham C.R., Halbert M.L., Woude A. Radiative capture of deuterons by protons// Phys. Rev.Lett. 1970. Vol.24, N 20. P. 1120-1123.

19. Barkas W.H., White M.G. Disintegration of deuterium by protons and P-N reactions in light gaseous elements// Phys.Rev. 1939.Vol.56, N 3. P. 288-289.

20. Henkel R.L., Perry J.E., Smith R.K. Breakup of deuterons on H, T, ^3He and ^4He // Ibid. 1955. Vol. 99, N 3. P. 1050-1053.

21. Gibbons J.H., Macklin R.L. Total neutron yields from light elements under proton and alpha bombardment// Ibid.1959. Vol. 114, N 2. P. 571-580.

22. Rybakov B.V., Sidorov V.A., Vlasov N.A. Breakup of deuterons on H, D, ^3He and ^4He // Nucl. Phys. 1961. Vol. 23, N 3. P. 491-498.
23. Cranberg L., Smith R.K. Breakup of deuterons by protons// Phys. Rev. 1959. Vol. 113, N 2. P. 587-589.
24. Nisimura K. Breakup of deuterons by the reactions $^1\text{H}(d,p)p$ with $E_d = 18$ MeV and $\text{D}(p,p)p$ with $E_p = 9$ MeV// J. Phys. Soc. Jap. 1961. Vol. 16, N 11. P. 2097-2100.
25. Van-Oers W.T.H., Brockman K.W. Phase shift analysis of elastic nucleon-deuteron scattering// Nucl. Phys. 1967. Vol. A92, N 3. P. 561-583.
26. Cecil F.E., Newman D.E. Diagnostics of high temperature deuterium and tritium plasmas by spectrometry of radiative capture// Nucl. Instr. Meth. 1984. Vol. 221, N 2. P. 449-452.
27. Cecil F.E., Cole D.M., Wilkinson E.G. Measurement and application of dd, dt and d ^3He reactions at low energy// Ibid. 1985. Vol. B10/11, N 1. P. 411-414.
28. Weller H.R., Colby P., Langenbrunner J. e.a. ^4He D-state effects in the $^2\text{H}(d,\gamma)^4\text{He}$ reaction at low energies// Phys. Rev. 1986. Vol. C34, N 1. P. 32-37.
29. Meyerhof W.E., Feldman W., Gilbert S. e.a. $^2\text{H}(d,\gamma)^4\text{He}$ reaction from 6 to 19 MeV// Nucl. Phys. 1969. Vol. A131, N 3. P. 489-500.
30. Zurmuhle R.W., Stephens W.E., Staub H.H. Gamma rays from neutron capture in helium-3 and deuteron capture in deuterium// Phys. Rev. 1963. Vol. 132, N 2. P. 751-754.
31. Poutissou J.M., Del Blanco W. Angular distributions of the $^2\text{H}(d,\gamma)^4\text{He}$ reaction// Nucl. Phys. 1973. Vol. A199, N 3. P. 517-529.
32. Jarmie H., Brown R.E. Low energy nuclear reactions with hydrogen isotopes// Nucl. Instr. Meth. 1985. Vol. B10/11. Pt 1. P. 405-410.
33. Drosch M. Unified absolute differential cross sections for neutron production by the hydrogen isotopes for charged-particle energies between 6 and 17 MeV// Nucl. Sci. Eng. 1978. Vol. 67, N 2. P. 190-220.
34. Krauss A., Becker H.W., Trautvetter H.P. e.a. Low-energy fusion cross sections of d+d and d+ ^3He reactions// Nucl. Phys. 1987. Vol. A465, N 1. P. 150-172.
35. Low energy cross sections measurement of d-d and d-t reactions// Phys. Energ. Port. at Phys. Nucl. 1985. Vol. 9, N 6. P. 723-735.
36. Chagnon P.R., Owen G.E. Angular distributions of the d-d neutrons// Phys. Rev. 1956. Vol. 101, N 6. P. 1798-1803.
37. Pavan P., Tonio D., Zagoga e.a. Forward absolute cross-section of the reaction $^2\text{H}(d,n)^3\text{He}$ for $E_d = (3-6)$ MeV// Nuovo Cim. 1981. Vol. A66, N 3. P. 285-271.
38. Manley J.H., Coon J.H., Graves E.R. Cross section of $\text{D}(d,n)^3\text{He}$ reaction// Phys. Rev. 1946. Vol. 70, N 1-2. P. 101.
39. Ганяев А.С., Говоров А.М., Осетинский Г.М. и др. Реакция D-D в интервале 100-1000 кэВ// Ядерные реакции на легких ядрах. М.: Атомиздат, 1957. С. 26-47.
40. Давиденко В.А., Погребов И.С., Сауков А.И. Определение формы кривой возбуждения реакции $\text{T}(d,n)^4\text{He}$ // Атомная энергия. 1957. Т. 2, № 4. С. 386-388.
41. Hunter G.T., Richards H.T. Yield and angular distribution of the d-d neutrons// Phys. Rev. 1949. Vol. 76, N 10. P. 1445-1451.
42. Schultze R.L., Cosack M., Obst A.W., Weill J.L. $^2\text{H}+d$ -reactions from 1,96 to 6,20 MeV// Nucl. Phys. 1972. Vol. A192, N 3. P. 609-624.
43. Okihana A., Fujiwara N., Nakamura-Yokota R. e.a. The $\text{D}(d,d)\text{D}$, $\text{D}(d,p)\text{T}$ and $\text{D}(d,^3\text{He})\text{n}$ reactions at 13,2 MeV// J. Phys. Soc. Jap. 1979. Vol. 46, N 3. P. 707-714.

44. Preston G., Shaw P.F.D., Young S.A. The cross sections and angular distributions of the d-d reactions between 150 and 450 keV//Proc. Roy.Soc. 1954. Vol. A226, N 1165. P. 206-216.

45. Booth D.L., Preston G., Show P.F.D. The cross section and angular distributions of the D-D reactions between 40 and 90 keV// Proc. Phys.Soc. 1956. Vol. 69A. Pt. 3, N 435. P.265-270.

46. Jarmie N., Jett J.H. Neutron source reaction cross sections//Phys.Rev. 1977. Vol. C16, N 1. P. 15-17.

47. Blair J.M., Freier G., Lampi E. e.a. The angular distributions of the products of the D-D reaction: 1 to 3,5 MeV// Ibid. 1948. Vol. 74, N 11. P. 1599-1603.

48. Ying N., Cox B.B., Barnes B.K., Barrows A.W. A study of the ${}^2\text{H}(d,p){}^3\text{H}$ and ${}^2\text{H}(d,n){}^3\text{He}$ reactions and the excited state of ${}^4\text{He}$ at 23,9 MeV//Nucl.Phys.1973. Vol. A206, N 3. P.481-497.

49. Dietrich F.S., Adelberger E.G., Meyerhof W.E. Study of the ${}^2\text{H}(d,n){}^3\text{He}$ reaction between 12 and 19 MeV// Ibid. 1972.Vol. A184, N 2. P. 449-457.

50. Broolley J.E., Putnam T.M., Rosen L. d-D reactions at 6 to 14 MeV input energy// Phys.Rev. 1957. Vol. 107, N 3.P.820-824.

51. Thornton S.T. The $\text{D}(d,n){}^3\text{He}$ reaction from $E_d=5$ to 10 MeV// Nucl.Phys.1969. Vol.A136, N 1. P.25-34.

52. Arnold W.R., Phillips J.A., Sawyer G.A. e.a. Cross sections for the reactions $\text{D}(d,p)\text{T}$, $\text{D}(d,n){}^3\text{He}$, $\text{T}(d,n){}^4\text{He}$, and ${}^3\text{He}(d,p){}^4\text{He}$ below 120 keV//Phys.Rev. 1954. Vol. 93, N 3. P. 483-499.

53. Goldberg M.D., Le-Blank J.M. Angular distributions of the $\text{D}(d,n){}^3\text{He}$ reaction for 5 to 12 MeV deuterons// Ibid.1960. Vol. 119, N 6. P.1992-1999.

54. Meyerhof W., Tombrello T. Energy levels of light nuclei $A = 4$ // Nucl.Phys. 1968. Vol. A109, N 1. P. 1-58.

55. Liskien H., Paulsen A. Neutron production cross section and energies for reactions $\text{T}(p,n){}^3\text{He}$, $\text{D}(d,n){}^3\text{He}$ and $\text{T}(d,n){}^4\text{He}$ // Nucl.Data. Tabl. 1973. Vol. A11, N 7. P. 569-579.

56. Greene S.L. Maxwell averaged cross section for some thermonuclear reactions on light isotopes//UCRL 70522. 1967. P. 1-46.

57. Gruebler W., Konig V., Schmelzbach P.A. e.a. Investigation of excited states of He via the ${}^2\text{H}(d,p){}^3\text{H}$ and ${}^2\text{H}(d,n){}^3\text{He}$ reactions using a polarized deuteron beams//Nucl.Phys. 1972. Vol. A193, N 1. P. 129-148.

58. Волков В.В., Воротников П.Е., Колтыпин Е.А. и др. Изучение d-d реакции в интервале энергий дейтронов 0,20-1,75 МэВ//Ядерные реакции на легких ядрах. М.: Атомиздат, 1957. С. 15-25.

59. Wenzel W.A., Whaling W. Cross section and angular distribution of the $\text{D}(d,p)\text{T}$ reaction//Phys.Rev.1952. Vol. 88. N 5.P.1149-1154.

60. Gruebler W., Konig V., Schmelzbach P.A. e.a. New highly excited He levels found by the ${}^2\text{H}(d,p){}^3\text{H}$ reaction// Nucl.Phys.1981. Vol. A369, N 3. P. 381-395.

61. Jarmie N., Jett J.H. Various cross sections for $A < 3$ nuclei// Phys.Rev.1974. Vol.C10, N 1. P. 54-56.

62. Allred J.C., Phillips D.D., Rosen L. Angular distribution of protons from the $\text{D}(d,p)\text{T}$ reaction at 10,3 MeV bombarding energy// Ibid. 1951. Vol. 82, N 6. P. 782-785.

63. Perry J.E., Bame S.J. $\text{T}(p,p){}^4\text{He}$ reaction//Ibid. 1955. Vol. 99, N 5. P. 1368-1375.

64. Del-Bianco W., Kajrys G. Angular distribution of the ${}^3\text{H}(p,p){}^4\text{He}$ reaction at proton energies below 1 MeV//Can.J.Phys. 1980. Vol.58, N 10. P. 1496-1499.

65. Meyerhof W.E., Suffer M., Feldman W. ${}^3\text{H}(p,\gamma){}^4\text{He}$ reaction from 3 to 18 MeV// Nucl.Phys. 1970. Vol. A148, N 1. P.211-224.

66. Gemmell D.S., Jones G.A. The $\text{T}(p,\gamma){}^4\text{He}$ reaction// Ibid. 1962. Vol. 33, N 1. P. 102-109.

67. Gardner C.C., Anderson J.D. Gamma yield from the proton bombardment of tritium// Phys.Rev. 1962. Vol. 125, N 2. P. 626-628.

68. Calarco J.R., Hanna S.S., Chang C.C. e.a. Absolute cross section $\text{H}(p,\gamma){}^4\text{He}$ and a review of ${}^4\text{He}(\gamma,p){}^3\text{H}$ measurements// Phys.Rev. 1983. Vol. C28, N 2. P. 483-488.

69. Brolley J.E., Putnam T.M., Rosen L., Stewart L. Hydrogen-helium isotope elastic scattering processes at intermediate energies//Ibid. 1960. Vol. 117, N 5. P.1308-1316.

70. Goldberg M.D. Neutron source, cross section and angular distributions//Progress in Fast Neutron Physics. University of Chicago Press, 1963. P. 3-21.

71. Jarvis G.A., Hemmendinger A., Argon H.V., Tasschek R.F. Reaction constants for ${}^3\text{H}(p,n){}^3\text{He}$ // Phys.Rev. 1950. Vol.79, N 6. P. 929-935.

72. Wilson W.E., Walter R.L., Fossan D.B. Differential cross sections for the $\text{T}(p,n){}^3\text{He}$ reaction//Nucl.Phys.1961. Vol. 27, N 3. P. 421-430.

73. Goldberg M.D., Anderson J.D., Stoering J.P., Wong C. Angular distribution of $\text{T}(p,n){}^3\text{He}$ neutrons for 3,4 to 12,4 MeV//Phys. Rev. 1961. Vol. 122, N 5. P. 1510-1513.

74. Богданов Г.Ф., Власов Н.А., Калинин С.П. и др. Реакция $\text{T}(p,n){}^3\text{He}$ при энергии протонов 7-12 МэВ// ЭТФ. 1959. Т.36, № 2. С.633-636.

75. Seagrave J.D. The $\text{T}(p,n){}^3\text{He}$ reaction and its inverse: Proc. of the Intern. Conf. "Nuclear Forces and the Few-Nucleon Problem", held at the Physics Dep. University College. London, 8-11 July 1959. London, Pergamon Press, 1960. P. 538-593.

76. Власов Н.А., Калинин С.П., Оглоблин А.А. и др. Взаимодействие протонов с тритием и возбужденное состояние ${}^4\text{He}$ //ЭТФ. 1955.Т.28, №6, С. 639-650.

77. Thambidurai P., Beyerle A.J., Gould C.R., Purser F.O. Tritium break-up contribution to the neutron source reaction ${}^3\text{H}(p,n)$ from 9 to 14 MeV//Nucl. Instr.Meth. 1982. Vol.196, N 2-3 P.415-420.

78. Hale G.M., Young P.G., Jarmie N. R-matrix analysis of the t+t reactions//BNL-NCS-26133. 1979. P. 127-136.

79. Morgan G.L., Lisowski P.W., Wender S.A. e.a. Measurement of the branching ratio ${}^3\text{H}(d,\gamma)/{}^3\text{H}(d,n)$ using thick tritium gas target// Phys.Rev. 1986. Vol. C33, N 4. P. 1224-1227.

80. Buss W., Waffler H., Ziegler B. Radiative capture of deuterons by ${}^3\text{H}$ //Phys.Lett. 1963. Vol. 4, N 3. P. 198-199.

81. Безотосный В.М., Жмайло В.А., Суоров Л.М. и др. Сечение реакции $\text{T}(d,\gamma){}^3\text{He}$ с испусканием 16,7 МэВ γ -квантов при энергии дейтронов 25-100 кэВ// Ядерная физика. 1969. Т. 10, № 2. С. 225-226.

82. Brown R.E., Jarmie N., Hale G.M. Fusion-energy reaction $\text{H}(d,\alpha)n$ at low energies// Phys.Rev. 1987. Vol. C35, N 6. P. 1999-2004.

83. Jarmie N., Brown R.E., Hardenkopf R.A. Fission-energy reaction $\text{H}(t,\alpha)n$ from $E_t = 12,5$ to 117 keV// Ibid.1984.Vol. C29, N 6. P. 2031-2046.

84. McDaniel D.K., Drosch M., Hopkins J.C., Seagrave J.D. Angular distributions and absolute cross sections for the $\text{T}(d,n){}^4\text{He}$ neutron-source reaction//Ibid.1973. Vol. C7, N 3. P. 882-888.

85. Galonky A., Johnson C.H. Cross sections for the $\text{T}(d,n){}^4\text{He}$ reactions//Phys. Rev. 1956. Vol.104, N 2. P.421-425.

86. Magiera E., Bormann M., Schewel W., Heiss P. Angular distributions of neutrons from the ${}^3\text{H}(d,n){}^4\text{He}$ reaction//Nucl.Phys. 1975. Vol. A246, N 2. P. 413-424.

87. Балабанов Е.М., Барит И.Я., Кацауров Л.Н. и др. Измерение эффективного сечения реакции $D(t,n)^4\text{He}$ в области энергий дейтронов 40-730 кэВ//Ядерные реакции на легких ядрах. М.: Атомиздат, 1957. С. 57-70.

88. Неммендингер А., Аргон Н.В. Reaction $D(t,\alpha)n$ at 1,5 MeV//Phys.Rev. 1955. Vol.98, N 1. P. 70-72.

89. Вампе С.Д., Пергу Дж.Е. $T(d,n)^4\text{He}$ reaction// Ibid. 1957. Vol. 107, N 6. P. 1616-1624.

90. Аргон Н.В., Тасчек Р.Ф., Агнью Н.М. е.а. Cross sections of the $D(t,n)^4\text{He}$ reaction for 80 to 1200 keV tritons//Ibid.1952. Vol.87, N 4. P. 612-618.

91. Порре С.Н., Холбров С.Н., Ворчерс Р.Р. Neutrons from $D+T$ and $D+H$ // Ibid. 1963. Vol. 129, N 2. P. 733-739.

92. Ненкел Р.Л., Пергу Дж.Е., Смитх Р.К. Breakup of deuterons on $H, T, ^3\text{He}$ and ^4He //Ibid. 1955. Vol. 99, N 3. P. 1050-1953.

93. Ягмие Н., Аллен Р.С. $T(t,\alpha)n,n$ reaction//Ibid. 1958. Vol.111, N 4. P.1121-1128.

94. Стрельников Ю.В., Абрамович С.Н., Моркин Д.А., Юрьева Н.Д. Функция возбуждения реакции $^3\text{H}(t,2n)^4\text{He}$ под углом 0° при энергиях 40-200 кэВ//Изв.АН СССР. Сер.Физическая. 1971. Т. 35, № 1. С. 165-168.

95. Серов В.И., Абрамович С.Н., Моркин Д.А. Измерение полного сечения реакции $T(t,2n)^4\text{He}$ //Атомная энергия. 1977. Т. 42, № 1. С.59-61.

96. Говоров А.М., Лигаен, Осетинский Г.М. и др. Полные сечения реакции $T+T$ в интервале энергий 60-1140 кэВ: Препринт № Р-764. Дубна: ОИЯИ, 1961.

97. Говоров А.М., Лигаен, Осетинский Г.М. и др. Спектры альфа-частиц и дифференциальные сечения реакции $^3\text{H}(t,2n)^4\text{He}$ под углом 90° //ЖЭТФ. 1961. Т. 41, № 3. С. 703-707.

98. Агнью Н.М., Леланд У.Т., Аргон Н.В. е.а. Measurement of the cross section for the reaction $T+T \rightarrow ^4\text{He}+2n+11,4$ MeV//Phys.Rev.1951. Vol. 84, N 4. P. 862-863.

99. Блаэтт С.Л., Янг А.М., Линг С.С. е.а. Reaction $T(^3\text{He},\gamma)^6\text{Li}$ in the energy range 0,5-11 MeV//Ibid.1968. Vol. 176, N 4. P.1147-1153.

100. Вентурга Е., Чанг С.С., Мейерхоф У.Е. The $^3\text{H}(^3\text{He},\gamma)^6\text{Li}$ capture reaction and the structure of ^6Li //Nucl.Phys.1971.Vol.A173, N 1. P.1-16.

101. Вентурга Е., Каларко Дж.Р., Мейерхоф У.Е., Янг А.М. Direct and resonant capture observed in the $^3\text{H}(^3\text{He},\gamma)^6\text{Li}$ reaction//Phys.Lett. 1973. Vol.B46, N 3.P.364-366.

102. Янг А.М., Блаэтт С.Л., Сейлер Р.Г. Direct radiative capture of ^3He by tritons and $T+^3\text{He}$ cluster states in ^6Li //Phys.Rev.Lett.1970. Vol.25, N 26. P. 1764-1767.

103. Краус Л., Суфферт М., Магдальга-Валетте Д. Etude de la reaction $^2\text{H}(^3\text{He},\gamma)^5\text{Li}$ а $E(^3\text{He})=5,5$ MeV//Nucl.Phys.1968. Vol. A109, N 3. P.593-602.

104. Блайр Дж.М., Хинтц Н.М., Ван-Паттер Д.М. Radiative capture of deuterons by ^3He //Phys.Rev.1954.Vol.96, N 4. P.1023-1029.

105. Бусс В., Дел-Бьянко В., Вайфлер Н., Зейглер В. Deuteron capture in ^3He //Nucl.Phys.1968. Vol. A112, N 1.P.47-64.

106. Шродер Н., Маусберг В. Study of ^5Li around 20 MeV excitation energy by a radiative capture reaction//Z.Phys.1970. Bd.235, N 3. S.234-243.

107. Кинг Н.Т., Мейерхоф У.Е., Хирко Р.Г. The $^2\text{H}(^3\text{He},\gamma)^5\text{Li}$ reaction from 2-26 MeV// Nucl.Phys. 1972. Vol.A178, N 2. P.337-349.

108. Аззенберг-Селове Ф. Energy levels of light nuclei $A=5-10$ //Ibid.1984. Vol. A413, N 1. P. 1-214.

109. M o l l e r W., B e s e n b a c h e r F.
A note on the $^3\text{He}+d$ nuclear-reaction cross section//Nucl.Instr.Meth.1980. Vol. 168, N 1/3.
P.111-114.
110. K l i n g e r W., D u s c h F., F l e i s c h m a n n R. The analyzing power of the reaction $^3\text{He}(d,p)^4\text{He}$ for vector-polarized deuterons between 2 and 13 MeV//Nucl.Phys.1971. Vol. A166, N 2.
P. 253-265.
111. L e e m a n n Ch., M e i n e r H., R o h r e r U. e.a. The $^3\text{He}(d,p)^4\text{He}$ reaction between 2,8 and 10 MeV//Polarization Phenomena in Nuclear Reactions, 1970. P. 548-549.
112. R o y R., S e i l e r F., C o n z e t t H.E., R a d F.N. Cross section and vector analyzing power $iT=11$ of the processes $^3\text{He}(d,d)^3\text{He}$, $^3\text{He}(d,p)^4\text{He}$ between 15 and 40 MeV//Phys.Rev.1981. Vol. C24, N 6. P. 2421-2434.
113. F r e i e r G., H o l m g r e n H. Interaction between ^2D and ^4He in the neighborhood of the 18,6 MeV level of ^5Li //Phys.Rev.1954.Vol.93, N 4. P. 825-826.
114. К л ю ч в р е в А.П., Е с е л ь с о н Б.А., В л ь т е р А.К. Изучение реакции $^3\text{He}+d$ дейтронами//Докл. АН СССР. 1956. Т.109, № 4.
С. 737-739.
115. Y a r n e l l J.L., L o v b e r g R.H., S t r a t t o n W.R. Angular distribution of the reaction $^3\text{He}(d,p)^4\text{He}$ between 240 keV and 3,56 MeV// Phys.Rev.1953.Vol.90, N 2. P. 292-297.
116. A l l r e d J.C. Differential cross section of the reaction $^3\text{He}(d,p)^4\text{He}$ at 10,2 MeV bombarding energy and search for excited state in ^4He // Ibid. 1951. Vol. 84, N 4. P. 695-699.
117. B o n n e r T.W., C o n n e r J.P., L i l l i e A.B. Cross section and angular distribution of the $^3\text{He}(d,p)^4\text{He}$ nuclear reaction//Ibid.1952. Vol. 88, N 3. P. 473-476.
118. J a r v i s R.G., R o a f D. Comparison of D-T and D- ^3He at low energies//Proc.Roy. Soc.1953. Vol.218, N 1134. P. 432-438.
119. B a k e r M.P., C a m e r o n J.M., C h a n t N.S., M a n g e l s o n N.F. A search for high-lying levels in the mass A=5 nuclei//Nucl.Phys. 1972. Vol. A184, N 1. P. 97-104.
120. S t e w a r t L., B r o l l e y J.E., R o s e n L. Interaction of 6 to 14 MeV deuterons with ^3He and tritium//Phys.Rev. 1960. Vol. 119, N 5. P. 1649-1653.
121. G r u e b l e r W., K o n i g V., R u h A. e.a. The differential cross sections and the analysing powers $iT=11$, $T=20$, between 2,8 and 11,5 MeV// Nucl.Phys. 1971. Vol. A176, N 3. P. 631-644.
122. K u n z W.E. Deuterium ^3He reaction//Phys. Rev. 1955. Vol. 97, N 2. P. 456-462.
123. В а н Н э н - М и н, Н о в а ц к и й Б.Н., О с е т я н с к и й Г.М. и др. Исследование реакции $^3\text{He}+^3\text{He}$ //Ядерная физика. 1966. Т. 3, № 6. С. 1064-1069.
124. K i n g T.R., S m u t h e R. Cross sections for $^2\text{H}(^3\text{He},^3\text{He})$ and $^2\text{H}(^3\text{He},^4\text{He})$ at 7 to 18 MeV centre-of-mass energy//Nucl.Phys. 1972. Vol. A183, N 3. P.657-665.
125. K e r r R.G. Neutrons from deuteron breakup on ^3He //Phys.Rev. 1966.Vol. 148, N 3. P.998-1002.
126. K u h n B., S c h l e n k B. Winkelverteilungen fur die reaction $^3\text{He}+t$ //Nucl.Phys.1963. Vol. 48, N 3. P. 353-360.
127. Л и Г а Е н, О с е т я н с к и й Г.М., С о д н о м Н. я др. Исследование реакции $^3\text{He}+^3\text{H}$ //ЖЭТФ. 1960. Т.39, № 2. С. 225-229.
128. К и м С ы н Н а м, О с е т я н с к и й Г.М., С е р г е е в В.А. О сохранении изоспина в реакции $^3\text{He}(t,d)^4\text{He}$ //Ядерная физика. 1969.Т.10, № 4. С. 705-712.
129. M o a k C.D. A study of the ^3H reactions// Phys.Rev. 1953. Vol. 92, N 2. P.383-388r

130. Nocken U., Quast U., Richter A., Schreider G. The reaction ${}^3\text{H}({}^3\text{He}, d){}^4\text{He}$ at very low energies: energy dependent violations of the Barchay-Temmer isospin theorem and highly excited states in ${}^6\text{Li}$ //Nucl.Phys. 1973. Vol. A213, N 1. P. 37-106.

131. Klopčič J.T., Darden S.E. Cross-section and polarization measurements for the ${}^3\text{H}({}^3\text{He}, n){}^6\text{Li}$ reaction// Phys.Rev.1971. Vol. C3, N 6. P. 2171-2179.

132. Harrison W.D., Stephens W.E., Tombrello T.A., Winkler H. Radiative capture of ${}^3\text{He}$ by ${}^3\text{He}$ //Phys.Rev. 1967. Vol. 160, N 4. P. 752-755.

133. Ventura E., Calarco J., Chang C.C. e.a. Resonant structure observed in the ${}^3\text{H}({}^3\text{He}, \gamma){}^6\text{Be}$ capture reaction//Nucl.Phys. 1974. Vol. A219, N 1. P. 157-170.

134. Dwarakanath M.R., Winkler H. ${}^3\text{He}({}^3\text{He}, 2p){}^4\text{He}$ total cross section measurements below the coulomb barrier//Phys.Rev. 1971. Vol. C4, N 5. P. 1532-1540.

135. Krauss A., Becker H.W., Trautvetter H.P., Rolfs C. Astrophysical S(E) factor of ${}^3\text{He}({}^3\text{He}, 2p){}^4\text{He}$ at solar energies//Nucl. Phys. 1987. Vol. A467, N 2. P. 273-290.

136. Tombrello T.A. Astrophysical problems//Nuclear research with low energy accelerators/edited by Marion J.B., Van-Patter D.M. New-York-London: Academic Press, 1967. P.195-212.

137. Brown B.E., Corell F.D., Hegland P.M. e.a. ${}^3\text{He}+{}^4\text{He}$ reaction cross sections at 17,9; 21,7; 24,0 MeV//Phys.Rev. 1987. Vol. C35, N 2. P. 383-392.

138. Dwarakanath M.R. ${}^3\text{He}({}^3\text{He}, 2p){}^4\text{He}$ and the termination p of the proton-proton chain// Ibid. 1974. Vol. C9, N 3. P.805-808.

139. Fowler W.A. Completion of the proton-proton reaction and the possibility of energetic neutrino emission by hot stars// Astrophysical Journal. 1958. Vol.127, N 3. P. 551-556.

140. Holmgren H.D., Johnston R.L. ${}^3\text{H}(\alpha, \gamma){}^6\text{Li}$ and ${}^3\text{He}(\alpha, \gamma){}^7\text{Be}$ reactions//Phys.Rev. 1959. Vol. 113, N 6. P.1556-1559.

141. Parker P.D., Kavanagh R.W. ${}^3\text{He}(\alpha, \gamma){}^7\text{Be}$ reaction//Phys.Rev. 1963. Vol.131, N 6. P. 2578-2582.

142. Nagatani K., Dwarakanath M.R., Ashery D. e.a. The ${}^3\text{He}(\alpha, \gamma){}^7\text{Be}$ reaction at very low energy//Nucl.Phys. 1969. Vol. A128, N 1. P. 325-332.

143. Krawinkel H., Becker H.W., Buchmann L. e.a. The ${}^3\text{He}(\alpha, \gamma){}^7\text{Be}$ reaction and the solar neutrino problem//Z.Phys. 1982. Bd. A304, N 4. S. 307-332.

144. Osborne J.L., Barnes C.A., Kavanagh R.V. e.a. Low-energy behavior of the ${}^3\text{He}(\alpha, \gamma){}^7\text{Be}$ cross section//Nucl.Phys.1984. Vol. A419, N 1. P. 115-132.

145. Robertson R.G.H., Dyer P., Bowles T.J. e.a. Cross section of the capture reaction ${}^3\text{He}(\alpha, \gamma){}^7\text{Be}$ //Phys.Rev. 1983. Vol. C27, N 1. P. 11-17.

146. Alexander T.K., Ball G.C., Leonard W.N. e.a. Measurement of the ${}^3\text{He}(\alpha, \gamma){}^7\text{Be}$ reaction at $E_{\alpha} = 252$ keV//Nucl.Phys.1984. Vol. A427, N 3. P. 526-544.

147. Griffiths G.M., Morrow R.A., Riley P.J. e.a. The $T(\alpha, \gamma){}^7\text{Li}$ reaction//Can. J.Phys. 1961. Vol.39. N 10. P. 1397-1408.

148. Robertson R.G., Dyer P., Warner R.A. e.a. Observation of the capture reaction ${}^2\text{H}(\alpha, \gamma){}^6\text{Li}$ and its role in production of Li in the big bang//Phys.Rev.Lett. 1981. Vol. 47, N 26. P.1867-1870.

149. Switkowski Z.E., Heggie J.C.P., Kennedy D.L. e.a. Cross section of the reaction ${}^7\text{Li}(p, \gamma){}^8\text{Be}$ // Nucl.Phys.1979. Vol. A331, N 1. P. 50-60.

150. Ostojic R., Subotic K., Stepanic B. Study of the direct radiative-capture reaction ${}^6\text{Li}(p,\gamma){}^7\text{Be}$ from 0,4 to 1,1 MeV//Nuovo Cim. 1983. Vol. A76, N 1. P. 73-82.

151. Bair J.K., Jones C.M., Williard H.B. Neutrons from the proton bombardment// Nucl. Phys. 1964. Vol. 53, N 2. P. 209-218.

152. Merchez F., Bouchez R., Hofswell R.A., Yavin A.I. L'excitation du niveau 0^+ de 3,56 MeV de ${}^6\text{Li}$ par diffusion (p,p) de 14 a 16 MeV// J.Physique. 1968. T. 29. N 11-12. P. 969-972.

153. Wakefield B., Macefield B.E.F. A study of the ${}^6\text{Li}(p,n){}^6\text{Be}$ reaction//Nucl. Phys. 1968. Vol. A114, N 3. P. 561-576.

154. Fiedler O., Kunze P. Wirkungsquerschnitte der kernreaktionen ${}^6\text{Li}(p,\alpha){}^3\text{He}$ und ${}^3\text{Li}(p,\alpha){}^4\text{He}$ bei kleinsten energien//Ibid 1967. Vol. A96, N 3. P. 513-520.

155. Sawyer// Report LA R-1578, 1953.

156. Gemeinhardt W., Kamke D., Von Rhoneck C. Wirkenverteilung und wirkungsquerschnitt der Reaktion ${}^6\text{Li}(p,\alpha){}^3\text{He}$ un Energiebereich von 50 bis 190 keV//Z.Phys. 1966. Bd.197, N 1.S.58-74.

157. Shinozuka T., Tanaka Y., Sugiyama K. Absolute cross sections for the ${}^6\text{Li}(p,{}^3\text{He}){}^4\text{He}$ reaction at energies below 1 MeV//Nucl. Phys. 1979. Vol. A326, N 1. P.47-54.

158. Elwyn A.J., Holland R.E., Davis C.N. e.a. Cross-sections for the ${}^6\text{Li}(p,{}^3\text{He}){}^4\text{He}$ reaction at energies between 0,1 and 3,0 MeV//Phys. Rev. 1979. Vol. C20, N 6. P.1984-1992.

159. Spinka H., Tambrello T., Winkler H. Low energy cross sections for ${}^7\text{Li}(p,\alpha){}^4\text{He}$ and ${}^6\text{Li}(p,\alpha){}^3\text{He}$ //Nucl.Phys. 1971. Vol. A164, N 1. P. 1-10.

160. Bertrand F., Grenier G., Pornet J. Etude des reactions ${}^6\text{Li}(p,\alpha){}^3\text{He}$, ${}^6\text{Li}(d,\alpha){}^4\text{He}$, ${}^6\text{Li}(d,p_0){}^7\text{Li}$, ${}^6\text{Li}(d,p_1){}^7\text{Li}$ de 300 keV a 1000 keV// Report CEA-R-3428, 1968.

161. Jeronimo J.M.F., Mani G.S., Sadeghi A. The ${}^6\text{Li}(p,\alpha){}^3\text{He}$ reactions// Nucl.Phys. 1963. Vol.43, N 3. P. 424-429.

162. Varnagy M., Csikai J., Szabo J. e.a. Application of T-cellit detector for the study of ${}^6,{}^7\text{Li}(p,\alpha){}^3,{}^4\text{He}$ reactions//Nucl.Instr. Meth. 1974. Vol. 119, N 3. P.451-461.

163. Gould C.R., Nelson R.O., Williams J.R., Boyce J.R. Cross-section requirements for charged-particle fussion-reaction: the ${}^6\text{Li}(p,{}^3\text{He})\alpha$ reaction//Nucl.Sci.and Eng. 1974. Vol. 55, N 3. P. 267-272.

164. Temmer G.M. Detailed (p, α) reaction studies the light nuclei with the Florida State University tandem accelerator: Proc.Conf. on direct interactions and nucl.react.measurements. Padua, New-York-London: Gordon and Breach Science Publishers, 1963. P. 1013-1024.

165. Werby M.F., Greenfield M.B., Kemper K.W. e.a. Study of α +d and ${}^3\text{He}+$ t clustering in ${}^6\text{Li}$ with a two-mode, finite-range analysis of the ${}^6\text{Li}(p,{}^3\text{He}){}^4\text{He}$ reaction//Phys.Rev. 1973. Vol. C8, N 1. P. 106-113.

166. Szabo J., Body Z.T., Szegedi S., Varnagy M. Low-energy cross section for ${}^6\text{Li}(d,n){}^7\text{Be}$ //Nucl.Phys. 1977. Vol. A289, N 2. P.526-532.

167. Elwyn A.J., Holland R.E., Davis C.N. e.a. Absolute cross sections for deuteron-induced reactions on ${}^6\text{Li}$ at energies below 1 MeV// Phys.Rev. 1977. Vol. C16, N 5.P.1744-1756.

168. М-С-Сленан С.Р., Сегал Р.Е. Cross sections for the ${}^7\text{Li}(d,p){}^8\text{Li}$, ${}^6\text{Li}({}^3\text{He},n){}^8\text{B}$, ${}^6\text{Li}(d,\alpha){}^4\text{He}$, ${}^6\text{Li}(d,p){}^7\text{Li}$ and ${}^6\text{Li}(d,n){}^7\text{Be}$ reactions//Phys.Rev. 1975. Vol. C11, N 2. P. 370-382.

169. Гужовский Б.Я., Абрамович С.Н., Звонигородский А.Г. и др. Полные сечения реакции ${}^6\text{Li}(d,n){}^7\text{Be}$, ${}^7\text{Li}(d,2n){}^7\text{Be}$, ${}^6\text{Li}(t,2n){}^7\text{Be}$ //Изв. АН СССР. Сер.Физическая. 1980. Т.44, № 9. С. 1983-1987.

170. Gangadharan S., Wolke R.L. Recoil angular distributions of the ${}^6\text{Li}(d,n){}^7\text{Be}$ and ${}^{12}\text{C}(d,n){}^{13}\text{C}$ reactions//Phys.Rev. 1970. Vol. C1, N 4. P. 1333-1341.

171. Абрамович С.Н., Гужовский Б.Я., Протопопов В.Н. О влиянии свойств парциальных каналов распада на структуру функций возбуждения реакции ${}^6\text{Li}(d,n){}^7\text{Be}$ // Изв. АН Казах. ССР. Сер. Физико-математическая. 1984, № 4. С. 24-29.

172. Гужовский Б.Я., Абрамович С.Н., Звенигородский А.Г. и др. Энергетические зависимости дольных сечений образования нейтронов в реакциях ${}^6\text{Li}+{}^2\text{H}$ // Прикладная ядерная спектроскопия. 1984. Вып. 13. С. 135-143.

173. Baggett L.M., Vame S.J. The disintegration of lithium by deuteron bombardment//Phys.Rev. 1952. Vol. 52, N 3. P. 434-436.

174. Slattery J.C., Chapman A.A., Bonner T.W. Excited states in ${}^7\text{Be}$ and ${}^8\text{Be}$ // Ibid. 1957. Vol. 108, N 3. P. 809-811.

175. Monahan J.E., Elwyn A.J., Sorduke P.J.D. Extrapolation of low-energy reaction cross sections// Nucl. Phys. 1976. Vol. A269, N 1. P. 61-73.

176. Powell D.L., Crawley G.M., Rao B.V., Robson B.A. Deuteron-induced reactions in ${}^6\text{Li}$, ${}^9\text{Be}$ and ${}^{10}\text{B}$ at bombarding energies of 4,5 to 6,0 MeV// Ibid. 1970. Vol. A147, N 1. P. 65-80.

177. Schiffer J.P., Morrison G.C., Siemssen R.H., Zeidman B. Study of the (d,p) reaction in the 1p shell//Phys. Rev. 1967. Vol. 164, N 4. P. 1274-1284.

178. Body Z.T., Szabo J., Varnagy M. Low energy cross sections for ${}^6\text{Li}(d,\alpha){}^4\text{He}$ and ${}^6\text{Li}(d,p){}^7\text{Li}$ reactions//Nucl. Phys. 1979. Vol. A330, N 2-3. P. 495-500.

179. Macklin R.L., Benta H.E. Tritium production from lithium by deuteron bombardment// Phys. Rev. 1955. Vol. 97, N 3. P. 753-757.

180. Holland R.E., Elwyn A.J., Davids C.N. e.a. Absolute cross section for three-body breakup reactions ${}^6\text{Li}(d,n){}^3\text{He}{}^4\text{He}$ and ${}^6\text{Li}(d,p+t){}^4\text{He}$ // Ibid. 1979. Vol. C19, N 3. P. 592-600.

181. Hamburger E.W., Cameron J.R. Study of some reactions of 14,8 MeV deuterons with lithium isotopes//Ibid. 1960. Vol. 117, N 3. P. 791-795.

182. Szabo J., Varnagy M., Body Z.T., Csikai J. Charged particle reaction cross sections relevant for nuclear astrophysics//Nucl. Data scienc and Technology, Antwerpen, 1982. P. 956-957.

183. Головков М.С., Куликаускас В.С., Борончев В.Т. и др. О сечениях дейтронных низкоэнергетических реакций на ядре ${}^6\text{Li}$ // Ядерная физика. 1981. Т. 34, № 3. С. 861-864.

184. Hirst F., Johnstone I., Poole M.J. The $d-{}^6\text{Li}$ reactions//Phil. Mag. 1954. Vol. 45, N 366. P. 762-766.

185. Mani G.S., Freeman R.M., Picard F. e.a. An experimental study of the ${}^6\text{Li}(d,\alpha)\alpha$ reaction//Proc. Phys. Soc. 1965. Vol. 85, N 544. P. 281-284.

186. Rislér R., Gruebler W., Debenham A.A. e.a. Investigation of the ${}^6\text{Li}(d,\alpha){}^4\text{He}$ reaction between 1,5 and 11,5 MeV// Nucl. Phys. 1977. Vol. A286, N 1. P. 115-130.

187. Durr W., Clausnitzer G., Fick D. e.a. Die analysierstarke der reaction ${}^6\text{Li}(d,\alpha){}^4\text{He}$ mit vektorpolarisierten der energie 2,1-10,9 MeV//Ibid. 1968. Vol. A120, N 3. P. 678-690.

188. Gould C.R., Joyce J.M., Boyce J.R. Cross section measurements for charged particle induced reactions on ${}^6\text{Li}$ //Neutron Cross Sect. and Technol. Vol. 2. 1975. P. 697-700.

189. Heidenburg N.S., Hundson C.M., Ingles D.R., Whitehead W.D. Angular distribution of alphas from ${}^6\text{Li}(d,\alpha){}^4\text{He}$ and ${}^7\text{Li}(p,\alpha){}^4\text{He}$ //Phys. Rev. 1948. Vol. 74, N 4. P. 405-410.

190. Jeronimo G.M., Mani G.S., Picard F., Sadeghi A. The ${}^6\text{Li}(d,\alpha){}^4\text{He}$ reaction//Nucl.Phys.1962. Vol. 38, N 1. P. 11-17.
191. Clark R.G., Horan H., Ray R.S., Titterton E.W. Evaluation of cross sections of the ${}^6\text{Li}(d,\alpha)\alpha$ reaction//Phys.Rev. 1978.Vol.C18, N 3. P. 1127-1132.
192. Серов В.И., Гужовский Б.Я. Исследования реакций ${}^6\text{Li}(t,n)$, ${}^7\text{Li}(t,n)$, ${}^7\text{Li}({}^3\text{He},n)$, ${}^9\text{Be}(t,n)$, ${}^{11}\text{B}$ и ${}^9\text{Be}({}^3\text{He},n){}^{11}\text{C}$ // Атомная энергия. 1962. Т. 12, № 1. С.5-II.
193. Seltz R., Magnag-Valette D. Courbes d'excitation et sections efficaces des reactions $\text{Li}(t,n)$ de 100 a 300 keV// Compt.Rend. 1960. T.251, N 19. P. 2006-2008.
194. Зальтер А.К., Вацет П.И., Колесников Л.Я. и др. Выход нейтронов из реакции ${}^6\text{Li}(t,n)$ и ${}^7\text{Li}(t,n)$ //Атомная энергия. 1961.Т. 10, № 6. С.577-586.
195. Абрамович С.Н., Гужовский Б.Я., Дунаева С.А. и др. Структура функций возбуждения каналов образования короткоживущих ядер ${}^6\text{He}$, ${}^8\text{Li}$, ${}^9\text{Li}$ и в реакциях ${}^7\text{Li}+n$ //ВАНТ.Сер. Ядерные константы. 1985, № 2. С. 14-18.
196. Ciric D., Sterancic B., Popic R. e.a. ${}^6\text{Li}(t,p){}^8\text{Li}$ reaction at low triton energy//Fizika. 1972. T.4.P. 193-194.
197. Farmer B.J. The ${}^6\text{Li}({}^3\text{He},n){}^8\text{Be}$ excitation//Bull.Amer.Phys.Soc.1961. Vol.6, N 4. P. 341.
198. Marrs R.E., Vodansky D., Adelberger E.G. Accelerator production of ${}^8\text{B}$ neutrons//Phys.Rev. 1973. Vol. C8, N 2. P. 427-430.
199. Ajzenberg-Selove F. Energy levels of light nuclei A = 11-12// Nucl.Phys. 1985. Vol. A433, N 1. P. 1-157.
200. Elwyn A.J., Holland R.E., Davids C.N. e.a. Cross-sections for the ${}^6\text{Li}({}^3\text{He},p)$ reaction at energies below 2 MeV//Phys.Rev. 1980. Vol. C22, N 4. P.1406-1419.
201. Schiffer J.P., Bonner T.W., Davis R.H., Prosser F.W. Study of the reaction mechanism for $({}^3\text{He},p)$ reactions with ${}^6\text{Li}$, ${}^{10}\text{B}$, ${}^{13}\text{C}$ // Ibid. 1956. Vol. 104, N 4. P.1064-1068.
202. Fletcher N.R., Marshall J.D., Davis R.H. Exchange effects in the ${}^6\text{Li}({}^3\text{He},p){}^8\text{Be}$ reaction//Nucl.Phys.1965.Vol. 70, N 2. P. 471-479.
203. Gould C.R., Boya J.R. Cross-section measurements for charged particle fusion reactors: the ${}^6\text{Li}({}^3\text{He},p)2\alpha$ reaction// Nucl.Sci.Eng.1976. Vol. 60, N 4. P. 477-481.
204. Ishad M., Rioux C., Asai J. e.a. Proton polarization and differential cross section for the $({}^3\text{He},p)$ reaction on ${}^6\text{Li}$ and ${}^9\text{Be}$ at 14 MeV//Nucl.Phys.1977. Vol. A286, N 3. P.483-493.
205. Pyle R.V., Ruby L., Sterbentz J.W. Measurements of the ${}^6\text{Li}({}^3\text{He},d){}^7\text{Be}$ and ${}^7\text{Li}({}^3\text{He},t){}^7\text{Be}$ cross sections//Trans.ANS.1978. Vol.30, N 1. P. 623-625.
206. Holland R.E., Elwyn A.J., Davids C.N. e.a. Nuclear cross sections for light ions on ${}^6\text{Li}$ // IEEE Trans.Nucl.Sci.1981. Vol.NS-28, N 2. P. 1344-1349.
207. Бужиньский С., Супраньский П., Русеяк К.И. и др. Измерение функций возмущения реакций ${}^6\text{Li}({}^3\text{He},{}^3\text{He}){}^6\text{Li}$ и ${}^6\text{Li}({}^3\text{He},d){}^7\text{Be}$ // Изв.АН СССР. Сер.Физическая. 1978.Т. 43, № 1. С. 156-159.
208. Ludesken H., Wan-Tjint T., Wegnar H., Zimmerer J. The reactions ${}^6\text{Li}({}^3\text{He},{}^3\text{He}){}^6\text{Li}$, ${}^6\text{Li}(d,d_0){}^6\text{Li}$, ${}^7\text{Li}(d,d_0){}^7\text{Li}$ and ${}^6\text{Li}({}^3\text{He},d_0){}^7\text{Be}$ // Nucl.Phys. 1968. Vol. A109, N 3. P. 676-688.
209. Абрамович С.Н., Гужовский Б.Я., Перешивкин В.А. Измерение полных сечений образования радиоактивного нуклида ${}^7\text{Be}$ при взаимодействии ${}^6\text{Li}$, ${}^7\text{Li}$, ${}^9\text{Be}$ и ${}^{10}\text{B}$ с ${}^3\text{He}$ // ВАНТ. Сер.Ядерные константы. 1980. Вып. 5. С.21-25.
210. Jarmie N., Seagrave J.D.// LA-2014, 1957.

211. Bonner T.W., Evans J.E. Resonances in the disintegration of fluorine and lithium by protons//Phys.Rev. 1948. Vol. 73, N 7. P. 666-674.

212. Kraus A.A. Gamma radiation from proton bombardment of ${}^7\text{Li}$ //Phys.Rev. 1954. Vol. 93, N 6. P. 1308-1310.

213. Fisher G.A., Paul P., Riggs F., Hanna S.S. Giant E1 resonances in ${}^8\text{Be}$ from the reaction ${}^7\text{Li}(p,\gamma){}^8\text{Be}$ //Ibid.1976. Vol.014, N 1. P. 28-36.

214. Schlueter D.J., Krone R.W., Prosser F.W. Measurements and analysis of angular distribution interference effects in the ${}^7\text{Li}(p,\gamma){}^8\text{Be}$ reaction//Nucl.Phys.1964.Vol. 58, N 2. P. 254-272.

215. Sweeney W.E., Marion J.B. Gamma-ray transitions involving isobaric-spin mixed states in ${}^8\text{Be}$ //Phys.Rev.1969. Vol. 182, N 4.P.1007-1021.

216. Liskien H., Paulsen A. Neutron production ${}^7\text{Li}(p,n){}^7\text{Be}$ and ${}^7\text{Li}(p,n){}^7\text{Be}$ //At.Data and Nucl.Data Tables.1975. Vol. 15, N 1. P. 57-85.

217. Sekharan K.K., Laumer H., Kern B.D., Gabbard F. A neutron detector for measurement of total neutron production cross sections//Nucl.Instr. Meth.1976. Vol. 133, N 2. P. 253-257.

218. Poppe C.H., Andersson J.D., Davic J.C. e.a. Cross sections for the ${}^7\text{Li}(p,n){}^7\text{Be}$ reaction between 4,2 and 26 MeV//Phys.Rev. 1976. Vol. C14, N 2.P. 438-445.

219. Presser G., Bass R. Reactions ${}^7\text{Li}+n$, ${}^7\text{Li}+p$ and excited states of the A=8 system//Nucl.Phys. 1972. Vol. A182, N 2. P. 321-341.

220. Freeman J.M., Hanna R.C., Monteague J. The nuclear reaction ${}^4\text{He}(\alpha,p){}^7\text{Li}$ and its inverse. The reaction ${}^7\text{Li}(p,\alpha){}^4\text{He}$ // Ibid.1958. Vol. 5, N 1. P. 148-149.

221. Marion J.B., Wilson M. The ${}^7\text{Li}(p,\gamma){}^8\text{Be}$ reaction and single-particle levels in ${}^8\text{Be}$ //Ibid.1966. Vol.77, N 1.P.129-148.

222. Pauhli R., Konner D., Snover K.A. Magnetic dipole transitions and isospin in ${}^8\text{Be}$ //Phys.Rev.1977. Vol. 173, N 4.P.919-930.

223. Rolfs C., Kavanagh R.N. The ${}^7\text{Li}(p,\gamma){}^4\text{He}$ cross section at low energies//Nucl. Phys. 1986. Vol. A455. P. 179-188.

224. King C.H., Austin S.M., Rossner H.H., Chien N.S. ${}^7\text{Li}$ and ${}^7\text{Be}$ production in the alpha+alpha reaction//Phys.Rev. 1977. Vol. C16, N 5. P. 1712-1722.

225. Slobodrian R.J., Conzett H.E. The ${}^4\text{He}(\alpha,p){}^7\text{Li}$, ${}^7\text{Li}^{n.o.478}$ reaction near threshold //Z.Phys. 1982. Bd. A308, N 1.S.15-20.

226. Ciric D.M., Popic R.V., Zakula R.B. e.a. The interaction of ${}^7\text{Li}$ isotope with low energy proton and triton beams//Zbornik Radova prirodno-mat faculteta - Univerzitet u novoy Sadu. 1976. T. 6. P. 115-126.

227. Mani G.S., Freeman B., Picard F. e.a. Study of the reaction ${}^7\text{Li}(p,\alpha){}^4\text{He}$ up to 12 MeV proton energy//Nucl.Phys. 1964. Vol. 60, N 4. P. 588-592.

228. Kilian K., Clausnitzer G., Durrr W. e.a. Untersuchung der reaktionen ${}^7\text{Li}(p,p){}^7\text{Li}$, ${}^7\text{Li}(p,p){}^7\text{Li}$ und ${}^7\text{Li}(p,\alpha){}^4\text{He}$ mit polarisierten protonen der energie 2,7 bis 10,8 MeV// Ibid. 1969. Vol. A126, N 3. P. 529-544.

229. Власов Н.А., Оглоблин А.А. Реакция ${}^7\text{Li}(p,t)$ //Ядерные реакции при малых и средних энергиях, 1966. С. 24.

230. Friedland E., Venter I. Die reaction ${}^7\text{Li}(d,\alpha){}^5\text{He}$ im energiegebiet von 0,6 bis 2,0 MeV//Z. Phys. 1971. Bd. 243, N 2. S.126-131.

231. Von-Mollendorff U., Janet A., Seiler F., Striebel H.R. The ${}^7\text{Li}(d,n){}^8\text{Be}$ reaction with polarized 800 keV deuterons//Nucl.Rhys. 1973. Vol. A209, N 2. P. 323-332.

232. Осетинский Г.М., Сикоро Б., Фрышин Б. Исследование реакции ${}^7\text{Li}(d,n){}^8\text{Be}$: Препринт № 5143. Дубна: ОИЯИ, 1970.

233. Milone S., Potenza R. The ${}^7\text{Li}+D$ reactions//Nucl.Phys.1966. Vol. 84, N 1. P.25-36.

234. Kavanagh R.W., Proton capture in ${}^7\text{Be}$ //Ibid. 1960. Vol. 15, N 3. P. 411-420.

235. Schilling A.E., Mangelson N.F., Nielson V.C. e.a. An accurate measurement of the ${}^7\text{Li}(d,p){}^8\text{Li}$ excitation function from $E_d = 0,6$ MeV to $2,0$ MeV//Ibid. 1976. Vol. A263, N 3. P. 389-396.

236. Абрамович С.Н., Гужовский Б.Я., Звенигородский А.Г. и др. Исследование высоковозбужденных состояний ядра ${}^9\text{Be}$ в реакциях ${}^6\text{Li}(t,p){}^8\text{Li}$ и ${}^7\text{Li}(d,p){}^8\text{Li}$ // Изв. АН СССР. Сер. Физическая. 1986. Т. 50, № 1. С. 65-67.

237. Filippone B.W., Elwyn A.J., Ray W., Kretke D.D. Absolute cross section for ${}^7\text{Li}(d,p){}^8\text{Li}$ and solar neutrino capture rates// Phys.Rev. 1982. Vol. C25, N 5. P.2174-2179.

238. Elwyn A.G., Holland R.E., Davids C.N., Ray W. ${}^7\text{Li}(d,p){}^8\text{Li}$ reaction cross section near $0,78$ MeV//Ibid. 1982. Vol. C25, N 5. P. 2168-2173.

239. Zander A.R., Kemper K.W., Fletcher N.R. Measurement and direct reaction analysis of the reactions ${}^7\text{Li}(d,t){}^6\text{Li}$ and ${}^7\text{Li}({}^3\text{He},\alpha){}^6\text{Li}$ // Nucl.Phys. 1971. Vol. A173, N 2. P. 273-285.

240. Levine S.N., Bender R.S., McGuire J.N. Angular distributions of deuteron-induced reactions in lithium//Phys.Rev. 1955. Vol. 97, N 5. P. 1249-1254.

241. Абрамович С.Н., Базь А.И., Гужовский Б.Я. Околопороговая аномалия в реакции ${}^7\text{Li}(p,{}^9\text{Li}){}^8\text{Li}$ // Н. Ч. 2// Ядерная физика. 1980. Т. 32, № 2. С. 402-406.

242. A Jensenberg-Selove F., Flynn B.R., Hanser O. (t,p) reactions on ${}^4\text{He}$, ${}^6\text{Li}$, ${}^7\text{Li}$, ${}^9\text{Be}$, ${}^{10}\text{B}$, ${}^{11}\text{B}$ and ${}^{12}\text{C}$ //Phys.Rev. 1978.Vol. C17, N 4. P. 1283-1293.

243. Young P.G., Stokes R.H. New states in ${}^9\text{Li}$ from the reaction ${}^7\text{Li}(t,p){}^9\text{Li}$ //Ibid. 1971. Vol. C4, N 5. P. 1597-1601.

244. Cecil F.E., Fahlsing R.F., Jarmie M. e.a. Low energy ${}^7\text{Li}(t,\alpha){}^6\text{He}$ cross section//Ibid.1983. Vol. C27, N 1. P. 6-10.

245. Almqvist E., Pepper T.P., Lorange P. The angular distribution of the ${}^7\text{Li}(t,\alpha){}^6\text{He}$ reactions at 240 keV triton energy// Can.J.Phys.1954. Vol.32, N 10. P.621-629.

246. Holmgren H.D., Cameron L.M. The ${}^7\text{Li}(t,\alpha){}^6\text{He}$ reaction: Proc. of the Rutherford Jubilee Intern.Conf. 1961. P.537-538.

247. Stokes R.H., Young P.G. Search for excited states of ${}^6\text{He}$ //Phys.Rev. 1971. Vol.C3, N 3. P.984-991.

248. A Jensenberg-Selove F., Watson J.W., Middleton R. Alpha particles from the triton bombardment of ${}^7\text{Li}$, ${}^{12}\text{C}$ and ${}^{16}\text{O}$ //Ibid. 1965. Vol. B139, N 3. P. 592-596.

249. Серов В.И., Стрельников Ю., Абрамович С.Н. и др. Состояние ядра ${}^{10}\text{Be}$ с энергией возбуждения $17,3$ МэВ// Изв. АН СССР. Сер. Физическая. 1987. Т. 51, № 5. С. 930-932.

250. Crews R.W. Neutron yield for the $\text{Li}+t$ reactions//Phys.Rev.1951. Vol. 82, N 1. P.100-101.

251. Серов В.И., Стрельников Ю., Абрамович С.Н. и др. Состояние ядра ${}^{10}\text{Be}$ с энергией возбуждения $17,3$ МэВ// Изв. АН СССР. Сер. Физическая. 1987. Т. 51, № 5. С.930-932.

252. Din G.U., Weil J.L. The reactions ${}^{11}\text{B}({}^3\text{He},n){}^{13}\text{N}$ and ${}^7\text{Li}({}^3\text{He},n){}^9\text{B}$ from 1,5 to 5,5 bombarding energy//Nucl.Phys. 1966. Vol. 86, N 3. P. 509-527.

253. Duggan J.L., Miller P.D., Gaby R.F. A study of the reactions ${}^9\text{Be}({}^3\text{He},n){}^{11}\text{C}$, ${}^7\text{Li}({}^3\text{He},n){}^9\text{Be}$ and ${}^{13}\text{C}({}^3\text{He},n){}^{15}\text{O}$ //Ibid.1963. Vol. 46, N 3. P. 336-352.

254. Dixon R.L., Edgell R.D. The ${}^7\text{Li}({}^3\text{He},d){}^8\text{Be}$ and ${}^7\text{Li}({}^3\text{He},p){}^9\text{Be}$ reactions//Ibid. 1970. Vol. A156, N 1. P. 33-42.

255. Bondouk I.I., Asfour F., Saleh Z., Machali F. An experimental investigation of the reactions, ${}^7\text{Li}({}^3\text{He},p_0){}^8\text{Be}$ and ${}^7\text{Li}({}^3\text{He},p_2){}^9\text{Be}$ in the ${}^3\text{He}$ energy range of 1,0 to 2,5 MeV//Rev.Rouv.Phys. 1975. Vol. 20, N 10. P. 1095-1098.

256. Wolicki E.A., Knudson A.R. ${}^7\text{Li}({}^3\text{He},p){}^9\text{Be}$, ${}^7\text{Li}({}^3\text{He},\alpha){}^6\text{Li}$ and ${}^7\text{Li}({}^3\text{He},t){}^7\text{Be}$ reactions//Bull. Amer.Phys.Soc. 1961. Vol. 6, N 5. P. 415.

257. Bondouk I.I., Saad S. Investigation of the reaction ${}^7\text{Li}({}^3\text{He},d_0){}^8\text{Be}$ in the ${}^3\text{He}$ energy range of 1,0 to 2,5 MeV//Atomkernenergie. 1977. Bd. 29, N 4. S. 270-271.

258. Liu Y.C.// Chin.J.Phys. 1972. Vol. 10, N 2. P. 76.

259. Bogart E., Devons S., Tatchell M. The ${}^3\text{He}-{}^3\text{H}$ reaction with mirror nuclei// Proc.Conf.Direct Interact. and Nucl.React.Mechanisms, Padua, 1963. P. 960-963.

260. Orihara H., Makagawa T., Ueno H. e.a. The $({}^3\text{He},t)$ reactions on ${}^7\text{Li}$ and ${}^9\text{Be}$ from 2,0 to 4,2 MeV//Nucl.Phys.1969. Vol. A139, N 1. P. 226-240.

261. Forsyth P.D., Perry R.R. The ${}^7\text{Li}({}^3\text{He},\alpha){}^6\text{Li}$ reaction between 1,3 and 5,5 MeV// Ibid. 1965. Vol. 67, N 3. P. 517-528.

262. Orihara H., Baba M., Akiyama M. e.a. The $({}^3\text{He},\alpha)$ reaction on ${}^7\text{Li}$ from 5,0 to 8,0 MeV// J.Phys.Soc.Jap. 1970. Vol. 29, N 3. P.533-539.

263. Link I., Bilwes R., Kraus L. e.a. Etude des premiers niveaux excites de ${}^6\text{Li}$ // J.Physique. 1969. T. 30, N 1. P. 17-28.

264. Paul P., Blatt S.L., Kohler D. Search for resonances in the reaction ${}^7\text{Li}({}^3\text{He},\alpha){}^6\text{Li}$ // Phys.Rev. 1965. Vol. B137, N 3. P. 499-501.

265. Sealock R.M., Hsiao-Yuan W.U., Overley J.C. ${}^7\text{Li}(\alpha,n){}^{10}\text{B}$ differential cross-section measurements from threshold to $E=5,1\text{MeV}$ //Nucl.Phys. 1981. Vol. A357, N 2. P. 279-292.

266. Van-Der-Zwan L., Geiger K.W. The ${}^7\text{Li}(\alpha,n){}^{10}\text{B}$ differential cross section for alpha-energies of up to 8 MeV//Ibid. 1972. Vol. A180, N 2. P.615-624.

267. Bichsel H., Bonner T.W. Neutrons from the nuclear reaction ${}^7\text{Li}(\alpha,n){}^{10}\text{B}$ // Bull.Amer.Phys.Soc. 1956. Vol. 1, N 2. P. 93.

268. Mehta M.K., Hunt W.E., Pledl H.S., Davis R.H. A study of the ${}^6\text{Li}(\alpha,n){}^9\text{Be}$ and ${}^7\text{Li}(\alpha,n){}^{10}\text{B}$ reactions//Nucl.Phys. 1963.Vol.48, N 1. P.90-96.

269. Meyerhof W.E., Tanner N.W., Hudson C.M. Radiative capture of protons by ${}^9\text{Be}$ //Phys.Rev.1959. Vol.115, N 5. P.1227-1237.

270. Szegedi S. Investigations on nuclear reactions induced by protons and deuterons in Be// Acta.Phys. Acad. Sci.Hung. 1973. Vol. 34, N 2-3. P. 215-223.

271. Forubayashi B., Teranishi T., Kageyama M. The 1330 keV resonance level of the ${}^9\text{Be}(p,\gamma){}^{10}\text{B}$ reaction and excited state of ${}^{10}\text{B}$ //J.Phys.Soc.Jap. 1963. Vol. 18, N 9. P. 1235-1246.

272. Hornyak W.F., Coor T. Capture gamma rays from the proton bombardment of ${}^9\text{Be}$ //Phys. Rev. 1953. Vol. 92, N 3. P. 675-680.

273. Rohrer U., Brown L. The ${}^9\text{Be}(p,n){}^9\text{B}$ reaction with polarized protons from 2,4 to 2,9 MeV// Nucl. Phys. 1976. Vol. A261, N 1. P. 141-148.

274. Marion J.B. Excited states in ${}^{10}\text{B}$ // Phys.Rev. 1956. Vol. 103, N 3. P. 713-717.

275. Marion J.B., Levin J.S. Investigation of the ${}^9\text{Be}(p,n){}^9\text{B}$ and ${}^9\text{Be}(p,\alpha){}^6\text{Li}$ reactions// Ibid. 1959. Vol. 115, N 1. P. 144-149.

276. Kelsey C.A., Lietz G.P., Trevino S.F., Darden S.E. Polarization and angular distribution measurements on the neutrons from the ${}^9\text{Be}(p,n){}^9\text{B}$ reaction//Ibid. 1963. Vol. 129, N 2. P. 759-764.

277. Walker B.D., Wong C., Anderson J.D., McClure J.W. Angular distribution and polarization of neutrons from the ${}^9\text{Be}(p,n_0){}^9\text{B}$ and ${}^{11}\text{B}(p,n_0){}^{11}\text{C}$ reactions//Ibid. 1965. Vol. B137, N 6. P. 1504-1507.

278. Anderson J.D., Wong C., McClure J.W., Walker B.D. Quasielastic (p,n) angular distributions//Phys.Rev. 1964. Vol. B136, N 1. P. 118-125.

279. Byrd R.C., Floyd C.E., Cuss P.P. e.a. Cross section measurement and Lane model analysis for the ${}^9\text{Be}(p,n){}^9\text{B}$ reaction// Nucl.Phys. 1983. Vol. A399, N 1. P. 94-118.

280. Verbinski V.V., Burrus W.R. Direct and compound-nucleus neutrons from 14-18 MeV protons on ${}^9\text{Be}$, ${}^{14}\text{N}$, ${}^{27}\text{Al}$, ${}^{56}\text{Fe}$, ${}^{119}\text{In}$, ${}^{181}\text{Ta}$ and ${}^{208}\text{Pb}$ from 33 MeV bremsstrahlung on ${}^{27}\text{Al}$, ${}^{206}\text{Pb}$, ${}^{208}\text{Pb}$ and ${}^{209}\text{Bi}$ //Phys.Rev. 1969. Vol. 177, N 4. P. 1671-1686.

281. Darden S.E., Murillo G., Sen S. The ${}^9\text{Be}(d,d){}^9\text{Be}$, ${}^9\text{Be}(d,p){}^{10}\text{Be}$, ${}^9\text{Be}(d,t){}^8\text{Be}$ and ${}^9\text{Be}(p,d){}^8\text{Be}$ reactions at 15 MeV//Nucl.Phys. 1976. Vol. A266, N 1. P. 29-59.

282. Becchetti P.D., Fieds C.A., Raymond R.S. e.a. Gost anomaly in ${}^8\text{Be}$ studies with ${}^9\text{Be}(p,d)$ at $E_p=14,3$ and $26,2$ MeV//Phys. Rev. 1981. Vol. C24, N 6. P. 2401-2408.

283. Sierk A.J., Tombrello T.A. The ${}^9\text{Be}(p,\alpha)$ and (p,d) cross section at low energies//Nucl.Phys.1973. Vol. A210, N 2.P. 341-354.

284. Weber G., Davis L.M., Marion J.B. (d,p) and (p, α) reactions in ${}^9\text{Be}$ //Phys.Rev. 1956. Vol. 104, N 5. P. 1307-1313.

285. Moller F.S. Elastic scattering of protons by beryllium//Ibid.1956. Vol. 104, N 5. P. 1386-1398.

286. Morita S., Tohei T., Nakagawa T. e.a. The ${}^9\text{Be}(p,\alpha){}^6\text{Li}$ and ${}^9\text{Be}(p,d){}^8\text{Be}$ reactions from 1 to 4,6 MeV//Nucl.Phys. 1965. Vol. 66. N 1. P. 17-24.

287. Hudson G.M., Crinean G.B., Kelly D.T., Spicer R.M. The ${}^9\text{Be}(p,d_0){}^8\text{Be}$ reaction and the BHMM theory of stripping reactions//Nucl.Phys.1972. Vol. A184, N 1. P. 175-192.

288. Blieden H.R., Tamm G.M., Warsch K.L. A study of the ${}^9\text{Be}(p,\alpha){}^6\text{Li}$ reaction from 3,5 to 12,5 MeV//Ibid.1963. Vol. 49, N 2. P. 209-238.

289. Yanaby T., Yamashita S., Kakigi S. e.a. Alpha emitting reactions on ${}^9\text{Be}$, ${}^{10}\text{B}$ and ${}^{11}\text{B}$ induced by protons, deuterons and alpha-particles//J.Phys.Soc.Jap. 1964.Vol.19, N 10. P. 1818-1823.

290. Rasmussen S.W. Interaction of 10 MeV protons with beryllium//Phys.Rev. 1956. Vol. 103, N 1. P. 186-189.

291. Summers - Gill R.G. Scattering of 12 MeV protons, 24 MeV deuterons and 48 MeV alpha particles by beryllium//Ibid.1958. Vol. 109, N 5. P. 1591-1603.

292. Becker J.A., Fox J.D. Capture of protons by ${}^{11}\text{B}$ in the giant resonance region// Nucl. Phys. 1963. Vol. 42, N 4. P. 669-675.

293. Suffert M. Study of the inverse photodeuteron reaction in ${}^{11}\text{B}$ and ${}^{16}\text{O}$ in the giant resonance energy region//Ibid.1966. Vol. 75. N 1. P.226-240.

294. Battleson K., McDaniel D.K. Resonance structure in reaction ${}^9\text{Be}(d,p){}^{11}\text{B}$ // Phys.Rev. 1971. Vol. C4. N 5. P. 1601-1610.

295. Del-Bianco W., Kundu S., Rouben B. The ${}^9\text{Be}(d,p){}^{11}\text{B}$ reaction in the region of the giant dipole resonance//Nucl.Phys. 1974. Vol. A232, N 2. P. 333-354.

296. Ш п е т н ы й А.И. Энергетическое и угловое распределение нейтронов из реакции ${}^9\text{Be}(d,n){}^{10}\text{B}$ // ЖЭТФ. 1957. Т. 32, № 3. С. 423-431.

297. К о л т а у Е. Investigation on the excitation function of the nuclear reaction ${}^9\text{Be}(d,n){}^{10}\text{B}$ by artificially accelerated particles in the 0,5-1,6 MeV energy range//Acta Phys. Acad. Sci. Hung. 1963. Vol. 16, N 2. P.93-100.

298. B a r d e s R., O w e n G. Angular distributions of the ${}^9\text{Be}(d,n){}^{10}\text{B}$ neutrons//Phys.Rev. 1960. Vol.120, N 4. P. 1369-1374.

299. C e c i l F.E., F a h l s i n g R.F., N e l s o n R.A. Total cross-section measurement for the production of nuclear gamma rays from light nuclei by low energy deuterons//Nucl.Phys. 1982. Vol. A376, N 2. P. 379-388.

300. S i e m s s e n R.H., C o s a c k M., F e l s t R. Reaction mechanism study of $L_p=1$ stripping processes on nuclei of the 1p shell. 1. The reactions ${}^9\text{Be}(d,n){}^{10}\text{B}$, ${}^{10}\text{B}(d,n){}^{11}\text{C}$ and ${}^{11}\text{B}(d,n){}^{12}\text{C}$ // Ibid. 1965. Vol. 69, N 1. P. 209-226.

301. P a r k Y., N i l l e r A., L i n d g r e n R. Spectroscopy of ${}^{10}\text{B}$ levels from the ${}^9\text{Be}(d,n){}^{10}\text{B}$ reaction//Phys.Rev. 1973. Vol. 8, N 5. P. 1557-1573.

302. D e - J o n g D., E n d t P.M., S i m o n s L.J.G. Angular dependence and yield of the ${}^9\text{Be}(d,p){}^{10}\text{Be}$ and ${}^9\text{Be}(d,t){}^8\text{Be}$ reactions//Physica. 1952. Vol. 18, N 10. P. 676-682.

303. J u r i c M.K. Angular distribution of disintegration products from the ${}^{16}\text{O}(d,p){}^{17}\text{O}$, ${}^9\text{Be}(d,p){}^{10}\text{Be}$ and ${}^9\text{Be}(d,t){}^8\text{Be}$ reactions//Phys. Rev. 1955. Vol. 98, N 1. P. 85-88.

304. F r i e d l a n d E., A l b e r t s H.W., V a n - S t a d e n J.C. Deuteron induced reactions on ${}^9\text{Be}$ at low energies//Z.Phys.1974. Bd. 267, N 2. S. 97-101.

305. B o n d o u k I., A s f o u r F., M a c h a l i F. An experimental investigation of the reactions ${}^9\text{Be}(d,p){}^{10}\text{Be}$, ${}^9\text{Be}(d,p){}^{10}\text{Be}$ and ${}^9\text{Be}(d,t){}^8\text{Be}$ in the deuteron energy range 0,9-2,5 MeV//Rev.Roum.Phys. 1974. Vol. 19, N 5. P. 551-553.

306. B i g g e r s t a f f J.A., H o o d R.F., S c o t t H., M c E l l i s t r e m M.T. Differential cross sections for (d, α) and (d,t) reactions in ${}^9\text{Be}$ //Nucl.Phys. 1962. Vol. 36, N 4. P.631-641.

307. Z w i e g l i n s k i B., S a g a n e k A., S l e d z i n s k a I., W i l h e l m i Z. Direct and resonance processes in ${}^9\text{Be}(d,p){}^{10}\text{Be}$ and ${}^9\text{Be}(d,t){}^8\text{Be}$ at low energies//Ibid.1975. Vol. A250, N 1. P. 93-105.

308. I s h i m a t s u T., T a k a n o N., H a c h i y a Y., N a k a s h i m a T. Angular distributions and excitation functions of the ${}^9\text{Be}(d,p){}^{10}\text{Be}$ ground-state reaction//J.Phys.Soc. Jap. 1961. Vol. 16, N 3. P. 367-371.

309. А н г у ф ь е в Ю.П., Д е й н е н к о А.С., З а л ю б о в с к и й И.И. и др. Угловые распределения дифференциальных сечений и векторных анализирующих способностей реакции ${}^9\text{Be}(d,p){}^{10}\text{Be}$, ${}^9\text{Be}(d,t){}^8\text{Be}$ и ${}^9\text{Be}(d,\alpha){}^6\text{Li}$ при $E_d = 2-2,8$ МэВ//Ядерная физика. 1984. Т. 40, № 1. С. 53-61.

310. C o x S.A., W i l l i a m s o n R.M. Angular distribution and correlation studies of ${}^9\text{Be}$, ${}^{10}\text{B}$ and ${}^{24}\text{Mg}(d,p)$ reactions//Phys.Rev. 1957. Vol. 105, N 6. P. 1799-1808.

311. F u l b r i g h t H.W., B r u n e r J.A., B r o m l e y D.A., G o l d m a n L.M. Angular distributions of protons and tritons from deuteron induced reactions on ${}^9\text{Be}$ // Ibid.1952. Vol. 88, N 4. P. 700-702.

312. R e a d F.H., C a l v e r t J.M., S c h o r k G. Some ${}^9\text{Be}(d,p){}^{10}\text{Be}$ angular correlation measurements off the stripping peak// Nucl.Phys.1961. Vol. 23, N 3. P. 386-398.

313. S c h m i d t - R o h r U., S t o c k R., T u r e k P. Die winkelverteilungen der protonen aus den reaktionen ${}^9\text{Be}(d,p){}^{10}\text{Be}$, ${}^{12}\text{C}(d,p){}^{13}\text{C}$, ${}^{16}\text{O}(d,p){}^{17}\text{O}$ and ${}^{40}\text{Ca}(d,p){}^{41}\text{Ca}$ bei 11,8 MeV//Nucl. Phys. 1964. Vol. 53, N 1. P. 77-86.

314. H e f t R.E., L i b b y W.F. Absolute cross sections for deuterons on beryllium//Phys. Rev. 1955. Vol. 100, N 3. P. 799-813.

315. W o l f g a n g R.L., L i b b y W.E. Absolute excitation function of the ${}^9\text{Be}(d,t)$ reaction// Ibid. 1952. Vol. 85, N 3. P. 437-440.

316. H a f f n e r J.M. Angular distribution of inelastically scattered deuterons//Ibid. 1956. Vol. 103, N 5. P. 1398-1407.

317. B o n d o u k I.I., A s f o u r P., M a c h a l i P. Investigation of the reaction ${}^9\text{Be}(d,t){}^8\text{Be}$ in the deuteron energy range 0,9-2,5 MeV// Ann. der Phys. 1975. Bd. 32, N 4. S. 255-260.

318. T a n a k a S. The ${}^9\text{Be}(d,t){}^8\text{Be}$ and ${}^9\text{Be}(d,\alpha){}^7\text{Li}$ reaction in the energy range from 12,17 MeV to 14,43 MeV//J.Phys.Soc.Jap. 1978. Vol. 44, N 5. P. 1405-1412.

319. A n n e g a r n H.J., M i n g a y D.W., S e l l s c h o p J.P.F. Evidence for a nuclear level in ${}^{11}\text{B}$ at 16,43 MeV//Phys.Rev. 1974. Vol. C9, N 1. P. 419-421.

320. И в а н ц ь к и й П.Г. Угловое распределение альфа-частиц из реакции ${}^9\text{Be}(d,\alpha){}^7\text{Li}$ //Укр.Физ.ж. 1962. Т.7, № II. С. II60-II63.

321. B e r t r a n d F., C r e n i e r G., P o r n a t J. Etude des reactions ${}^9\text{Be}(d,\alpha){}^7\text{Li}$, ${}^9\text{Be}(d,\alpha){}^7\text{Li}$, ${}^9\text{Be}(d,t){}^8\text{Be}$ et ${}^9\text{Be}(d,p){}^{10}\text{B}$ de 300 keV a 1000 keV//CEA-R-3504, 1968.

322. S l e d z i n s k a I., S a g a n e k A., W i l h e l m i Z., Z w i e g l i n s k i B. Analysis of the ${}^9\text{Be}(d,\alpha){}^7\text{Li}$ and ${}^9\text{Be}(d,\alpha){}^7\text{Li}$ (470 keV) reaction in terms of the two nucleon distorted wave born approximation// Acta Phys.Polon 1977. T.19, N3. P.227-235.

323. В а л ь т е р А.К., В а с и л ь т П.И., К о л е с н и к о в Л.Я. и др. Выход нейтронов в реакции ${}^9\text{Be}(t,n)$ //Укр.Физ.ж. 1961. Т.6, № 4. С. 457-460.

324. М а л у ш и н ь с к а К., Н е д в е д ь о к К., С а л а ц к и й В.И., Х а л ь в е к И. Исследование реакции ${}^9\text{Be}(t,n){}^{11}\text{B}$ в диапазоне энергий мюнов трития 1,1-1,7 МэВ: Препринт № Р.15-9986. Дубна:ОИЯИ, 1976.

325. A n d e r s B., H e r g e s P., S c o b e l W. Excitation functions of nuclear reactions producing ${}^{11}\text{C}$ // Z.Phys. 1981. Bd. A301, N 4. S. 353-361.

326. H a h n R.L., R i c c i E. Interactions of ${}^3\text{He}$ particles with ${}^9\text{Be}$, ${}^{12}\text{C}$, ${}^{16}\text{O}$, ${}^{19}\text{F}$ // Phys.Rev. 1966. Vol. 146, N 3. P. 650-659.

327. А б р а м о в и ч С.Н., Г у ж о в с к и й Б.Я., П е р е ш и в к и н В.А. Полные сечения образования радионуклида ${}^{11}\text{C}$ в реакциях ${}^9\text{Be}({}^3\text{He},n){}^{11}\text{C}$, ${}^{10}\text{B}(d,n){}^{11}\text{C}$ и ${}^{11}\text{B}(d,2n){}^{11}\text{C}$ // ВАНТ.Сер.Ядерные константы. 1984. Вып.2(56). С. 55-60.

328. D i n G.U., W e i l J.L. The reaction ${}^9\text{Be}({}^3\text{He},n){}^{11}\text{C}$ from 1,3 to 5,4 MeV// Nucl.Phys. 1956. Vol. 71, N 3. P. 641-661.

329. O s m a n A., D i n G.U. ${}^9\text{Be}({}^3\text{He},n){}^{11}\text{C}$ and ${}^{11}\text{B}({}^3\text{He},n){}^{13}\text{N}$ reaction of energies below coulomb barrier// Ann. der Phys. 1979. Ed. 36, N 1. S. 56-63.

330. T o w l e J.H., M a c e f i e l d B.E.F. A study of the ${}^9\text{Be}({}^3\text{He},n){}^{11}\text{C}$ reaction//Nucl.Phys. 1965. Vol. 66, N 1. P. 65-79.

331. H i n d s S., M i d d l e t o n R. A study of the ${}^9\text{Be}({}^3\text{He},p){}^{11}\text{B}$ and the ${}^9\text{Be}({}^3\text{He},d){}^{10}\text{B}$ reactions in the energy range 5,7 to 10,2 MeV//Proc.Phys. Soc. 1960. Vol. 75, N 485. Pt.5. P. 754-761.

332. W o l i c k i E.A., H o l m g r e n H.D., J o n s t o n R.L., I l l s l e y E.G. Differential cross sections for ${}^9\text{Be}({}^3\text{He},p){}^{11}\text{B}$ reaction//Phys.Rev. 1959.Vol.116, N 6. P. 1585-1591.

333. W e i n m a n J.A., S m i t h e r R.K. The observation of ${}^8\text{Be}$ in the ground state//Nucl. Phys. 1963. Vol. 45, N 2. P. 260-272.

334. Poulriot J., Roy R., Bricault P. e.a. Polarization et mesures de section efficace dans la réaction ${}^9\text{Be}({}^3\text{He}, p){}^{11}\text{B}$ //Can.J.Phys. 1963. Vol. 61, N 12. P. 1609-1612.

335. Holmgren H.D., Bullock M.L., Kunz W.E. Differential cross sections for the ${}^9\text{Be}({}^3\text{He}, p){}^{11}\text{B}$ reaction//Phys.Rev. 1956. Vol. 104, N 5. P. 1446-1450.

336. Coker W.R., Duncan M.M., Duggan J.L., Miller P.D. An investigation of the ${}^9\text{Be}({}^3\text{He}, p){}^{11}\text{B}$ reaction at low energies//Nucl.Phys. 1967. Vol. A91, N 1. P.97-111.

337. Gibbons J.H., Macklin R.L. Total cross section for ${}^9\text{Be}(\alpha, n)$ //Phys.Rev. 1965. Vol. B137, N 6. P.1508-1509.

338. Van-der-Zwan L., Geiger K.W. The ${}^9\text{Be}(\alpha, n){}^{12}\text{C}$ cross section between 1,5 and 7,8 MeV//Nucl.Phys. 1970. Vol. A152, N 3. P. 481-494.

339. Geiger K.W., Van-der-Zwan L. Radioactive neutron source - spectra from ${}^9\text{Be}(\alpha, n)$ cross section data//Nucl.Instr.Meth. 1975. Vol.131, N 2. P. 315-321.

340. Obst A.W., Grandy T.B., Weil J.L. Reaction ${}^9\text{Be}(\alpha, n){}^{12}\text{C}$ from 1,7 to 6,4 MeV//Phys.Rev. 1972. Vol. C5, N 3. P. 738-754.

341. Verbinski V.V., Perey F.G., Dickens J.K., Burrus W.R. Neutrons from ${}^9\text{Be}(\alpha, n)$ reaction for $E(\alpha)$ between 6 and 10 MeV//Phys.Rev. 1968. Vol. 170, N 4. P. 916-923.

342. Risser J.R., Price J.E., Class C.M. Resolved neutrons from the $\text{Be}(\alpha, n)$ reaction//Ibid. 1957. Vol. 105, N 4. P. 1288-1293.

343. James D.B., Jones G.A., Wilkinson D.H. The reactions ${}^9\text{Be}(\alpha, n){}^{12}\text{C}$ //Phyl. Mag. 1956. Vol. 1, N 10. P. 949-963.

344. Davids C.N. A study of (α, n) reactions on ${}^9\text{Be}$ and ${}^{13}\text{C}$ at low energies//Nucl.Phys. 1968. Vol. A110, N 3. P. 619-636.

345. Seaborn J.B., Mitchell G.E., Fletcher N.R., Davis R.H. Gamma rays from the ${}^9\text{Be}(\alpha, n){}^{12}\text{C}$ reaction//Phys.Rev. 1963. Vol. 129, N 5. P.2217-2219.

346. Bonner T.W., Kraus A.A., Marion J.B., Schiffer J.P. Neutrons and gamma rays from the alpha-particle bombardment of ${}^9\text{Be}$, ${}^{10}\text{B}$, ${}^{11}\text{B}$, ${}^{13}\text{C}$ and ${}^{18}\text{O}$ //Ibid. 1956. Vol. 102, N 5. P. 1348-1354.

347. Klages H.O., Scholermann H. Polarisation und differentieller Wirkungsquerschnitt der Neutronen aus der Reaktion ${}^9\text{Be}(\alpha, n){}^{12}\text{C}$ //Z.Phys. 1969. Bd. 227, N 4. S. 344-351.

348. Nilsson A., Kjellman J. Neutron angular distributions from the ${}^9\text{Be}(\alpha, n){}^{12}\text{C}$ reaction at 14,1; 13,9 and 13,5 MeV// Nucl.Phys. 1962. Vol. 32, N 2. P. 177-189.

349. Kondo M., Yamazaki T., Yamaube S. Angular distributions of (α, n) reactions on Be and C// J.Phys.Soc.Jap. 1963. Vol. 18, N 1. P. 22-28.

350. Deconninck G., De-Vroey M., Meulders J.P., Simonet J. (α, n) reactions in light nuclei// Nucl.Phys. 1963. Vol. 49, N 3. P. 424-432.